



**MONASH** University

**APPLICATIONS OF ANTIMICROBIAL BISMUTH-  
NANOCELLULOSE MATERIALS**

by

**Maisha Maliha**

B.Sc. Engg. (Chem)

Thesis submitted in the fulfilment of the requirement for the degree of  
*Doctor of Philosophy in Chemical Engineering*

Bioresource Processing Institute of Australia (BioPRIA)  
Department of Chemical Engineering  
Faculty of Engineering  
Monash University

April 2021

THIS PAGE HAS BEEN INTENTIONALLY LEFT BLANK

*Dedicated to my beloved parents*

*~ Abbu & Ammu ~*

THIS PAGE HAS BEEN INTENTIONALLY LEFT BLANK

## **Copyright notice**

© Maisha Maliha, 2021. Except as provided in the Copyright Act 1968, this thesis may not be reproduced in any form without written permission of the author.

I certify that I have made all reasonable efforts to secure copyright permissions for third-party content included in this thesis and have not knowingly added copyright content to my work without the owner's permission.

.....  
**Maisha Maliha**

THIS PAGE HAS BEEN INTENTIONALLY LEFT BLANK

## **General Declaration**

This thesis is an original work of my research and contains no material which has been accepted for the award of any other degree or diploma at any university or equivalent institution and that, to the best of my knowledge and belief, this thesis contains no material previously published or written by another person, except where due reference is made in the text of the thesis.

Signature: .....

Print Name: Maisha Maliha

Date: 1 April, 2021

THIS PAGE HAS BEEN INTENTIONALLY LEFT BLANK

## Table of Contents

Copyright notice.....	v
General Declaration.....	vii
Table of Contents .....	ix
Thesis including published works declaration .....	xi
Acknowledgements .....	xiii
Abstract .....	xv
Publications during enrolment .....	xvii
List of Figures .....	xviii
List of Tables.....	xxii
List of Abbreviations.....	xxiv
List of Nomenclature.....	xxvi
<b>Chapter 1:</b> Introduction and Literature Review .....	1
<b>Chapter 2:</b> Bismuth phosphinate incorporated nanocellulose sheets with antimicrobial and barrier properties for packaging applications .....	69
<b>Chapter 3:</b> The effect of pulp type on the barrier and antimicrobial performance of microfibrillar lignocellulosic bismuth-based active packaging material ...	103
<b>Chapter 4:</b> Biocompatibility and selective antibacterial activity of a bismuth phosphinato-nanocellulose hydrogel.....	131
<b>Chapter 5:</b> Bismuth phosphinato incorporated antibacterial filter paper for drinking water disinfection .....	165
<b>Chapter 6:</b> Conclusion and Perspectives.....	195
<b><u>Appendix I:</u></b> <b><u>Supplementary Information</u></b>	
<b>Appendix IA:</b> Bismuth phosphinate incorporated nanocellulose sheets with antimicrobial and barrier properties for packaging applications .....	I-3
<b>Appendix IB:</b> The effect of pulp type on the barrier and antimicrobial performance of microfibrillar lignocellulosic bismuth-based active packaging material ...	I-11

**Appendix IC:** Biocompatibility and selective antibacterial activity of a bismuth phosphinato-nanocellulose hydrogel .....I-13

**Appendix ID:** Bismuth phosphinato incorporated antibacterial filter paper for drinking water disinfection.....I-17

**Appendix II: Publications included in thesis in their published format**

**Appendix IIA:** Bismuth phosphinate incorporated nanocellulose sheets with antimicrobial and barrier properties for packaging applications..... II-3

**Appendix IIA:** Biocompatibility and selective antibacterial activity of a bismuth phosphinato-nanocellulose hydrogel ..... II-15

**Appendix III: Co-authored publications not included in thesis**

**Appendix IIIA:** Engineering laminated paper for SARS-CoV-2 medical gowns ..... III-3

**Appendix IIIA:** High-performance homogenized and spray coated nanofibrillated cellulose-montmorillonite barriers ..... III-13

## Thesis including published works declaration

I hereby declare that this thesis contains no material which has been accepted for the award of any other degree or diploma at any university or equivalent institution and that, to the best of my knowledge and belief, this thesis contains no material previously published or written by another person, except where due reference is made in the text of the thesis.

This thesis includes 2 original papers published in peer reviewed journals and no submitted publications. The core theme of the thesis is *Bismuth phosphinate loaded nanocellulose antimicrobial materials*. The ideas, development and writing up of all the papers in the thesis were the principal responsibility of myself, the student, working within the Department of Chemical Engineering, Monash University under the supervision of Associate Professor Warren Batchelor, Professor Philip Andrews and Dr. Melissa Werrett.

The inclusion of co-authors reflects the fact that the work came from active collaboration between researchers and acknowledges input into team-based research.

In the case of Chapter 2 and Chapter 4, my contribution to the work involved the following:

Thesis Chapter	Publication Title	Status (published, in press, accepted or returned for revision, submitted)	Nature and % of student contribution	Co-author name(s) Nature and % of Co-author's contribution*	Co-author (s), Monash student Y/N*
2	Bismuth phosphinate incorporated nanocellulose sheets with antimicrobial and barrier properties for packaging applications	Published	60% Initiation, key ideas, experimental work, analysis of results, writing up.	<ol style="list-style-type: none"> <li>1. Megan Herdman, experimental work, paper reviewing and editing, 5%</li> <li>2. Rajini Brammananth, experimental work, 2%</li> <li>3. Michael McDonald, experimental work, 2%</li> <li>4. Ross Coppael, paper reviewing and editing, 1%</li> <li>5. Melissa Werrett, key ideas, experimental work, paper reviewing and editing, 10%</li> <li>6. Philip Andrews, key ideas, paper reviewing and editing, 10%</li> </ol>	<p>Yes</p> <p>No</p> <p>No</p> <p>No</p> <p>No</p> <p>No</p>

PREFACE

				7. Warren Batchelor, key ideas, paper reviewing and editing, 10%	No
4	Biocompatibility and Selective Antibacterial Activity of a Bismuth Phosphinato-Nanocellulose Hydrogel	Published	60% Initiation, key ideas, experimental work, analysis of results, writing up.	1. Rajini Brammananth, experimental work, 3% 2. Jennifer Dyson, experimental work, paper reviewing and editing 5% 3. Ross Coppel, paper reviewing and editing, 2% 4. Melissa Werrett, experimental work, paper reviewing and editing, 10% 5. Philip Andrews, paper reviewing and editing, 10% 6. Warren Batchelor, key ideas, paper reviewing and editing, 10%	No No No No No No

I have renumbered sections of submitted or published papers in order to generate a consistent presentation within the thesis.

**Student name: Maisha Maliha**

**Student signature:**

**Date:**

I hereby certify that the above declaration correctly reflects the nature and extent of the student's and co-authors' contributions to this work. In instances where I am not the responsible author I have consulted with the responsible author to agree on the respective contributions of the authors.

**Main Supervisor name: Warren Batchelor**

**Main Supervisor signature:**

**Date:**

## Acknowledgements

I would like to start by thanking the Almighty for this opportunity and for giving me the patience and determination during the entire PhD journey.

I would like to express my humble gratitude to my supervisor Associate Professor Warren Batchelor for his wise guidance, expertise and constant support throughout the tenure of my PhD. He is truly an amazing supervisor, huge thanks to him for always being very understanding and supporting. I would like to extend my gratefulness to my co-supervisors Professor Philip Andrews and Dr. Melissa Werrett. I have learnt a lot from them which has helped me complete my study successfully and will also help me in my research career in the future. My supervisors formed a very dynamic team with great expertise from both chemistry and engineering ends and I thoroughly enjoyed my time working with them.

I would like to acknowledge the financial support provided by The National Health and Medical Research Council (APP1139844) for my research and the Australian Government Research Training Program (RTP) Scholarship.

I would like to express my sincere thanks to Professor Gil Garnier for giving me the opportunity to work with him on the COVID-19 Task Force team alongside my PhD project. It was a great experience for me to work with such a lovely and lively leader. I would like to thank Janette Anthony for keeping the laugh and love alive in the workplace by organising all the social events. Thanks to Scot Sharman for the trainings and lab inductions and his jokes every time I see him. Thanks to all the staff members in BioPRIA and the Department of Chemical Engineering- Dr. Joanne Tanner, Dr. Christine Browne, Dr. Vikram Raghuwanshi, Heather McLeish, Dr. Rosi Eka, Clare Manderson, Kim Phu, Anthony De Girolamo and Ross Ellingham. I would like to acknowledge Rajini Brammananth and Ross Coppel for their assistance with the microbiology studies and Jennifer Dyson for training me with the cell biology and tissue culture techniques.

I would like to thank my noisy friends cum colleagues - Aysu Onur, Rodrigo Curvello, Marek Bialkower, Ruth Barajas, David Mendoza, Diana Alves, Wriju Kargupta, Mahdi Naseri Nosar, Humayun Nadeem, Mostafa Dehghani, Megan Herdman, Kirubanandan Shanmugam, Simin Miri and Thilina Gunawardhana. All of you made each day at work enjoyable. I would like to express my love and appreciation to my dearest friend, colleague and roomie, Laila Hossain. Thanks to Laila and Afifa Tamanna for being the best roomies and my family away from home. When I am thanking my friends, I can never miss out on my childhood buddies. I would like to express my love to my best friends Raihana Mohsina, Arunima Hassan, Tarina Monzur and Shabnaz Zubaid for always being just one call or message away. I would also like to thank my dearest friends Israt

Jahan and Samavi Farnush, with whom I learned the ABC's of research together. These two incredible women play a huge role in my career. I have to acknowledge my previous research supervisors Associate Professor Shoeb Ahmed and Associate Professor Mohidus Samad Khan. It was these two knowledgeable and brilliant people who taught me to think like a scientist and built me what I am today. Thanks to you both, Sir.

I express my affection and love to my sister-in-law, Tanzima Farheen and brother-in-law Mehedee Hasan for their warmth and care and for being my family in Melbourne. You both are amazing elder siblings, and it is a blessing that I always have your back. I would like to thank another two amazing human beings, my mother-in-law (Maa), Anjuman Ara Begum and father-in-law (Baba), Kazi Mahiuddin. Maa, who was an academic herself, has been a woman I can always look up to and aspire to become. And Baba is the person who taught me the art of patience and perseverance and helped me grow the maturity I have today. Thanks for treating me as your little kid and always being supportive. I thank you all from the bottom of my heart. I would like to express my love to my sweet nieces Mehree Farzeen and Marnia Fariba for their playful presence. Little Marnia was always there with the warm hugs and all the cute gestures to brighten my day. I want to express my admiration and affection to my darling sisters- Dr. Anusha Anjum, Bushra Tasnim, Iffat Adury and Tahifa Tanzib. I am extremely proud that you all are growing up to such smart and capable women. I always strive to be a better version of myself, a big reason for that is I know you are looking upto me.

Saving the best for the last. I would have to thank my handsome and ever-so-supporting husband, Kazi Naveed Ridwan. He has been there through thick and thin, and supported me in every possible way to fulfil my dreams. Dealing with my frustrations during experiments failure, feeding my mind with positivity, encouraging me to go ahead and filling my life so full of love are only some of the many things you have done for me. Long-distance relationship is hard itself, and the travel restrictions made it worse. But with your love and effort, even from miles away, every difficulty became easier. For some people, a mention in the acknowledgement is never enough. At that place stands my beloved parents- Nur Nabi and Ashma Nur. I would never be where I am today without your love and blessings. I cannot thank you enough for everything you have done for me, so I wouldn't even try. I am dedicating my PhD thesis to you.

## Abstract

Antimicrobial resistance is a major threat to public health. Antimicrobial materials are a great tool for infection control and so various antimicrobial agents in different materials have been studied. Since the widespread use of the most commonly used antimicrobial agents has given rise to antimicrobial resistance in bacterial populations, it is vital that new antimicrobial agents are discovered. One such new antimicrobial agent is the organometallic complex, diphenyl *bis*-phosphinato bismuth (III). This has been studied previously and shown to exhibit antibacterial activity as well as very low solubility. These two properties make the bismuth (III) complex a strong choice to be incorporated into materials. This thesis explores the potential of the complex for producing antibacterial materials. While various polymeric materials have been studied for carrying antimicrobial agents, most of them are petroleum-based. The global demand for sustainability has driven the interest of this research in using a renewable biopolymer. Cellulose is the most abundant natural polymer and is environmentally friendly due to its renewability, biodegradability and non-toxicity. Cellulose can be isolated to nano and micron sized fibrils known as nanocellulose. This thesis aims to understand the utility of the bismuth complex nanocellulose-based materials to engineer its use in three distinct applications.

In the first part of the thesis, the potential of the complex in nanocellulose composites for active packaging applications was investigated. *Bis*-phosphinato bismuth complex-nanocellulose composites were produced by spray coating technique. The complex exist as cylindrical structures and are present not just on the surface but are also embedded within the material. The composites showed both antibacterial and antifungal properties. The water vapor barrier and the mechanical properties of the composites remained in the acceptable range for packaging materials. All these provided well-defined results to ensure nanocellulose-bismuth complex composites are suitable for active packaging applications. The study was further extended to understand the suitability of different types of lignocellulosic matrices for this application. The release behaviour of the complex plays a major role in the antibacterial activity of materials. Lignin-containing matrices form a strong interaction with the hydrophobic complex, resulting in lower release and hence lower activity. Hence hydrophilic fibrous materials are preferred for such applications.

In the second part of this thesis, an important biomedical application for infection control has been studied. The utility of the complex in wound care applications has been introduced by incorporating the complex in nanocellulose hydrogel. The Bi-complex loaded hydrogel behaves like a true gel, with solid-like behaviour beyond the yield point. Nanocellulose hydrogels are completely safe to mammalian fibroblast cells, as proven by *in-vitro* studies. But the complex was shown to induce reduced fibroblast viability at high concentrations. An optimised concentration

of 9 µg/g was found. At this concentration it remained bactericidal to Gram-negative bacteria (*Pseudomonas aeruginosa* and *Acinetobacter baumannii*) and bacteriostatic to Gram-positive bacteria (Methicillin-resistant *Staphylococcus aureus* and Vancomycin-resistant *Enterococci*), while not inhibiting fibroblast growth. The complex concentration to achieve selective toxicity to bacterial cells over mammalian cells, that was established in this thesis, will be the basis for future pre-clinical studies.

Finally, the potential of the complex in water disinfection was explored. Two different approaches are studied in this thesis. The first hypothesis was that the microorganisms in contaminated water will be deactivated or killed as it passes through a filter coated with the *bis*-phosphinato bismuth complex. Unfortunately, this hypothesis was not proven, as the filtered water showed no change in bacterial content. So, the complex does not have instantaneous effect on bacteria. However, when the filtrate was stored at 37 °C for 24 hours, up to 100% bacterial removal was observed. Hence this can be an easy-to-use approach in developing countries to filter contaminated water and consume it only after storing it. However, if immediate removal of bacteria was desired a second approach was proposed. Herein, highly fibrillated nanocellulose was used to prepare microfiltration membranes to eliminate the bacteria by size exclusion. For filtration systems in prolonged contact with microbial load, biofouling is an issue. The bismuth complex in these microfiltration membranes was shown to inhibit the surface growth of bacteria and hence prevent biofilm formation.

Overall, this thesis has significantly expanded the knowledge about the *bis*-phosphinato bismuth complex in nanocellulose material and has developed new applications where the complex could be utilised.

## **Publications during enrolment**

The following published papers are included in this thesis as individual chapters. The papers in their published form is included as Appendix II. The sections have been renumbered for a consistent presentation within the thesis.

1. **Maliha, M.**, M. Herdman, R. Brammananth, M. McDonald, R. Coppel, M. Werrett, P. Andrews and W. Batchelor (2019). *Bismuth phosphinate incorporated nanocellulose sheets with antimicrobial and barrier properties for packaging applications*. Journal of Cleaner Production 246.
2. **Maliha, M.**, R. Brammananth, R. Coppel, J. Dyson, M. Werrett, P. Andrews and W. Batchelor (2021). *Biocompatibility and Selective Antibacterial Activity of a Bismuth Phosphinato-Nanocellulose Hydrogel*. Cellulose.

The following co-authored published papers are not included in this thesis.

1. Shanmugam, K., S. Ang, **M. Maliha**, V. Raghuvanshi, S. Varanasi, G. Garnier and W. Batchelor (2021). *High-performance homogenized and spray coated nanofibrillated cellulose-montmorillonite barriers*. Cellulose 28(1): 405-416.
2. Hossain, L., **M. Maliha**, R. Barajas, J. Kim, K. Putera, D. Subedi, J. Tanner, J. Barr, M. B. Holl, G. Garnier. (2021) *Engineering laminated paper for SARS-CoV-2 medical gown*. Polymer.

## List of Figures

### Chapter 1

- Figure 1: Different mechanisms of action of antimicrobial metals.
- Figure 2: Bacterial mechanism of adapting and dealing with the toxic effects of antimicrobial metals.
- Figure 3: Experimentally confirmed resistance genes for metals.
- Figure 4: Chemical structure of the *bis*-phosphinato bismuth complex.
- Figure 5: Chemical reaction for the synthesis of the *bis*-phosphinato bismuth complex.
- Figure 6: Antibacterial activity of the complex determined by the zone of inhibition method against MRSA. Here, the sample labelled “1” is the *bis*-phosphinato complex.
- Figure 7: Details of cellulose fibre structure originating from cellulosic source.
- Figure 8: Different pathways of MFC and CNC production from plant cellulose.
- Figure 9: Oxidation of primary alcohol of cellulose to carboxylate using TEMPO/NaBr/NaClO.
- Figure 10: Schematic showing the basic difference between conventional and antimicrobial packaging.
- Figure 11: Change in pore size with change in fibre diameter at 80% porosity.

### Chapter 2

- Figure 1: Experimental setup for lab scale spraying of the bismuth (III) phosphinato-MFC suspension onto stainless steel plates.
- Figure 2: SEM images of the surface of 4.37 wt.% Bi-MFC composite at different magnifications:(a)  $\times 3500$  (b)  $\times 12500$ .
- Figure 3: (a) Particle length distribution (n=140) and (b) Aspect ratio distribution (n=40) of bismuth (III) phosphinato complex on the surface of 4.37 wt.% Bi-MFC sheet.
- Figure 4: SEM images of the 4.37 wt.% Bi-MFC composite using (a) secondary electron imaging (b) EDX mapping of the selected area.
- Figure 5: SEM images of the 4.37 wt.% Bi- MFC sheets using (a) secondary electron imaging and their corresponding (b) Back scattered electron imaging.
- Figure 6: Back scattered electron image of the 4.37 wt.% Bi- MFC sheet at low magnification ( $\times 200$ ).
- Figure 7: Effect of bismuth complex loading on zone of inhibition with different bacteria from disk diffusion assay and the top images show their picture representation against *S. aureus*.

- Figure 8: Zone of inhibition (a) and the amount of bismuth content leached out into the zone of inhibition (b) for the 4.37 wt.% and 0.94 wt.% loaded bismuth sheets with time.
- Figure 9: Physical appearance of the 0.39 wt.%, 0.94 wt.% and 2.10 wt.% bismuth (III) phosphinato-MFC sheets (left to right).
- Figure 10: Pore size distribution for pure MFC and Bi-MFC composite.
- Figure 11: Effect of bismuth complex loading on the water vapour permeability of the phenyl bismuth *bis*(diphenylphosphinato) functionalized MFC.

### Chapter 3

- Figure 1: Representation of the sources and types of the pulp used for Bi-MFC composites preparation. The dashed box shows the simplified flowchart of the major processes in the paper mills. The green and the orange arrows show the preparation of the softwood and the hardwood pulp respectively. Here the acronyms UPK, BPK, BEK, UTMP and BTMP stands for unbleached pine kraft pulp, bleached pine kraft pulp, bleached eucalyptus kraft pulp, unbleached thermomechanical pulp and bleached thermomechanical pulp respectively.
- Figure 2: Physical appearance of the composites using bleached eucalyptus kraft pulp (BEK), bleached (BPK) and unbleached (UPK) radiata pine kraft pulp and bleached (BTMP) and unbleached (UTMP) radiata pine thermomechanical pulp.
- Figure 3: Micrographs of the composite films from bleached eucalyptus kraft pulp (BEK) (top), bleached (BPK) and unbleached (UPK) radiata pine kraft pulp (middle panel), bleached (BTMP) and unbleached (UTMP) radiata pine thermomechanical pulp (bottom panel) showing the fibre dimensions.
- Figure 4: Optical profilometry images of the surface of blank films (no bismuth) (top panel) and the height profiles of the surface along the horizontal centre line shown (bottom panel). The scale bars indicate 50  $\mu\text{m}$ .
- Figure 5: FTIR spectrum of the Bi-complex loaded films prepared from bleached eucalyptus kraft pulp (BEK), bleached (BPK) and unbleached (UPK) radiata pine kraft pulp and bleached (BTMP) and unbleached (UTMP) radiata pine thermomechanical pulp showing the difference in chemical composition.
- Figure 6: The zones of inhibition of the bismuth loaded composites of bleached eucalyptus kraft pulp (BEK), bleached (BPK) and unbleached (UPK) radiata pine kraft pulp and bleached (BTMP) and unbleached (UTMP) radiata pine thermomechanical pulp against different bacteria after 24 hours (A) and against *S. aureus* over a period of 5 days (B). There was no zone observed where it is labelled with a zero (0) in the graph.

- Figure 7: The percentage of Bi-complex released into water from composite films of bleached eucalyptus kraft pulp (BEK), bleached (BPK) and unbleached (UPK) radiata pine kraft pulp and bleached (BTMP) and unbleached (UTMP) radiata pine thermomechanical pulp. The bars represent the percentage of bismuth complex present in the leachate after 24 hours with respect to the mass of the complex contained in the composites. The error bars represent the standard deviation.
- Figure 8: The water vapor transmission rate (WVTR) of the films prepared from bleached eucalyptus kraft pulp (BEK), bleached (BPK) and unbleached (UPK) radiata pine kraft pulp and bleached (BTMP) and unbleached (UTMP) radiata pine thermomechanical pulp with and without the bismuth complex at 23°C and 50% relative humidity. The error bars indicate standard deviations.
- Figure 9: Mechanical properties from tensile testing for composite films from bleached eucalyptus kraft pulp (BEK), bleached (BPK) and unbleached (UPK) radiata pine kraft pulp and bleached (BTMP) and unbleached (UTMP) radiata pine thermomechanical pulp with and without bismuth complex loading expressed as an average tensile index (A) and Young modulus (B). Error bars represent 95% confidence interval.

#### **Chapter 4**

- Figure 1: SEM image of air-dried Bi-NC hydrogel. (a) Secondary electron image (b) Back-scattered electron image of the same area (c) secondary electron image showing a nanofibre bundle.
- Figure 2: Viscosity profile of blank hydrogel and bismuth-complex loaded hydrogel compared to commercial wound hydrogel.
- Figure 3: Dynamic strain sweep of blank hydrogel and bismuth-complex loaded hydrogel compared to commercial wound hydrogel.
- Figure 4: Viability of L929 cells after treatment with (A) nanocellulose hydrogels loaded with the indicated target concentrations of Bi-complex (green) or Ag-compound (blue) and (B) the indicated commercial hydrogel and blank nanocellulose hydrogel, determined by MTS assay. Percentage viability normalised over no treatment DMEM control. The data presented are expressed as mean  $\pm$  standard error of mean of technical triplicates from four independent sets of biological replicates. The number of asterisks over the bars show the level of significance of the data when compared with no treatment control. \* represents  $p \leq 0.05$ , \*\* represents  $p \leq 0.01$ , \*\*\* represents  $p \leq 0.001$  and \*\*\*\* represents  $p \leq 0.0001$ .

- Figure 5: Live-dead staining of L929 cells after 24 hours of incubation with the indicated target concentration of the bismuth complex in nanocellulose hydrogel, the blank nanocellulose hydrogel (NC-gel) or DMEM culture media only. The green and red fluorescence show live and dead/dying cells respectively. Scale bar represents 100  $\mu\text{m}$ .
- Figure 6: Light microscopy of L929 cells after 24 hours of incubation with the indicated target concentration of the bismuth complex in nanocellulose hydrogel, or blank nanocellulose hydrogel (NC-gel) without the bismuth complex or DMEM media only. Scale bar represents 100  $\mu\text{m}$  in the images and 20  $\mu\text{m}$  in the inset.
- Figure 7: Time-kill kinetics of the Bi-NC hydrogel at indicated target concentration of the bismuth complex against the Gram-negative bacterial strains of *A. baumannii*, *P. aeruginosa* and *E. coli* and the Gram-positive strains of MRSA and VRE for 24 hours period performed in triplicates. The values expressed represent mean  $\pm$  standard deviation ( $n=3$ ). All measurements were done in triplicate and all data included except for the following three instances where two replicates were in agreement and one was an outlier, which was excluded: *A. baumannii* at 6 and 3  $\mu\text{g/g}$  at 12 hours and *P. aeruginosa* at 6  $\mu\text{g/g}$  at 12 hours.
- Figure 8: SEM images of untreated *P. aeruginosa* cells (a-b), and treated with Bi-NC hydrogel with bismuth complex concentrations of 12  $\mu\text{g/g}$  (c) and 9  $\mu\text{g/g}$  (d).
- Figure 9: SEM images of a single *P. aeruginosa* cell with no treatment (control), and treated with Bi-NC hydrogel with bismuth complex concentrations of 12  $\mu\text{g/g}$  and 9  $\mu\text{g/g}$ . Scale bar represents 1  $\mu\text{m}$ .

## Chapter 5

- Figure 1: SEM image of the base sheets Advantec (a) and Whatman (b), the 5 wt% Bi-complex loaded coated side on Advantec (A-M5-S) (c-d) and the 5 wt% Bi-loaded NFC membranes (N5-F) (e-f) at two different magnifications.
- Figure 2: Pore size distribution of the blank and 5 wt% Bi-loaded NFC membranes (N0-F and N5-F) and coating (A-M0-S and A-M5-S). The highlighted area shows the size range of *S. aureus* bacteria.
- Figure 3: Logarithmic bacterial colony count of *S. aureus* in the filtrate after passing through the composite filters (error bars show standard deviations,  $n=3$ ).
- Figure 4: Logarithmic bacterial colony count of *S. aureus* in the filtrate after passing through the composite filters with Advantec at different loadings in different storage conditions showing the reduction in bacterial growth when stored at 37  $^{\circ}\text{C}$  for 24 hours

- Figure 5: Schematic presentation of the filtration set up for the MFC coated filter papers and for the NFC microfiltration membranes. The results from the gravity filtration test using Bi-MFC coated filter papers, with antibacterial activity observed for stored water at 37 °C (a), Microfiltration setup with a representative plate showing colony count of *S. aureus* in the inlet liquid and the filtrates after passing through the NFC membranes with no bacterial presence (b).
- Figure 6: Cytotoxicity of the filtrates at different concentrations of the bismuth complex on murine fibroblast cell line expressed as a percentage of the negative control (DMEM media only, no treatment). The culture medium was diluted with the filtrate from 10 wt% Bi-loaded NFC membranes to achieve these concentrations. Culture medium containing 10% DMSO is the positive control, showing high level of toxicity. The box plot shows the interquartile range, the marker ‘×’ represents the mean and the line represents the median and the whiskers presents the range of data from independent biological replicates. The horizontal blue line shows the limit for cytotoxic material according to ISO 10993-5 (< 70%).
- Figure 7: SEM image bacterial attachment on the blank NFC membrane or N0-F (left) and the 2.5 wt% Bi-loaded NFC membrane or N2.5-F (right) after 24 hours of contact showing lesser attachment on the Bi-loaded membrane.
- Figure 8: SEM image bacterial attachment on the blank NFC membrane or N0-F (left) and the 2.5 wt% Bi-loaded NFC membrane or N2.5-F (right) after 4 days of contact showing lesser attachment on the Bi-loaded NFC membrane but a mature biofilm formation on the blank NFC membrane.

## List of Tables

### Chapter 1

- Table 1: Mechanical properties of pure nanocellulose films produced in different techniques
- Table 2: Mechanical properties of different plastic materials
- Table 3: Commercial active packaging working under the four main principles
- Table 4: Cellulose based packaging material loaded with different antimicrobial agent
- Table 5: Some of the commercial wound dressings using silver as the active agent
- Table 6: Nanocellulose hydrogel studied as antimicrobial wound dressings
- Table 7: Cellulose based filters for water disinfection using metal antimicrobial agent

## Chapter 2

- Table 1: Percentage of phenyl bismuth *bis*(diphenylphosphinato) from ICP-OES analysis for the different loaded Bi-MFC composites
- Table 2: Antifungal activity of the Bi-MFC composites determined by the zone of inhibition assay
- Table 3: Pore properties of the pure MFC sheet and Bi-MFC composite
- Table 4: Literature comparison of WVP of common packaging materials with Bi-MFC composites

## Chapter 3

- Table 1: Physical properties of the blank films and the Bi-loaded composite films from bleached eucalyptus kraft pulp (BEK), bleached (BPK) and unbleached (UPK) radiata pine kraft pulp and bleached (BTMP) and unbleached (UTMP) radiata pine thermomechanical pulp
- Table 2: Average aspect ratio values calculated from the gel point determined using the EMT and CN empirical equations
- Table 3: Actual bismuth complex content of the composite films analysed from ICP-OES analysis

## Chapter 5

- Table 1: Properties of coated filter papers: grammage and flux measured
- Table 2: Pore properties of the MFC coated filters and NFC membranes
- Table 3: Bismuth complex concentration in the filtrate from the MFC coated Advantec filter paper and the NFC membranes

## Chapter 6

- Table 1: Table showing how the different preparation parameters influences the major properties of the *bis*-phosphinato bismuth complex-nanocellulose materials

**List of Abbreviations**

<i>A. baumannii</i>	<i>Acinetobacter baumannii</i>
<i>A. niger</i>	<i>Aspergillus niger</i>
Ag	Silver
AM	Antimicrobial
AMR	Antimicrobial resistance
ASTM	American Society for Testing and Materials
ATR-FTIR	Attenuated total reflectance- Fourier transform infrared
<i>B. amyloliquefaciens</i>	<i>Bacillus amyloliquefaciens</i>
<i>B. subtilis</i>	<i>Bacillus subtilis</i>
BEK	Bleached eucalyptus kraft
BET	Brunauer–Emmett–Teller
BHI	Brain Heart Infusion
Bi	Bismuth
BNC	Bacterial nanocellulose
BPK	Bleached pine kraft
BSE	Back-scattered electron
BSS	Bismuth subsalicylate
BTMP	Bleached thermomechanical pulp
<i>C. albicans</i>	<i>Candida albicans</i>
<i>C. glabrata</i>	<i>Candida glabrata</i>
CBS	Colloidal bismuth subcitrate
CFU/mL	Colony forming units/millilitre
CN	Crowding Number
CNC	Cellulose nanocrystal
DLS	Dynamic light scattering
DMEM	Dulbecco’s modified Eagle medium
DMSO	Dimethyl sulfoxide
DPPA	Diphenyl phosphinic acid
DSC	Differential scanning calorimetry
<i>E. coli</i>	<i>Escherichia coli</i>
EDX	Electro dispersive X-ray
EMT	Effective medium theory
EtOH	Ethanol
FBS	Fetal bovine serum
FEG-SEM	Field emission gun- scanning electron microscopy

HDPE	High density polyethylene
ICP-MS	Inductively coupled plasma- mass spectroscopy
ICP-OES	Inductively coupled plasma- optical emission spectroscopy
<i>L. innocua</i>	<i>Listeria innocua</i>
<i>L. monocytogene</i>	<i>Listeria monocytogenes</i>
LB	Lysogeny broth or Luria–Bertani
LDPE	Low density polyethylene
LMH	litre per square meter per hour
LVR	Linear viscoelastic region
MDR	Multidrug resistance
MFC	Microfibrillated cellulose
MRSA	Methicillin resistant <i>Staphylococcus aureus</i>
MTS	(3-(4,5-dimethylthiazol-2-yl)-5-(3-carboxymethoxyphenyl)-2-(4-sulfophenyl)-2H-
NaBr	Sodium bromide
NaClO	Sodium hypochlorite
NC	Nanocellulose
NCC	Nanocrystalline cellulose
NFC	Nanofibrillated cellulose
NP	Nanoparticle
<i>P. aeruginosa</i>	<i>Pseudomonas aeruginosa</i>
PBS	Phosphate buffered saline
PET	Polyethylene terephthalate
PGA	polyglycolic acid
PI	Propidium iodide
PLA	Polylactic acid
PP	Polypropylene
<i>S. aureus</i>	<i>Staphylococcus aureus</i>
<i>S. cerevisiae</i>	<i>Saccharomyces cerevisiae</i>
<i>S. pombe</i>	<i>Schizosaccharomyces pombe</i>
SE	Secondary electron
SEM	Scanning electron microscope
TCPS	tissue culture polystyrene)
TEMPO	(2,2,6,6-tetramethylpiperidine-1-oxyl)
TGA	Thermogravimetric analysis
TMP	Thermomechanical pulp
TOCN	TEMPO oxidised cellulose nanofibres

UPK	Unbleached pine kraft
UTMP	Unbleached thermomechanical pulp
UV	Ultraviolet
VRE	Vancomycin resistant <i>Enterococcus</i>
WVP	Water vapor permeability
WVTR	Water vapor transmission rate

## List of Nomenclature

MPa	Mega Pascal
%	percentage
$\mu\text{L}$	microlitre
$\mu\text{g}$	microgram
$^{\circ}\text{C}$	degree Celsius
g	gram
G'	storage modulus
G''	loss modulus
h	hour
kg	kilogram
gsm	grams per square metre
nm	nanometer
$\mu\text{m}$	micrometer
wt%	weight percentage
cm/s	centimeter per second
$\mu\text{g/g}$	micrograms per gram
psi	pounds per square inch
ppm	parts per million
ppb	parts per billion
$h_0$	initial height of the suspension
$h_s$	final sedimentation height of the suspension
$C_C$	gel point
p	level of significance (statistics)
v/v	volume/ volume
COS-7	cell line derived from monkey kidney tissue
L929	fibroblast cell line derived from mouse subcutaneous connective tissue

---

---

# **CHAPTER 1**

## **INTRODUCTION AND LITERATURE REVIEW**

---

---

THIS PAGE HAS BEEN INTENTIONALLY LEFT BLANK

**CHAPTER 1: INTRODUCTION AND LITERATURE REVIEW**

<b>1.1. Introduction .....</b>	<b>5</b>
<b>1.2. Literature Review.....</b>	<b>7</b>
<b>1.2.1. Antimicrobial resistance and health issues .....</b>	<b>7</b>
<b>1.2.2. Antimicrobial Agents .....</b>	<b>7</b>
1.2.2.1. Current metal-based antimicrobial agents.....	8
1.2.2.1.1. Silver .....	9
1.2.2.1.2. Arsenic and Antimony .....	10
1.2.2.1.3. Others .....	11
1.2.2.2. Necessity of new antimicrobial agents.....	11
<b>1.2.3. Bismuth and its compounds .....</b>	<b>14</b>
1.2.3.1. General Chemistry.....	14
1.2.3.2. Antimicrobial Activity of Bismuth compounds .....	15
1.2.3.3. Mechanism of action .....	16
1.2.3.4. Toxicity concerns of bismuth compounds .....	16
1.2.3.5. Phenyl <i>bis</i> -diphenyl phosphinato bismuth (III) complex.....	17
<b>1.2.4. Translation to antimicrobial materials- .....</b>	<b>19</b>
<b>1.2.5. Nanocellulose .....</b>	<b>20</b>
1.2.5.1. General aspects of nanocellulose .....	20
1.2.5.2. Production of nanocellulose .....	21
1.2.5.3. Nanocellulose films.....	23
1.2.5.3.1. Preparation methods.....	23
1.2.5.3.2. Properties and applications.....	23
1.2.5.4. Nanocellulose hydrogel.....	25
1.2.5.4.1. Preparation methods.....	26
1.2.5.4.2. Properties and applications.....	27
<b>1.2.6. Applications of antimicrobial materials.....</b>	<b>28</b>
1.2.6.1. Packaging materials.....	28
1.2.6.1.1. Current active packaging technologies .....	28
1.2.6.1.2. Nanocellulose antimicrobial packaging .....	30
1.2.6.2. Wound dressing.....	35
1.2.6.2.1. Wound infection.....	35
1.2.6.2.1.1. Wound pathogens.....	35
1.2.6.2.2. Current antimicrobial wound dressings.....	36
1.2.6.2.3. Hydrogels as wound dressings .....	39
1.2.6.2.4. Nanocellulose antimicrobial hydrogel .....	40

1.2.6.3.	Water purification .....	43
1.2.6.3.1.	Issues with non-active filters .....	43
1.2.6.3.2.	Nanocellulose filters .....	44
<b>1.2.7.</b>	<b>Perspectives .....</b>	<b>47</b>
<b>1.3.</b>	<b>Gaps in knowledge .....</b>	<b>48</b>
<b>1.4.</b>	<b>Research Objectives.....</b>	<b>49</b>
<b>1.5.</b>	<b>Thesis outline.....</b>	<b>50</b>
<b>1.6.</b>	<b>References.....</b>	<b>53</b>

## 1.1. Introduction

Dealing with antimicrobial resistance is a major global challenge. Overuse and misuse of antimicrobials has caused development of resistance in microorganisms. Treatment to cure diseases caused by these resistant microorganisms are becoming more difficult, leading to the need for longer treatment periods, additional medications and more expensive treatments [1, 2]. Moreover, the treatment options for such infections are limited [3]. Development of multidrug resistance in microorganisms makes the situation worse, and the world is in constant need for new antimicrobials to replace the old obsolete ones. Metal-based antimicrobials are unique as they have a combination of different modes of action and so it is difficult for microbes to develop resistance against them [4, 5]. They also have the flexibility to be incorporated into various matrices such as fabric, paper, medical devices, coatings, sensitive surfaces etc. for different applications [6]. Some metals have historical uses in medicine. Metals like gold, silver, zinc, arsenic and bismuth are being investigated by researchers across the world for antibacterial property in various forms, e.g. nanoparticles, inorganic compounds, organometallic complexes [5]. However, many cannot be used for most applications due to their toxicity [6]. On the other hand, for the ones that are already in commercial products, microorganisms may develop resistant genes towards them. A huge number of bacterial genes have already gained resistance against the most widely used metal-based antimicrobial agents like silver, copper etc. [7]. Therefore, it is evident that the commercial market will need new antimicrobials to replace them. Thus, it is necessary to discover new antimicrobial materials that are versatile, minimally toxic to humans, and are environmentally safe.

Bismuth is one of the metals that exhibits low antimicrobial resistance in bacterial communities with a low level of toxicity [8]. Bismuth salts are used for treatment of various gastrointestinal disorders as well as syphilis and malaria [9, 10]. Bismuth complexes have the advantages of being generally sparingly soluble in most solvents, showing antimicrobial activity at very low concentrations and exhibiting low toxicity against mammalian cells [11, 12]. Bismuth is exceptionally safe and the human body gets rid of it fairly rapidly. Poisoning is very rare and is only caused by excessive long-term exposure [9]. In this thesis, an organobismuth complex, phenyl *bis*-diphenylphosphinato bismuth (III) complex  $[\text{BiPh}(\text{OP}(=\text{O})\text{Ph}_2)_2]$ , is being investigated, which showed good antibacterial performance [13]. However, its activity in polymeric materials is not yet understood.

Bacteria attaches to a surface and grows there to form an extensive biofilm layer. This layer increases the spread of microbes to other surfaces, promoting transmission and contamination. Biofilm formation can be inhibited by preventing attachment of the microorganisms to the surface [14]. Antimicrobial materials can minimise the spread and growth of microorganisms, and thereby

reduce infections [3]. Antimicrobial materials have prospective applications in active packaging, healthcare and biomedical devices, as well as in water purification and textiles [15]. Researchers are constantly investigating new antimicrobial materials using polymers with inherent antimicrobial activity, or incorporating antimicrobial agents [6, 16, 17].

The challenge for using antimicrobial agents into such applications is the choice of a suitable carrier matrix. [18]. Cellulose being the most abundant natural biopolymer, along with being biodegradable and biocompatible, is a good choice for most applications [18]. Cellulose in its nanofibrillated form provides effective barrier properties, and allows the antimicrobial agents to be incorporated due to its porous structures [19]. There is little information in the literature about the antimicrobial activity of the bismuth complex of interest and hardly any on incorporation of such types of compounds into a polymer matrix. To address this, this dissertation aims to establish the effect of incorporating the organobismuth complex into a nanocellulose network and fabricate it into sheet and hydrogel form. The bismuth-functionalised nanocellulose material will potentially prevent the biofilm formation on the surfaces and inhibit their growth in the surrounding areas. The bismuth-based sheets can be used for food packaging, in hospitals and health care facilities and water purification. The antimicrobial hydrogels have prospective applications as coatings on medical devices, implants and in wound dressings. Herein, the application of the bismuth phosphinato loaded nanocellulose materials were studied for three different applications: active packaging materials, wound dressings and water filter.

To begin this thesis, a detailed literature review is presented in this chapter to demonstrate the importance and significance of this research. The literature review initially gives an overview of the selection of the antimicrobial agent and the nanocellulose polymeric matrix in this research, followed by the background and current status of the particular applications of interest in this thesis. This leads to the identification of the gaps in knowledge and research objectives. The thesis outline is given at the end of the chapter.

## **1.2. Literature Review**

### **1.2.1. Antimicrobial resistance and health issues**

Antimicrobial resistance (AMR) is a major global threat to public health. Inappropriate use of antibiotics has given rise to a global problem of antibiotic resistance in microorganisms. Selective pressure from antibiotics causes the weak microbes to die, thereby favouring the growth of the antibiotic resistant ones. Moreover, the antibiotic resistance gene is transferred to other organisms by phages, plasmids etc. and exchange of genes, thus spreading through the population of microorganisms. Once a bacterium has acquired a specific resistance, this ability is not lost easily. Moreover, they become more capable of gaining additional resistance thus becoming multi-drug resistant [1, 2]. Not only humans are using antibiotics, but they are also fed to livestock, fish and pets. Antibiotic resistant bacteria have entered human food chain and water bodies, and are widespread throughout the environment. The situation is worse in developing countries, where effluents from hospitals and drug manufacturing factories has been reported to have high levels of antibiotics and resistant microorganisms [20].

Therefore, the threat by resistant pathogenic microorganisms is increasing with time. This is a major issue for a number of reasons like medical treatment failure, rise in health care costs etc. [1]. Infection caused by resistant bacteria are more difficult to cure and treatment requires additional medications and longer periods of time. It has been predicted that there might be an additional 10 million deaths per year by 2050 [21]. The annual treatment cost of such infections in the US has been estimated to be over \$4-7 billion in 2015, and might rise up to 100 billion dollars in 2050 if strategies to deal with it are not established [2, 21]. So, it has become very important to explore ways to minimise the spread of these bacteria. Infection control is a basic requirement to deal with this, which includes careful use of antibiotics and hygiene improvement [3]. There is the crucial need to look for alternative ways to control the spread, transmission and growth of these resistant organisms. Antibacterial materials can help prevent the growth of bacteria on surfaces and prevent its spread to surrounding environment. Advances in nanotechnology can be utilised to assemble bactericidal agents into complex nano-structured matrix to make antimicrobial materials. The next section reviews the different antimicrobial agents to identify their limitations and the need for new antimicrobial agent.

### **1.2.2. Antimicrobial Agents**

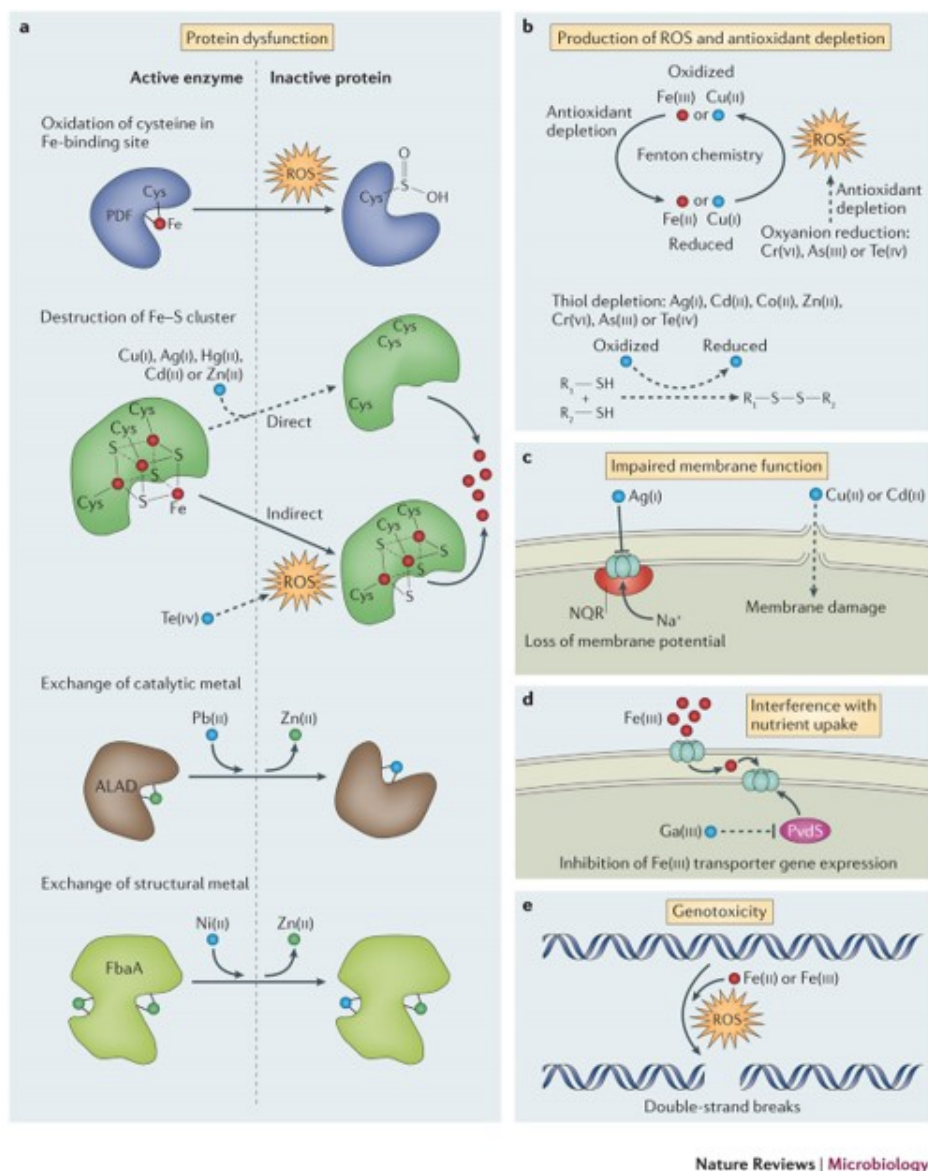
There are different classes of antibacterial products. Antibiotics are organic compounds, mainly synthetic, and are used as drugs to treat infections inside human body [17]. They can be taken in several ways- by oral intake, injection or as topical creams and lotions. There are six different classes of antibiotics- penicillins, cephalosporins, aminoglycosides, tetracyclines, macrolides and

fluoroquinolones [22]. Antiseptics and disinfectants are also antimicrobial compounds, mainly organic, that inhibit the growth and/or kill microorganisms on surfaces. Antiseptics are meant to be used for application on living tissue or skin whereas disinfectants are more generally used to sanitise non-living object surfaces [17]. Ethyl alcohol is the most generally used disinfectant used in storage of medical syringes etc and formaldehyde is mainly used for the cold sterilization of surgical equipment. Alcohols and formaldehyde are bacteriostatic (inhibits the growth of bacteria) at low concentrations, and are bactericidal (kills bacteria) at higher concentrations. Phenols are antibacterial as well, showing more activity at higher temperatures and lower pH. The most studied surface active organic antimicrobials are the quarternary ammonium compounds [23]. Dealing with multidrug resistance (MDR) pathogens is a challenge, and the antibacterial agents in the market is not enough to address this challenge. Thus, new antimicrobials with a new mechanism of action are in great demand [5]. Scientists are continuously developing new antimicrobials to respond to the rise in AMR. The ability of metals to interact with intracellular processes has recently driven attention to metal-based antimicrobial agents as an emerging opportunity to combat the AMR threat [6].

#### **1.2.2.1. Current metal-based antimicrobial agents**

Metal-based antimicrobials have the unique ability to interact with the intracellular proteins and enzymes and initiate various biochemical reactions, and thereby can act by a combination of several mechanisms of action. This makes metal-based antimicrobials a promising alternative to combat infections from multidrug resistant strains. Also, metal-based bactericidal agents can be incorporated into various materials like fabric, medical devices or coatings on sensitive surfaces. Only a few of the metallic element have been researched as antimicrobial agents. Among them, some present toxicity and environmental issues or are not suitable for medical applications [6]. So, it is worthwhile to explore and utilise the antimicrobial activity of the metals not yet investigated.

Novel antimicrobial compounds can be developed by utilizing the advances in inorganic and metal coordination chemistry, including both essential and non-essential metals. Synthesised metal complexes provide a different mechanism than pure organic drugs [10]. The mechanism of action of the metal-based antimicrobials depends on the physicochemical properties of the specific metal and its ligand [6]. Microbial growth can be inhibited by one or a combination of different mechanisms. The metal-based antimicrobials can lead to protein dysfunction, and inactivate enzymes or also cause cell membrane disruption. They can also facilitate the reactive oxygen species production and thus kill microbial cells by creating oxidative stress. Some metal antimicrobials interfere with nutrient uptake and some are genotoxic [4]. These different possible mechanisms are shown in Figure 1.



Nature Reviews | Microbiology

**Figure 1:** Different mechanisms of action of antimicrobial metals. Reproduced from [4], Copyright © 2013, with permission from Springer Nature.

Metals like silver, gold, arsenic, bismuth, antimony, copper, mercury, platinum, palladium, ruthenium, cobalt etc. and their compounds have been shown to exhibit antimicrobial properties. This includes inorganic compounds, organometallic complexes, metal organic frameworks, metal nanoparticles (NPs) etc. [10].

#### 1.2.2.1.1. Silver

Silver is the most widely known metal antimicrobial agent. Silver nanoparticles (Ag-NPs) can prevent microbial infections due their high potency against various pathogenic microbes. These nanoparticles can be used for applications like treatment of gastrointestinal infections, water purification systems, active packaging, cleaning and personal hygiene products as well as various

biomedical applications such as drug delivery [24-27]. In addition to being antibacterial, Ag-NPs are also reported to act against various fungal infections. Kim et al investigated the effect on fungal strains like *Trichophyton mentagrophytes* and *Candida albicans* fungi and reported the effective antifungal properties of Ag-NPs [28].

Ag-NPs have been used as composites with synthetic and natural polymers like cellulose, chitosan, gelatin, chitin collagen for various applications [24, 29, 30]. With all the antimicrobial activity exhibited by Ag-NPs, they are already being used in prostheses, catheters, vascular grafts and wound dressings. Ag-NP incorporated in artificial heart valves and stents, and hip and knee joint implantation and other implanted materials could be used to eliminate the dangers of microbial infections from implanted materials. Catheters with Ag-NPs can be useful in avoiding catheter associated infections during surgeries. Also, research has showed quicker healing using bandages containing silver compared to that without Ag-NPs [25]. Food packaging with materials coated with Ag-NPs prevents contamination of food by microbes by slow release of Ag<sup>+</sup> and prevents microbial growth on the surface of the packaging [31]. Nanosilver is currently being used in a lot of consumer products, including personal care, healthcare, textile, household and hygiene products. Examples of commercially available silver-based products include wound dressings, dietary supplements, medications, creams, silicone and latex catheters. Consequently, the extensive exposure of the microorganisms to silver is eventually resulting in the development of resistance [32].

In addition, like any other antimicrobial agent, there is the concern of its impact on human health and on the environment. These small sized particles can easily enter human and animal bodies through ingestion, breathing or even penetrating the skin, and thereby penetrate through organs to reach the cytoplasm. Therefore, the cytotoxicity of these particles is a very important parameter to be determined. Experiments by Ji *et al.* on Sprague-Dawley rats inhaling Ag-NPs suggested no abnormal behaviour or change in blood or weight of the rats over time for 28 days [33]. However, other studies report that prolonged exposure can affect the immune system and cause neural and pulmonary diseases. Some researchers have also suggested that these NPs might cause reproductive disorder and morphological deformation. [34, 35]. Soluble silver also causes harm to organs like the liver and kidneys [34, 36]. In spite of all the advantages, the issues related to cytotoxicity, environmental accumulation and the usage limitations point out the need to develop antimicrobial materials with less toxicity.

#### **1.2.2.1.2. Arsenic and Antimony**

Despite arsenic, antimony and bismuth being in the same group on the periodic table, their biological and medicinal properties are quite different. Organoarsenical complex have been

shown to have antimicrobial properties through the discovery of Salvarsan® (1910) and Neosalvarsan® (1912) [5]. Salvarsan® is an arsenic-based antimicrobial agent that is used for the treatment of syphilis and trypanosomiasis. Although it has already been replaced, this gives an indication of how metals are an important tool against microbes. Salvarsan® is metal complex with 3-amino-4-hydrophenyl ligands and works against microbes by redox reaction to release its active form [10]. Other arsenic based antimicrobial compounds like sulfarsphenamine and bismuth arsphenamine sulphonate (also known as Bismarsen®) are also used for the treatment of syphilis. In spite of the arsenic being a toxic metalloid, Bismarsen® had lower toxicity. However, in many parts of the world, including Europe and USA, all arsenic based drugs have been withdrawn due to their carcinogenic effects [37].

Antimony compounds are used for treatment of Leishmania, a parasitic infection [38]. Antimony has two oxidation states,  $Sb^{3+}$  and  $Sb^{5+}$ . Although the  $Sb^{5+}$  has low toxicity similar to bismuth,  $Sb^{5+}$  is more toxic. However, it was found to slowly accumulate in the human body and the resulting emerging development of resistance has raised concerns around using them [39].

#### **1.2.2.1.3. Others**

Oxides and nanoparticles of zinc, copper and iron have been reported to be good antibacterial agents. Azam *et al.* studied the antibacterial effect of these metal oxides against both Gram-positive and Gram-negative bacteria, and found that ZnO is the most effective against both, followed by CuO and  $Fe_2O_3$  [40]. The pathogenicity and drug susceptibility of a bacterial species is largely affected by the cell envelop structure, which determines the gram reaction of the bacteria. Both Gram-positive and Gram negative bacteria has a cell wall and cell membrane, while the Gram-negative bacteria has an additional outer membrane [41]. Jones *et al.* tested a number of metal oxide nanoparticles and showed that ZnO and  $Al_2O_3$  have significantly better antibacterial effect against *Staphylococcus aureus* (Gram-positive), whereas MgO,  $TiO_2$ , CuO and  $CeO_2$  showed no activity at all.  $Al_2O_3$  is toxic to human cells, and is not a good option to work with. The study also showed that the nanoparticle form of zinc oxide shows more bactericidal activity than larger particles. Although ZnO was more effective against *S. aureus*, CaO and MgO works better against *E. coli* (Gram-negative) [42]. A recent study showed that 2.5% loaded ZnO microfibrillated cellulose sheets exhibited effective antibacterial properties for food packaging applications [43]. However, Zn and its oxides are toxic to human cells at high concentrations [44].

#### **1.2.2.2. Necessity of new antimicrobial agents**

It is hard to find a compound with good pharmaceutical attributes which also has low toxicity to mammalian cells, and hence there is a shortage of new antibiotics. Bacteria develops resistance

very quickly for a new class of antibiotics, with its effectiveness remaining for an average of 5 years. Therefore, the need for alternative strategies to deal with the AMR problem is an urgent issue [20]. Bacteria develops some mechanisms to survive the effects of antibacterial agents. The bacterial resistance develops as the microorganisms develops the ability to protect themselves by either altering its active binding site or by production of molecules to interfere with the binding. Some bacteria protect themselves by altering the cell wall to reduce the permeability of the agent into the cell or by transporting it out by efflux pumps [45]. Metal-based antimicrobials, on the other hand, work by a different mode of action which makes it hard for bacteria to develop resistance [5]. Such metal-based antimicrobials are being used in various commercial products, with silver being the most widely used. The widespread use of the silver-based materials in applications from disinfectants to high-end medical products is facilitating the development of resistance in bacteria [32]. Such is the scenario for many other metal-based antimicrobials [7].

The microorganisms learn to adapt with the stress created by these antimicrobials in a number of different ways and thereby develop resistance, as described in Figure 2. The microorganisms can evolve mechanisms to regulate the uptake of the metal as well as to transport toxic metals out of the cell. The cells also develop mechanisms of trapping the metal ions, making them inactive by extracellular and intracellular sequestration. Bacterial cells can also develop repair mechanisms to reverse the effect of the metal ions on the proteins or follow an alternative metabolic pathway to avoid the effect of the toxic metal [4].

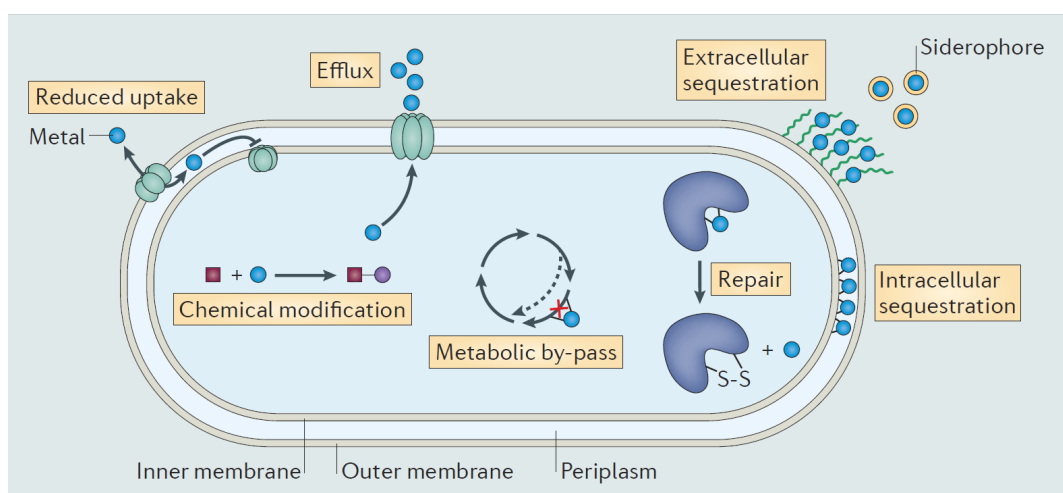


**Figure 2:** Bacterial mechanism of adapting and dealing with the toxic effects of antimicrobial metals. Reproduced from [4], Copyright © 2013, with permission from Springer Nature.

Pal *et al.* compiled data on bacterial genes conferring resistance against antibiotics and metals from more than 400 published articles. The study included 20 metals, with the highest number of resistant genes being against copper (60 genes), zinc (58 genes) and nickel (51 genes), as

presented in Figure 3 [7]. Another study showed that 75.3% of the livestock MRSA isolates are resistant to at least one metal among arsenic, cadmium, copper and zinc [46]. A large number of bacterial strains isolated from Cu-polluted agricultural soil showed copper resistant genes along with resistance to other heavy metals [47]. Another study has shown that heavy metal pollution has led to copper resistant genes in bacteria isolates of *Pseudomonas*, *Lysinibacillus* and *E.coli* from a river polluted from industrial activities [48].

Silver based antibacterial agents are widely accepted as biocides in various healthcare and hygiene products. However, the efficacy of these products towards the Ag resistant mutant bacteria remains a concerns [49]. Studies have suggested that silver resistance is particularly concerning for Gram-negative bacteria with *E. coli* evolving resistant genes in just 6 days of exposure [50]. A study has shown that *Enterobacter cloacae* isolated from burn patients are resistant to silver sulfadiazine, one of the common biocides in burn ointments [51]. The presence of silver resistance in bacterial genes is not a recent discovery. In fact, a study in 1989 showed *E.coli* isolates from burn patients contains plasmids responsible for silver resistance and showed that they are able to grow and replicate in the presence of high concentration of silver nitrate [52]. Another study in 1994 showed an environmental isolate of *A. baumannii* was also resistant to a high concentration of silver nitrate [53]. Although there are a lot of studies that report silver resistance, the mechanisms of resistance development are not fully understood. The most likely mechanisms could be genetic mutation and transfer of plasmid to be able to either reduce the uptake of silver in bacterial cells or help with efflux [54]. Silver resistant *E.coli* strains were found to have active Ag<sup>+</sup> efflux capability [55]. A number of studies have been done to understand the genetic mutation and molecular biology of bacterial silver resistance [56, 57]. A study tested two commercial silver-based wound dressings against silver-resistant *Enterobacter cloacae* wound isolates and showed that both are not effective against one of the three strains tested. It is quite concerning because that particular strain demonstrated strong resistance to the two dressings that have different concentrations and release kinetics of silver [58].

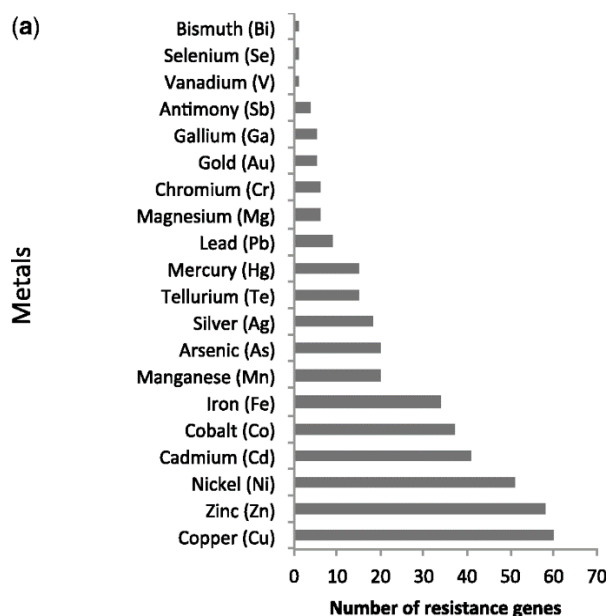


**Figure 3:** Experimentally confirmed resistance genes for metals Reproduced from [7], Copyright © 2013, with permission from Oxford University Press.

Therefore, there is a chance of the current metal-based antimicrobials being ineffective in the near future. The current metal-based antimicrobials will no longer be able to deal with the threat posed by increasing antibiotic resistance [32]. Hence, the study of a new antimicrobial agent is of particular interest in this thesis. Herein, a new metal-based antibacterial agent is being studied with bismuth as the metal centre. The next section gives an overview of bismuth-based antimicrobial agents and the motivation to use the *bis*-phosphinato bismuth complex in this thesis.

### 1.2.3. Bismuth and its compounds

#### 1.2.3.1. General Chemistry

Bismuth is the 83<sup>rd</sup> element in the periodic table and is ranked as 69<sup>th</sup> in abundance in nature, found present in minerals. Common ores of the metals are bismite ( $\alpha$ - $\text{Bi}_2\text{O}_3$ ), bismuthinite ( $\text{Bi}_2\text{S}_3$ ) and bismutite ( $(\text{BiO})_2\text{CO}_3$ ) [59]. It is a silver-white metal with a lustrous finish. Bismuth has a ground state electronic configuration of  $[\text{Xe}] 4f^{14}5d^{10}6s^26p^3$ . It has an oxidation state of +3 for majority of the compounds using the three 6p electrons for bonding, but can also form pentavalent compounds. Bismuth can have coordination numbers of 2,3,4,5 and 6 in organometallic compounds. Although it belongs to the same group, the chemical behaviour of bismuth is quite different from phosphorus, antimony or arsenic [9]. Moreover, it is unique due to its low-toxicity compared to its neighbouring metals [8].

### 1.2.3.2. Antimicrobial Activity of Bismuth compounds

Bismuth has a long history of being used for treating intestinal disorders. Inorganic bismuth salts like carbonates, phosphates, silicates, subcarbonates and subnitrates as well as phenolic salts like salicylates are used for various gastrointestinal treatments. Bismuth complexes generally have very low solubility in a range of common solvents. Bismuth compounds like Pepto-Bismol (BSS or bismuth subsalicylate) and De-Nol (CBS or colloidal bismuth subcitrate) and its derivatives are being used for gastrointestinal disorders [11]. Bismuth salicylate has been used for treatment of diarrhoea and other gastrointestinal illnesses, as well as syphilis and rheumatoid arthritis. Bismuth subcitrate is used for the treatment of ulcers, as it is effective against the bacteria *Helicobacter Pylori*. Also, previously used antisyphilitic drugs using bismuth are disodium pentaiodobismuthate tetrahydrate ( $\text{Na}_2\text{BiI}_5 \cdot 4\text{H}_2\text{O}$ ) and cacodylate ( $\text{Bi}[\text{Me}_2\text{As}(=\text{O})\text{O}]_3 \cdot 8\text{H}_2\text{O}$ ) [9, 10]. Aliphatic carboxylate salts of bismuth have also been in use for treatment of tonsillitis, syphilis and appendicitis. Examples of such salts include butylthiolaurate, camphorate, citrate, dipropylacetate, ethylcamphorate, potassio(sodio)tartarate and succinate. Moreover, colloidal tripotassium dicitratobismuthate and micronized bismuth subnitrate helps with the treatment of intestinal ulcers [9]. Some bismuth compounds have been reported to show antimicrobial activity at very low concentrations along with low toxicity. However, the demand for this heavy metal and its compounds was reduced with the emergence of antibiotics [11].

Bismuth thiols have also been suggested to inhibit slime production of 16 strains of *S. epidermidis* at sub-inhibitory concentrations, and thus can be considered as a promising tool to prevent colonization of the bacteria on surfaces treated with them. On the contrary,  $\text{AgNO}_3$  showed no slime inhibition at sub-inhibitory concentration. So, bismuth thiols have been reported to be bacteriostatic and bactericidal, as well as show unique properties of biofilm inhibition [60]. Thiolato bismuth (III) complexes have been suggested to exhibit antibacterial properties, and five mixed thiolatobismuth (III) complexes have been studied by Luqman *et al.* All five complexes were reported to be non-toxic to mammalian COS-7 cell line at a maximum tolerance limit of 20  $\mu\text{g}/\text{mL}$ . Their study suggested that heteroleptic bismuth (III) complexes (at least one different ligand) are more effective against bacteria relative to its homoleptic (all identical ligands) analogue. Their tested compounds also showed less antibacterial activity towards Gram-negative bacteria like *E.coli* [12]. This fact that bismuth (III) compounds are more effective towards inhibition of Gram-positive bacteria has been reported by other researchers too [8]. This phenomena could be explained by the fact that the double membrane in Gram-negative bacteria forms a barrier against penetration of antimicrobial agents [61].

In another study, cyclic organobismuth compounds were investigated, and results suggested that eight membered rings are more active against bacteria compared to six membered ring compounds.

Thus, cyclic organobismuth compounds and bismuth thiol compounds have been recognised by previous research as effective antibacterial agents, with the potential of various medical applications [8]. Hydrogel coated polyurethane rods, treated with bismuth-2-3-dimercaptopropanol (BisBAL) inhibited growth of *S. epidermidis* for more than a month, and can thus be used for indwelling medical devices [60]. In addition to being antimicrobial, bismuth also has anti-cancer and anti-leishmanial attributes.

### 1.2.3.3. Mechanism of action

Various researchers have studied different forms of bismuth based compounds and proposed possible pathways for their mechanisms of action. It is proposed that bismuth works by binding to proteins with thiol containing metal binding sites [62]. Possible binding sites are the iron, zinc and nickel sites in enzymes and proteins [38]. The Bi (III) was shown to bind with the ferric uptake regulator protein in *Helicobacter pylori* bacteria, resulting it to oligomerise [63]. This protein is involved in DNA transcription and is a cause of the bacterial pathogenesis [64]. A recent study has shown that the bismuth (III) compounds works by inhibiting the  $\beta$ -lactamase enzyme, which is normally resistant towards  $\beta$ -lactam antibiotics [65, 66]. The effectiveness of these compounds is largely dependent on the type of ligand and the structure of the complex [12, 67].

### 1.2.3.4. Toxicity concerns of bismuth compounds

Unlike other heavy metals, bismuth is exceptionally safe due to its non-toxic and non-carcinogenic nature [8]. Although it is a heavy metal in the nitrogen family, where toxicity is supposed to increase down the group, bismuth is unique for its low toxicity. Similar compounds of arsenic and antimony are very toxic compared to their bismuth counterpart. For bismuth telluride and bismuth/antimony metal compounds, the toxicity is mainly derived from the tellurium or antimony. However, large doses of bismuth during medical therapy might cause accidental poisoning. Some water-soluble salts ingested orally might cause mild kidney damage but most are excreted by the urinary tract. Bismuth and its oxide are barely soluble in plasma and quickly enters the urinary system. On the other hand, water-insoluble salts are not absorbed and are excreted with faeces. Thus, poisoning is rare. The body generally gets rid of all bismuth within 10 to 60 days. However, long-term oral intake of bismuth should not exceed dosage of 1 g/day, which might cause mental disorders. Long-term exposure to high levels of bismuth results in hypersalivation, stomatitis and a darkish layer around gum. No bismuth compounds have been found to be carcinogenic, teratogenic or mutagenic [9].

### 1.2.3.5. Phenyl *bis*-diphenyl phosphinato bismuth (III) complex

In this thesis, the antimicrobial agent of interest is an organobismuth complex- phenyl *bis*-diphenyl phosphinato bismuth (III) complex  $[\text{BiPh}(\text{OP}(=\text{O})\text{Ph}_2)_2]$  as shown in Figure 4.

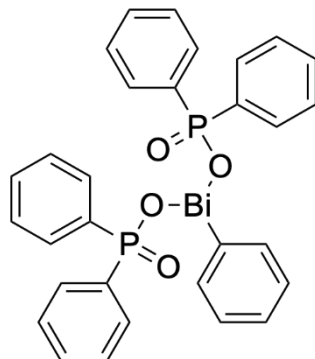


**Figure 4:** Chemical structure of the *bis*-phosphinato bismuth complex (Drawn from the general structure of the class of phosphinato bismuth (III) complexes,  $[\text{BiPh}(\text{OP}(=\text{O})\text{R}^1\text{R}^2)_2]$ , from Werrett *et al.* [67])

The complex is formed by heating triphenyl bismuth ( $\text{BiPh}_3$ ) and diphenyl phosphinic acid in ethanol at reflux [13]. The phosphinic acid deprotonates to substitute two of the phenyl groups in  $\text{BiPh}_3$ , eliminating benzene and forming the heteroleptic complex. The chemical reaction is shown in Figure 5.

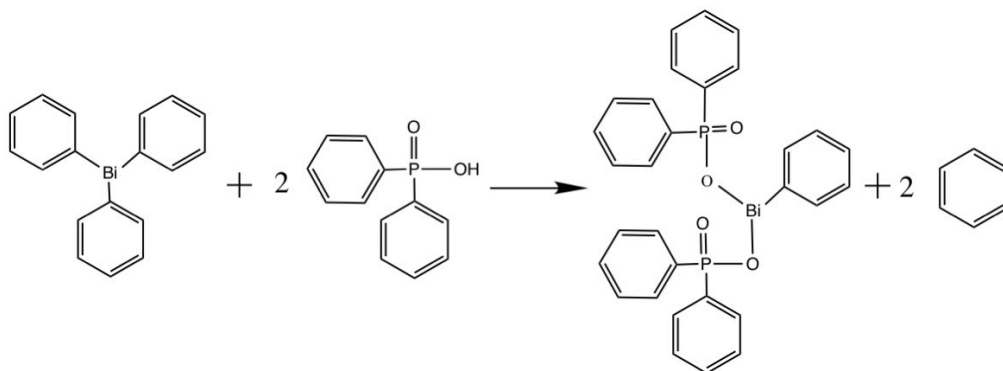


**Figure 5:** Chemical reaction for the synthesis of the *bis*-phosphinato bismuth complex (Drawn from the general synthesis scheme of the class of phosphinato bismuth (III) complexes,  $[\text{BiPh}(\text{OP}(=\text{O})\text{R}^1\text{R}^2)_2]$ , from Werrett *et al.* [67])

The complex exists as a white powder and has good thermal stability. The decomposition and melting temperatures are above  $300^\circ\text{C}$ , which means that they are suitable to be used in high-melt polymeric materials [67]. This particular complex has been recently shown to have antibacterial activity [13]. The antibacterial activity of the complex determined by the zone of inhibition is

shown in Figure 6. The zone of inhibition is used to measure the ability of a compound to inhibit bacterial growth. It is the clear circular area on the agar plate where bacterial growth did not occur. Here, the sample labelled 1 (on the right plate) is the *bis*-phosphinato bismuth complex showing antibacterial activity. The precursors  $\text{BiPh}_3$  (on the right plate) and the diphenyl phosphinic acid (labelled as (i) on the left plate) do not show any zones of inhibition.

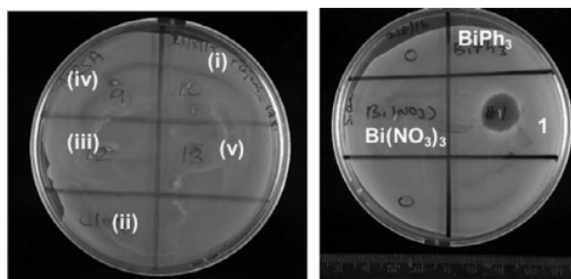


**Figure 6:** Antibacterial activity of the complex determined by the zone of inhibition method against MRSA. Here, the sample labelled “1” is the *bis*-phosphinato complex. Reproduced from [67]. Copyright © 2018, with permission from John Wiley and Sons.

A recent study has shown that homoleptic analogue of this complex (tris phosphinato) does not have any antibacterial activity [68]. The *bis*-phosphinato complexes also have very low solubility in water and most solvents (ethanol, dichloromethane, tetrahydrofuran, toluene, DMSO). This complex needs 16.3kg of water to dissolve 1 gram, whereas the homoleptic analogue required 9.4 kg. It was suggested that the low solubility was due to its possible existence in polymeric forms [67]. Although the very low solubility makes it difficult to analyse its crystal structure, similar mono-phosphinato bismuth complex have been studied by single-crystal X-ray diffraction and has been reported to exist as one-dimensional co-ordination polymers [68]. Thus, it is expected to have a slow release of the complex and thereby reduced release to the environment. This property makes it a good candidate to be used as an additive in antimicrobial materials. Preliminary mammalian cytotoxicity results suggested this complex shows very low level of toxicity at 1 mg/mL and no toxicity at 0.5 mg/mL to eukaryotic cells (COS-7 cell line) when treated with these solid powders [67]. The promising antibacterial activity, low solubility and low mammalian toxicity indicates this complex to be a good candidate to be used as an additive in antimicrobial materials. However, the behaviour of the complex in materials is not understood. There is a significant gap in understanding the antibacterial efficacy and influence of the complex on material properties of any material loaded with the complex. This motivated us to understand its behaviour in polymeric matrices to develop new antimicrobial materials.

#### 1.2.4. Translation to antimicrobial materials-

Microbial growth on surfaces and cross-contamination from there spreads infection. This has become a major concern to human health because of the difficulty to treat them due to AMR. Antimicrobial materials can overcome this issue. Such materials can inhibit the microbial growth and surface contamination by killing or inactivating the microorganisms. Due to the rise of AMR to the current antimicrobial materials there is a need to study novel compounds inside materials. For development of antimicrobial materials, the antimicrobial agent must be physically or chemically entrapped in a suitable carrier matrix. The challenges for application of antimicrobials agents are firstly the sustained release of the agent over time and its ability to retain its efficacy over the period of usage. In addition, there is a maximum loading of the agent that is allowable to ensure non-cytotoxicity [69]. Therefore, a trade-off must be made between the minimum loading for activity and the maximum loading to ensure non-cytotoxicity. However, the required loading of the *bis*-phosphinato complex to impart antibacterial properties to a material is not known. The leachability of the complex from its composite material to the surrounding environment and its effect on its efficacy or cytotoxicity is also not fully understood.

Another technical challenge for translation of the antimicrobial compound to material lies on the choice for suitable matrix to use for supporting them. Polymers have been widely used as the carrier matrix to incorporate the biocides to improve their stability and activity due to their macromolecular properties, such as insolubility in water and most solvents [15]. The compatibility of the polymer properties for particular applications, e.g. biocompatibility of antimicrobial polymers for biomedical applications is also an important factor [69]. Non-leachable antimicrobial polymers with inherent antimicrobial properties provide long term efficacy as well as reduce the risk of resistance development. Although it reduces the environmental contamination and cytotoxicity, the limited leaching ability might reduce the accessibility of the antimicrobial agents to the microbes [70].

The most studied matrices for antimicrobial materials have been petroleum based polymers, e.g. polyethylene, polypropylene, polystyrene, polyethylene terephthalate, ethylene vinyl alcohol copolymer, acrylamide etc. [15, 30, 71, 72]. Environmental accumulation of these, and the resulting impacts from plastic pollution, are driving interest in biodegradable polymers like polylactic acid (PLA), polyglycolic acid (PGA), and more importantly the renewable natural biopolymers like cellulose, starch, chitosan, alginate, collagen etc. [15]. Among all available polymers, hydrophilic polymers are favoured for antimicrobial surfaces, due to their increased wettability and lubricity. This reduces the undesired bacterial adhesion and colonization on these surfaces [69]. Nanocellulose is one such hydrophilic biopolymer. Nanocellulose is an effective physical barrier layer, along with providing a porous structure for antimicrobial agents to be

attached both physically and chemically. Moreover, its biocompatibility makes it suitable for various medical uses [19]. The following section gives a detailed review of nanocellulose, the matrix used in this thesis.

## 1.2.5. Nanocellulose

### 1.2.5.1. General aspects of nanocellulose

Cellulose is one of the most abundant and important natural biopolymers, occurring in all plant-based materials [18, 73]. Cellulose is biodegradable and renewable, along with being inexpensive and non-toxic [74, 75]. Isolated cellulosic materials, with at least one dimension in the nanometre range can be termed as nanocellulose. Nanocellulose is unique due to its hydrophilicity, biocompatibility, easy chemical functionalization, large surface area, ability to form semi-crystalline fibre morphologies combined with the high surface area of a nanostructured material [18, 76]. The hierarchical breakdown of a cellulose source (tree) to its the constituent cellulose chain is shown in Figure 7.

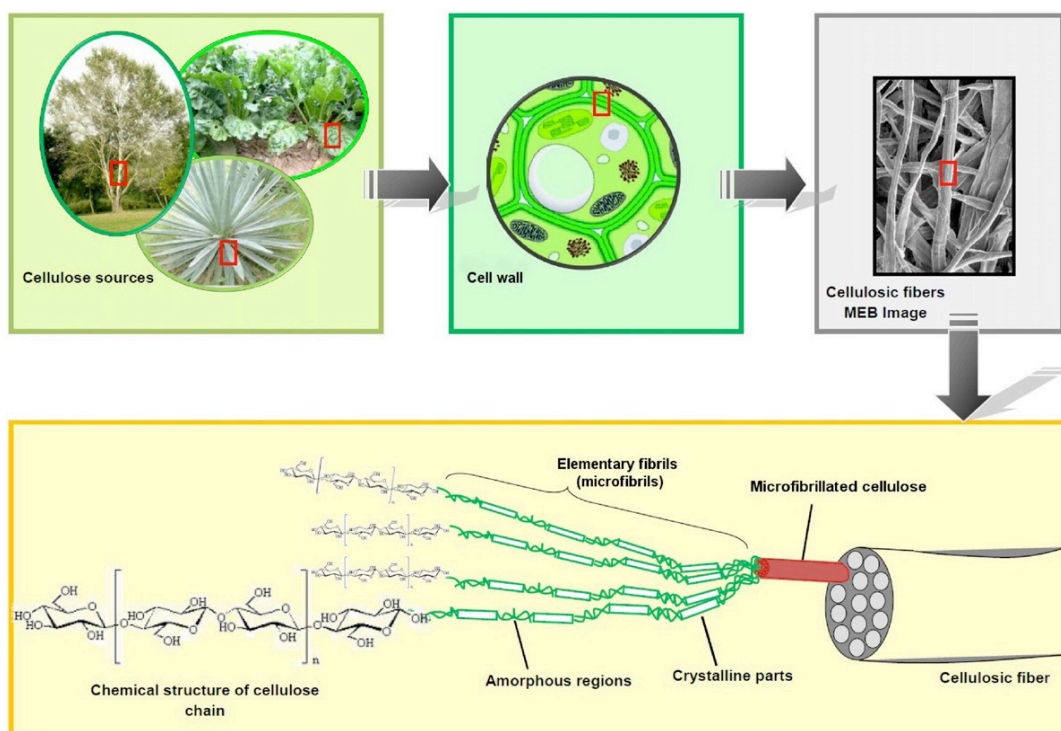


**Figure 7:** Details of cellulose fibre structure originating from cellulosic source. Reproduced from [77], Copyright © 2012, with permission from Elsevier.

Nanocellulose can be categorised into three major divisions:

- Cellulose nanofibres (CNF)/ Nanofibrillated cellulose (NFC)/ microfibrillated cellulose (MFC)
- Cellulose nanocrystals (CNC)/ Nanocrystalline cellulose (NCC)
- Bacterial nanocellulose (BNC)

Cellulose nanofibers are composed of nanosized cellulose fibrils having a high aspect ratio (i.e. length to diameter ratio), with diameters of 5-60 nm and several micrometres long. This class is usually obtained by mechanical high shear fibrillation. Before mechanical treatment, the fibres are sometimes pre-treated chemically or enzymatically [18, 78]. Nanocellulose fibres has been denoted interchangeably in the literature by various terms, like nanofibrils, microfibrils, nanofibrillated cellulose, microfibrillated cellulose, nanocellulose and nanofibers. In most literature, MFC refers to nanocellulose prepared by mechanical treatment and NFC refers to even thinner fibres produced by a chemical pre-treatment before mechanical fibrillation [73].

Nanocrystalline cellulose is made up of crystalline rigid nanoparticles formed by acid hydrolysis of the CNFs. These are shorter than nanofibrils, with a length of 100-250 nm for plant cellulose and diameter of 5-70 nm [18].

Bacterial nanocellulose, also known as microbial cellulose, is produced by aerobic bacteria and is a highly pure form of cellulose. This type of nanocellulose is more crystalline and has higher strength than NFC or MFC and has a fibre diameter of around 20-100 nm. However, the large scale industrial production of BNC is expensive and not fully established. Different bacterial strains and production parameters needs different processing techniques after production [18].

In this thesis, only nanofibrillated cellulose(NFC)/ microfibrillated cellulose(MFC) has been used and any referral to nanocellulose means the high-aspect ratio microfibrils. Microfibrillated cellulose has its major application as a reinforcing filler in composites of paper and polymers, smooth coating material on paper surfaces, nanofiller for glues and resins, and additives in paints, cosmetics [78]. These have great potential as barrier material, due to its film having nanoscale pores [77]. The major issue associated with MFC commercialization is the huge energy required (around 25000 kWh per ton) for MFC production [18]. However, a lot of research is being done to reduce the production cost by carrying out various pre-treatments, e.g. physical treatment, chemical treatment, and enzymatic degradation to make it more energy efficient.

#### **1.2.5.2. Production of nanocellulose**

Nanocellulose are obtained by high shear disintegration of the cellulose pulp, with or without a pre-treatment, to fibrillate the cellulose. Pre-treatment methods include a biological or chemical

step to reduce the energy consumption in the mechanical disintegration. Chemical pre-treatment includes TEMPO-oxidation, carboxymethylation etc. and mechanical treatment includes refining, homogenization, microfluidization and grinding [18]. The mechanically treated fibres tend to form thicker bundles compared to the chemically pre-treated ones, which are relatively shorter and thinner. Thus, the pre-treated nanocellulose fibres have a higher aspect ratio [77]. The degree of crystallinity of the nanocellulose is not affected by the pre-treatment, but decreases with each pass in the high shear homogeniser. However, pre-treated fibres tend to be less crystalline after the mechanical treatment. If the aqueous dispersions of the nanofibers have a dense network and have small enough gaps between them to avoid light scattering, optically transparent films can be made from them. These suspensions are pseudoplastic, which increases in viscosity under shear strain [78]. Creating charged groups on the cellulose fibres helps with the separation of the fibres. Low concentrations of such nanocellulose suspensions containing charged groups can form gels [18]. The different nanocellulose production techniques are shown in Figure 8. Production of nanocellulose was not the main aim of this thesis, and hence either purchased commercial MFC or already established NFC production methods were used herein.

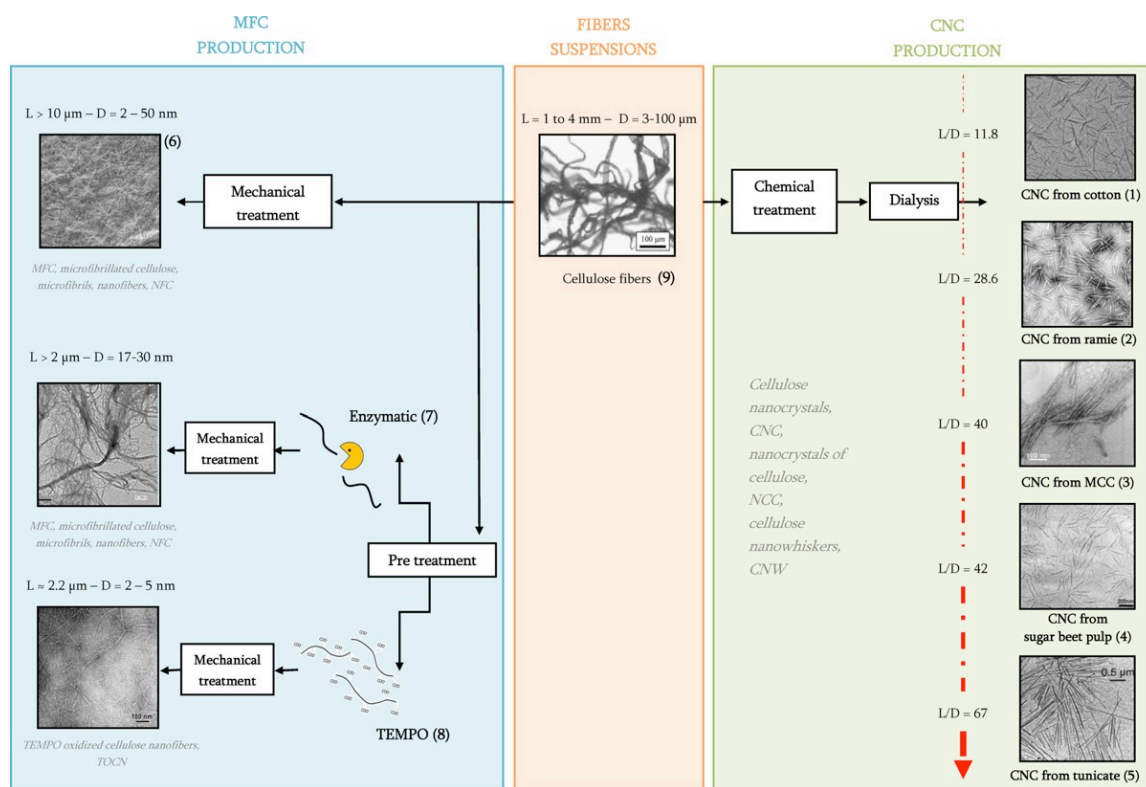


**Figure 8:** Different pathways of MFC and CNC production from plant cellulose Reproduced from [77], Copyright © 2012, with permission from Elsevier.

### **1.2.5.3. Nanocellulose films**

#### **1.2.5.3.1. Preparation methods**

Nanocellulose suspensions can be converted to sheets and films by various methods like vacuum filtration [79], casting [80] and spraying [81-83]. Casting is the most time-consuming process, followed by vacuum filtration and spraying [84]. Spraying can be done on impermeable surfaces to produce standalone sheets [84, 85] or coated on substrate/base paper [86, 87] and is a great method for large scale production of nanocellulose films [88]. This can be done by spraying the suspension over a substrate moving on a conveyor belt. Although this process has the advantage of quick preparation allowing large scale production, the disadvantages include the longer time required to dry the sheet and inhomogeneity in the sheets/films [85, 88]. A large number of factors affect the properties of the sheet including the drying method [89, 90], the substrate roughness [91], the spraying conditions (e.g. conveyor speed) and suspension concentration [88]. In the vacuum filtration method, the nanocellulose suspension is processed through a filter, where the fibres settle to form a wet film. The film is then pressed between blotters and dried. The limiting factor here is the drainage time, which varies depending on the filter medium and fibre properties and can take up to 4 hours [84]. Both these methods have been used in this thesis to prepare the Bi-MFC composite films.

#### **1.2.5.3.2. Properties and applications**

The unique properties of the nanocellulose films draws attention of the researchers to utilise them in practical applications as a renewable, sustainable and environmental-friendly resource. Firstly, the mechanical strength of nanocellulose films is quite high compared to other paper-based materials [92]. The high fibrillation of the cellulose fibres provides more surface for the hydrogen bonding to strengthen the fibrous network in the film and hence the mechanical properties depends on the source of cellulose and the extent of fibrillation. The mechanical properties of nanocellulose films are shown in Table 1. Here, the tensile strength is the maximum stress that the film can withstand and does not break. The tensile strength normalised by the film density gives the tensile index. They both signify how resistant a material is to breakage under tension. A calculated value of the tensile index has been provided in the table where the sheet density data was available for better comparison. The Young modulus is a measure of the elasticity and denotes the stress required per unit strain (proportional deformation). The elongation at break is the maximum stretch with respect to the original length before the film breaks and is a measure of the ductility of the material [93]. The tensile strength of copy paper composed of cellulose macrofibres is only 25 MPa [94]. The tensile strength and Young Modulus of the nanocellulose films are quite high, even higher than some of the petroleum derived plastics (Table 2). However, most of the plastic based polymers have exceptionally high strains at break.

**Table 1:** Mechanical properties of pure nanocellulose films produced by different techniques

NC preparation	Film preparation	Tensile Strength at break (MPa)	Elongation at break (%)	Young's Modulus (GPa)	Tensile Index (Nm/g)	Reference
TEMPO oxidisation followed by sonication	Casting	53.4±3.8	2.6±0.6	3.4±0.6	43.4 (calculated)	[95]
TEMPO oxidisation followed by homogenisation	Suction filtration	233±44 (SW) 222±11 (HW)	7.6±0.02 (SW) 7.0±2.5 (HW)	6.9±1.4 (SW) 6.2±1.6 (HW)	160 (SW) (Calculated) 153 (HW) (Calculated)	[96]
Homogenisation	Vacuum filtration	--	--	--	116	[97]
Commercial MFC	Spraying	--	--	2-8	40-80	[88]
Enzymatic pre-treatment followed by homogenisation	Spraying	38±6	0.8±0.3	16±1	30 (Calculated)	[83]

**Table 2:** Mechanical properties of different plastic materials

Type of polymer	Tensile Strength at break (MPa)	Elongation at break (%)	Young's Modulus (GPa)	Reference
Polylactic acid (PLA)	59	7	1.3	[98]
Polyethylene terephthalate (PET)	79	335	2.8	[99, 100]
Low density polyethylene (LDPE)	~10	512	~0.3	[101, 102]
High density polyethylene (HDPE)	~26	714	~0.5	[101, 103]
Polypropylene (PP)	~39	131	~1	[101]

Secondly, the barrier properties of nanocellulose films are a great advantage providing opportunities for packaging applications as alternatives to petroleum based plastic materials. This includes both oxygen and water vapor barrier properties. The oxygen permeability of nanocellulose films is quite low[104]. The water vapor permeability depends on the various parameters like cellulose source, method of nanocellulose production, and film preparation technique [80, 105, 106]

The great mechanical and barrier properties of the MFC films/sheets make them a promising material for applications like packaging materials, printed electronics substrates and sensors [73, 77, 80]. Their high mechanical strength and biodegradability also make them suitable as reinforcing agents in paper, packaging materials and nanocomposites [18]. Various researchers have developed nanocellulose-based antimicrobial packaging material using different metal nanoparticles [43, 107, 108]. The microporous structure of the nanocellulose films also makes them suitable for microfiltration and ultrafiltration applications [109, 110]. This thesis studies the applications of nanocellulose films as active packaging and water filters.

#### 1.2.5.4. Nanocellulose hydrogel

Physical entanglement and chemical crosslinking of polymers capable of absorbing large quantities of water results in the formation of a three-dimensional network known as hydrogel. This network can be achieved from natural, synthetic or hybrid polymers, with water filled in voids or bonded with hydrophilic groups [111, 112]. Their structure is largely dependent on trapped moisture, and removal of water results in hydrogen bonding reformation and significant volume reduction [113]. There are a wide variety of design options for the preparation of

hydrogels of different structures and properties [112]. Nanocellulose hydrogels are formed by charged cellulose polymer which are insoluble in water. This makes them quite different from most other hydrogels which are water soluble [114].

#### **1.2.5.4.1. Preparation methods**

Nanocellulose hydrogels are prepared by entanglement of nanocellulose fibres suspended in water as a colloidal suspension [114]. This can be achieved in two ways- physical or chemical crosslinking [115]. Physical hydrogels are formed by physical and reversible interactions like hydrogen bonding, ionic interaction, hydrophobic interaction, Vander Waals force or even simple chain entanglement [115]. Physical crosslinking can be achieved by functionalising the nanocellulose fibres. Chemically crosslinked hydrogels have crosslinker chemicals bonded to the polymer chains by irreversible covalent bond. [115]. Examples of irreversible chemical crosslinkers include poly(N-isopropylacrylamide) (PNIPAAm) [116], hexamethylenediamine (HMDA), ethylenediamine (EDA) [117], epichlorohydrin [118] and many others. For biomedical applications, physically cross-linked hydrogels are preferred over chemically crosslinked ones since it avoids the use of chemicals/crosslinking agents or organic solvents and eliminates the risks and toxicity associated with those [119]. So, nanocellulose hydrogels physically cross-linked by hydrogen bonding was chosen herein. This was produced by TEMPO-mediated oxidation of the cellulose followed by mechanical fibrillation.

TEMPO (2,2,6,6-tetramethylpiperidine-1-oxyl) is a radical that catalyses the oxidation of the primary alcohol group on the cellulose chains to carboxylic acid using a hypochlorite oxidant. The reaction pathway is shown in Figure 9. The sodium dissociates to create negatively charged carboxylic groups on the cellulose chains which causes the fibres to repel each other. The mechanical fibrillation separates the nanofibres, eventually forming the hydrogel [120, 121].

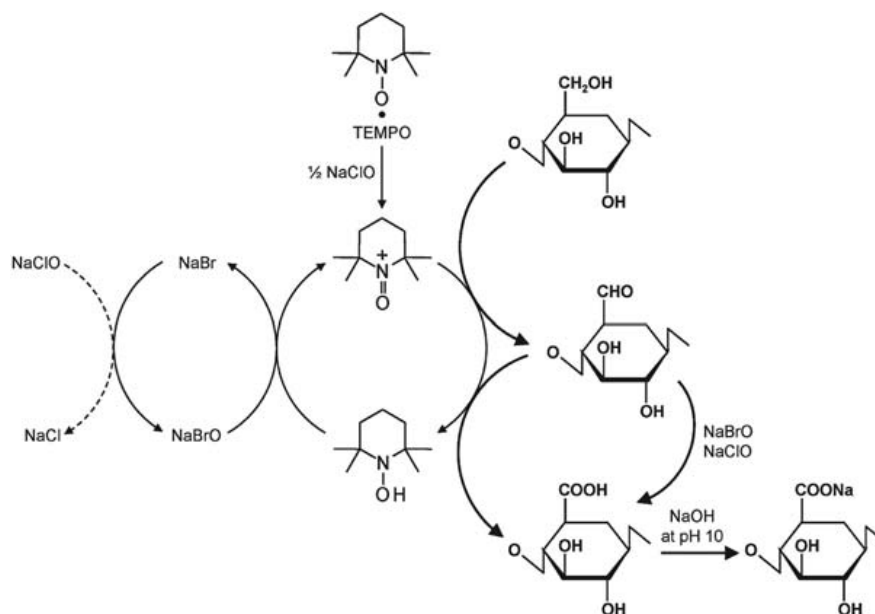


**Figure 9:** Oxidation of primary alcohol of cellulose to carboxylate using TEMPO/NaBr/NaClO. Reproduced from [122], Copyright © 2011, with permission from Royal Society of Chemistry

#### 1.2.5.4.2. Properties and applications

Nanocellulose hydrogels, like all other hydrogels, are highly hydrated containing large amounts of water [123]. Being highly hydrated, hydrogel structures possess excellent biocompatibility and have a vast scope in biomedical and pharmaceutical applications [111]. Hydrogels are used for soft contact lenses, as drug and protein carriers, medical implants in soft tissue, as well as for tissue engineering [112]. Hydrogels of nanocellulose are biodegradable. Moreover these hydrogels are stable and their mechanical properties are tunable by varying the solids content and crosslinking method [121]. Nanocellulose hydrogels exhibit swelling behaviour [124, 125] and can be used to prepare superabsorbent materials (i.e. materials that can absorb and retain significantly large amounts of liquid relative to their own weight) [126]. This property makes them a promising choice for wound dressing that can absorb wound exudates. The rheological properties of the hydrogel must also be tightly controlled for biomedical applications [127]. The structural and functional properties of the hydrogels can be altered by chemical modification of the cellulose chain, by immobilising/grafting biomolecules (like proteins and enzymes) or by formation of functional groups [114]. The cellulose content in the hydrogel determines the porosity of the structure and hence the diffusion of biomolecules and any additives physically entrapped within the network [128]. Drugs and other additives can be added to the hydrogel matrix to impart desired properties like antimicrobial properties. Antimicrobial hydrogels can be used in various medical applications including wound dressings, medical implant coating etc. Such hydrogels can be prepared by immobilization or dispersion of antimicrobial agents in them

or by making them with polymers having inherent antimicrobial properties [129]. A very important property required for biological applications is a low level of cytotoxicity. Pure nanocellulose hydrogel has been shown to be non-toxic to mammalian cells [130-132]. To summarise, nanocellulose hydrogels are a great material for biomedical applications and hence its potential as antimicrobial wound dressing was studied in this thesis.

### **1.2.6. Applications of antimicrobial materials**

This section provides an understanding of the applications of antimicrobial materials that are studied in this thesis and the context of nanocellulose in it.

#### **1.2.6.1. Packaging materials**

Conventional packaging only serves as a physical barrier between the environment and the product contained in it, protecting the product from contaminants, oxygen, and water vapor [31]. Active packaging materials offer enhanced protection and has emerged due to a demand for quality assurance and product safety, especially for sensitive products like food and medicines [86, 133].

##### **1.2.6.1.1. Current active packaging technologies**

Active packaging materials interact with the product or the environment within the packaging by either containing antimicrobial agents or by absorbing gases (oxygen, ethylene, water vapor) [31]. Additives can be used to modify the atmosphere inside the packaging by absorbing gases to reduce the chances of microbial growth. Oxygen scavengers typically work by oxidation of iron or enzymatic reactions and ethylene scavengers works by using potassium permanganate to oxidise the ethylene to carbon dioxide. These scavenger chemicals are contained in a permeable sachet. Thus, these are not suitable for liquid products [31, 134]. Moisture absorption is done by means of absorbent pads containing silica gel, propylene glycol or polyvinyl alcohol. [135]. There are a number of limitations with these modified atmosphere techniques since these mainly rely on the reactive chemical contained in a sachet. Consumer concerns over accidental ingestion or children's safety makes them undesirable [135]. These gas scavengers help by altering the atmosphere inside the packaging to reduce the chances of microbial growth. On the other hand, antimicrobial packaging are able to inhibit microbial surface growth and contamination and thus provides better protection [134]. Some commercial antimicrobial packaging products with the above mentioned working principles are listed in Table 3.

**Table 3:** Commercial active packaging working under the four main principles

Working principle	<u>Commercial Name</u>				<u>Reference</u>
Oxygen scavengers	ActiTUF™	Cryovac®	Ciba®	FreshCard®	[31, 136]
	Ageless	O2S®O-Buster®	Shelfplus™	Freshlizer	
	Amosorb®	Oxbar®	Wonderkeep	Oxyguard	
	Celox™	DiamondClear®	Freshmax®	Zero <sub>2</sub>	
	Getter Pak®	Bioka	Freshpax®		
Ethylene scavengers	Neupalon	Ethylene Control	Retarder®		[31, 135, 136]
	Peakfresh	Evert-Fresh	Profresh		
Moisture Absorber	Dri-Loc®	Pichit®	StripPax®	Desi Pak®	[31, 136]
	Tenderpac®	Humidipak	Natrasorb®	Dri-Fresh™	
	Supa-Loc®	Luquasorb®	Trisorb®	Eat-fresh™	
	Lite-Loc®	Minipax	Sorb-it®		
Antimicrobial agent	Agion®	Antimicrobial (Ag)	Biomaster®	(Ag)	[31, 137] [138]
	Food Touch™	(Ag)	Microban®	(Triclosan)	
	Ciba®	IRGAGUARD® B (Ag)	Novaron®	(Ag)	
	Microbeguard®	(Ag)	Duretham®	(Ag)	
			Kodak®	(Ag)	

The antimicrobial agents in these packaging in Table 3 are shown in parenthesis next to the commercial names and majority of them are silver-based. Antimicrobial active packaging can be obtained by incorporating or immobilizing antibacterial and antifungal agents into the material [26, 86, 108]. Antimicrobial agents in packaging materials offers better protection by reducing

chances of microbial contamination and growth in the product and thereby increasing shelf life, product quality and safety [31, 137]. This is illustrated in Figure 10. Herein, the conventional packaging provides physical barrier to moisture and oxygen, but cannot provide protection from bacterial growth. Antimicrobial packaging with the required barrier properties against water vapor and oxygen can protect the product from microbial growth as well.

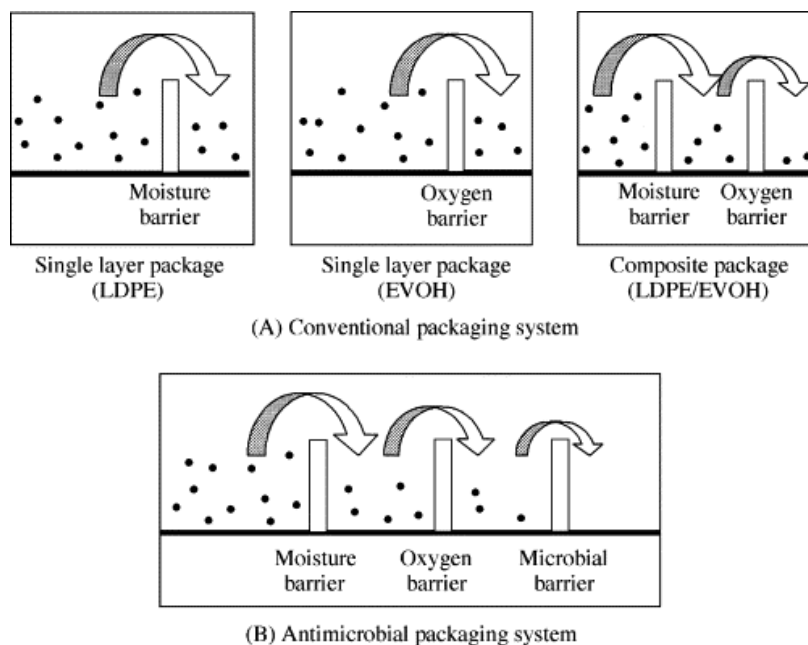


**Figure 10:** Schematic showing the basic difference between conventional and antimicrobial packaging. Reproduced from [134], Copyright © 2003, with permission from Elsevier.

Antimicrobial packaging has been studied in a number of publications in different matrices including polyethylene (like LDPE, HDPE), ethylene vinyl alcohol (EVOH), polylactic acid (PLA) as well as nanocellulose [139, 140]. Most of the commercial ones use petroleum based polymers as the matrix, which is not environmentally friendly. Bacterial cellulose has been studied in a number of research papers but its high cost of production makes it practical only for very high value product packaging [141].

#### 1.2.6.1.2. Nanocellulose antimicrobial packaging

There is a trend to shift the packaging materials to more sustainable and environmentally friendly materials from the more generally used petroleum based polymers. Paper based materials are great in that aspect, however lacks in the required barrier properties. Current paper based packaging materials have layers of lamination of polyethylene to impart the hydrophobicity and barrier performance required. These layers contribute to the non-biodegradability of the composite materials. In these composites, the paper layer provides the support and the lamination gives the barrier properties. Nanocellulose films have the potential to overcome this limitation.

Nanocellulose films have very low oxygen permeability and lower water vapor permeability compared to its macro-cellulosic materials counterpart [104].

A number of publications have reported the use of nanocellulose materials for active packaging materials, some of which are presented in Table 4. The method of antibacterial performance analysis is different in each study making it hard for comparisons. Moreover, the actual loading of the active agent on the finished composite was not reported in most studies which also makes comparison difficult. However, an overall observation is that all the metal oxides and nanoparticles (Ag, Zn and Cu) tabulated here showed activity towards a range of bacteria when formed into nanocellulose-based packaging. It is not known how such nanocellulose-based composites loaded with the *bis*-phosphinato bismuth complex would compare with these. The antibacterial efficacy of different loading levels of the bismuth complex in MFC composites and with different types of MFC will be studied in this thesis.

The most commonly studied antimicrobial agent are silver-based. As discussed previously, there are many commercial food packaging and other food contact materials as well that employs silver as the antimicrobial agent[152]. Silver nanoparticles can be released from the packaging into the food contained in it [153, 154]. After 24 days of storage, the silver concentration in food has been reported to exceed the regulatory limits set for food contact materials [155]. The maximum silver intake of 10 g in lifetime is considered to be safe [156]. These, along with the issues with resistance development, has driven us to study the application of the *bis*-phosphinato bismuth complex for packaging materials.

**Table 4:** Cellulose based packaging material loaded with different antimicrobial agents

<u>Metal used</u>	<u>Form of cellulose</u>	<u>Metal compound/form</u>	<u>Microorganism tested</u>	<u>Method</u>	<u>Antibacterial efficacy or performance</u>	<u>Loading level</u>	<u>Reference</u>
Silver	Bleached Eucalyptus MFC, TEMPO-oxidised NFC	Ag-NPs	<i>E. coli</i>	Zone of inhibition, CFU	Up to 12 mm, 100% reduction with MFC, Partial reduction with NFC	2.3 to 5 %	[24]
	TEMPO-oxidised CNF	Ag nanowires	<i>E. coli</i> , <i>S. aureus</i>	CFU	89.3% ( <i>E.coli</i> ), 100% ( <i>S. aureus</i> ) reduction	N/A	[142]
	Bacterial nanocellulose	Ag-NPs	<i>E. coli</i>	CFU	Up to 7 log CFU/ml reduction	N/A	[143]
	Anionic nanocellulose	Ag-NPs	<i>E. coli</i> , <i>S. aureus</i>	Zone of inhibition	1.9 mm ( <i>E. coli</i> ), 2.1 mm ( <i>S. aureus</i> )	N/A	[144]
	Regenerated cellulose	Ag-NPs	<i>E. coli</i> and <i>L. monocytogene</i>	CFU	Up to 100% reduction for both	102 mg Ag/g fibre	[145]

	Commercial CNF	Ag-NPs	<i>E. coli, S. aureus</i>	CFU	Up to 100% reduction for both	N/A	[26]
	CNC reinforcement	CNC Ag nanohybrids	<i>E. coli, S. aureus</i>	CFU	2.2 mm, up to 99.6% ( <i>E. coli</i> ), 3.6 mm, up to 96.6% ( <i>S. aureus</i> ) reduction	N/A	[146]
	CNC reinforcement	Ag-NPs	<i>E. coli, S. aureus</i>	Zone of inhibition, CFU	4.5 mm, up to 99.8% ( <i>E. coli</i> ), 2.3 mm, up to 97.4% ( <i>S. aureus</i> ) reduction	N/A	[139]
	CNC reinforcement	Ag-NPs	<i>E. coli, S. aureus</i>	CFU	Good bactericidal properties; efficacy varies with Ag content, time and temperature of incubation and CNC source	0.1 and 0.5 %	[147]
Zinc	Bleached acid hydrolysed CNC	ZnO	<i>E. coli, S. aureus</i>	Zone of inhibition	Up to 20 mm ( <i>E. coli</i> ), 24mm ( <i>S. aureus</i> )	N/A	[148]
	MFC paper	ZnO	<i>E. coli, S. aureus</i>	Zone of inhibition	>15mm for both	2.5%	[43]

	Bleached Eucalyptus chemi-mechanical cellulose	ZnO-NPs	<i>A. niger</i> , <i>B. subtilis</i> , <i>E. coli</i> , <i>S. aureus</i> ,	Zone of inhibition	Up to 13.2 mm ( <i>A. niger</i> ), 12.6 mm ( <i>B. subtilis</i> ), 5.6 mm ( <i>E. coli</i> ), 11.8 mm ( <i>S. aureus</i> )	0.79-4.86%	[149]
	Regenerated cellulose	ZnO-NPs	<i>E. coli</i> and <i>L. monocytogene</i>	CFU	Up to 100% reduction for both	29 mg Ag/g fibre	[145]
	Bacterial nanocellulose	ZnO	<i>E. coli</i> , <i>S. aureus</i>	Zone of inhibition	Up to 20.4 mm ( <i>S. aureus</i> ), 7.6 mm ( <i>E.coli</i> )	5 % (wt%)	[150]
Copper	Regenerated cellulose	CuO-NPs,	<i>E. coli</i> and <i>L. monocytogene</i>	CFU	Bacteriostatic	4 mg Ag/g fibre	[145]
	Bacterial cellulose	CuO	<i>E. coli</i> , <i>L. monocytogenes</i> <i>P. aeruginosa</i>	Zone of inhibition	13.76 mm ( <i>E.coli</i> ), 13.0 mm ( <i>P. aeruginosa</i> ), 16.76 mm ( <i>L. monocytogenes</i> )	N/A	[151]

### **1.2.6.2. Wound dressing**

Treatment of wounds is a very complex process. It involves three stages, the inflammation phase, the proliferation phase and the tissue remodelling phase. The wound prepares for healing in the inflammation phase and new blood vessels are generated, followed by rebuilding of the skin tissue in the second phase and reaches its final form to function normally in the third phase. Disruption in any one phase increases the complexity of the process [157]. Hence, wound management using appropriate dressing techniques and proper dressing materials is very important. The type of dressing varies depending on the type of wound. However, in general all dressings should ideally be able to hydrate the wound, control the exudates (like blood, puss) and non-adherent for painless removal. Very importantly, they would be able to protect the wound from microorganisms [158].

#### **1.2.6.2.1. Wound infection**

A wound can be contaminated (containing non-replicating bacteria), colonised (containing replicating bacteria that does not cause any damage to host cells) or infected (replicating cells harming host cells). Infection by bacteria can hinder healing, by jamming the wound healing in the inflammation and proliferation stage, delaying healing. On top of that, wound healing is a slower process than the spreading of infection [157]. The wound management and wound healing processes are affected by the level and severity of the infection, making infection control in wounds very important [159]. Researchers have reported by modelling and simulation that low or high densities of harmless bacteria in a wound does not delay the wound healing process. However, virulent bacteria in both low and high densities interferes with the wound healing mechanism. For a low density of virulent bacteria, the wound starts to heal normally initially, and then slows down when compared to non-infected wound. In the case of a high density virulent bacteria, the capillaries fail to propagate at all [157].

##### **1.2.6.2.1.1. Wound pathogens**

Several clinical studies on wound microbiota have reported the most frequently isolated pathogens in different kinds of wounds. The results suggest that most chronic wounds are infected with Gram-negative bacteria [160]. The World Health Organisation has identified the Gram-negative bacteria *Pseudomonas aeruginosa* and *Acinetobacter baumannii* as critical priority pathogens [161]. A two years long study on specimens collected from burn patients in the Traumatology and Burn Centre, Tunisia showed that *A. baumannii* has been isolated from 12% of total burn infection cases. Of them, a large proportion were resistant to antibiotics. 87, 60 and 99% of the bacterial isolates were resistant to ciprofloxacin, imipenem and ceftazidime respectively. Similarly, 35% of the *P. aeruginosa* strains isolated from 16% of the total burn cases

were resistant to multiple antibiotics [162]. Methicillin-resistant *Staphylococcus aureus* and vancomycin-resistant *Enterococcus* are also major causes of infections in burn wounds [163, 164]. Around 20% of burn wound infections are caused by *S. aureus*, as the dominant species, of which 68% is Methicillin resistant type [162]. Burn patients are at very high risk of MRSA infection and combinations of infection control strategies are needed [165].

#### **1.2.6.2.2. Current antimicrobial wound dressings**

Active wound dressing that delivers drugs or contains antibacterial agents are very popular due to the high risk of infection in wounds [166]. Although different kinds of antimicrobial agents have been studied in wound dressings, silver and its compounds has been the most popular among researchers. Examples of commercial wound care products that uses silver as the antimicrobial agent are shown in Table 5. The silver based wound dressings are available in various forms- as amorphous hydrogels, foams, gauze etc. The data for the loading level is available only for a few of these products and has been mentioned in the table.

**Table 5:** Some of the commercial wound dressings using silver as the active agent

<b>Product Name</b>	<b>Form of silver</b>	<b>Form of matrix</b>	<b>Loading level</b>	<b>Company/ manufacturer</b>	<b>Reference</b>
Acticoat	Ag <sup>+</sup>	Flexible absorbent sheet	104mg/ 100cm <sup>2</sup>	Smith +Nephew	[167-169]
Actisorb™	N/A	Cloth with activated charcoal	220 mg Ag/100g or 33 ug/cm <sup>2</sup>	3M+KCI	[170, 171]
Aquacel ®	Ag <sup>+</sup>	Hydrofiber absorbent material	1.2% ionic silver or 900 µg/100 cm <sup>2</sup>	ConvaTec	[167, 170, 172]
DermaSyn/Ag™	N/A	Water based amorphous gel	N/A	Dermarite	[173]
Gentell Calcium Alginate Ag	N/A	Calcium alginate absorbent pad	N/A	Gentell	[173]
PolyMem Silver®	Ag <sup>+</sup>	Polymeric membrane-hydrophilic polyurethane matrix	13 mg/100 cm <sup>2</sup>	Ferris Mfg. Corp	[167, 174]

## CHAPTER 1

PolyMem WIC®	N/A	Polymeric membrane	N/A	Ferris Mfg. Corp.	[175]
Silvasorb™	Ag <sup>+</sup>	Amorphous gel	N/A	Medline	[170, 173]
Silvercel™	Ag <sup>+</sup>	Alginate-carboxymethylcellulose non-woven pad	N/A	3M+KCI	[176]
Silverderm 7®	Ag <sup>+</sup> from 99% Ag and 1% Ag <sub>2</sub> O	Porous non-adherent knitted nylon dressing	N/A	Dermarite Industries, LLC	[158]
Silverlon®	Ag <sup>+</sup>	Calcium alginate non-woven pad	N/A	Argentum Medical, LLC	[169]
Silverlon® Lifesavers™ IV/ Catheter dressings	Ag <sup>+</sup>	Circular disk dressing with centre hole for catheter	N/A	Argentum Medical, LLC	[177]
SilverMed™	Ag <sup>+</sup>	Liquid spray	N/A	MPM Medical	[173]
Urgotul™ Ag/Silver	Ag <sup>+</sup> from Ag <sub>2</sub> SO <sub>4</sub>	Flexible non-adherent polyester mesh with lipid-hydrocolloid matrix	14 mg/ 100cm <sup>2</sup>	Urgo Medical	[49, 167]

### 1.2.6.2.3. Hydrogels as wound dressings

Hydrogels, due to its ability to keep the wound moist and having the “tissue-like” structure, is one of the best forms of dressing for wound healing [119]. The ability to maintain the pH and moisture in the wound is an important attribute for wound healing, which can be provided by hydrogels [114].

Various antimicrobial agents in hydrogel matrices have already been studied, like salicylate in carboxybetaine ester hydrogel [178], polyhexamethylene biguanide (PHMB) in cross-linked poly (N-isopropylacrylamide) (PNIPAAm)-based hydrogels [72], light-activated No-donor ([Mn(PaPy<sub>3</sub>)(NO)]ClO<sub>4</sub>) in pHEMA-based (poly(2-hydroxyethyl methacrylate) hydrogels [179] etc. for wound dressing and biomedical applications. Hydrogels loaded with antibiotic have also been studied for wound dressing applications, e.g. Ciprofloxacin in poly(2-hydroxyethyl methacrylate) hydrogel [180, 181], poly(ethylene-glycol diacrylate) (PEGDA-AA) hydrogel [181], in peptide hydrogels [182] etc. Although different kinds of antimicrobial agents have been studied in hydrogels, silver and its compounds has been the most popular among researchers. Experiments already conducted by researchers includes incorporation of silver NPs in poly(vinyl alcohol)/poly(*N*-vinyl pyrrolidone) (PVA-PVP) hydrogels [183], poly(vinyl alcohol) (PVA) hydrogel films [184], polyvinyl pyrrolidone (PVP) and alginate hydrogels [185], poly (acrylamide-co-acrylic acid) hydrogels [186], cross-linked poly (acrylamide) hydrogel network [71, 187], poly(acrylamide)/poly(vinyl alcohol) hydrogel [188], Poly(acrylamide)/poly (ethylene glycol) (PAM-PEG) semi-IPN hydrogel, poly(acrylamide)/poly(vinyl sulfonic acid) (PAM-PVSA) semi-IPN hydrogel, poly(acrylamide-co-acrylic acid) (PAM-AAc) hydrogels [187] etc for wound dressings and other medical uses. Acrylic acid, acrylamides and vinyl based polymers exhibit poor environmental degradation. Moreover, acrylamides are neurotoxic, carcinogenic and mutagenic, posing potential health risk [189].

Hebeish *et al.* (2013) suggested a technique of in situ synthesis of Ag-NPs inside carboxymethyl cellulose (CMC) hydrogel network to produce an effective antibacterial activity for medical applications [190]. Gelatin hydrogel pads with AgNO<sub>3</sub> in acetic acid showed antimicrobial growth inhibition properties for potential wound dressing applications [166]. Although the biopolymer gelatin is cheap and abundant, its dried form is brittle and its hydrated form is too soft [191]. Thus, the mechanical property of gelatin is not suitable for wound dressing applications, and researchers have to use crosslinkers. Rattanuengsrikul *et al.* studied gelatin hydrogel pads by crosslinking with glutaraldehyde (GTA) to overcome this limitation of mechanical strength and used Ag-NPs as the antibacterial agent. They reported slight increase in toxicity with increase in GTA content and incubation time, and suggested the reason to be unreacted GTA that came out of the hydrogel

network could have been toxic [166]. Thus, GTA level is crucial in this type of hydrogel for dermal application. Other researchers have studied the chemical modification of gelatin structure with methacrylic anhydride-methacrylamide (MA) to obtain gelatin methacrylate with better mechanical properties. However cell attachment on the hydrogel surface was reduced due to presence of MA, which is hydrophobic [191]. Nanocellulose hydrogels are great materials for biomedical applications [192].

#### **1.2.6.2.4. Nanocellulose antimicrobial hydrogel**

The most commonly studied form of nanocellulose hydrogels for such applications is bacterial cellulose (BC) [193]. Periodate oxidate of BC can be used to obtain dialdehyde cellulose. Laçın studied dialdehyde bacterial cellulose hydrogel, with chloramphenicol (CAP) as the antibacterial agent [193]. Bacterial cellulose has also been studied by Wei *et al.*, but this study involved dry films of BC, rather than the hydrogel form. This study involved the use of benzalkonium chloride as the antibacterial agent. Swelling and antimicrobial performance were investigated and it was found that it had good swelling ratio and has antimicrobial activity for at least 24 hours [194]. Commercial BC based wound healing products include Biofill, Gengifelix, XCell [193]. Bacterial cellulose and wood-based cellulose has the same chemical structure, with the same sugar molecule forming the polymer. However, BC is a weak hydrogel, and is hard to modify to other forms [195]. Moreover, cost of production of BC is very high, making the hydrogel quite expensive [141].

Limited research exists looking at wood-based nanocellulose as wound dressings. The surface chemistry of nanocellulose has been studied and reported to be quite suitable for wound dressing applications [196]. Hakkarainen, Koivuniemi *et al.* studied the use of wood based nanocellulose as wound dressing for burns in patients [195]. Nanocellulose/polydopamine hydrogels crosslinked with  $\text{Ca}^{2+}$  with a broad-spectrum antibiotic (tetracycline hydrochloride) showed wound healing after 10 days, compared to 15 days for the control [197]. In this thesis, wood-based nanocellulose hydrogel matrix was studied as the carrier matrix for the antibacterial bismuth complex. Very few studies have reported nanocellulose hydrogel loaded with metal based antibacterial agents for wound care applications and are listed in Table 6. The metals previously studied are calcium, copper and silver ions and nanoparticles. The potential of bismuth based antibacterial agent in hydrogel matrices for wound care applications has not been explored. So, there is a lack of understanding of the effect of the complex to reduce the chances of infection or its impact on mammalian cells. These will be explored in this thesis.

**Table 6:** Nanocellulose hydrogel studied as antimicrobial wound dressings

<u>Metal used</u>	<u>Form of cellulose</u>	<u>Metal compound/form</u>	<u>Microorganism tested</u>	<u>Method</u>	<u>Antibacterial efficacy or performance</u>	<u>Loading level</u>	<u>Reference</u>
Calcium	TEMPO oxidised NFC hydrogel	Ca <sup>2+</sup>	<i>S. epidermidis</i> , <i>P.aeruginosa</i>	Growth curve	No effect ( <i>P. aeruginosa</i> ), lag time 266%↑, doubling time 36% ↑ ( <i>S. epidermidis</i> )	N/A	[198]
Copper	TEMPO oxidised NFC hydrogel	Cu <sup>2+</sup>	<i>S. epidermidis</i> , <i>P.aeruginosa</i>	Growth curve	Lag phase 49% ↑, doubling time 78%↑ ( <i>P. aeruginosa</i> ), lag time 137%↑, doubling time 191% ↑ ( <i>S. epidermidis</i> )	N/A	[198]
Silver	TEMPO-oxidised CNF hydrogel	Ag-NH <sub>2</sub> NPs	<i>S. aureus</i> , <i>P. aeruginosa</i>	Zone of inhibition	Up to 2 mm (approx.)	N/A	[199]
Silver	Bacterial cellulose ( <i>Acetobacter xylium</i> )	Ag-NPs	<i>E. coli</i> , <i>S. aureus</i>	Zone of inhibition, CFU	2 mm, 99.7% reduction ( <i>E. coli</i> ), 3.5 mm, 99.9 % reduction ( <i>S. aureus</i> )	N/A	[200]

Silver	Bacterial cellulose	Ag-NPs	<i>E. coli, S. aureus, P. aeruginosa</i>		1 – 2.35 mm, 98.8 – 100 % reduction for all	1.09 to 3.40 % or 14 - 45 mg Ag/100 cm <sup>2</sup>	[201]
Silver	Carboxymethyl cellulose hydrogel	Ag-NPs	<i>S. aureus, P. aeruginosa</i>	Zone of inhibition	N/A Qualitative study	N/A	[202]

### **1.2.6.3. Water purification**

Lack of safe drinking water is a serious issue in most developing countries. Drinking contaminated water can lead to diseases like diarrhoea and typhoid. This is very common in developing countries due to lack of basic facilities and poverty [203, 204]. Current drinking water purification techniques include boiling, chlorination and ultraviolet (UV) treatment. However, boiling and UV treatment are expensive and time-consuming and chlorine-based chemicals have cytotoxicity risks [205, 206]. Low cost water filters are a great solution for such applications since they are cheap, often easy to operate, and portable to be taken to remote areas in developing countries [207, 208]. Most commonly used low cost water filter material include ceramic, polymeric materials, polyurethanes and paper-based filters [208]. In this thesis, a paper-based filter material will be studied.

#### **1.2.6.3.1. Issues with non-active filters**

Liquid filtration is often a preferred method due to its non-destructive separation and easy operation. However, fouling is a major limitation to membrane based separations. Different types of fouling can occur, which includes blockage of the filtration area by various sizes of suspended molecules and protein and biological fouling [209]. Biofouling involves the formation of bacterial biofilm and is a major problem in membrane based filtration systems. [210, 211]. It affects the performance of the filters by reducing the permeate flux, separation efficiency and membrane longevity [210]. Properties of membranes that can reduce the chances of bacterial attachment for biofouling are hydrophilicity, electrical charge and smoothness of membranes. However, for applications with longer bacterial exposure antimicrobial functionalities of the membrane are required [210]. This can be done by making the membrane reactive, instead of being just a physical barrier to the microorganisms, by incorporating antimicrobial agents [211]. Researchers have studied incorporation of metal nanoparticles, especially silver nanoparticles, in filter media for such applications. If nanoparticles are incorporated, retention of these particles in the membrane matrix remains a challenge. Low retention is undesirable due to the cost of the nanoparticles lost and the risks of them escaping into the filtrate posing a danger to humans and the environment. Immobilization of the active agent can be a solution to this, but this lowers the available active surface area and hence lowers the disinfection efficiency [211]. Ultrafiltration membranes of polysulfone loaded with Ag-NPs showed antifouling behaviour on the membrane, along with high leaching behaviour of Ag leading to quick loss of antibacterial properties [212]. Thus, the amount of biocidal additive in the membrane and its leachability decides how long the membrane is effective [210]. Research is needed to achieve slow release behaviour to reduce the loss of biocide from the membrane and minimise the risks to human health and ecosystem

[210, 211]. Since the *bis*-phosphinato bismuth complex studied herein is highly hydrophobic, it is hypothesised that it will show a slow release behaviour from the filter media. However, the role of the complex to inhibit biofilm formation is not yet known and will be studied in this thesis.

#### **1.2.6.3.2. Nanocellulose filters**

A range of metal-based antimicrobial agents have been studied for water purification filters. Examples include silver [27, 205, 213-215], copper [205, 207] and zinc [205, 216]. Some of the cellulose-based filters using metal based antimicrobial agents are listed in Table 7.

Commercial water purification systems like Marathon® and Aquapure® also use silver as the antimicrobial agents [219]. These filters are highly effective, but the silver nanoparticles wash out into the drinking water posing potential risks to human health [27, 208]. Regulatory bodies have set a maximum concentration of 0.1 mg/L of silver in drinking water [220]. Given the concerns about silver ingestion discussed in section 1.2.2.1.1, a new antimicrobial agent in water filters application is needed. Hence in this thesis, the bismuth phosphinato complex was studied for this particular application.

Nanocellulose has been gaining interest for many environmental applications. The highly entangled nature and small pore size in nanocellulose paper makes them a great choice as filter membranes [221]. The high mechanical strength, high surface area and chemical inertness of nanocellulose make it a great choice for membrane and filter applications [222]. A number of researchers have shown the potential of using nanocellulose membranes for the removal of contaminants like metals, dyes, organics and microorganisms [222]. Nanocellulose filter paper has been shown to be able to remove very small biological particles like viruses by controlling the pore size distribution of the filter [209, 223, 224].

Pressure driven filtration can be microfiltration, ultrafiltration, nanofiltration and reverse osmosis. For bacterial separation, microfiltration is required, which is usually performed below 1 bar or 100kPa and is employed for the separation of particles in the size range of 0.1 to 10  $\mu\text{m}$  [209, 225, 226]. Most bacteria are larger than 0.2  $\mu\text{m}$ , and hence the pore size distribution of the filter media needs to be lower than that range. In non-woven structures, the fibre diameter and bulk porosity decides the pore size distribution [227]. This can be understood from the Figure 11. Nanocellulose coating on filter paper substrates produced by vacuum filtration can be used for high efficiency ultrafiltration [109]. This thesis studies water disinfection using nanocellulose based filters both as coating on filter paper and standalone nanocellulose films.

**Table 7:** Cellulose based filters for water disinfection using metal antimicrobial agent

<b>Metal used</b>	<b>Form of cellulose</b>	<b>Metal compound/form</b>	<b>Microorganism tested</b>	<b>Method</b>	<b>Antibacterial efficacy or performance</b>	<b>Loading level</b>	<b>Reference</b>
Silver, Copper	Filter paper	Ag-NPs, Cu-NPs	<i>E. coli</i>	Filtration followed by total coliform and CFU	Log 5.1 (Ag-paper) and log 4.8 (Cu-paper) reduction for >5x 10 <sup>7</sup> CFU/ml influent water. Complete inactivation (both) for <1.5 x 10 <sup>6</sup> CFU/ml water.	1.39-3.21 mg Ag/g paper; 64.9 mg Cu/g paper	[217]
Silver	Bleached softwood Kraft blotters	Ag-NPs	<i>E. coli</i> , <i>E. faecalis</i>	Filtration followed by CFU	Up to 7.5 ( <i>E.coli</i> ) and 3.2 ( <i>E. faecalis</i> ) log CFU/ml reduction	0.26 – 26.5 mg Ag/ dry g paper	[27]
Iron	Filter paper	Fe <sup>3+</sup> - saturated montmorillonite	<i>E. coli</i>	Filtration followed by CFU	> 99% deactivation efficiency	N/A	[218]

Silver	Nitrocellulose membrane filter	Biosynthesised Ag-NPs	<i>E. coli</i> , <i>E. faecalis</i> , <i>P. aeruginosa</i>	Filtration followed CFU after 48 hour incubation	Complete inhibition after 48 hours	N/A	[213]
Copper, Zinc, Silver	Cellulose foam filter	Metal oxide NPs	<i>E. coli</i> , <i>B. cereus</i> , <i>B. subtilis</i> , <i>P. aeruginosa</i> ,	Zone of inhibition	Up to 18mm ( <i>E.coli</i> ), 13 mm ( <i>B. cereus</i> ), 18mm ( <i>B. subtilis</i> ), 17mm ( <i>P. aeruginosa</i> )	N/A	[205]
Copper	Bleached softwood Kraft blotters	Cu-NPs	<i>E. coli</i>	Filtration followed by total coliform count	8.8 log CFU/mL reduction	10-65 mg Cu/g paper	[207]
Silver	Cellulose filter paper	Ag-NPs	<i>E. coli</i>	Filtration followed by CFU	Suitable for bacterial removal from rainwater, tap water and river water.	N/A	[214]

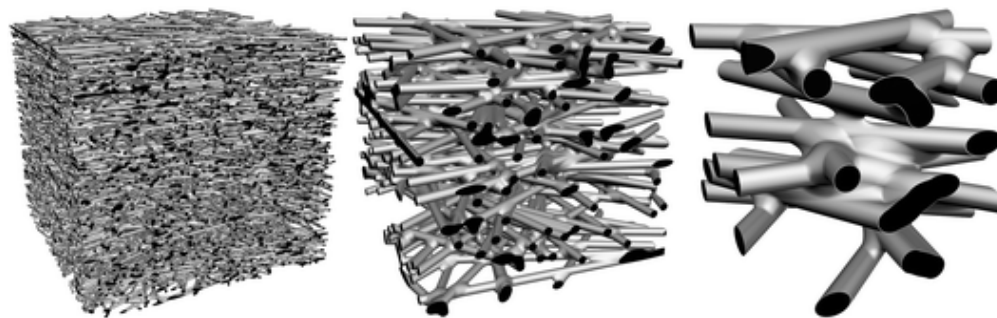


**Figure 11:** Change in pore size with change in fibre diameter at 80% porosity. Reproduced from [227], Copyright © 2011, with permission from Royal Society of Chemistry.

### 1.2.7. Perspectives

Rise in antimicrobial resistance has driven many researchers towards the development of new antimicrobials and engineering antimicrobial materials by putting them into polymer matrices for different applications. Metal-based antimicrobials can be justified to be an ideal choice due to their flexibility to be incorporated into different matrices, their ability to affect microorganisms by multiple mechanisms and the reduced capacity for microorganisms to grow resistance against them. However, many metal-based antimicrobials have concerns regarding toxicity and environmental accumulation. In addition, microorganisms' genes are already gaining resistance to silver, copper and other metals used in commercial products [7]. Bismuth, despite being one of the metals that microorganisms have the least resistance to, as well as being known for its remarkably low toxicity [8], has not been much researched. Herein, a synthesised insoluble organobismuth complex, phenyl *bis*-diphenylphosphinato bismuth (III) complex invented recently in 2016, has been studied as the antimicrobial agent [13]. This complex showed promising antimicrobial performance. However, the properties and bioactivity of this in polymer matrices is not known. Incorporation of this complex into a suitable polymer can open up applications, including active packaging, wound dressings, water filters, antimicrobial textiles and many others. Most of these rely on petroleum based polymers as the carrying matrix. But these have environmental issues and thus the necessity for sustainable and environmentally friendly materials has pushed natural biopolymers forward. Cellulose is the most abundant biopolymer. Nanocellulose is an emerging nanomaterial that is not only a green polymer, but also has unique properties making them very appealing to researchers. Nanocellulose has not been studied as matrix for bismuth-based antimicrobials. Therefore, research to use nanocellulose for developing antimicrobial materials is required.

### 1.3. Gaps in knowledge

This review discusses the global concerns of AM resistance and the current AM agents in different materials. It identifies the need for new alternatives in such materials and introduces the phenyl *bis*-phosphinato bismuth complex. The *bis*-phosphinato bismuth complex has been shown to have antimicrobial properties as well as very low solubility. These two properties make it a great choice to be incorporated into materials. However, there is a significant gap in understanding how this complex behaves within a polymeric matrix. Moreover, although various metal compounds have been studied in different matrices, these are mainly metal NPs studied in plastic-based matrix. There are not any studies to explore the material application of the *bis*-phosphinato bismuth complex. While the chemistry and biological properties of various bismuth compounds and organobismuth complexes have been studied, very few studies looked into the engineering aspect of them to develop AM materials. It is extremely vital to understand the structural, chemical and biological behaviour of the complex within a material for utilising its antimicrobial properties for a particular application. This is the major gap in knowledge that this thesis has aimed to answer.

The specific questions left unanswered that are addressed in this thesis are:

1. Behaviour of the *bis*-phosphinato bismuth complex in nanocellulose materials
  - Are the antimicrobial properties retained when inside materials?
  - What loading level is required to achieve antibacterial properties and how does the complex affect other properties of the material?
  - How is the complex distributed within the fibrous matrix?
  - If the type of matrix it is incorporated into makes a difference in terms of its antibacterial properties?
  - What is the leachability of the complex from materials and how does it govern the antibacterial properties or cytotoxicity?
2. Development of nanocellulose-based antimicrobial materials for different applications
  - Packaging application:
    - Does the bismuth complex provide antimicrobial protection in nanocellulose composites for active packaging materials?
    - Does the complex have an effect on the barrier performance, mechanical properties and other required properties for packaging applications?
    - Does the composition and the fibre dimensions have an effect on the properties?

- Water purification:
  - Can the bismuth complex provide instant killing of bacteria in water purification filters?
  - Can the bismuth complex reduce biofilm formation on filtration membranes?
  - How do different sheet formation techniques and extent of fibrillation affects the filtration performance?
- Wound dressings:
  - How does the complex affect mammalian cells for use in wound care applications?
  - Can wound dressings with the bismuth complex reduce chances of infection?

These gaps in knowledge for utilising the complex into applications have been addressed in this thesis and are discussed next.

#### **1.4. Research Objectives**

This doctoral thesis aims to explore the applications of the novel *bis*-phosphinato bismuth complex in nanocellulose matrix to develop renewable antimicrobial materials. The applications of interest in this thesis are active packaging material, water disinfection filter and wound care hydrogel. The main objective of this thesis is to study the engineering of nanocellulose- bismuth complex composite sheets and hydrogel and simultaneously increase the understanding about the physico-chemical and biological properties of the complex within nanocellulose matrix.

The specific objectives of this thesis are:

1. To understand the properties of pure nanocellulose- bismuth complex composite sheet as active packaging material
2. To understand the effect of using lignocellulosic materials having different composition and fibre properties on the barrier and antimicrobial properties for active packaging applications
3. To understand the biocompatibility and selective antibacterial activity of the bismuth complex for wound hydrogel application
4. To develop antibacterial filter composites and understand its capability as an antibiofilm membrane

## 1.5. Thesis outline

This thesis is presented in the format of “Thesis including published works” according to the Monash University guidelines. It consists of four experimental chapters, two of which are published and accepted. The content of all published/accepted papers are unchanged but are formatted for a consistent presentation. The original publications are presented in Appendix II.

The thesis outline with a brief summary of each of the chapters are as follows:

- **Chapter 1- Introduction and Literature Review**

This chapter aims to provide a context of the research area to identify the gaps in knowledge. It discusses the issues of antimicrobial resistance and the need for new antimicrobial agents. It introduces the bismuth complex of interest in this thesis (the *bis*-phosphinato bismuth complex) and discusses all that is known about it, and thereby highlights the need for further research using the complex. It also provides a detailed background of nanocellulose and its attributes. Furthermore, it provides an in-depth literature review of the recent studies of antimicrobial materials for each of the applications of interest and finally recognises the questions left unanswered and states the research aims.

- **Chapter 2: Bismuth phosphinate incorporated nanocellulose sheets with antimicrobial and barrier properties for packaging applications**

*Maisha Maliha, Megan Herdman, Rajini Brammananth, Michael McDonald, Ross Coppel, Melissa Werrett, Philip Andrews, Warren Batchelor (2019). Bismuth phosphinate incorporated nanocellulose sheets with antimicrobial and barrier properties for packaging applications. Journal of Cleaner Production 246. Impact factor: 7.246*

This chapter aims to study the application of the *bis*-phosphinato bismuth complex in nanocellulose composites for active packaging materials. Morphological studies of the sheets were done and the images revealed overall distribution of the complex throughout the nanocellulose matrix, with occasional clustering behaviour on the surface. Water vapour permeability of the paper sheets increased very slightly with loading of the bismuth complex, however still remained in the acceptable range for packaging materials within  $10^{-11}$  g/m.Pa.s. Microbiological investigations showed the composite sheets to have antimicrobial effectiveness against multidrug resistant microorganisms, including both bacteria and fungus. Moreover, studies showed continued release of the bismuth complex over time with effective lifetime depending on the loading. Overall, this chapter describes the preparation of a new type of

freestanding antimicrobial composite paper, using the poorly soluble bismuth complex dispersed into nanocellulose matrix, which showed the potential to be used as an active packaging material.

- **Chapter 3: The effect of pulp type on the barrier and antimicrobial performance of microfibrillar lignocellulosic bismuth-based active packaging material**

*Maisha Maliha, Rajini Brammananth, Ross L. Coppel, Melissa Werrett, Philip Andrews, Warren Batchelor. The effect of pulp type on the barrier and antimicrobial performance of microfibrillar lignocellulosic bismuth-based active packaging material. (Manuscript prepared for Cellulose)*

This chapter is an extension to the previous one and aims to optimise the best type of pulp to be used for *bis*-phosphinato bismuth complex-nanocellulose composites for active packaging applications. Microfibrillated cellulose from different sources containing different amounts of cellulose, hemicellulose, lignin and extractives was used as the matrix phase with the antimicrobial organobismuth complex as the disperse phase. The aim of the study was to investigate the effect of the source and type of fibres on the antibacterial, barrier and mechanical properties of the composites for active packaging application. It was observed that the kraft pulp are more easily fibrillated than the thermomechanically treated pulp. The highly fibrillated nanocellulose fibres form a close network resulting in low water vapor transmission rate and high tensile index. While the mechanical and barrier properties are governed by the physical dimensions of the fibres, the antibacterial property is more dependent on the chemical composition of the matrix. The hydrophilicity of the kraft pulp (due to low lignin content) results in weak bond with the hydrophobic bismuth complex. This causes the complex to leach out more resulting in larger zones of inhibition with both the Gram-positive and Gram-negative bacteria. On the other hand, the high level of lignin in the thermomechanically treated pulp holds the bismuth complex within the matrix, resulting in less availability and thereby lower antibacterial activity. Moreover, the bismuth complex further reduces the water vapor transmission rate. This chapter presents the idea of using the different lignocellulosic matrices commonly available in most paper mills for developing lignocellulosic-bismuth complex composites and studies their performance as sustainable active packaging material.

- **Chapter 4: Biocompatibility and Selective Antibacterial Activity of a Bismuth Phosphinato-Nanocellulose Hydrogel**

*Maisha Maliha, Rajini Brammananth, Jennifer Dyson, Ross Coppel, Melissa Werrett, Philip Andrews, Warren Batchelor. (2021) Biocompatibility and Selective Antibacterial Activity of a Bismuth Phosphinato-Nanocellulose Hydrogel, Cellulose. Impact factor 4.210*

This chapter investigates the use of the bismuth phosphinato complex in a medical application where the performance of antimicrobial properties is extremely important. This chapter introduces the concept of using this complex in nanocellulose hydrogel matrix for wound dressings. An active wound dressing that contains antibacterial agents are very popular due to the high risk of infection in wounds. In this study, TEMPO-oxidized cellulose nanofibers hydrogel is combined with the *bis*-phosphinato bismuth complex. The rheological properties of the bismuth loaded hydrogel is comparable to commercial over-the-counter burn hydrogel. The nanocellulose hydrogel is shown to have no harmful effect on mammalian fibroblast cells. Selective cytotoxicity of the different concentrations of the complex is studied against a range of bacteria and mammalian fibroblast cells to establish the safe and active loading that can be used. An optimum target loading of 9  $\mu\text{g/g}$  showed bactericidal activity against the Gram-negative bacteria (*Acinetobacter baumannii* and *Pseudomonas aeruginosa*) and bacteriostatic effect against the Gram-positive ones (MRSA and VRE). However, the same concentration exhibited no toxic effect on mammalian fibroblast cells. So, this chapter identifies the safe level of bismuth loading for designing antibacterial nanocellulose hydrogel for potential active wound dressing applications and can serve as a very useful preliminary study for future in-vivo investigations.

- **Chapter 5: Bismuth Phosphinato Incorporated Antibacterial Filter Paper for Drinking Water Disinfection**

*Maisha Maliha, Benjamin Tan, Karmen Wong, Simin Miri, Rajini Brammananth, Ross Coppel, Melissa Werrett, Philip Andrews, Warren Batchelor. Bismuth Phosphinato Incorporated Antibacterial Filter Paper for Drinking Water Disinfection. (Manuscript prepared for Colloids and Surfaces A: Physicochemical and Engineering Aspects)*

The chapter develops *bis*-phosphinato bismuth complex loaded papers for filtration applications for drinking water purification. Here, two approaches for drinking water purification with different mechanisms of disinfection are proposed. The first approach is the deactivation of bacteria in water after passing through *bis*-phosphinato bismuth complex coated filter paper. Herein, the objective is to make an antibacterial coating with bismuth phosphinato on paper filters to develop a cheap water purification system for bacteria-free water that is driven by gravity filtration. The antibacterial activity of the filter arrangement was studied by filtering bacterial broth of *Staphylococcus aureus* through it and analysing the live bacteria in the filtrate. There was no sign of instantaneous killing but the filtrate showed reduction in live bacterial population after storing it at 37°C for 24 hours. This suggests a simple water purification system that can be operated by simple gravity filtration for storage water and can be useful in developing countries in tropical regions. The second approach focuses on the size exclusion principle by microfiltration through membrane with small pores to trap the bacteria. These filters showed immediate

elimination of bacteria and the bismuth complex prevented biofilm formation on the membrane. The chapter also studies the leaching behaviours of the complex to the water (filtrate) and evaluates its *in-vitro* toxicity for potential ingestion purposes. This chapter provides the prototypes of sustainable water filter designs that can be developed utilising the *bis*-phosphinato bismuth complex and nanocellulose and can serve as a useful tool for stored or immediate water purification.

### 1.6. References

1. Levy, S.B., *Antimicrobial Resistance: A Global Perspective*, in *Antimicrobial Resistance: A Crisis in Health Care*, D.L. Jungkind, et al., Editors. 1995, Springer US: Boston, MA. p. 1-13.
2. Smith, R.D. and J. Coast. *Antimicrobial drug resistance*. 2003 [cited 2018 January 23]; Available from: [http://www.who.int/trade/distance\\_learning/gpgh/gpgh4/en/](http://www.who.int/trade/distance_learning/gpgh/gpgh4/en/).
3. Warren, K.D. and J.V. Fraser, *Infection control measures to limit antimicrobial resistance*. *Critical Care Medicine*, 2001. **29**(4 Suppl): p. N128-N134.
4. Lemire, J.A., J.J. Harrison, and R.J. Turner, *Antimicrobial activity of metals: mechanisms, molecular targets and applications*. *Nature Reviews Microbiology*, 2013. **11**: p. 371.
5. Patra, M., G. Gasser, and N. Metzler-Nolte, *Small organometallic compounds as antibacterial agents*. *Dalton Transactions*, 2012. **41**(21): p. 6350-6358.
6. Abd-El-Aziz, A.S., C. Agatemor, and N. Etkin, *Antimicrobial resistance challenged with metal-based antimicrobial macromolecules*. *Biomaterials*, 2017. **118**: p. 27-50.
7. Pal, C., et al., *BacMet: antibacterial biocide and metal resistance genes database*. *Nucleic acids research*, 2014. **42**(Database issue): p. D737.
8. Kotani, T., et al., *Antibacterial Properties of Some Cyclic Organobismuth(III) Compounds*. *Antimicrobial Agents and Chemotherapy*, 2005. **49**(7): p. 2729.
9. Suzuki, H. and Y. Matano, *Chapter 1 - Introduction*, in *Organobismuth Chemistry*, Y. Matano, Editor. 2001, Elsevier Science: Amsterdam. p. 1-20.
10. Barry, N.P.E. and P.J. Sadler, *Exploration of the medical periodic table: towards new targets*. *Chem. Commun.*, 2013. **49**(45): p. 5106-5131.
11. Briand, G.G. and N. Burford, *Bismuth Compounds and Preparations with Biological or Medicinal Relevance*. *Chemical Reviews*, 1999. **99**(9): p. 2601-2658.
12. Luqman, A., et al., *The Importance of Heterolepticity in Improving the Antibacterial Activity of Bismuth(III) Thiolates*. *European Journal of Inorganic Chemistry*, 2016. **2016**(17): p. 2738-2749.
13. Philip, A., M. Werrett, and B. Madleen, *Antibacterial Bismuth Complexes*. 2016: Australia.

14. Alhede, M., T.H. Jakobsen, and M. Givskov, *Novel and Future Treatment Strategies*, in *Biofilm Infections*, T. Bjarnsholt, et al., Editors. 2011, Springer New York: New York, NY. p. 231-249.
15. Alvarez-Paino, M., A. Munoz-Bonilla, and M. Fernandez-Garcia, *Antimicrobial Polymers in the Nano-World*. Nanomaterials (Basel), 2017. **7**(2).
16. Rodríguez-Hernández, J., *Applications and Current Status of Antimicrobial Polymers*, in *Polymers against Microorganisms: On the Race to Efficient Antimicrobial Materials*. 2017, Springer International Publishing: Cham. p. 255-278.
17. Carmona-Ribeiro, A. and L. de Melo Carrasco, *Cationic Antimicrobial Polymers and Their Assemblies*. International Journal of Molecular Sciences, 2013. **14**(5): p. 9906.
18. Klemm, D., et al., *Nanocelluloses: A New Family of Nature-Based Materials*. Angewandte Chemie International Edition, 2011. **50**(24): p. 5438-5466.
19. Lin, N. and A. Dufresne, *Nanocellulose in biomedicine: Current status and future prospect*. Eur. Polym. J., 2014. **59**: p. 302-325.
20. Harbarth, S., et al., *Antimicrobial resistance: one world, one fight!* Antimicrobial Resistance and Infection Control, 2015. **4**(1): p. 49.
21. Shallcross, L.J., et al., *Tackling the threat of antimicrobial resistance: from policy to sustainable action*. Philos Trans R Soc Lond B Biol Sci, 2015. **370**(1670): p. 20140082.
22. 2016; Available from: <https://www.nhs.uk/conditions/antibiotics/>.
23. Hamilton, W.A., *Membrane Active Antibacterial Compounds*, in *Inhibition and Destruction of the Microbial Cell*. 1971, Academic Press. p. 77-93.
24. Yan, J., et al., *Antibacterial activity of silver nanoparticles synthesized In-situ by solution spraying onto cellulose*. Carbohydr Polym, 2016. **147**: p. 500-8.
25. Haider, A. and I.K. Kang, *Preparation of Silver Nanoparticles and Their Industrial and Biomedical Applications: A Comprehensive Review*. Advances in Materials Science and Engineering, 2015. **2015**: p. 1-16.
26. Amini, E., et al., *Silver-nanoparticle-impregnated cellulose nanofiber coating for packaging paper*. Cellulose, 2016. **23**(1): p. 557-570.
27. Dankovich, T.A. and D.G. Gray, *Bactericidal paper impregnated with silver nanoparticles for point-of-use water treatment*. Environ Sci Technol, 2011. **45**(5): p. 1992-8.
28. Kim, K., et al., *Antifungal effect of silver nanoparticles on dermatophytes*. J. Microbiol. Biotechnol., 2008. **18**(8): p. 1482-1484.
29. Xiong, Z.C., et al., *One-Step Synthesis of Silver Nanoparticle-Decorated Hydroxyapatite Nanowires for the Construction of Highly Flexible Free-Standing Paper with High Antibacterial Activity*. Chemistry, 2016. **22**(32): p. 11224-31.

30. Martínez-Abad, A., J.M. Lagaron, and M.J. Ocio, *Development and Characterization of Silver-Based Antimicrobial Ethylene–Vinyl Alcohol Copolymer (EVOH) Films for Food-Packaging Applications*. Journal of Agricultural and Food Chemistry, 2012. **60**(21): p. 5350-5359.
31. Pereira De Abreu, D.A., J.M. Cruz, and P. Paseiro Losada, *Active and Intelligent Packaging for the Food Industry*. Food Reviews International, 2012. **28**(2): p. 146-187.
32. Gunawan, C., et al., *Widespread and Indiscriminate Nanosilver Use: Genuine Potential for Microbial Resistance*. ACS Nano, 2017. **11**(4): p. 3438-3445.
33. Ji, J.H., et al., *Twenty-Eight-Day Inhalation Toxicity Study of Silver Nanoparticles in Sprague-Dawley Rats*. Inhalation Toxicology, 2007, Vol.19(10), p.857-871, 2007. **19**(10): p. 857-871.
34. Drake, P.L. and K.J. Hazelwood, *Exposure-related health effects of silver and silver compounds: a review*. Ann Occup Hyg, 2005. **49**(7): p. 575-85.
35. Stensberg, M.C., et al., *Toxicological studies on silver nanoparticles: challenges and opportunities in assessment, monitoring and imaging*. Nanomedicine (Lond), 2011. **6**(5): p. 879-98.
36. Maillard, J.-Y. and P. Hartemann, *Silver as an antimicrobial: facts and gaps in knowledge*. Critical Reviews in Microbiology, 2013. **39**(4): p. 373-383.
37. Gibaud, S. and G. Jaouen, *Arsenic-Based Drugs: From Fowler's Solution to Modern Anticancer Chemotherapy*, in *Medicinal Organometallic Chemistry*, G. Jaouen and N. Metzler-Nolte, Editors. 2010, Springer Berlin Heidelberg: Berlin, Heidelberg. p. 1-20.
38. Ge, R. and H. Sun, *Bioinorganic chemistry of bismuth and antimony: target sites of metallodrugs*. Accounts of chemical research, 2007. **40**(4): p. 267.
39. Gielen, M., E.R.T. Tiekink, and ProQuest, *Metallotherapeutic drugs and metal-based diagnostic agents : the use of metals in medicine*. 2005, Hoboken, N.J.: Hoboken, N.J. : Wiley.
40. Azam, A., et al., *Antimicrobial activity of metal oxide nanoparticles against Gram-positive and Gram-negative bacteria: a comparative study*. International Journal of Nanomedicine, 2012. **7**: p. 6003-6009.
41. Goto, M., *Chapter 2 - Morphology, Structure, and Composition*, in *Fundamentals of Bacterial Plant Pathology*, M. Goto, Editor. 1992, Academic Press: San Diego. p. 8-25.
42. Sawai, J., *Quantitative evaluation of antibacterial activities of metallic oxide powders (ZnO, MgO and CaO) by conductimetric assay*. Journal of Microbiological Methods, 2003. **54**(2): p. 177-182.

43. Pang, X., Y.Z. Chen, and Z.J. Zhang, *Study on the Antibacterial Paper Coated by ZnO/MFC for Food Packaging*. Applied Mechanics and Materials, 2015. **731**(Advanced Printing and Packaging Materials and Technologies): p. 457-461.
44. Jones, N., et al., *Antibacterial activity of ZnO nanoparticle suspensions on a broad spectrum of microorganisms*. FEMS Microbiology Letters, 2008. **279**(1): p. 71-76.
45. Hevener, K.E., et al., *Special Challenges to the Rational Design of Antibacterial Agents*, in *Annual Reports in Medicinal Chemistry*, M.C. Desai, Editor. 2013, Academic Press. p. 283-298.
46. Argudin, M.A., et al., *Heavy metal and disinfectant resistance genes among livestock-associated methicillin-resistant Staphylococcus aureus isolates*. Vet Microbiol, 2016. **191**: p. 88-95.
47. Altimira, F., et al., *Characterization of copper-resistant bacteria and bacterial communities from copper-polluted agricultural soils of central Chile*. BMC Microbiology, 2012. **12**(1): p. 193.
48. Chihomvu, P., P. Stegmann, and M. Pillay, *Characterization and structure prediction of partial length protein sequences of pcoA, pcoR and chrB genes from heavy metal resistant bacteria from the Klip River, South Africa*. Int J Mol Sci, 2015. **16**(4): p. 7352-74.
49. Silver, S., T. Phung le, and G. Silver, *Silver as biocides in burn and wound dressings and bacterial resistance to silver compounds*. J Ind Microbiol Biotechnol, 2006. **33**(7): p. 627-34.
50. Randall, C.P., et al., *Silver resistance in Gram-negative bacteria: a dissection of endogenous and exogenous mechanisms*. Journal of Antimicrobial Chemotherapy, 2015. **70**(4): p. 1037-1046.
51. GAYLE, W.E.J., et al., *Resistant Enterobacter cloacae in a Burn Center: The Ineffectiveness of Silver Sulfadiazine*. Journal of Trauma and Acute Care Surgery, 1978. **18**(5): p. 317-323.
52. Starodub, M.E. and J.T. Trevors, *Silver resistance in Escherichia coli R1*. Journal of Medical Microbiology, 1989. **29**(2): p. 101-110.
53. Deshpande, L.M. and B.A. Chopade, *Plasmid mediated silver resistance in Acinetobacter baumannii*. Biometals, 1994. **7**(1): p. 49-56.
54. Chopra, I., *The increasing use of silver-based products as antimicrobial agents: a useful development or a cause for concern?* J Antimicrob Chemother, 2007. **59**(4): p. 587-90.
55. Li, X.Z., H. Nikaido, and K.E. Williams, *Silver-resistant mutants of Escherichia coli display active efflux of Ag<sup>+</sup> and are deficient in porins*. Journal of Bacteriology, 1997. **179**(19): p. 6127.

56. Gupta, A., et al., *Diversity of silver resistance genes in IncH incompatibility group plasmids*. Microbiology, 2001. **147**(Pt 12): p. 3393-402.
57. Silver, S., *Bacterial silver resistance: molecular biology and uses and misuses of silver compounds*. FEMS Microbiology Reviews, 2003. **27**(2): p. 341-353.
58. Percival, S.L., P. Bowler, and J. Dolman, *Susceptibility of silver resistant bacteria to silver containing wound dressings*. Burns, 2007. **33**(1).
59. Norman, N.C., *Chemistry of arsenic, antimony, and bismuth*. 1st ed. 1998: Springer Netherlands.
60. Domenico, P., et al., *Activities of Bismuth Thiols against Staphylococci and Staphylococcal Biofilms*. Antimicrobial Agents and Chemotherapy, 2001. **45**(5): p. 1417.
61. Tegos, G., et al., *Multidrug Pump Inhibitors Uncover Remarkable Activity of Plant Antimicrobials*. Antimicrobial Agents and Chemotherapy, 2002. **46**(10): p. 3133.
62. Keogan, D. and D. Griffith, *Current and Potential Applications of Bismuth-Based Drugs*. Molecules, 2014. **19**(9): p. 15258.
63. He, X., et al., *Bismuth-Induced Inactivation of Ferric Uptake Regulator from Helicobacter pylori*. Inorganic chemistry, 2017. **56**(24): p. 15041.
64. Porcheron, G. and C.M. Dozois, *Interplay between iron homeostasis and virulence: Fur and RyhB as major regulators of bacterial pathogenicity*. Vet Microbiol, 2015. **179**(1-2): p. 2-14.
65. Wang, R., et al., *Bismuth antimicrobial drugs serve as broad-spectrum metallo- $\beta$ -lactamase inhibitors*. Nature Communications, 2018. **9**(1): p. 439.
66. Stephens, L.J., et al., *Is Bismuth Really the "Green" Metal? Exploring the Antimicrobial Activity and Cytotoxicity of Organobismuth Thiolate Complexes*. Inorg. Chem, 2020. **59**(6): p. 3494-3508.
67. Werrett, M., et al., *Bismuth Phosphinates in Bi-Nanocellulose Composites and their Efficacy towards Multi-Drug Resistant Bacteria*. Chemistry- A European Journal, 2018.
68. Herdman, M.E., et al., *Impact of structural changes in heteroleptic bismuth phosphinates on their antibacterial activity in Bi-nanocellulose composites*. Dalton Trans., 2020. **49**(22): p. 7341-7354.
69. Zhang, Z. and V.E. Wagner, *Antimicrobial coatings and modifications on medical devices*. 2017, Cham: Cham : Springer.
70. Lagaron, J.M., M.J. Ocio, and A. Lopez-Rubio, *Antimicrobial Polymers*. 2011, Hoboken, UNITED STATES: Wiley.
71. Vimala, K., et al., *Controlled silver nanoparticles synthesis in semi-hydrogel networks of poly(acrylamide) and carbohydrates: A rational methodology for antibacterial application*. Carbohydrate Polymers, 2009. **75**(3): p. 463-471.

72. Jiang, B., et al., *Investigation of lysine acrylate containing poly(N-isopropylacrylamide) hydrogels as wound dressings in normal and infected wounds*. Journal of Biomedical Materials Research Part B: Applied Biomaterials, 2012. **100B**(3): p. 668-676.
73. Siró, I. and D. Plackett, *Microfibrillated cellulose and new nanocomposite materials: a review*. Cellulose, 2010. **17**(3): p. 459-494.
74. Xu, Q., et al., *A facile route to prepare cellulose-based films*. Carbohydrate Polymers, 2016. **149**: p. 274-281.
75. O'Sullivan, A.C., *Cellulose: the structure slowly unravels*. Cellulose, 1997. **4**(3): p. 173-207.
76. Klemm, D., et al., *Cellulose: Fascinating Biopolymer and Sustainable Raw Material*. Angewandte Chemie International Edition, 2005. **44**(22): p. 3358-3393.
77. Lavoine, N., et al., *Microfibrillated cellulose - its barrier properties and applications in cellulosic materials: a review*. Carbohydr Polym, 2012. **90**(2): p. 735-64.
78. Ioelovich, M., *Characterization of Various Kinds of Nanocellulose*, in *Handbook of Nanocellulose and Cellulose Nanocomposites*. 2017, Wiley-VCH Verlag GmbH & Co. KGaA. p. 51-100.
79. Varanasi, S. and W.J. Batchelor, *Rapid preparation of cellulose nanofibre sheet*. Cellulose, 2013. **20**(1): p. 211-215.
80. Kumar, V., et al., *Comparison of nano- and microfibrillated cellulose films*. Cellulose, 2014. **21**(5): p. 3443-3456.
81. Beneventi, D., E. Zeno, and D. Chaussy, *Rapid nanopaper production by spray deposition of concentrated microfibrillated cellulose slurries*. ATIP. Association Technique de L'Industrie Papetiere, 2016. **70**(2): p. 6-14.
82. Krol, L.F., et al., *Microfibrillated cellulose-SiO<sub>2</sub> composite nanopapers produced by spray deposition*. Journal of Materials Science, 2015. **50**(11): p. 4095-4103.
83. Beneventi, D., et al., *Highly Porous Paper Loading with Microfibrillated Cellulose by Spray Coating on Wet Substrates*. Industrial & Engineering Chemistry Research, 2014. **53**(27): p. 10982-10989.
84. Shanmugam, K., et al., *Rapid preparation of smooth nanocellulose films using spray coating*. Cellulose, 2017. **24**(7): p. 2669.
85. Nadeem, H., et al., *An energy efficient production of high moisture barrier nanocellulose/carboxymethyl cellulose films via spray-deposition technique*. Carbohydrate Polymers, 2020. **250**: p. 116911.
86. Lavoine, N., et al., *Antibacterial paperboard packaging using microfibrillated cellulose*. J Food Sci Technol, 2015. **52**(9): p. 5590-600.

87. Kumar, V., et al., *Substrate role in coating of microfibrillated cellulose suspensions*. Cellulose, 2017. **24**(3): p. 1247-1260.
88. Shanmugam, K., et al., *Flexible spray coating process for smooth nanocellulose film production*. Cellulose (London), 2018. **25**(3): p. 1725-1741.
89. Peng, Y.C., et al., *Influence of drying method on the material properties of nanocellulose I: thermostability and crystallinity*. Cellulose, 2013. **20**(5): p. 2379-2392.
90. Peng, Y.C., D.J. Gardner, and Y.S. Han, *Drying cellulose nanofibrils: in search of a suitable method*. Cellulose, 2012. **19**(1): p. 91-102.
91. Shanmugam, K., et al., *Engineering surface roughness of nanocellulose film via spraying to produce smooth substrates*. Colloids and surfaces. A, Physicochemical and engineering aspects, 2020. **589**: p. 124396.
92. Gan, P.G., et al., *Thermal properties of nanocellulose-reinforced composites: A review*. Journal of applied polymer science, 2020. **137**(11): p. 48544-n/a.
93. TAPPI, *Tensile properties of paper and paperboard (using constant rate of elongation apparatus) (T494 om-01) 2006*, Technical Association of the Pulp and Paper Industry.
94. Machmud, M., et al., *Alternative Fiber Sources from Gracilaria Sp and Eucheuma Cottonii for Papermaking*. International Journal of Science and Engineering, 2013. **6**.
95. Bideau, B., et al., *Mechanical and antibacterial properties of a nanocellulose-polypyrrole multilayer composite*. Mater Sci Eng C Mater Biol Appl, 2016. **69**: p. 977-84.
96. Fukuzumi, H., et al., *Transparent and High Gas Barrier Films of Cellulose Nanofibers Prepared by TEMPO-Mediated Oxidation*. Biomacromolecules, 2009. **10**(1): p. 162-165.
97. Rodionova, G., et al., *Surface chemical modification of microfibrillated cellulose: improvement of barrier properties for packaging applications*. Cellulose, 2011. **18**(1): p. 127-134.
98. Farah, S., D.G. Anderson, and R. Langer, *Physical and mechanical properties of PLA, and their functions in widespread applications — A comprehensive review*. Adv Drug Deliv Rev, 2016. **107**: p. 367-392.
99. Karayannidis, G.P., et al., *Thermal behavior and tensile properties of poly(ethylene terephthalate-co-ethylene isophthalate)*. Journal of Applied Polymer Science, 2000. **78**(1): p. 200-207.
100. Ávila Córdoba, L., et al., *Effects on Mechanical Properties of Recycled PET in Cement-Based Composites*. International journal of polymer science, 2013. **2013**: p. 1-6.
101. Abd Alsalam, A., *Comparison of the Characteristics of LDPE : PP and HDPE : PP polymer blends*. Modern Applied Science, 2013.

102. Jokar, M., et al., *Melt Production and Antimicrobial Efficiency of Low-Density Polyethylene (LDPE)-Silver Nanocomposite Film*. Food and Bioprocess Technology, 2012. **5**(2): p. 719-728.
103. Mahmoud, M.E., et al., *Design and testing of high-density polyethylene nanocomposites filled with lead oxide micro- and nano-particles: Mechanical, thermal, and morphological properties*. Journal of applied polymer science, 2019. **136**(31): p. 47812-n/a.
104. Nair, S.S., et al., *High performance green barriers based on nanocellulose*. Sustainable Chemical Processes, 2014. **2**(1): p. 23.
105. Spence, K., et al., *The effect of chemical composition on microfibrillar cellulose films from wood pulps: water interactions and physical properties for packaging applications*. Cellulose, 2010. **17**(4): p. 835-848.
106. Shanmugam, K., et al., *Nanocellulose films as air and water vapour barriers: A recyclable and biodegradable alternative to polyolefin packaging*. Sustainable Materials and Technologies, 2019. **22**: p. e00115.
107. El-Samahy, M.A., et al., *Synthesis of hybrid paper sheets with enhanced air barrier and antimicrobial properties for food packaging*. Carbohydrate Polymers, 2017. **168**(Supplement C): p. 212-219.
108. Lavoine, N., et al., *Active bio-based food-packaging: Diffusion and release of active substances through and from cellulose nanofiber coating toward food-packaging design*. Carbohydr Polym, 2016. **149**: p. 40-50.
109. Wang, Z., et al., *Preparation of nanocellulose/filter paper (NC/FP) composite membranes for high-performance filtration*. Cellulose, 2018. **26**(2): p. 1183-1194.
110. Onur, A., et al., *Engineering cellulose fibre inorganic composites for depth filtration and adsorption*. Separation and Purification Technology, 2018. **203**: p. 209-216.
111. Abou-Yousef, H. and S. Kamel, *High efficiency antimicrobial cellulose-based nanocomposite hydrogels*. Journal of Applied Polymer Science, 2015. **132**(31).
112. Kopecek, J., *Hydrogels: From soft contact lenses and implants to self-assembled nanomaterials*. Journal of Polymer Science Part A: Polymer Chemistry, 2009. **47**(22): p. 5929-5946.
113. Xia, Z., et al., *Structure and relaxation in cellulose hydrogels*. Journal of Applied Polymer Science, 2015. **132**(24): p. n/a-n/a.
114. Curvello, R., V.S. Raghuwanshi, and G. Garnier, *Engineering nanocellulose hydrogels for biomedical applications*. Advances in Colloid and Interface Science, 2019.
115. Shen, X., et al., *Hydrogels based on cellulose and chitin: fabrication, properties, and applications*. Green Chemistry, 2016. **18**(1): p. 53-75.

116. Masruchin, N., B.-D. Park, and V. Causin, *Dual-responsive composite hydrogels based on TEMPO-oxidized cellulose nanofibril and poly( N -isopropylacrylamide) for model drug release*. Cellulose, 2018. **25**(1): p. 485-502.
117. Mendoza, L., et al., *Nanocellulose for gel electrophoresis*. Journal of Colloid and Interface Science, 2019. **540**: p. 148-154.
118. Navarra, M.A., et al., *Synthesis and Characterization of Cellulose-Based Hydrogels to Be Used as Gel Electrolytes*. Membranes (Basel), 2015. **5**(4): p. 810-23.
119. Kamoun, E.A., E.-R.S. Kenawy, and X. Chen, *A review on polymeric hydrogel membranes for wound dressing applications: PVA-based hydrogel dressings*. Journal of Advanced Research, 2017. **8**(3): p. 217-233.
120. Saito, T., et al., *Cellulose nanofibers prepared by TEMPO-mediated oxidation of native cellulose*. Biomacromolecules, 2007. **8**(8): p. 2485.
121. Mendoza, L., et al., *Gelation mechanism of cellulose nanofibre gels: A colloids and interfacial perspective*. Journal of Colloid and Interface Science, 2018. **509**(Supplement C): p. 39-46.
122. Isogai, A., T. Saito, and H. Fukuzumi, *TEMPO-oxidized cellulose nanofibers*. Nanoscale, 2011. **3**(1): p. 71-85.
123. Gun'ko, V.M., I.N. Savina, and S.V. Mikhalovsky, *Properties of Water Bound in Hydrogels*. Gels, 2017. **3**(4).
124. Grignon, J. and A.M. Scallan, *Effect of pH and neutral salts upon the swelling of cellulose gels*. Journal of applied polymer science, 1980. **25**(12): p. 2829-2843.
125. Hossain, L., et al., *Structure and swelling of cross-linked nanocellulose foams*. J Colloid Interface Sci, 2020. **568**: p. 234-244.
126. Mendoza, L., et al., *Carboxylated nanocellulose foams as superabsorbents*. J Colloid Interface Sci, 2019. **538**: p. 433-439.
127. Jawaid, M.e. and F.e. Mohammad, *Nanocellulose and nanohydrogel matrices : biotechnological and biomedical applications*. 2017: Weinheim, Germany : Wiley-VCH.
128. Lopez-Sanchez, P., et al., *Diffusion of macromolecules in self-assembled cellulose/hemicellulose hydrogels*. Soft Matter, 2015. **11**(20): p. 4002-10.
129. Salomé Veiga, A. and J.P. Schneider, *Antimicrobial hydrogels for the treatment of infection*. 2013. p. 637-644.
130. Alexandrescu, L., et al., *Cytotoxicity tests of cellulose nanofibril-based structures*. Cellulose, 2013. **20**(4): p. 1765-1775.
131. Basu, A., et al., *In Vitro and in Vivo Evaluation of the Wound Healing Properties of Nanofibrillated Cellulose Hydrogels*. ACS Applied Bio Materials, 2018. **1**(6): p. 1853-1863.

132. Lopes, V.R., et al., *In vitro biological responses to nanofibrillated cellulose by human dermal, lung and immune cells: surface chemistry aspect*. Particle and Fibre Technology, 2017. **14**(1).
133. Inamuddin, *Green Polymer Composites Technology : Properties and Applications*. 2016, Boca Raton, United Kingdom: Chapman and Hall/CRC.
134. Han, J.H., *Antimicrobial food packaging*, in *Novel Food Packaging Techniques*. 2003. p. 50-70.
135. Ozdemir, M. and J.D. Floros, *Active food packaging technologies*. Crit Rev Food Sci Nutr, 2004. **44**(3): p. 185-93.
136. Biji, K.B., et al., *Smart packaging systems for food applications: a review*. J Food Sci Technol, 2015. **52**(10): p. 6125-35.
137. Appendini, P. and J.H. Hotchkiss, *Review of antimicrobial food packaging*. Innovative Food Science & Emerging Technologies, 2002. **3**(2): p. 113-126.
138. Hoseinnejad, M., S.M. Jafari, and I. Katouzian, *Inorganic and metal nanoparticles and their antimicrobial activity in food packaging applications*. Crit Rev Microbiol, 2018. **44**(2): p. 161-181.
139. Yu, H.Y., et al., *Fabrication of multifunctional cellulose nanocrystals/poly(lactic acid) nanocomposites with silver nanoparticles by spraying method*. Carbohydr Polym, 2016. **140**: p. 209-19.
140. Oun, A.A., S. Shankar, and J.W. Rhim, *Multifunctional nanocellulose/metal and metal oxide nanoparticle hybrid nanomaterials*. Crit Rev Food Sci Nutr, 2020. **60**(3): p. 435-460.
141. Nguyen, V.T., M.J. Gidley, and G.A. Dykes, *Potential of a nisin-containing bacterial cellulose film to inhibit Listeria monocytogenes on processed meats*. Food Microbiol, 2008. **25**(3): p. 471-8.
142. Spieser, H., et al., *Cellulose nanofibrils and silver nanowires active coatings for the development of antibacterial packaging surfaces*. Carbohydrate Polymers, 2020. **240**: p. 116305.
143. Wang, W., et al., *Properties and antimicrobial activity of polyvinyl alcohol-modified bacterial nanocellulose packaging films incorporated with silver nanoparticles*. Food Hydrocolloids, 2020. **100**.
144. Gopiraman, M., et al., *Silver coated anionic cellulose nanofiber composites for an efficient antimicrobial activity*. Carbohydr Polym, 2016. **149**: p. 51-9.
145. Shankar, S., A.A. Oun, and J.W. Rhim, *Preparation of antimicrobial hybrid nanomaterials using regenerated cellulose and metallic nanoparticles*. Int J Biol Macromol, 2018. **107**(Pt A): p. 17-27.

146. Yu, H., et al., *Reinforcement of biodegradable poly(3-hydroxybutyrate-co-3-hydroxyvalerate) with cellulose nanocrystal/silver nanohybrids as bifunctional nanofillers*. J Mater Chem B, 2014. **2**(48): p. 8479-8489.
147. Fortunati, E., et al., *Ternary PVA nanocomposites containing cellulose nanocrystals from different sources and silver particles: part II*. Carbohydr Polym, 2013. **97**(2): p. 837-48.
148. Lefatshe, K., C.M. Muiva, and L.P. Kebaabetswe, *Extraction of nanocellulose and in-situ casting of ZnO/cellulose nanocomposite with enhanced photocatalytic and antibacterial activity*. Carbohydr Polym, 2017. **164**: p. 301-308.
149. Li, Z.H., et al., *ZnO Deposit on O-ZrP as Paper Filler and its Potential Antibacterial Property*. Bioresources, 2015. **10**(3): p. 6001-6013.
150. Shahmohammadi Jebel, F. and H. Almasi, *Morphological, physical, antimicrobial and release properties of ZnO nanoparticles-loaded bacterial cellulose films*. Carbohydr Polym, 2016. **149**: p. 8-19.
151. Almasi, H., P. Jafarzadeh, and L. Mehryar, *Fabrication of novel nanohybrids by impregnation of CuO nanoparticles into bacterial cellulose and chitosan nanofibers: Characterization, antimicrobial and release properties*. Carbohydr Polym, 2018. **186**: p. 273-281.
152. Chaudhry, Q., et al., *Assessment of Current and Projected Applications of Nanotechnology for Food Contact Materials in Relation to Consumer Safety and Regulatory Implications*, F.S. Agency, Editor. 2008.
153. Echegoyen, Y. and C. Nerín, *Nanoparticle release from nano-silver antimicrobial food containers*. Food and Chemical Toxicology, 2013. **62**: p. 16-22.
154. Huang, Y., et al., *Nanosilver Migrated into Food-Simulating Solutions from Commercially Available Food Fresh Containers*. Packaging Technology and Science, 2011. **24**(5): p. 291-297.
155. Pezzuto, A., et al., *Food safety concerns deriving from the use of silver based food packaging materials*. Frontiers in microbiology, 2015. **6**: p. 1109-1109.
156. Cao, H., *Silver nanoparticles for antibacterial devices : biocompatibility and toxicity*. 2017: Boca Raton : CRC Press, Taylor & Francis Group.
157. Agyingi, E., S. Maggelakis, and D. Ross, *The Effect of Bacteria on Epidermal Wound Healing*. Mathematical Modelling of Natural Phenomena, 2010. **5**(3): p. 28-39.
158. Rajendran, S., *Chronic wound care: synthetic and natural antimicrobials*. Nursing And Residential Care, 2018. **20**(8): p. 370-378.
159. Ashtikar, M. and M. Wacker, *Nanopharmaceuticals for wound healing –Lost in translation?* Vol. 129. 2018.

160. Percival, S.L. and K.F. Cutting, *Microbiology of wounds*. 2010, Boca Raton: Boca Raton : Taylor & Francis.
161. *Prioritization of pathogens to guide discovery, research and development of new antibiotics for drug resistant bacterial infections, including tuberculosis*. 2017: Geneva: World Health Organization.
162. Thabet, L., et al., *Bacteriological profile and antibiotic resistance of bacteria isolates in a burn department*. La Tunisie medicale, 2008. **86**(12): p. 1051-1054.
163. Cook, N., *Methicillin-resistant Staphylococcus aureus versus the burn patient*. Burns, 1998. **24**(2): p. 91-98.
164. Norbury, W., et al., *Infection in Burns*. Surgical infections, 2016. **17**(2): p. 250-255.
165. Andrade, C., et al., *Methicillin-resistant Staphylococcus aureus: An assessment of environmental contamination in a burn center*. American Journal of Infection Control, 2009. **37**(6): p. 515-517.
166. Rattanuengsrikul, V., N. Pimpha, and P. Supaphol, *Development of Gelatin Hydrogel Pads as Antibacterial Wound Dressings*. Macromolecular Bioscience, 2009. **9**(10): p. 1004-1015.
167. Parsons, D., et al., *Silver antimicrobial dressings in wound management: A comparison of antibacterial, physical and chemical characteristics*. Wounds: a compendium of clinical research and practice, 2005. **17**: p. 222-232.
168. Yin, H.Q., R. Langford, and R.E. Burrell, *Comparative evaluation of the antimicrobial activity of ACTICOAT antimicrobial barrier dressing*. The Journal of burn care & rehabilitation, 1999. **20**(3): p. 195.
169. Heggors, J.P., et al., *Acticoat versus Silverlon: The Truth: 150*. Journal of Burn Care & Rehabilitation, 2002. **23**: p. S115.
170. Castellano, J.J., et al., *Comparative evaluation of silver-containing antimicrobial dressings and drugs*. International Wound Journal, 2007. **4**(2): p. 139-140.
171. Soriano, J.V., et al., *Effects of an activated charcoal silver dressing on chronic wounds with no clinical signs of infection*. Journal of Wound Care, 2004. **13**(10): p. 419-423.
172. Caruso, M.D., et al., *Randomized Clinical Study of Hydrofiber Dressing With Silver or Silver Sulfadiazine in the Management of Partial-Thickness Burns*. Journal of Burn Care & Research, 2006. **27**(3): p. 298-309.
173. Finnegan, S. and S.L. Percival, *Clinical and Antibiofilm Efficacy of Antimicrobial Hydrogels*. Adv Wound Care (New Rochelle), 2015. **4**(7): p. 398-406.
174. Beitz, A.J., et al., *A polymeric membrane dressing with antinociceptive properties: analysis with a rodent model of stab wound secondary hyperalgesia*. J Pain, 2004. **5**(1): p. 38-47.

175. Benskin, L.L., *PolyMem® Wic® Silver® Rope: A Multifunctional Dressing for Decreasing Pain, Swelling, and Inflammation*. Adv Wound Care (New Rochelle), 2012. **1**(1): p. 44-47.
176. Meaume, S., et al., *Evaluation of a silver-releasing hydroalginate dressing in chronic wounds with signs of local infection*. Journal of wound care, 2005. **14**(9): p. 411.
177. Karlnoski, R., et al., *Reduction in Central Line-Associated Bloodstream Infections Correlated With the Introduction of a Novel Silver-Plated Dressing for Central Venous Catheters and Maintained for 6 Years*. J Intensive Care Med, 2019. **34**(7): p. 544-549.
178. Cheng, G., et al., *Integrated Antimicrobial and Nonfouling Hydrogels to Inhibit the Growth of Planktonic Bacterial Cells and Keep the Surface Clean*. Langmuir, 2010. **26**(13): p. 10425-10428.
179. Halpenny, G.M., et al., *Characterization of pHEMA-based hydrogels that exhibit light-induced bactericidal effect via release of NO*. Journal of Materials Science: Materials in Medicine, 2009. **20**(11): p. 2353.
180. Tsou, T.-L., et al., *Poly(2-hydroxyethyl methacrylate) wound dressing containing ciprofloxacin and its drug release studies*. Journal of Materials Science: Materials in Medicine, 2005. **16**(2): p. 95-100.
181. De Giglio, E., et al., *Ciprofloxacin-modified electrosynthesized hydrogel coatings to prevent titanium-implant-associated infections*. Acta Biomaterialia, 2011. **7**(2): p. 882-891.
182. Marchesan, S., et al., *Self-assembly of ciprofloxacin and a tripeptide into an antimicrobial nanostructured hydrogel*. Biomaterials, 2013. **34**(14): p. 3678-3687.
183. Yu, H., et al., *Preparation and antibacterial effects of PVA-PVP hydrogels containing silver nanoparticles*. Journal of Applied Polymer Science, 2007. **103**(1): p. 125-133.
184. Zan, X., et al., *Covalently Attached, Silver-Doped Poly(vinyl alcohol) Hydrogel Films on Poly(L-lactic acid)*. Biomacromolecules, 2010. **11**(4): p. 1082-1088.
185. Singh, R. and D. Singh, *Radiation synthesis of PVP/alginate hydrogel containing nanosilver as wound dressing*. Journal of Materials Science: Materials in Medicine, 2012. **23**(11): p. 2649-2658.
186. Thomas, V., et al., *A versatile strategy to fabricate hydrogel–silver nanocomposites and investigation of their antimicrobial activity*. Journal of Colloid And Interface Science, 2007. **315**(1): p. 389-395.
187. Murali Mohan, Y., et al., *Controlling of silver nanoparticles structure by hydrogel networks*. Journal of Colloid and Interface Science, 2010. **342**(1): p. 73-82.
188. Varaprasad, K., et al., *Hydrogel–silver nanoparticle composites: A new generation of antimicrobials*. Journal of Applied Polymer Science, 2010. **115**(2): p. 1199-1207.

189. Tepe, Y., et al., *Acrylamide in Environmental Water: A Review on Sources, Exposure, and Public Health Risks*. Exposure and health, 2019. **11**(1): p. 3-12.
190. Hebeish, A., et al., *Development of CMC hydrogels loaded with silver nano-particles for medical applications*. Carbohydrate Polymers, 2013. **92**(1): p. 407-413.
191. Resmi, R., et al., *Synthesis and characterization of silver nanoparticle incorporated gelatin-hydroxypropyl methacrylate hydrogels for wound dressing applications*. Journal of Applied Polymer Science, 2017. **134**(10).
192. De France, K., T. Hoare, and E. Cranston, *Review of Hydrogels and Aerogels Containing Nanocellulose*, in *Chem. Mat.* 2017. p. 4609-4631.
193. Laçın, N.T., *Development of biodegradable antibacterial cellulose based hydrogel membranes for wound healing*. International Journal of Biological Macromolecules, 2014. **67**(Supplement C): p. 22-27.
194. Wei, B., G. Yang, and F. Hong, *Preparation and evaluation of a kind of bacterial cellulose dry films with antibacterial properties*. Carbohydrate Polymers, 2011. **84**(1): p. 533-538.
195. Hakkarainen, T., et al., *Nanofibrillar cellulose wound dressing in skin graft donor site treatment*. Journal of Controlled Release, 2016. **244**: p. 292-301.
196. Chinga-Carrasco, G. and K. Syverud, *Pretreatment-dependent surface chemistry of wood nanocellulose for pH-sensitive hydrogels*. Journal of Biomaterials Applications, 2014. **29**(3): p. 423-432.
197. Liu, Y., et al., *A physically crosslinked polydopamine/nanocellulose hydrogel as potential versatile vehicles for drug delivery and wound healing*. Carbohydrate Polymers, 2018. **188**: p. 27-36.
198. Basu, A., et al., *Ion-crosslinked wood-derived nanocellulose hydrogels with tunable antibacterial properties: Candidate materials for advanced wound care applications*. Carbohydrate Polymers, 2018. **181**: p. 345-350.
199. Liu, R., et al., *Antibacterial and hemostatic hydrogel via nanocomposite from cellulose nanofibers*. Carbohydrate Polymers, 2018. **195**: p. 63-70.
200. Maneerung, T., S. Tokura, and R. Rujiravanit, *Impregnation of silver nanoparticles into bacterial cellulose for antimicrobial wound dressing*. Carbohydrate Polymers, 2008. **72**(1): p. 43-51.
201. Wu, J., et al., *In situ synthesis of silver-nanoparticles/bacterial cellulose composites for slow-released antimicrobial wound dressing*. Carbohydrate Polymers, 2014. **102**: p. 762.
202. Marques Fortes, A., et al., *In Situ Synthesis of Silver Nanoparticles in a Hydrogel of Carboxymethyl Cellulose with Phthalated-Cashew Gum as a Promising Antibacterial and Healing Agent*. International Journal of Molecular Sciences, 2017. **18**(11): p. 2399.

203. *Water for life : making it happen*, in *WHO/UNICEF Joint Monitoring Programme 2005*. 2005, World Health Organization, Geneva.
204. *Drinking Water*. World Health Organization, Geneva 2019 [cited 2019 8 July 2019]; Available from: <https://www.who.int/en/news-room/fact-sheets/detail/drinking-water>.
205. Jain, S., et al., *Enhanced antibacterial profile of nanoparticle impregnated cellulose foam filter paper for drinking water filtration*. Carbohydrate Polymers, 2018. **202**: p. 219-226.
206. Thompson, T., et al., *Chemical safety of drinking-water: Assessing priorities for risk management*, in *World Health Organization, Geneva*. 2007.
207. Dankovich, T.A. and J.A. Smith, *Incorporation of copper nanoparticles into paper for point-of-use water purification*. Water Research, 2014. **63**: p. 245-251.
208. Praveena, S. and A. Aris, *Application of Low-Cost Materials Coated with Silver Nanoparticle as Water Filter in Escherichia coli Removal*. Water Quality, Exposure and Health, 2015. **7**(4): p. 617-625.
209. Cui, Z.F., Y. Jiang, and R.W. Field, *Fundamentals of Pressure-Driven Membrane Separation Processes*, in *Membrane Technology*. 2010. p. 1-18.
210. Mansouri, J., S. Harrisson, and V. Chen, *Strategies for controlling biofouling in membrane filtration systems: challenges and opportunities*. Journal of Materials Chemistry, 2010. **20**(22).
211. Li, Q., et al., *Antimicrobial nanomaterials for water disinfection and microbial control: potential applications and implications*. Water Res, 2008. **42**(18): p. 4591-602.
212. Zodrow, K., et al., *Polysulfone ultrafiltration membranes impregnated with silver nanoparticles show improved biofouling resistance and virus removal*. Water Res, 2009. **43**(3): p. 715-23.
213. Fernández, J.G., et al., *Development of nitrocellulose membrane filters impregnated with different biosynthesized silver nanoparticles applied to water purification*. Talanta, 2016. **146**: p. 237-243.
214. Praveena, S., K. Karuppiyah, and L. Than, *Potential of cellulose paper coated with silver nanoparticles: a benign option for emergency drinking water filter*. Cellulose, 2018. **25**(4): p. 2647-2658.
215. Reza, I., et al., *Production of antibacterial filter paper from wood cellulose*. BioResources, 2011. **6**(1): p. 891-900.
216. Huang, J., et al., *Performance of ceramic disk filter coated with nano ZnO for removing Escherichia coli from water in small rural and remote communities of developing regions.(Report)*. Environmental Pollution, 2018. **238**: p. 52.

217. Dankovich, T.A., et al., *Inactivation of bacteria from contaminated streams in Limpopo, South Africa by silver- or copper-nanoparticle paper filters*. Environmental Science: Water Research & Technology, 2016. **2**(1): p. 85-96.
218. Qin, C., et al., *Deactivation of E. coli in water using Fe<sup>3+</sup>-saturated montmorillonite impregnated filter paper*. Science of the Total Environment, 2019. **652**: p. 643-650.
219. Qu, X., P.J.J. Alvarez, and Q. Li, *Applications of nanotechnology in water and wastewater treatment*. Water research, 2013. **47**(12): p. 3931.
220. *Silver as a drinking-water disinfectant*, in *Alternative drinking-water disinfectants: bromine, iodine and silver*. 2018, World Health Organization, Geneva.
221. Ling, S., et al., *Biopolymer nanofibrils: Structure, modeling, preparation, and applications*. Progress in Polymer Science, 2018. **85**: p. 1-56.
222. Voisin, H., et al., *Nanocellulose-Based Materials for Water Purification*. Nanomaterials (Basel), 2017. **7**(3).
223. Metreveli, G., et al., *A Size-Exclusion Nanocellulose Filter Paper for Virus Removal*. Advanced Healthcare Materials, 2014. **3**(10): p. 1546-1550.
224. Gustafsson, S., et al., *Mille-feuille paper: a novel type of filter architecture for advanced virus separation applications*. Materials Horizons, 2016. **3**(4): p. 320-327.
225. Van der Bruggen, B., *Microfiltration, ultrafiltration, nanofiltration, reverse osmosis, and forward osmosis*, in *Fundamental Modelling of Membrane Systems*. 2018. p. 25-70.
226. Gustafsson, S. and A. Mihranyan, *Strategies for Tailoring the Pore-Size Distribution of Virus Retention Filter Papers*. ACS Appl Mater Interfaces, 2016. **8**(22): p. 13759-67.
227. Ma, H., et al., *Ultra-fine cellulose nanofibers: new nano-scale materials for water purification*. Journal of Materials Chemistry, 2011. **21**(21).

---

---

## **CHAPTER 2**

**BISMUTH PHOSPHINATE INCORPORATED NANOCELLULOSE SHEETS WITH  
ANTIMICROBIAL AND BARRIER PROPERTIES FOR PACKAGING  
APPLICATIONS**

---

---

THIS PAGE HAS BEEN INTENTIONALLY LEFT BLANK

## PREFACE

Although antimicrobial packaging materials using nanocellulose has been studied previously, bismuth based compounds for such applications have not been explored. The *bis*-phosphinato bismuth (III) complex has low solubility and thus can be a useful antimicrobial agent incorporate into materials. This chapter studies the development and characterisation of *bis*-phosphinato bismuth complex loaded nanocellulose composites. This chapter introduces the concept of using such composites as active packaging materials and addresses the gaps in understanding the effect of the complex on barrier and mechanical properties of nanocellulose sheets. Herein, composites with pure cellulose were studied to address the first research objective of this thesis.

THIS PAGE HAS BEEN INTENTIONALLY LEFT BLANK

---

**CHAPTER 2: BISMUTH PHOSPHINATE INCORPORATED NANOCELLULOSE SHEETS WITH ANTIMICROBIAL AND BARRIER PROPERTIES FOR PACKAGING APPLICATIONS**

<b>2.1.</b>	<b>Abstract.....</b>	<b>75</b>
<b>2.2.</b>	<b>Keywords .....</b>	<b>76</b>
<b>2.3.</b>	<b>Introduction.....</b>	<b>76</b>
<b>2.4.</b>	<b>Materials and Method .....</b>	<b>78</b>
2.4.1.	Materials .....	78
2.4.2.	MFC Suspension Preparation .....	79
2.4.3.	Sheet preparation .....	79
2.4.4.	Characterization .....	80
2.4.4.1.	ICP-OES Analysis .....	80
2.4.4.2.	Bi-complex characterization .....	81
2.4.4.3.	SEM Imaging .....	81
2.4.5.	Material performance.....	81
2.4.5.1.	Antimicrobial Test .....	81
2.4.5.2.	Duration of antimicrobial action:.....	82
2.4.5.3.	Physical and mechanical properties .....	82
2.4.5.4.	Water vapor permeability .....	82
<b>2.5.</b>	<b>Results and Discussion.....</b>	<b>83</b>
2.5.1.	Characterisation .....	83
2.5.1.1.	ICP-OES Analysis: .....	83
2.5.1.2.	Bi-complex characterization .....	83
2.5.1.3.	SEM Imaging .....	84
2.5.2.	Material performance.....	87
2.5.2.1.	Antibacterial Activity .....	87
2.5.2.2.	Antifungal Activity .....	89
2.5.2.3.	Duration of antimicrobial action.....	90
2.5.2.4.	Physical and Mechanical properties.....	91
2.5.2.5.	Water vapour permeability .....	93
<b>2.6.</b>	<b>Conclusion .....</b>	<b>95</b>
<b>2.7.</b>	<b>Acknowledgements .....</b>	<b>96</b>
<b>2.8.</b>	<b>References.....</b>	<b>96</b>

THIS PAGE HAS BEEN INTENTIONALLY LEFT BLANK

**BISMUTH PHOSPHINATE INCORPORATED NANOCELLULOSE SHEETS WITH  
ANTIMICROBIAL AND BARRIER PROPERTIES FOR PACKAGING  
APPLICATIONS**

Maisha Maliha<sup>1</sup>, Megan Herdman<sup>2</sup>, Rajini Brammananth<sup>3</sup>, Michael McDonald<sup>4</sup>, Ross Coppel<sup>3</sup>,  
Melissa Werrett<sup>2</sup>, Philip Andrews<sup>2</sup>, Warren Batchelor<sup>1</sup>

<sup>1</sup>*Bioresource Processing Research Institute of Australia (BioPRIA), Department of Chemical Engineering,  
Monash University, VIC 3800, Australia*

<sup>2</sup>*School of Chemistry, Monash University, VIC 3800, Australia*

<sup>3</sup>*Department of Microbiology, Monash University, VIC 3800, Australia*

<sup>4</sup>*Centre for Geometric Biology, School of Biological Sciences, Monash University, VIC 3800, Australia*

Corresponding author email: warren.batchelor@monash.edu

### **2.1. Abstract**

The incorporation of an organobismuth complex into a nanocellulose matrix to develop a free-standing antimicrobial barrier material was investigated. The non-toxic complex, phenyl bismuth bis(diphenylphosphinato) was used as the additive to impart antimicrobial properties to nanocellulose sheets for the development of paper-based renewable and biodegradable active packaging material. A spraying technique was used to prepare sheets with different loadings of the organobismuth complex and its effects on antimicrobial and barrier properties were studied. Morphological studies of the sheets revealed the overall distribution of the complex throughout the nanocellulose matrix, with occasional clustering behaviour on the surface. Water vapour permeability of the paper sheets increased very slightly with loading of the bismuth complex, but remained in the range acceptable for packaging materials. The physical and mechanical properties of the sheets were also affected by the addition of the bismuth complex in the structure, and hence a trade-off needs to be made between the loading level and the material performance for commercialization. The composite sheets were able to inhibit the growth of bacteria and fungi, including strains of multidrug resistant bacteria. Moreover, the paper showed continued release of the bismuth complex over time with effective lifetime depending on the loading. In summary, this paper describes the preparation and characterization of a sustainable and ecofriendly antimicrobial composite paper, using a poorly soluble bismuth complex dispersed into nanocellulose matrix, which shows the potential to be used as an active packaging material.

## 2.2. Keywords

nanocellulose, bismuth, antimicrobial, packaging, barrier

## 2.3. Introduction

Packaging plays a vital role for most products in terms of consumer safety. Conventional packaging serves only as a barrier layer between the product and the environment and shields it from oxygen, water vapour and other contaminants [1]. Demand for quality assurance and product safety of sensitive items such as food and medical products has led to the emergence of high-value active packaging material that offers enhanced protection [2, 3]. Active packaging has the ability to either interact with the product or alter the environment enclosed within the packaging. Examples include incorporating compounds that can absorb and remove oxygen, ethylene or moisture, or have antimicrobial properties [1]. The latter offers better protection by inhibiting the microbial contamination of the products reducing the risk of deterioration. It can also inhibit contamination of the packaging surface, thus reducing microbial cross-contamination from the packaging. This is an effective strategy with proven improvements in product protection and quality [1, 4]. Antimicrobial active packaging can be obtained by incorporating or immobilizing antibacterial and antifungal agents into the material [3, 5, 6].

The use of metal-based antimicrobial agents, in the form of nanoparticles and compounds, has been increasing [7-9]. This is due to metals often showing greater efficacy and resilience to bacterial resistance than the organic compounds. [10]. Metals such as silver, gold, arsenic, bismuth, antimony, copper, mercury, platinum, palladium, ruthenium, and cobalt, and their compounds have shown antimicrobial activity [11, 12]. This includes inorganic compounds, organometallic complexes, metal organic frameworks and metal nanoparticles [8, 9, 11]. Of them, silver has been the most popular metal used as an antimicrobial additive in materials [6, 13-17]. Silver nanoparticles have been studied as composites with synthetic and natural polymers, such as cellulose, chitosan, gelatine, chitin, and collagen [15, 18, 19]. Silver is also used in various commercial products, including packaging materials, clothing, and healthcare and personal care products. This widespread use of silver has raised concerns about its toxicity for various organisms including humans and environmental accumulation [20-22]. The most severe toxic effect of long-term silver exposure to humans is the condition of blue coloration of the skin, known as argyria. Other harmful effects of soluble silver include damage to liver, kidney and blood cells [23, 24]. Silver nanoparticles can enter the human body through gastrointestinal absorption from food contact materials (e.g. silver based food-packaging) as well as through the respiratory tract [20]. The maximum safe level of lifetime silver intake is only 10g as declared

by the World Health Organization [25]. Studies have shown that silver nanoparticles can migrate into food from silver-based food-packaging materials [26, 27]. It has also been reported that the concentration of silver released into food from a commercial packaging material can exceed the regulatory limits set for food contact materials after 24 days of storage [28]. This suggests there is a necessity to develop new active packaging materials, with more attention to safety and health concerns. In addition, the prolonged use of silver has raised the risk of induction of silver resistance in bacteria [24, 29, 30], a scenario common for many other metal-based antimicrobials [31]. As a result, it has been suggested that silver-based antimicrobials be regulated by governments and reserved for medical uses only [32]. Accordingly, there is a need for a new generation of antimicrobial compounds for use in active packaging for food, medical supplies and other sensitive products.

The purpose of this study is to investigate a poorly soluble bismuth complex as an active species for packaging applications. Many bismuth complexes have been reported to possess antibacterial activity [33-37]. Bismuth has a long history of being used for treating intestinal disorders: Pepto-Bismol (BSS or bismuth subsalicylate) and De-Nol (CBS or colloidal bismuth subcitrate) are used as gastrointestinal treatments, for example traveller's diarrhoea, and are effective agents against the bacteria *Helicobacter pylori* [9, 38, 39]. It is proposed that bismuth works by binding to proteins with metal binding sites, e.g. thiol (cysteine) rich protein structures [40]. Unlike other heavy metals, bismuth displays a low level of toxicity in humans and is non-carcinogenic [36]. Although it is a heavy metal in the pnictide (Gp 15) family, where toxicity is assumed to increase with molecular weight, bismuth is unique in its comparatively low-toxicity [39]. In this paper, a new class of organobismuth complex, phenyl bismuth bis(diphenylphosphinato), has been chosen as the active agent. This has been reported to have little or no toxicity to mammalian cells and has significantly low solubility in water [33]. As a result, in the context of packaging, the risks of migration into the product or into the environment is also greatly reduced.

The technical challenge for applications in active packaging lies in the choice of material that is suitable for use in supporting the antimicrobial agents. In this regard, polymers have been widely used as the carrier matrix for antimicrobial agents to improve their stability and activity due to their macromolecular properties [12]. The most studied materials for antimicrobial films are petroleum based polymers, e.g. polyethylene, polypropylene, polystyrene and polyethylene terephthalate [12, 19]. The packaging industry is also mainly dependant on petroleum-based polymers [2]. Environmental accumulation of plastics, and the resulting impact from plastic pollution, have driven interest in the use of biodegradable polymers such as polylactic acid (PLA), polyglycolic acid (PGA), and more importantly renewable natural biopolymers such as cellulose,

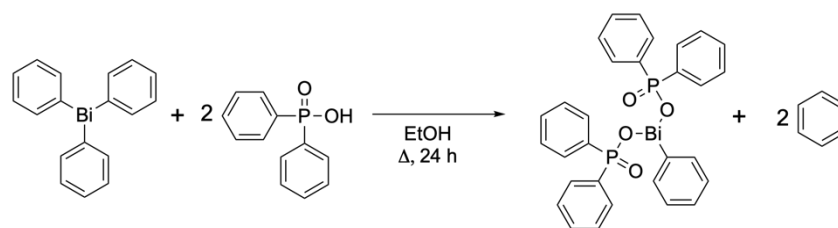
starch, chitosan, alginate, and collagen [12]. Of them, cellulose is the most abundant, biodegradable and renewable, as well as inexpensive and non-toxic [41, 42]. However, while cellulose fibres can be formed into strong and stiff paper-based packaging, the barrier properties are inferior to that of petroleum-based polymers. This limitation can be overcome by breaking down cellulose-containing materials into microfibrils or bundles of microfibrils. The product, which is generally known as nanocellulose, has excellent strength and greatly improved barrier properties when compared to conventional paper [43-45]. Nanocellulose is unique due to its hydrophilicity, biocompatibility and large surface area in addition to all the attributes of nanostructured materials [46, 47]. Nanocellulose films also provide a porous structure for antimicrobial agents to attach to, both physically and chemically [48], making nanocellulose a promising material for active packaging applications. Nanocellulose suspensions can be converted to sheets and films by various methods such as vacuum filtration [49], casting [45], spraying [50-52] or coated on a substrate /base paper [3, 53].

The objective of this study was to incorporate a new class of organobismuth complex, phenyl bismuth bis(diphenylphosphinato), into a nanocellulose matrix for the development of cleaner antimicrobial sheets for active packaging applications. Antimicrobial performance, physical, mechanical and barrier properties of the free-standing nanocellulose paper sheets were thoroughly studied to demonstrate the hypothesis that these materials can potentially serve as an active barrier layer as a standalone sheet or as coatings on other materials.

## **2.4. Materials and Method**

### **2.4.1. Materials**

Microfibrillated Cellulose (MFC) purchased from DAICEL Chemical Industries Limited, Japan (grade Celish KY-100G) was used as the nanocellulose matrix. The MFC used was characterized in previous work by Varanasi et al. to have a mean diameter of 73 nm and an aspect ratio of 147 [54]. Phenyl bismuth bis(diphenylphosphinato) was prepared according to Andrews et al. [33]. Triphenyl bismuth and diphenyl phosphinic acid were mixed in the ratio of 1:2 in ethanol and heated at reflux for 24 hours. The reaction mixture was then filtered, and the insoluble phenyl bismuth bis(diphenylphosphinato) was isolated as a white powder. Following filtration, the complex was washed with hot ethanol to remove all unreacted chemicals and the by-product benzene, after which no further purification was required.



Scheme 1: Chemical reaction for the synthesis of phenyl bismuth bis(diphenylphosphinato)

All analytical data matches that previously reported for the phenyl bismuth bis(diphenylphosphinato) complex (as shown in Scheme 1). The complex is sparingly soluble in water and the solubility as reported is 16.3 kg of water required to dissolve 1 g complex. The complex was also previously reported to have limited solubility in organic solvents like ethanol, dichloromethane, tetrahydrofuran, toluene, and dimethyl sulfoxide (DMSO). Moreover, preliminary toxicity results has been reported previously and it was shown that the complex has no toxic effect on mammalian COS-7 cells at a concentration of 0.5 mg/mL [33].

#### 2.4.2. MFC Suspension Preparation

Phenyl bismuth bis(diphenylphosphinato) was dispersed in small amounts of water using a magnetic stirrer and mixed with the MFC. This was then diluted to make a suspension of 2 wt.% MFC and mixed with a hand blender, followed by disintegration. In the disintegrator, the suspension is contained in a 3 L vessel and a small propeller running at 3000 revolutions separates the fibres from each other. The suspensions were made with varying amount of the bismuth complex. The suspensions were made with target loadings of 5, 2.5, 1.0, 0.5, and 0.1 wt.% of the bismuth complex with respect to the mass of cellulose fibres in the suspension. Thus, the composition was 2 g fibre and 0.1g, 0.05g, 0.02g, 0.01g or 0.002g of the bismuth complex in 100 grams of the 5, 2.5, 1.0, 0.5, and 0.1 wt.% suspensions respectively, the remaining being DI water. The experimental consistency of the suspensions are given in Table A1 in the supplementary information. The suspensions were sprayed immediately without any time delay to ensure no settling of the particles, thus confirming uniform dispersibility in the suspensions.

#### 2.4.3. Sheet preparation

Bismuth(III) phosphinato-MFC composites were prepared using a spraying technique as described by Shanmugam et al. [55]. The composites were made using the suspensions described with target loadings of 5, 2.5, 1.0, 0.5, and 0.1 wt.% of the bismuth. The consistency of the fibres in the suspension was kept constant throughout. The MFC suspension was sprayed onto square stainless steel plates moving on a variable speed conveyor set at  $1 \pm 0.2$  cm/s. The suspension

was sprayed using a Professional Wagner spray system (Model number 117) at 200 bar from a height of  $30 \pm 1$  cm. A spray tip of 517 type was used. After spraying, the MFC on the plates was dried at ambient temperature of  $25^\circ\text{C}$  under constraint at the edges until the sheets separated from the plate and started to roll off at the edges. The sheets were then peeled from the plates and stored in a controlled temperature and humidity condition maintained at  $23^\circ\text{C}$  and 50 % relative humidity.

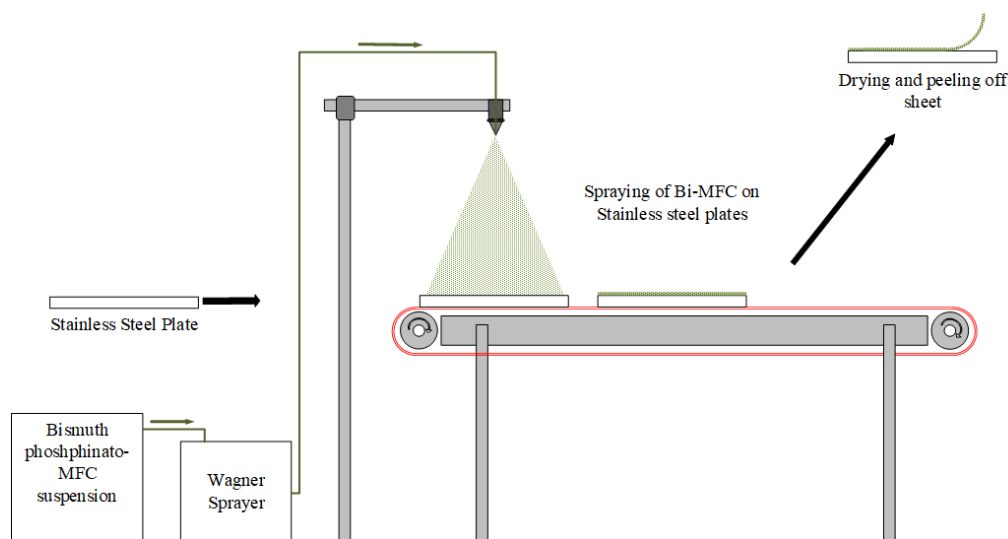


**Figure 1:** Experimental Setup for lab scale spraying of the bismuth (III) phosphinato-MFC suspension onto stainless steel plates

## 2.4.4. Characterization

### 2.4.4.1. ICP-OES Analysis

Weighed samples of the sheets were ashed using a muffle furnace in crucibles. During ashing, the temperature was ramped to  $600^\circ\text{C}$  over three hours and maintained at this temperature for a further three hours. Above  $100^\circ\text{C}$  all moisture, and at about  $525^\circ\text{C}$  all cellulose, is removed. The inorganic complex decomposes at about  $330^\circ\text{C}$ . The bismuth-based residue left in the crucible was dissolved in small quantities of concentrated nitric acid and diluted. This was then analysed using Perkin-Elmer Avio 200 ICP-OES (inductively coupled plasma-optical emission spectrometry). The concentration of the elemental bismuth in the sample solution was analysed by ICP-OES, and back calculated to the amount of bismuth complex in the paper. Each sheet was analysed in triplicate and reported as percentage of the mean mass of the bismuth complex per gram of dry paper  $\pm$  standard deviation.

#### **2.4.4.2. Bi-complex characterization**

The hydrodynamic diameter of the particles was estimated using dynamic light scattering (DLS) using a Nanobrook Omni Particle Size Analyser (Brookhaven Instruments) with a dilute suspension of 0.02 wt.% Bi-complex in Milli-Q water.

#### **2.4.4.3. SEM Imaging**

Scanning Electron Microscope (SEM) imaging of the bismuth(III) phosphinato-MFC sheets was performed using the FEI Nova NanoSEM 450 FEG SEM and FEI Magellan 400 FEG SEM using an accelerating voltage of 5 keV and spot size 2 to study the morphology and distribution of the bismuth complex in the sheets. The samples were prepared by cutting a small piece of the composite sheet and mounting it onto a metal stub secured properly using carbon tape. The samples were coated with a thin conducting layer of Iridium metal.

#### **2.4.5. Material performance**

##### **2.4.5.1. Antimicrobial Test**

The antibacterial and antifungal activities of differently loaded bismuth(III) phosphinato-MFC sheets were measured using disk diffusion assays. The Gram-positive bacteria, viz. *Staphylococcus aureus* (*S. aureus*), Vancomycin-resistant *enterococcus* (VRE), and Methicillin-resistant *Staphylococcus aureus* (MRSA) and Gram-negative bacteria viz. *Escherichia coli* (*E. coli*) and *Pseudomonas aeruginosa* (*P. aeruginosa*) were examined. The fungi used for the tests were the non-pathogenic model organisms *Saccharomyces cerevisiae* YJM789 and *Schizosaccharomyces pombe* H-, which are known for their multidrug resistance [56], as well as the pathogenic species, *Candida albicans* SC5314 and *Candida glabrata* BG99. *C. albicans* BG99 is a pathogenic and virulent strain often used in lab and genomic studies [57]. *C. glabrata* BG99 is the lab model for the third most common cause of fungal infection in humans [58]. The growth media Lysogeny broth (LB) was used for the bacteria *S. aureus*, *E. coli* and *P. aeruginosa* and Brain Heart Infusion (BHI) was used for VRE and MRSA. The LB or BHI agar plates were inoculated with 100µl of the specific stationary phase bacteria. CSM plates were inoculated with 100 ml of a stationary phase overnight culture of the yeasts. The composite sheets was cut into discs of 6 mm using a standard hole punch, which were placed on the agar plate that had already been spread with the microbial culture. All strains were incubated at 37 °C for 24 hours except for *S. cerevisiae*, *S. pombe* and *C. glabrata*, which were incubated at 30 °C. For the samples that inhibited the growth of the microorganism, a clear zone was observed. The plates were then

photographed and the diameter of the zone of inhibition was measured. These tests were performed in triplicate for each type of test microorganism.

#### **2.4.5.2. Duration of antimicrobial action:**

The 0.94 wt.% and 4.37 wt.% loaded bismuth(III) phosphinato-MFC sheets were tested to investigate the activity of the antimicrobial paper over time. The Gram-positive bacterium *Staphylococcus epidermidis* was chosen for this analysis because it is a part of human microbiota. *S. epidermidis* is the most dominant species of bacteria in human skin and mucosal surfaces, and are carried by healthy people [59]. The zone of inhibition experiment was done in the same way as for the other bacterial strains. After 24 hours, the discs were transferred aseptically to a new fresh agar plate inoculated with the same bacterial strain and incubated for another 24 hours. This was repeated until no visible zone of inhibition was observed. Furthermore, the agar around the disks in each of these plates were analysed for presence of any bismuth in there. This was done by scooping out some agar samples, dissolving it in nitric acid and then analysing the bismuth concentration by ICP-OES.

#### **2.4.5.3. Physical and mechanical properties**

The mass of the sheets per unit area was measured by drying the sheet in an oven at 105°C to determine the grammage. The tensile index and Young's Modulus were measured using an Instron tensile tester (model 5965). The papers were cut into 15 mm width strips and conditioned before the test at 23°C and 50% relative humidity for 24 hours. The span tested was 50 mm with a constant strain rate of 10mm/min. Five replicated were measured for each test. The pore size distribution and porosity were determined by mercury porosimetry using Micromeritics Autopore IV. The sheets were cut into 8 mm squares and degassed for 24 hours at 100°C in the sample holder. The measurements were done in a penetrometer (Model 14, 3cc). The surface area and pore shape were determined by physisorption of nitrogen gas at 77K using a Micromeritics 3Flex.

#### **2.4.5.4. Water vapor permeability**

The water vapour transmission rate of the bismuth (III) phosphinato-MFC sheets were measured at 23 °C and 50 % relative humidity by following ASTM E96, using the desiccant method [60]. The sheets were pre-dried in an oven at 105 °C for at least four hours. Cups complying with the standard were filled with dried desiccant, calcium chloride, and sealed with the test sample. This arrangement was kept in the test condition chamber and the variation in mass of the permeability cups over time was recorded. The rate of change in mass quantifies the water vapour transmission rate (WVTR). The WVTR was then normalized by the thickness of the paper to determine water

vapour permeability (WVP). The thickness of the composite sheets was measured using L&W thickness tester. A number of readings were taken for each sheet, and the mean thickness was calculated.

## 2.5. Results and Discussion

### 2.5.1. Characterisation

#### 2.5.1.1. ICP-OES Analysis:

ICP-OES was used to quantify the actual amount of bismuth complex present in the sheets. Table 1 shows the mean percentage of bismuth complex to dry paper determined using ICP-OES analysis, along with the standard deviation ( $n=3$ ). The results were found to be close to the expected values. However, the minor difference could be accounted for by loss of the complex while preparing the suspension or due to sticking of the complex within the spray system. The maximum loss (30%) was observed for 0.1wt%. loading which could mean that a larger proportion of the complex was lost on the surfaces in contact with the suspension at low loadings than at high loadings of 5.0 wt.% (13% loss), with the 1.0 wt.% (6% loss) being an outlier. In this instance the preparation of the composites was done in small laboratory scale, with a much greater surface to volume ratio than would be the case in large scale production. When scaling this up to a large-scale production, these losses would be expected to be minimal.

**Table 1:** Percentage of phenyl bismuth bis(diphenylphosphinato) from ICP-OES analysis for the different loaded Bi-MFC composites

Target loading of bismuth complex wt. % (g bismuth complex/g cellulose)	Mean actual percentage of bismuth complex wt. % from ICP $\pm$ standard deviation (g bismuth complex/g dry paper)
0.1	$0.07 \pm 0.01$
0.5	$0.39 \pm 0.05$
1.0	$0.94 \pm 0.02$
2.5	$2.10 \pm 0.05$
5.0	$4.37 \pm 0.07$

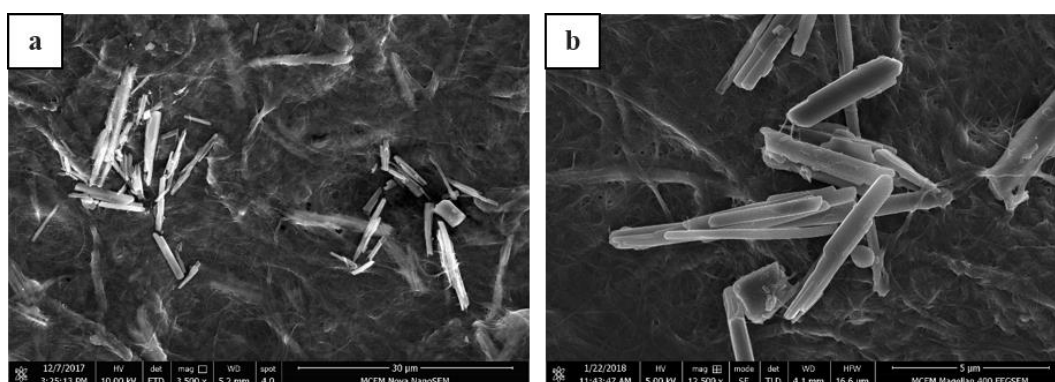
#### 2.5.1.2. Bi-complex characterization

The bismuth(III) phosphinato complex precipitates from the reaction as long thin needles, as shown in the optical image of the bismuth complex alone in Figure A13. The particle size of the

dispersed phase plays a significant role in the properties of composite materials. Due to the particles being non-spherical, light/laser scattering techniques do not define the actual dimensions of the particles. However, scattering techniques can be used to measure the hydrodynamic diameter of an equivalent sphere of the particle that has the same diffusion coefficient. The hydrodynamic diameter of the particle was found to be  $1.25 \pm 0.18 \mu\text{m}$ , with a polydispersity index of  $0.33 \pm 0.04$ . The complex is stable upto a temperature of  $300 \text{ }^\circ\text{C}$ , found by TGA (Figure A12). The melting point and the decomposition point of the complex is  $300 \text{ }^\circ\text{C}$  and  $330 \text{ }^\circ\text{C}$  respectively and has been reported previously as well [33].

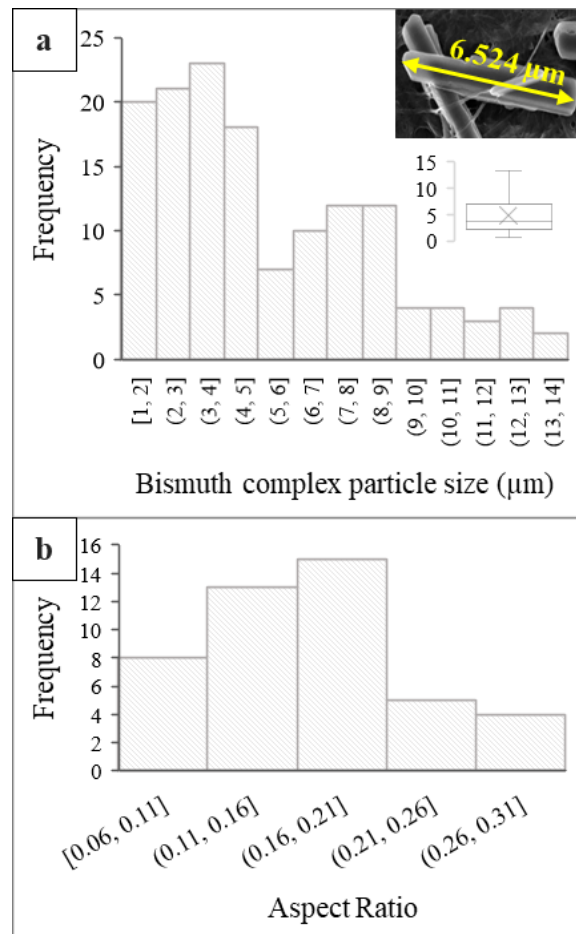
### 2.5.1.3. SEM Imaging

Scanning Electron Microscope (SEM) was used to study the distribution of the complex within the microfibrillated cellulose fibres. Secondary electron (SE) imaging was done to obtain surface information of the 4.37 wt.% Bi-MFC composite as shown in Figure 2. It is clear from the images that nanofibers form a highly entangled network, and the cylindrical inorganic complex particles are present on the surface entangled within the MFC fibres. It is evident that the particles vary in size and are arranged in random orientation with occasional clustering at different regions on the surface.



**Figure 2:** SEM images of the surface of 4.37 wt.% Bi-MFC composite at different magnifications: (a)  $\times 3500$  (b)  $\times 12500$

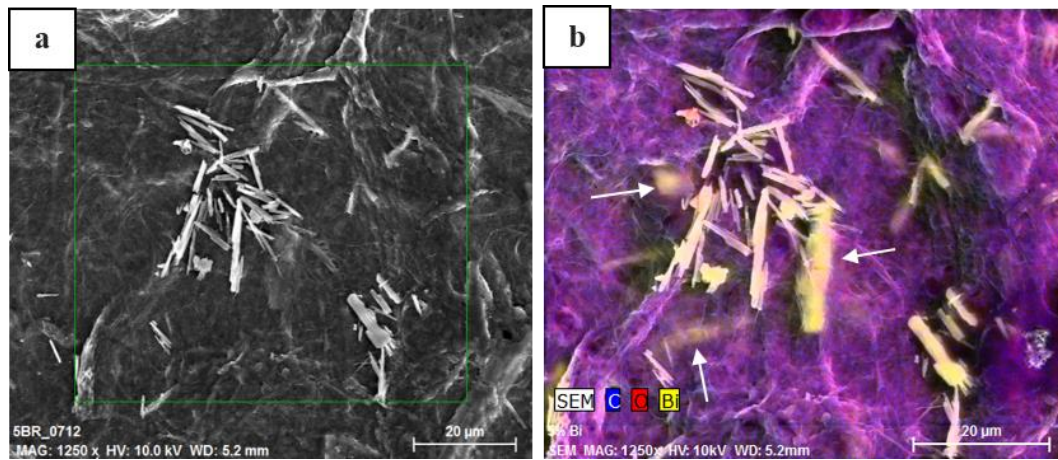
The dimensions of randomly selected particles on the surface were measured, and the particle size distribution is as illustrated in the Figure 3. The smallest particle was  $525 \text{ nm}$ , and the largest one detected was  $13.3 \mu\text{m}$ . The shape of the particles can be observed to be cylindrical needle-shaped from Figure 2. For such a form, a simple parameter, aspect ratio, can be used to describe the shape. The aspect ratio, the ratio of the width to length of the particle, has been measured from SEM images and the aspect ratio distribution curve is shown in Figure 3(b).



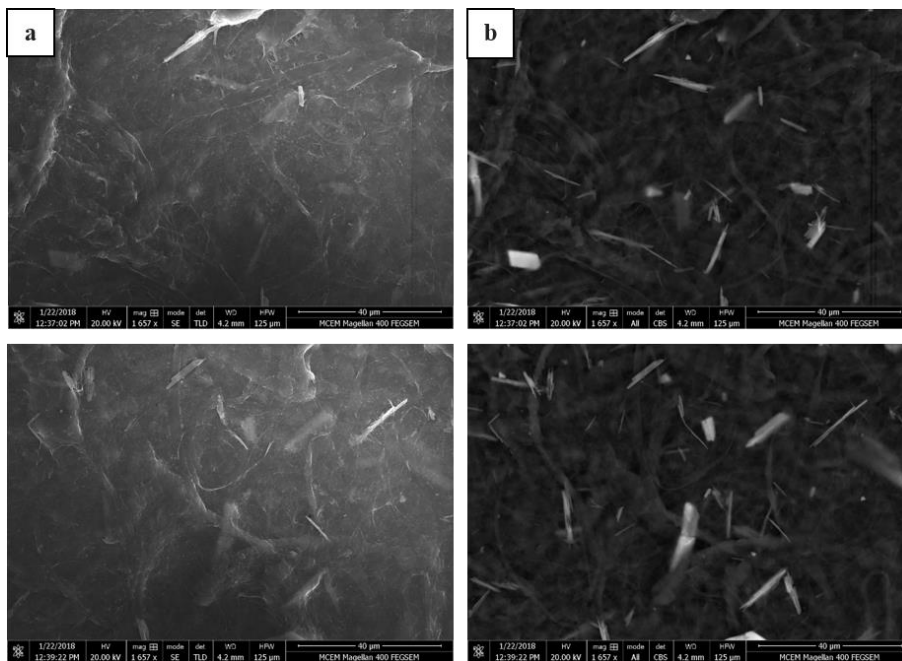
**Figure 3:** (a) Particle length distribution (n=140) and (b) Aspect ratio distribution (n=40) of bismuth (III) phosphinato complex on the surface of 4.37 wt.% Bi-MFC sheet

Figure 4 shows the secondary electron image and its corresponding energy-dispersive X-ray (EDX) mapping of the same bismuth (III) phosphinato-MFC composite. This, along with Figure A14 showing the EDX point analysis of the composite, confirms the presence of bismuth at the cylindrical needle-like structures. Moreover, it also shows that not only are the particles present on the surface, but that they are also buried inside the material (as indicated by arrows in Figure 4). This phenomenon of the particles being embedded deeper under the surface has also been supported by the back scattered electron images in Figure 5. The high atomic number of bismuth, compared to carbon, oxygen and hydrogen found in the cellulose, means that the bismuth complex appears much brighter in the BSE images. The bright needle-like structures in the BSE images indicate the presence of the bismuth (III) phosphinato complex. BSE imaging in Figure 5 was done in areas where not many cylindrical particles could be spotted with secondary electron imaging, but it was found that bismuth was present in those areas. A BSE image taken at low magnification, in Figure 6, shows that the bismuth (III) phosphinato structures can be seen

throughout the space indicating that the inorganic complex is well distributed throughout the matrix.



**Figure 4:** SEM images of the 4.37 wt.% Bi-MFC composite using (a) secondary electron imaging (b) EDX mapping of the selected area



**Figure 5:** SEM images of the 4.37 wt.% Bi- MFC sheets using (a) secondary electron imaging and their corresponding (b) Back scattered electron imaging

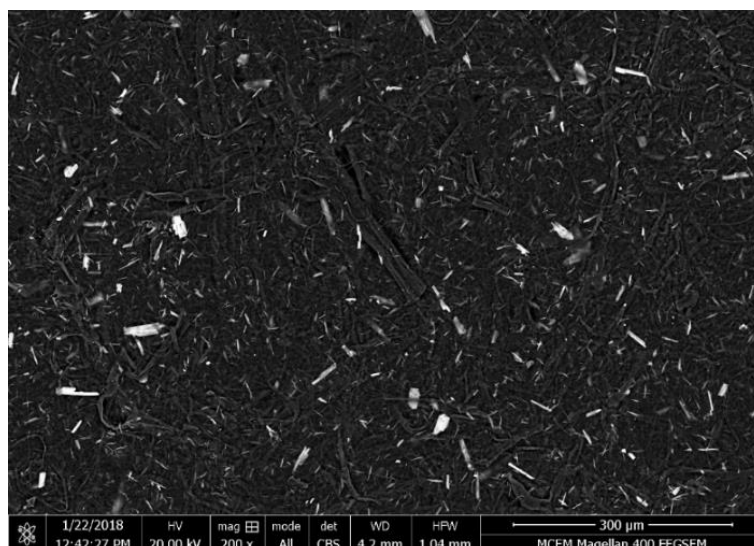


**Figure 6:** Back scattered electron image of the 4.37 wt.% Bi- MFC sheet at low magnification ( $\times 200$ )

Although the secondary images show some clustering of the complex, the BSE images and EDX mapping give clear evidence of the particles being buried under the surface and that there is an overall even distribution of the particles within the matrix. The fact that the particles are entrapped within the fibres also mean that the particles are well secured within the matrix, and this along with the insolubility of the complex should limit the release of bismuth out of the material, thereby minimizing the risks of environmental accumulation. Figure A15 shows the entanglement of the Bi-complex within the nanocellulose fibres. This suggests that the bismuth complex is quite securely held within the composite structure.

## 2.5.2. Material performance

### 2.5.2.1. Antibacterial Activity

The disk diffusion assays show that sheets with higher bismuth complex loadings produce greater zones of inhibition. The agar plates for the zones of inhibition is shown in Figures A1-A5 in the supplementary information and the results summarized in Figure 7. Figure 7 shows that the Gram-negative bacteria, *P. aeruginosa* and *E. coli*, are less susceptible to the Bi-MFC composite, as evidenced by smaller zones of inhibition compared to the Gram-positive bacteria. The composites provided little or no inhibition of Gram-negative bacteria at loadings below 0.94 wt.%. In contrast, Gram-positive bacteria showed evidence of growth inhibition even at the lowest levels of bismuth loading tested, which is 0.07 wt.%. These observations agree with previous work that showed that the bismuth (III) complex is more active against Gram-positive bacteria than Gram-negative strains [33, 34, 36]. Gram-negative bacteria are in general harder to kill or inhibit as these cells

are surrounded by an outer membrane of lipopolysaccharide, which is absent in Gram-positive bacteria. This extra outer membrane in Gram-negative bacteria acts as a permeability barrier to antibiotics and bactericidal agents making attack more difficult [61]. Figure 7 also shows that the increase in effectiveness with increased loadings becomes less pronounced for higher loadings and the antibacterial activity seems to reach a plateau beyond 2.10 wt. %, as observed by the trends for *E. coli*, *P. aeruginosa* and MRSA.

The results also showed the bismuth-loaded composites were as effective against the drug-resistant form of *S. aureus*, i.e. MRSA as it was to the more sensitive strain of this medically-important bacterium. MRSA is very difficult to treat by most antibiotics and is a major problem in the hospital system [8]. Silver-resistance has been reported in 33 strains of MRSA [62]. We examined a limited set of MRSA strains in this study but it raises the possibility that these bismuth-based materials could potentially replace silver-based ones. Based on the results, it was demonstrated that bismuth (III) phosphinato loaded sheets are active against the Gram-positive bacteria and to a lesser extent the Gram-negative bacteria.

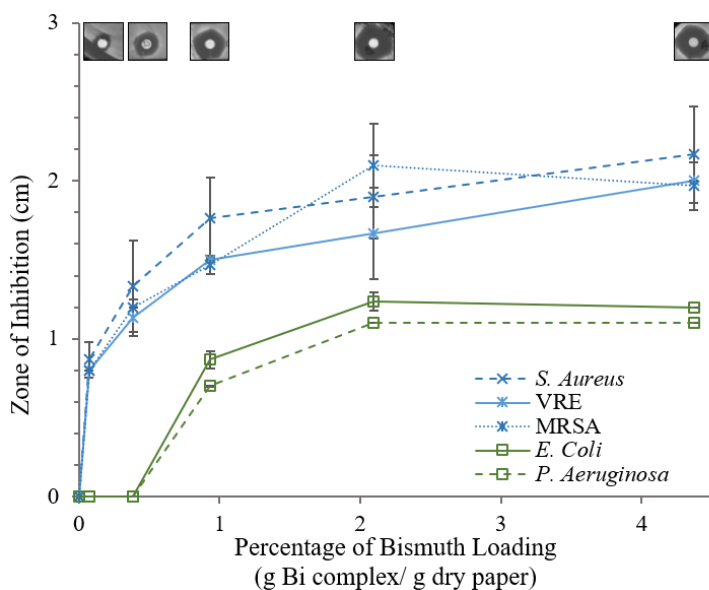


**Figure 7:** Effect of bismuth complex loading on zone of inhibition with different bacteria from disk diffusion assay and the top images show their picture representation against *S. aureus*

Previous research showed bacterial nanocellulose- silver nanoparticle composite with 1.01 wt% loading produced small zones of inhibition against *E. coli*, *S. aureus* and *P. aeruginosa*, with all results being below 8mm [63]. When compared to bismuth composites, with a similar loading of 0.94 wt.%, the zones of inhibitions were 8.7 mm, 17 mm and 7 mm respectively. Also, it was reported that silver sulfadiazine loaded nanocellulose sheets with 0.43 wt.% loading produced a

9 mm zone of inhibition against VRE [33]. Whereas in Figure 7, we can observe that bismuth composites with a much lower loading of 0.072 wt.% produced an 8 mm diameter zone of inhibition diameter against the same bacteria. Based on the zones of inhibition, it can be inferred that the bismuth loaded nanocellulose composites have an equal or greater activity than similar composites loaded with silver-based antibacterial agents.

### 2.5.2.2. Antifungal Activity

It was found that the bismuth (III) phosphinato loaded composites were effective against several fungi species, including the pathogenic *C. glabrata* and *C. albicans*. The zone of inhibition on the fungal plates were similar in size to that observed for *P. aeruginosa* and *E.coli*, suggesting a lower level of inhibition but one that may still prove useful to control contamination of products inside the packaging. Table 2 shows the zones of inhibition of the composites against fungal species. Some of the fungal species were hard to grow evenly across the plate, which made visual assessment difficult, as shown in Figures A6-A9 in the supplementary information. However, close examination and measurement of the halo allowed an objective comparison of the effect of the composite on all of the yeasts. Since the results for *C. glabrata* were inconclusive for all samples tested, further experiments were done with a higher composite loading of 10.53 wt.% and a zone in the range 0.6 cm to 0.8 cm was observed. On the other hand, for *C. albicans*, a zone of inhibition was observed even at the low loading of 0.94 wt.%. Overall, this composite is shown to be effective not only on bacteria but also on some pathogenic fungi strains.

**Table 2:** Antifungal activity of the Bi-MFC composites determined by the zone of inhibition assay

Test Fungus	Percentage of bismuth loading (g Bi complex/ g dry paper)						
	0	0.07	0.39	0.94	2.01	4.37	10.53
<i>S. pombe</i>	–	–	–	±	±	+	++
<i>S. cerevisiae</i>	–	–	–	+	++	++	++
<i>C. glabrata</i>	–	–	–	±	±	±	+
<i>C. albicans</i>	–	–	–	+	++	++	++

– no inhibition  
± not clear/ inconclusive  
+ clear zone of 0.6-0.8 cm  
++ clear zone greater than 0.8 cm

### 2.5.2.3. Duration of antimicrobial action

It was observed that the activity of the bismuth(III) phosphinato-MFC composites decreased with time for both samples, illustrated by the decreasing zone of inhibition with time in Figure 8(a) and Figure A10, which was performed in triplicates. The 0.94 wt.% and 4.37 wt.% loaded sheets remained active for 3 and 5 days respectively. Also, the zone of inhibition was greater for the 4.37 wt.% sheets at all times due to presence of higher amounts of active complex shown in Figure 8(b).

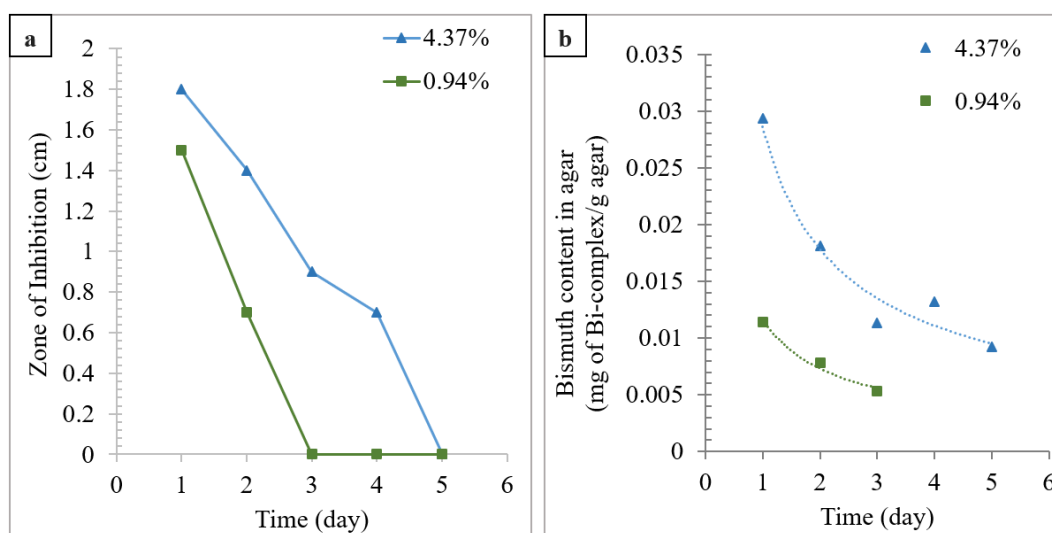


**Figure 8:** Zone of inhibition (a) and the amount of bismuth content leached out into the zone of inhibition (b) for the 4.37 wt.% and 0.94 wt.% loaded bismuth sheets with time

Exhausted composites were further analysed by ICP-OES, and the final bismuth content was found to be 0.15 wt.% and 0.04 wt.% (g of Bi-complex/g dry paper) for the 4.37 wt% and 0.94 wt.% original composites respectively after 5 days of agar testing. Thus, the complex will eventually leach out of the composite to work on the bacteria when in contact with it, but remains securely held within the fibres while being transported or handled.

#### 2.5.2.4. Physical and Mechanical properties

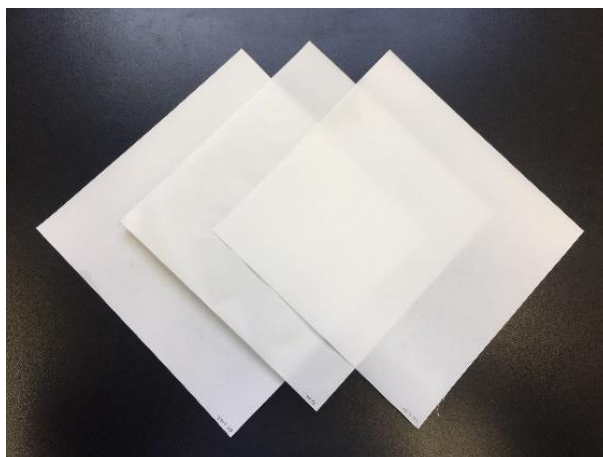


**Figure 9:** Physical appearance of the 0.39 wt.%, 0.94 wt.% and 2.10 wt.% bismuth (III) phosphinato-MFC sheets (left to right)

The pure MFC sheet and all the composites are white and opaque, with no visible difference among them to the naked eye. The sheets are satisfactorily homogenous in terms of thickness and basis weight, as reported in Table A2 in the supplementary information. It was observed that the addition of the Bi-complex into MFC affects the mechanical strength of the sheets formed. The tensile index for the pure MFC sheet was found to be  $76.5 \pm 5.8$  Nm/g. However, with only 0.07 wt.% Bi-complex additive added to the composite, the tensile index dropped to  $55.8 \pm 1.0$  Nm/g. On a higher loading of 4.37 wt.%, the tensile index further dropped to  $40.0 \pm 1.5$  Nm/g. These values are comparable to the mechanical strength of similar MFC sheets, which were reported to be in the range 45-104 Nm/g [50]. Similar trends were observed for the Young's modulus, which were  $8.4 \pm 0.4$  GPa,  $7.6 \pm 0.3$  GPa and  $5.4 \pm 0.3$  GPa for 0 wt.%, 0.07 wt.% and 4.37 wt.% Bi-loaded composites, respectively. The Young's modulus of pure MFC has been reported by various researchers to be up to 6 GPa [64]. It can be suggested that the Bi-complex particles interferes with the inter-fibre bonding, which has been recognised to directly impact the mechanical properties of such composites [65]. At higher loadings, any agglomerated hydrophobic cluster can thus result in poor bonding between the cellulose chains. A similar effect was reported for high loading of nanoclay in MFC composites [64, 66].

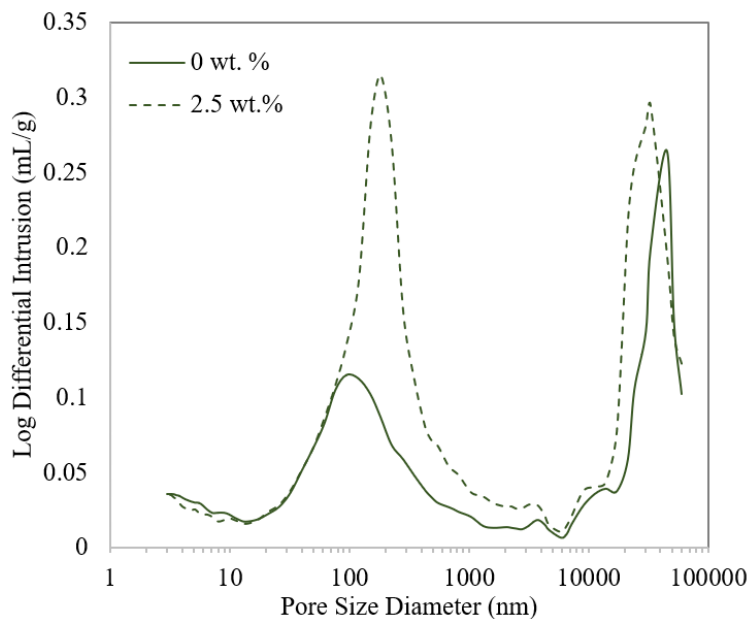


**Figure 10:** Pore size distribution for pure MFC and Bi-MFC composite

The pore structure analysis was done, where the 2.10 wt.% Bi-MFC composite was chosen as it was the closest to the pure MFC sheet in terms of grammage. Figure 10 shows bimodal distribution of pore size in both the pure MFC sheet and the Bi-MFC composite. The modal pore size range did not seem to change much with the addition of bismuth complex. However, there seems to be significantly higher number of smaller pores as well as slightly more larger pores for the Bi-loaded composite than the pure MFC sheet, hence also explaining the rise in overall porosity reported in Table 3. The increased number of pores, along with the added surface from the bismuth particles, explains the rise in BET surface area for the Bi-MFC composite as reported in Table 3. The shape of the adsorption-desorption isotherm obtained from physisorption of nitrogen, in Figure A16, also tells us the material has slit-shaped pores, rather than cylindrical ones, according to the IUPAC classification of porous materials [67].

**Table 3:** Pore properties of the pure MFC sheet and Bi-MFC composite

Property	Pure MFC	2.10 wt. % Bi-MFC composite
Porosity (%)	19.3	28.9
Total intrusion volume (mL/g)	0.2357	0.3678
BET surface area (m <sup>2</sup> /g)	0.4112 ± 0.0011	0.7552 ± 0.0020

### 2.5.2.5. Water vapour permeability

Packaging materials must be able to act as a barrier to the entry of water vapour in order to protect packaged goods from contamination and degradation. Molecule migration across a polymer film depends on the adsorption and desorption ability of the molecule on the surface and particularly on the rate of molecule diffusion across the film [68]. The dense network of the microfibrillated cellulose fibres creates small pores across the surface of the MFC sheets and increases the mean free path that the water molecule has to travel to reach the other end, i.e. it increases the tortuosity of travel as compared to normal cellulose.

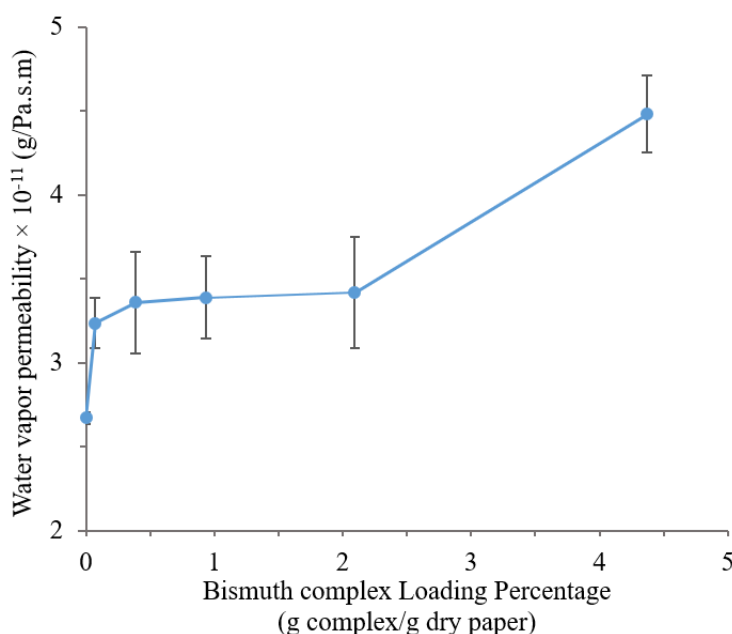


**Figure 11:** Effect of bismuth complex loading on the water vapour permeability of the phenyl bismuth bis(diphenylphosphinato) functionalized MFC

However, with addition of the bismuth complex, the WVP was observed to increase slightly as shown in Figure 11. The SEM images and EDX mapping confirmed the even distribution of the complex throughout the material, with evidence of them being distributed under the surface. It

was also observed that the particles were large, with the largest observed dimension of 13 microns. It can be proposed that arrangement of some of the particles with its largest dimension parallel to the diffusion pathway allowed water vapour molecules to follow a more direct path rather than a tortuous path. This resulted in minor reductions in the WVP performance. Increasing the loading from 0.07 wt.% to 2.10 wt. % did not significantly alter WVP performance. Surprisingly, increasing the loading to 4.37 wt.% showed a sudden increase. It can be proposed that after a certain loading, the complex becomes interconnected due to aggregation of the hydrophobic complexes. It is possible that at this point the percolation threshold might have been reached, creating a conducting pathway that increases the WVP. It has been reported that diffusion across a material with embedded tubular particles increases with an increase in concentration of the particles within, and the most significant change occurs near the percolation threshold [69, 70]. The barrier properties are dependent on a number of factors, which include the size and shape of the additive agent, its distribution as well as the total amount present in the structure [66]. All these parameters have been studied to support the hypothesis. However, the effect of the complex was very minor and was still in the range of  $10^{-11}$  when compared to the WVP of commercial plastic based packaging materials, which are within  $10^{-12}$  to  $10^{-13}$  range [71, 72].

**Table 4:** Literature comparison of WVP of common packaging materials with Bi-MFC composites

Film	WVP $\times 10^{-11}$ (g/m.Pa.s)	Relative Humidity (%)	Temperature (°C)	Reference
Experimental sheets				
Pure MFC sheet	2.67	0-50%	23	-
Bi-MFC composites	3.23-4.48	0-50%	23	-
Synthetic Films				
HDPE	0.002	0-100	27.6	[71]
LDPE	0.014	-	27.6	
PP	0.010	-	25	
PVC	0.041		27.6	
PSs	0.5	0-100	25	[72]
Biobased Films				
Cellulose derivatives	9.2-11	0-85%	21	[73]
Chitosan	13	76.2	25	[74]

Table 4 compares the values of WVP for various packaging materials. The published data were obtained using different testing conditions and so are not exactly comparable to our values without considering the relative humidity and temperature. A higher relative humidity gives higher permeability values for a test sample. However, these values provide an indication of the Bi-MFC sheets performance with respect to commercial packaging materials. The WVP values of the bismuth-based sheets are not as low as those for synthetic films, but further modifications may be possible to arrive at similar performance levels. Additionally, of course, the bismuth-impregnated material has the advantage of being antimicrobial against some of the medically important microorganisms. However, to be used as a packaging material for food packaging applications in particular, further investigation with food pathogens will be required. Moreover, the antimicrobial additive will get used up during its application, thereby losing its effectiveness over time and ensuring that the material is recyclable and biodegradable. The biodegradability and renewability of nanocellulose further makes this material a sustainable and eco-friendly product that not only safeguards public health but also protects the environment throughout its life cycle.

This material can be the answer to a number of environmental issues from a broad cleaner production perception that has the antimicrobial and barrier properties for use as a packaging material along with

- being a safer alternative to silver-based material, addressing all the issues of overuse of silver, viz. environmental accumulation, cytotoxicity and induction of resistance in bacteria
- using a biodegradable and renewable natural polymer as the matrix

## **2.6. Conclusion**

The study investigated the preparation of bismuth-based nanocellulose composites on an industrial scale using a spraying system for the development of a biodegradable and renewable active packaging material. The composites prepared in this study have antimicrobial properties against some of the most medically-important bacteria and fungi, along with the virtue of having activity at relatively low loadings. There is a clear dose effect on the performance of these sheets. In addition, the composites have reasonable barrier performance against water vapour, with the bismuth complex not having any significant effect on the barrier performance unless present at relatively high levels. The physical and mechanical properties are also affected by the addition of the complex, but were still in expected range within the scope of study. Bismuth-based nanocellulose composites have potential to serve as a cleaner antimicrobial barrier material and can potentially replace silver-based packaging material. However, a proper understanding of the

loading and its corresponding material properties needs to be fully understood, and this paper provides a fair direction for doing so.

## 2.7. Acknowledgements

We would like to thank Kirubanandan Shanmugam (BioPRIA) for assistance with sheet preparation. The authors thank Monash University and The National Health and Medical Research Council (APP1139844) for financial support. The authors would like to acknowledge the use of the facilities in the Monash Centre for Electron Microscopy. Maisha Maliha and Megan Herdman would like to acknowledge the Australian Government for the Research Training Program (RTP) Scholarship.

## 2.8. References

1. Pereira De Abreu, D.A., J.M. Cruz, and P. Paseiro Losada, *Active and Intelligent Packaging for the Food Industry*. Food Reviews International, 2012. **28**(2): p. 146-187.
2. Inamuddin, *Green Polymer Composites Technology : Properties and Applications*. 2016, Boca Raton, United Kingdom: Chapman and Hall/CRC.
3. Lavoine, N., et al., *Antibacterial paperboard packaging using microfibrillated cellulose*. J Food Sci Technol, 2015. **52**(9): p. 5590-600.
4. Appendini, P. and J.H. Hotchkiss, *Review of antimicrobial food packaging*. Innovative Food Science & Emerging Technologies, 2002. **3**(2): p. 113-126.
5. Lavoine, N., et al., *Active bio-based food-packaging: Diffusion and release of active substances through and from cellulose nanofiber coating toward food-packaging design*. Carbohydr Polym, 2016. **149**: p. 40-50.
6. Amini, E., et al., *Silver-nanoparticle-impregnated cellulose nanofiber coating for packaging paper*. Cellulose, 2016. **23**(1): p. 557-570.
7. Dizaj, S.M., et al., *Antimicrobial activity of the metals and metal oxide nanoparticles*. Materials Science and Engineering: C, 2014. **44**: p. 278-284.
8. Patra, M., G. Gasser, and N. Metzler-Nolte, *Small organometallic compounds as antibacterial agents*. Dalton Transactions, 2012. **41**(21): p. 6350-6358.
9. Barry, N.P.E. and P.J. Sadler, *Exploration of the medical periodic table: towards new targets*. Chem. Commun., 2013. **49**(45): p. 5106-5131.
10. Lemire, J.A., J.J. Harrison, and R.J. Turner, *Antimicrobial activity of metals: mechanisms, molecular targets and applications*. Nature Reviews Microbiology, 2013. **11**: p. 371.

11. Abd-El-Aziz, A.S., C. Agatemor, and N. Etkin, *Antimicrobial resistance challenged with metal-based antimicrobial macromolecules*. *Biomaterials*, 2017. **118**: p. 27-50.
12. Alvarez-Paino, M., A. Munoz-Bonilla, and M. Fernandez-Garcia, *Antimicrobial Polymers in the Nano-World*. *Nanomaterials (Basel)*, 2017. **7**(2).
13. Carbone, M., et al., *Silver nanoparticles in polymeric matrices for fresh food packaging*. *Journal of King Saud University - Science*, 2016. **28**(4): p. 273-279.
14. Haider, A. and I.K. Kang, *Preparation of Silver Nanoparticles and Their Industrial and Biomedical Applications: A Comprehensive Review*. *Advances in Materials Science and Engineering*, 2015. **2015**: p. 1-16.
15. Xiong, Z.C., et al., *One-Step Synthesis of Silver Nanoparticle-Decorated Hydroxyapatite Nanowires for the Construction of Highly Flexible Free-Standing Paper with High Antibacterial Activity*. *Chemistry*, 2016. **22**(32): p. 11224-31.
16. Dankovich, T.A. and D.G. Gray, *Bactericidal paper impregnated with silver nanoparticles for point-of-use water treatment*. *Environ Sci Technol*, 2011. **45**(5): p. 1992-8.
17. Huang, J.-Y., X. Li, and W. Zhou, *Safety assessment of nanocomposite for food packaging application*. *Trends in Food Science & Technology*, 2015. **45**(2): p. 187-199.
18. Yan, J., et al., *Antibacterial activity of silver nanoparticles synthesized In-situ by solution spraying onto cellulose*. *Carbohydr Polym*, 2016. **147**: p. 500-8.
19. Martínez-Abad, A., J.M. Lagaron, and M.J. Ocio, *Development and Characterization of Silver-Based Antimicrobial Ethylene–Vinyl Alcohol Copolymer (EVOH) Films for Food-Packaging Applications*. *Journal of Agricultural and Food Chemistry*, 2012. **60**(21): p. 5350-5359.
20. Cushen, M., et al., *Nanotechnologies in the food industry – Recent developments, risks and regulation*. *Trends in Food Science & Technology*, 2012. **24**(1): p. 30-46.
21. Stensberg, M.C., et al., *Toxicological studies on silver nanoparticles: challenges and opportunities in assessment, monitoring and imaging*. *Nanomedicine (Lond)*, 2011. **6**(5): p. 879-98.
22. Restuccia, D., et al., *Chapter 16 - Industrial Applications: Regulatory Issues and Life Cycle Assessment of Food Packaging*. 2016, Elsevier Inc. p. 215-227.
23. Drake, P.L. and K.J. Hazelwood, *Exposure-related health effects of silver and silver compounds: a review*. *Ann Occup Hyg*, 2005. **49**(7): p. 575-85.
24. Maillard, J.-Y. and P. Hartemann, *Silver as an antimicrobial: facts and gaps in knowledge*. *Critical Reviews in Microbiology*, 2013. **39**(4): p. 373-383.

25. Cao, H., *Silver nanoparticles for antibacterial devices : biocompatibility and toxicity*. 2017: Boca Raton : CRC Press, Taylor & Francis Group.
26. Echegoyen, Y. and C. Nerín, *Nanoparticle release from nano-silver antimicrobial food containers*. *Food and Chemical Toxicology*, 2013. **62**: p. 16-22.
27. Huang, Y., et al., *Nanosilver Migrated into Food-Simulating Solutions from Commercially Available Food Fresh Containers*. *Packaging Technology and Science*, 2011. **24**(5): p. 291-297.
28. Pezzuto, A., et al., *Food safety concerns deriving from the use of silver based food packaging materials*. *Frontiers in microbiology*, 2015. **6**: p. 1109-1109.
29. Silver, S., *Bacterial silver resistance: molecular biology and uses and misuses of silver compounds*. *FEMS Microbiology Reviews*, 2003. **27**(2): p. 341-353.
30. Gunawan, C., et al., *Widespread and Indiscriminate Nanosilver Use: Genuine Potential for Microbial Resistance*. *ACS nano*, 2017. **11**(4): p. 3438.
31. Pal, C., et al., *BacMet: antibacterial biocide and metal resistance genes database*. *Nucleic acids research*, 2014. **42**(Database issue): p. D737.
32. Crocetti, G., *Save the nano-silver for where it's needed*. *Chain Reaction*, 2013(117): p. 16.
33. Werrett, M., et al., *Bismuth Phosphinates in Bi-Nanocellulose Composites and their Efficacy towards Multi-Drug Resistant Bacteria*. *Chemistry- A European Journal*, 2018.
34. Luqman, A., et al., *The Importance of Heterolepticity in Improving the Antibacterial Activity of Bismuth(III) Thiolates*. *European Journal of Inorganic Chemistry*, 2016. **2016**(17): p. 2738-2749.
35. Svoboda, T., et al., *NCN Chelated Organoantimony(III) and Organobismuth(III) Phosphinates and Phosphites: Synthesis, Structure and Reactivity*. *European Journal of Inorganic Chemistry*, 2010. **2010**(33): p. 5222-5230.
36. Kotani, T., et al., *Antibacterial Properties of Some Cyclic Organobismuth(III) Compounds*. *Antimicrobial Agents and Chemotherapy*, 2005. **49**(7): p. 2729.
37. Domenico, P., et al., *Activities of Bismuth Thiols against Staphylococci and Staphylococcal Biofilms*. *Antimicrobial Agents and Chemotherapy*, 2001. **45**(5): p. 1417.
38. Briand, G.G. and N. Burford, *Bismuth Compounds and Preparations with Biological or Medicinal Relevance*. *Chemical Reviews*, 1999. **99**(9): p. 2601-2658.
39. Suzuki, H. and Y. Matano, *Chapter 1 - Introduction*, in *Organobismuth Chemistry*, Y. Matano, Editor. 2001, Elsevier Science: Amsterdam. p. 1-20.

40. Keogan, D. and D. Griffith, *Current and Potential Applications of Bismuth-Based Drugs*. *Molecules*, 2014. **19**(9): p. 15258.
41. Xu, Q., et al., *A facile route to prepare cellulose-based films*. *Carbohydrate Polymers*, 2016. **149**: p. 274-281.
42. O'Sullivan, A.C., *Cellulose: the structure slowly unravels*. *Cellulose*, 1997. **4**(3): p. 173-207.
43. Siró, I. and D. Plackett, *Microfibrillated cellulose and new nanocomposite materials: a review*. *Cellulose*, 2010. **17**(3): p. 459-494.
44. Lavoine, N., et al., *Microfibrillated cellulose - its barrier properties and applications in cellulosic materials: a review*. *Carbohydr Polym*, 2012. **90**(2): p. 735-64.
45. Kumar, V., et al., *Comparison of nano- and microfibrillated cellulose films*. *Cellulose*, 2014. **21**(5): p. 3443-3456.
46. Klemm, D., et al., *Nanocelluloses: A New Family of Nature-Based Materials*. *Angewandte Chemie International Edition*, 2011. **50**(24): p. 5438-5466.
47. Klemm, D., et al., *Cellulose: Fascinating Biopolymer and Sustainable Raw Material*. *Angewandte Chemie International Edition*, 2005. **44**(22): p. 3358-3393.
48. Lin, N. and A. Dufresne, *Nanocellulose in biomedicine: Current status and future prospect*. *Eur. Polym. J.*, 2014. **59**: p. 302-325.
49. Varanasi, S. and W.J. Batchelor, *Rapid preparation of cellulose nanofibre sheet*. *Cellulose*, 2013. **20**(1): p. 211-215.
50. Beneventi, D., E. Zeno, and D. Chaussy, *Rapid nanopaper production by spray deposition of concentrated microfibrillated cellulose slurries*. *ATIP. Association Technique de L'Industrie Papetiere*, 2016. **70**(2): p. 6-14.
51. Krol, L.F., et al., *Microfibrillated cellulose-SiO<sub>2</sub> composite nanopapers produced by spray deposition*. *Journal of Materials Science*, 2015. **50**(11): p. 4095-4103.
52. Beneventi, D., et al., *Highly Porous Paper Loading with Microfibrillated Cellulose by Spray Coating on Wet Substrates*. *Industrial & Engineering Chemistry Research*, 2014. **53**(27): p. 10982-10989.
53. Kumar, V., et al., *Substrate role in coating of microfibrillated cellulose suspensions*. *Cellulose*, 2017. **24**(3): p. 1247-1260.
54. Varanasi, S., H. Chiam, and W. Batchelor, *Application and interpretation of zero and short-span testing on nanofibre sheet materials*. *Nord. Pulp Paper Res. J.*, 2012. **27**(2): p. 343-351.
55. Shanmugam, K., et al., *Rapid preparation of smooth nanocellulose films using spray coating*. *Cellulose*, 2017. **24**(7): p. 2669.

56. Kawashima, S.A., et al., *Analyzing fission yeast multidrug resistance mechanisms to develop a genetically tractable model system for chemical biology*. Chem Biol, 2012. **19**(7): p. 893-901.
57. Hua, X., et al., *Morphogenic and genetic differences between Candida albicans strains are associated with keratomycosis virulence*. Mol Vis, 2009. **15**: p. 1476-84.
58. Fidel, P.L., Jr., J.A. Vazquez, and J.D. Sobel, *Candida glabrata: review of epidemiology, pathogenesis, and clinical disease with comparison to C. albicans*. Clin Microbiol Rev, 1999. **12**(1): p. 80-96.
59. Fey, P.D. and M.E. Olson, *Current concepts in biofilm formation of Staphylococcus epidermidis*. Future microbiology, 2010. **5**(6): p. 917-933.
60. E96/E96M-16, A., *Standard Test Methods for Water Vapor Transmission of Materials*. 2016, ASTM International West Conshohocken, PA.
61. Tegos, G., et al., *Multidrug Pump Inhibitors Uncover Remarkable Activity of Plant Antimicrobials*. Antimicrobial Agents and Chemotherapy, 2002. **46**(10): p. 3133.
62. Loh, J.V., et al., *Silver resistance in MRSA isolated from wound and nasal sources in humans and animals*. International Wound Journal, 2009. **6**(1): p. 32-38.
63. Wu, J., et al., *In situ synthesis of silver-nanoparticles/bacterial cellulose composites for slow-released antimicrobial wound dressing*. Carbohydrate Polymers, 2014. **102**: p. 762.
64. Gabr, M.H., et al., *Mechanical, thermal, and moisture absorption properties of nano-clay reinforced nano-cellulose biocomposites*. Cellulose, 2013. **20**(2): p. 819-826.
65. Sehaqui, H., et al., *Fast preparation procedure for large, flat cellulose and cellulose/inorganic nanopaper structures*. Biomacromolecules, 2010. **11**(9): p. 2195-8.
66. Garusinghe, U.M., et al., *Nanocellulose-montmorillonite composites of low water vapour permeability*. Colloids and Surfaces A: Physicochemical and Engineering Aspects, 2018. **540**: p. 233-241.
67. Alothman, Z., *A Review: Fundamental Aspects of Silicate Mesoporous Materials*. Materials, 2012. **5**(12): p. 2874-2902.
68. Nair, S.S., et al., *High performance green barriers based on nanocellulose*. Sustainable Chemical Processes, 2014. **2**(1): p. 23.
69. Likhomanova, P.A., et al., *Modeling of Particle Diffusion in Heterogeneous Structure Near to the Percolation Threshold*. Physics Procedia, 2015. **72**: p. 42-46.
70. Grekhov, A.M., et al., *Percolation of composite poly(vinyltrimethylsilane) membranes with carbon nanotubes*. Petroleum Chemistry, 2013. **53**(8): p. 549-553.

71. Bourlieu, C., et al., *Edible Moisture Barriers: How to Assess of their Potential and Limits in Food Products Shelf-Life Extension?* Critical Reviews in Food Science and Nutrition, 2009. **49**(5): p. 474-499.
72. Aulin, C. and T. Lindstrom, *Biopolymer Coatings for Paper and Paperboard*, in *Biopolymers – New Materials for Sustainable Films and Coatings*.
73. Park, H.J. and M.S. Chinnan, *Gas and water vapor barrier properties of edible films from protein and cellulosic materials*. Journal of Food Engineering, 1995. **25**(4): p. 497-507.
74. Rhim, J.-W. and P.K.W. Ng, *Natural Biopolymer-Based Nanocomposite Films for Packaging Applications*. Critical Reviews in Food Science and Nutrition, 2007. **47**(4): p. 411-433.

THIS PAGE HAS BEEN INTENTIONALLY LEFT BLANK

---

---

## **CHAPTER 3**

**THE EFFECT OF PULP TYPE ON THE BARRIER AND ANTIMICROBIAL  
PERFORMANCE OF MICROFIBRILLAR LIGNOCELLULOSIC BISMUTH-BASED  
ACTIVE PACKAGING MATERIAL**

---

---

THIS PAGE HAS BEEN INTENTIONALLY LEFT BLANK

**PREFACE**

Although the potential of the use of the *bis*-phosphinato bismuth (III) complex in nanocellulose packaging materials was proved in the previous chapter, isolation of pure cellulose and nanocellulose production from pure cellulosic source is not very common. The commonly used pulp in most paper mills has been studied in this chapter for developing lignocellulosic-bismuth complex composites and their potential for active packaging material was established. The aim of this chapter was to investigate the effect of the different types of pulp on the interaction of the complex with the matrix phase and its influence on the properties of the composites. This chapter not only identifies the optimal pulp as a carrier matrix for the *bis*-phosphinato bismuth complex, but also explores new avenues about the retention of the complex within composites and how this plays a role in the antimicrobial properties. This chapter also identifies a major difference in the bismuth complex arrangement within the composites when the sheets are prepared via spraying vs. vacuum filtration and how this affects the mechanical and barrier properties of the composites. Overall, this chapter follows the second research objective of this thesis.

THIS PAGE HAS BEEN INTENTIONALLY LEFT BLANK

---

**CHAPTER 3: THE EFFECT OF PULP TYPE ON THE BARRIER AND ANTIMICROBIAL PERFORMANCE OF MICROFIBRILLAR LIGNOCELLULOSIC BISMUTH-BASED ACTIVE PACKAGING MATERIAL**

<b>3.1. Abstract.....</b>	<b>109</b>
<b>3.2. Keywords.....</b>	<b>110</b>
<b>3.3. Introduction .....</b>	<b>110</b>
<b>3.4. Methodology .....</b>	<b>112</b>
3.4.1. Materials.....	112
3.4.2. Preparation of the films.....	112
3.4.3. Characterisation.....	113
3.4.3.1. Physical properties .....	113
3.4.3.2. SEM characterisation .....	113
3.4.3.3. Surface characterisation .....	113
3.4.3.4. Aspect Ratio measurement.....	113
3.4.3.5. FTIR analysis .....	113
3.4.3.6. ICP-OES analysis.....	114
3.4.4. Antibacterial properties.....	114
3.4.5. Release behaviour .....	114
3.4.6. Water vapor transmission rate.....	115
3.4.7. Mechanical properties .....	115
<b>3.5. Results and Discussion.....</b>	<b>115</b>
3.5.1. Visual Observation.....	115
3.5.2. Characterisation.....	116
3.5.2.1. Physical properties .....	116
3.5.2.2. SEM characterisation .....	116
3.5.2.3. Surface characterisation .....	117
3.5.2.4. Aspect Ratio .....	118
3.5.2.5. FTIR analysis .....	119
3.5.2.6. ICP-OES analysis.....	120
3.5.3. Antibacterial properties.....	120
3.5.4. Release behaviour .....	122
3.5.5. Water vapor transmission rate.....	123

3.5.6. Mechanical properties.....	124
<b>3.6. Conclusion .....</b>	<b>126</b>
<b>3.7. Acknowledgements .....</b>	<b>126</b>
<b>3.8. References.....</b>	<b>127</b>

**THE EFFECT OF PULP TYPE ON THE BARRIER AND ANTIMICROBIAL  
PERFORMANCE OF MICROFIBRILLAR LIGNOCELLULOSIC BISMUTH-BASED  
ACTIVE PACKAGING MATERIAL**

Maisha Maliha<sup>1</sup>, Rajini Brammananth<sup>2</sup>, Ross L. Coppel<sup>2</sup>, Melissa Werrett<sup>3</sup>, Philip Andrews<sup>3</sup>,  
Warren Batchelor<sup>1\*</sup>

<sup>1</sup>*Bioresource Processing Research Institute of Australia (BioPRIA), Department of Chemical Engineering, Monash University, VIC 3800, Australia*

<sup>2</sup>*Department of Microbiology, Monash University, VIC 3800, Australia*

<sup>3</sup>*School of Chemistry, Monash University, VIC 3800, Australia*

Corresponding author email: warren.batchelor@monash.edu

### **3.1. Abstract**

Microfibrillated cellulose from pulps with different cellulose, hemicellulose, lignin and extractive content were used as the matrix phase with antimicrobial *bis*-phosphinato bismuth complex as the dispersed phase. The aim of the study was to investigate the effect of the source and type of pulp on the composite properties and identify the best pulp to develop active packaging material. Bleached and unbleached kraft and thermomechanical pulp (TMP) were refined to the same degree and the breakdown was observed to be relatively higher in the kraft pulp. The thin fibres of the kraft pulp observed in the SEM images and their high aspect ratio indicates that these are more fibrillated than the TMP. These fibrillated cellulose fibres form a strong close network resulting in low water vapor transmission rate (WVTR) and high tensile index. The bismuth complex does not have any detrimental effect on the mechanical properties and further improves the barrier properties of the composites. The high hydrophilicity of the bleached kraft pulp, from both softwood and hardwood, results in a weak bond with the hydrophobic bismuth complex, causing its higher leachability and thereby resulting in larger zones of inhibition against both Gram-positive and Gram-negative bacteria. Therefore, bleached kraft pulp was found to be the most suitable with promising barrier, mechanical and antibacterial properties, followed by unbleached kraft pulp, bleached TMP and then the unbleached TMP.

### 3.2. Keywords

Bismuth, kraft, thermomechanical, packaging, antibacterial

### 3.3. Introduction

Polymeric materials are used for packaging applications to protect its content from contaminants and gases like water vapor and oxygen [1]. While conventional packaging only acts as a physical barrier, antimicrobial (AM) packaging provides additional protection by protecting them from microbial contamination. Antimicrobial packaging helps prevent microbial growth on its surface, thus reducing chances of contamination and spoilage [2]. AM packaging can be achieved by incorporation of antimicrobial agents into the polymeric matrix.

Metal based antimicrobial agents are becoming increasingly popular among researchers; examples include nanoparticles, inorganic compounds and organometallic complexes of gold, silver, zinc etc [3]. Metal based antimicrobials can have multiple mechanisms of action on microorganisms, making it difficult for bacteria to develop resistance [3, 4]. Due to the overuse of the common antimicrobial agents, large fraction of bacterial population has developed antimicrobial resistance towards them [5]. So, there is a constant need to study new antimicrobial agents. One such agent is the *bis*-phosphinato bismuth complex. We have shown recently this compound to have good antimicrobial properties [6]. The complex is very sparingly soluble in water, opening up opportunities to be incorporated into materials [7].

Active packaging materials have been studied using different polymers like polyethylene, ethylene vinyl alcohol etc. [8, 9]. Commercial AM packaging also uses such petroleum based polymeric matrices. Recently, the attention towards green and sustainable polymers as replacement to them is rising for such applications. Lignocellulosic materials are of great interest because of their biodegradability, renewability and ready availability. Microfibrillated cellulose (MFC) films are an interesting material for packaging applications, as the process of mechanical treatment to reduce fibre size substantially improves barrier and mechanical properties [10]. We have recently shown that MFC films loaded with the *bis*-phosphinato bismuth complex can serve as high performance packaging material with antimicrobial activity towards some of the most concerning drug-resistant bacteria and fungi [11].

Commercialisation of pure MFC products is still challenging and the current market is quite small. Bacterial cellulose and some plant sources like cotton are composed of pure cellulose and can be directly used for MFC production [12]. However, most paper mills use wood based sources to produce pulp with different compositions, containing different levels of cellulose and other

components (hemicellulose, lignin and extractives). Integrating the Bi-MFC composite production into conventional pulp and paper mills can reduce production cost. Hence, this paper presents the preparation and characterisation of Bi-MFC composites using the pulp from conventional pulp and paper mills. The wood is processed to pulp in different ways in the mills to separate the fibres either chemically (kraft, sulphite and soda pulping), mechanically or thermomechanically. The kraft process, the most common chemical pulping method, uses NaOH and Na<sub>2</sub>S to break the bonds among the cellulose, hemicellulose and lignin, getting rid of most of the lignin [13]. It was reported that a bleached kraft pulp contains 79% cellulose and 18% hemicellulose, and very small amounts of lignin, extractives and ash [14]. Bleached kraft pulp is the most commonly used pulp for MFC production [15] or for preparation of MFC films and composites [16-19]. Thermomechanical pulping uses heat and mechanical refining to soften the lignin to separate the fibres but does not remove the lignin, leaving approximately 30% lignin [20]. There are limited studies using thermomechanical pulp (TMP) for antimicrobial composites, and so the effect of such pulp on the film properties for active packaging is not understood. In fact, only a few studies have investigated the use of TMP for MFC production [21].

The treated wood pulp fibres are often bleached, using chlorine-based chemicals, hydrogen peroxide or other bleaching agents, to increase their brightness for paper-making. Bleaching of chemical pulp removes the residual lignin to whiten the pulp. The removal of lignin increases the fibre-fibre bonding. Bleaching mechanical pulp involves a very different approach. The large amounts of lignin present are not removed, but the chromophores (part of the lignin molecule responsible for the colour) are altered by redox reactions. Paper from thermomechanical treatment is usually used for newspapers, which can yellow as it ages due to production of new chromophores from the lignin present there [13]. Moreover, the source of fibres also plays an important role since softwood and hardwood differ in physical dimensions. Softwood fibres are longer and thicker compared to hardwood fibres and so are harder to fibrillate [22]. Composites from natural fibres have different properties, depending on the type and content of fibre, fibre orientation, porosity, and hydrophilicity which is determined by the feedstock source and pulping process involved [23, 24]. Herein, composites were made with MFC from different pulp type and sources as the matrix phase and the antimicrobial organobismuth complex as the dispersed phase. Figure 1 shows the sources and types of pulp studied herein describing where they are obtained from in a paper mill. The aim of the study was to characterise bismuth phosphinato loaded MFC composites and understand the effect of the carrier matrix on its properties for packaging applications.

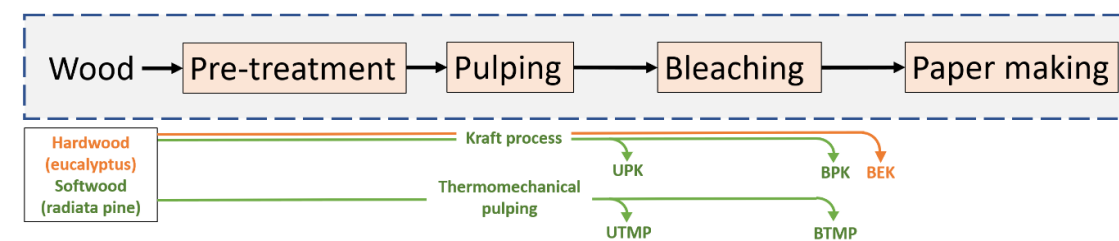


**Figure 1:** Representation of the sources and types of the pulp used for Bi-MFC composites preparation. The dashed box shows the simplified flowchart of the major processes in the paper mills. The green and the orange arrows show the preparation of the softwood and the hardwood pulp respectively. Here the acronyms UPK, BPK, BEK, UTMP and BTMP stands for unbleached pine kraft pulp, bleached pine kraft pulp, bleached eucalyptus kraft pulp, unbleached thermomechanical pulp and bleached thermomechanical pulp respectively.

### 3.4. Methodology

#### 3.4.1. Materials

Bleached eucalyptus kraft pulp (BEK) was obtained from Australian Paper, Maryvale, Australia. Bleached (BPK) and unbleached (UPK) Radiata pine kraft pulp were obtained from Oji Fibre Solutions, New Zealand. The bleached (BTMP) and unbleached (UTMP) Radiata Pine thermomechanical pulp were obtained from Norske Skog, Australia. The *bis*-phosphinato bismuth complex was prepared as described in our previous works [7, 25]. In brief, diphenyl phosphinic acid and triphenyl bismuth were heated under reflux for 24 hours and the complex was then separated from the reaction mixture as dry powder.

#### 3.4.2. Preparation of the films

The different types of pulp were subjected to mechanical treatment using PFI mill refiner. The pulp was diluted to 10 wt% and was then subjected to 20,000 PFI mill refining revolutions. The fibres were then diluted to 1.2wt% and disintegrated in a 3L Mavis standard disintegrator (Model 8522) for 15000 revolutions. The stock suspension was diluted to 0.2 wt% with either deionised water or Bi-complex and water suspension to make blank films or Bi-loaded composite films respectively. The Bi-complex suspension was prepared by suspending a known mass of bismuth complex in deionised water and subjected to high speed dispermat at 2000 rpm for 1 hour. The amount of bismuth complex in the suspension was determined to achieve a target loading of 1% Bi complex (g of Bi-complex/g composite film). The pulp suspensions were then made into films of target basis weight of 60g/m<sup>2</sup> using the British Handsheet Maker according to the TAPPI

standard T205. Films were prepared by pouring the suspension into the handsheet maker over filter paper (GE Whatman 541 Hardened Ashless filter paper) on top of the 150-mesh screen.

### **3.4.3. Characterisation**

#### **3.4.3.1. Physical properties**

The basis weight of the film was determined by measuring the dried weight of a known area of sample and dividing the weight by the area. The thickness of the films were measured using an L&W thickness tester and expressed as an average of 7 points from 3 different films and expressed as mean  $\pm$  st. dev. The density is calculated by dividing the basis weight by the thickness.

#### **3.4.3.2. SEM characterisation**

The composites were cut into small pieces and mounted on a metal stub. The sample was secured using carbon tape and sputter coated with iridium metal. Scanning electron microscope (SEM) imaging of the coated samples were then done using FEI Magellan 400 FEGSEM.

#### **3.4.3.3. Surface characterisation**

The surface of the blank films was studied using an OLS 5000 optical profilometer (Olympus Corporation). A height profile was analysed using the Analysis application software supplied with the instrument at the centre line of the 2D image.

#### **3.4.3.4. Aspect Ratio measurement**

The aspect ratio of the refined fibres were determined using the gel-point measurement method as described in Varanasi *et al.* [26]. MFC suspensions of different solid concentrations ranging from 0.01 wt% to 0.1 wt% were poured into measuring cylinders and allowed to sediment for 48 hours. The initial height of the suspension ( $h_0$ ) and the final sedimentation height ( $h_s$ ) were measured. The concentration vs. ratio of final to initial height ( $h_s/h_0$ ) was fitted with a smoothing spline using the Curve Fitting Tool in MATLAB [27]. The gel point is the y-intercept of its first derivative curve. The Effective Medium Theory (EMT) and Crowding Number (CN) empirical equations were then used to determine the aspect ratio.

#### **3.4.3.5. FTIR analysis**

The FTIR analysis was carried out using Agilent Technologies Cary 630 ATR-FTIR (Attenuated total reflectance-Fourier Transform Infrared). The samples were placed on the diamond and scans at  $4\text{cm}^{-1}$  in the range of 4000 to  $800\text{cm}^{-1}$  were done.

#### 3.4.3.6. ICP-OES analysis

To quantify the amount of the bismuth complex in the composite films, ICP-OES (Inductively coupled plasma- optical emission spectroscopy) analysis was performed. Known mass of the films (10-20 mg) were ashed in a muffle furnace where the temperature was ramped from 25 °C to 600 °C over 3 hours and maintained at 600°C for an additional three hours. The ash was then dissolved in nitric acid and the amount of bismuth dissolved in the acid was then analysed using ICP-OES. This was then calculated to quantify the amount of the complex per gram of the composite films.

#### 3.4.4. Antibacterial properties

The antibacterial activity of the films were analysed using the Gram-positive strains *Staphylococcus aureus* (A134/ATCC 6538) and MRSA (M118797, methicillin-resistant *Staphylococcus aureus*) and the Gram-negative strains *Escherichia coli* (G102), and *Acinetobacter baumannii* (C403/ATCC17978). LB (Luria-Bertani) agar plate was used for all bacteria except for *S. aureus*, for which nutrient agar plate was used. Agar plates were spread with 20 µL of overnight culture of a specific bacterium and 6 mm discs of the film was placed on the agar plate. The plates were incubated at 37 °C for 24 hours and the zone of inhibition was measured. For each type of pulp, blank films (no bismuth) were tested as the control. Each experiment was repeated three times.

The overtime effectiveness study was performed for a specific bacteria – *S.aureus* for 5 days. Herein, the experiment was performed the same way as mentioned above. After 24 hours of incubation of the plate, the discs were transferred using a sterile tweezer to a new agar plate freshly spread with the same bacterial strain. The plates were then incubated for 24 hours to measure the zone of inhibition formed on day 2. This was repeated until 5 days total incubation time was reached.

#### 3.4.5. Release behaviour

The release behaviour was studied by suspending 5 circles of the composites of 6 mm diameter in 10 mL of Milli-Q water contained in a falcon tube. The tubes were kept in an incubator shaker at 25 °C at 150 rpm for 24 hours. The water was then analysed using ICP-MS (Inductively coupled plasma- mass spectroscopy).

### 3.4.6. Water vapor transmission rate

The water vapor transmission rate (WVTR) was studied using ASTM E96 desiccant method. Standard cups containing the desiccant were sealed with the sample and incubated at 23 °C and 50 % relative humidity. Weight of the cups were recorded at regular intervals and the loss in mass was plotted as a function of time. The rate of change of mass obtained from the slope was used to calculate the water vapor transmission rate.

### 3.4.7. Mechanical properties

The mechanical properties of the films were determined using Instron Tensile Tester (Model 5965). The samples were cut into 15 mm wide strips and conditioned for 24 hours at 23 °C and 50% relative humidity. 50 mm span was tested using a constant strain rate of 10 mm/min. The results were presented as an average of six replicates.

## 3.5. Results and Discussion

### 3.5.1. Visual Observation

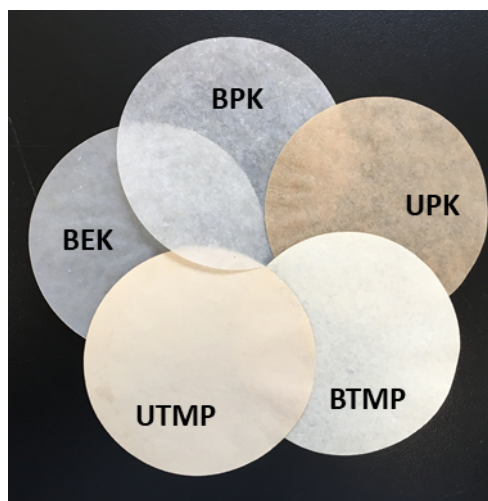


**Figure 2:** Physical appearance of the composites using bleached eucalyptus kraft pulp (BEK), bleached (BPK) and unbleached (UPK) radiata pine kraft pulp and bleached (BTMP) and unbleached (UTMP) radiata pine thermomechanical pulp

Figure 2 shows the physical appearance of the composites. It can be seen that the bleached composites are whiter compared to its unbleached counterpart (BPK vs UPK and BTMP vs. UTMP), as expected. Bleached kraft pulp from both the softwood (BPK) and hardwood (BEK) looked similar. However, the bleached thermomechanical pulp film (BTMP) is more yellow,

which is due to its higher lignin content. Hence the pulping method and the bleaching step has a significant influence on the appearance of the composites.

### 3.5.2. Characterisation

#### 3.5.2.1. Physical properties

**Table 1:** Physical properties of the blank films and the Bi-loaded composite films from bleached eucalyptus kraft pulp (BEK), bleached (BPK) and unbleached (UPK) radiata pine kraft pulp and bleached (BTMP) and unbleached (UTMP) radiata pine thermomechanical pulp

Source of wood	Type of pulp	Sample	Basis weight (g/m <sup>2</sup> )	Thickness (μm)	Density (g/cm <sup>3</sup> )	
Hardwood (eucalyptus)	Kraft	BEK	Blank	69±3	87±6	0.80
			Bi-loaded	69±1	85±5	0.81
BPK		Blank	62±3	94±7	0.66	
		Bi-loaded	62±3	91±5	0.68	
Softwood (radiata pine)		UPK	Blank	64±2	107±6	0.59
			Bi-loaded	69±1	107±5	0.65
	BTMP	Blank	64±2	101±4	0.63	
		Bi-loaded	66±2	105±8	0.63	
	UTMP	Blank	62±2	115±11	0.54	
		Bi-loaded	62±1	120±10	0.52	

#### 3.5.2.2. SEM characterisation

Figure 3 shows the secondary electron images of the composites prepared from the different kinds of pulp. Herein, it is clearly seen that the composites from the kraft pulp (BEK, BPK, UPK) is made of significantly thinner fibres compared to the thermomechanical pulp (BTMP, UTMP). The kraft pulp films consist of a closely arranged network of mostly very thin fibres with a few thicker fibre bundles. The thermomechanical films, on the other hand, are made up of thick bundles of fibres forming an open and more porous network. Spence et al. reported that kraft pulps produces fibres in nanometre range, but the same fibrillation treatment resulted in TMP fibres in micron scale. Unrefined fibres from both bleached and unbleached softwood pulp were reported to be around 30 μm, bleached and unbleached hardwood pulp to be 20 μm, and TMP to be 34 μm [28]. The secondary electron images gives an understanding of the fibre dimensions to better understand the film properties. The back-scattered electron (BSE) images in figure S1

shows that the bismuth complex (shown as bright structures) are distributed throughout the material in all the composites.

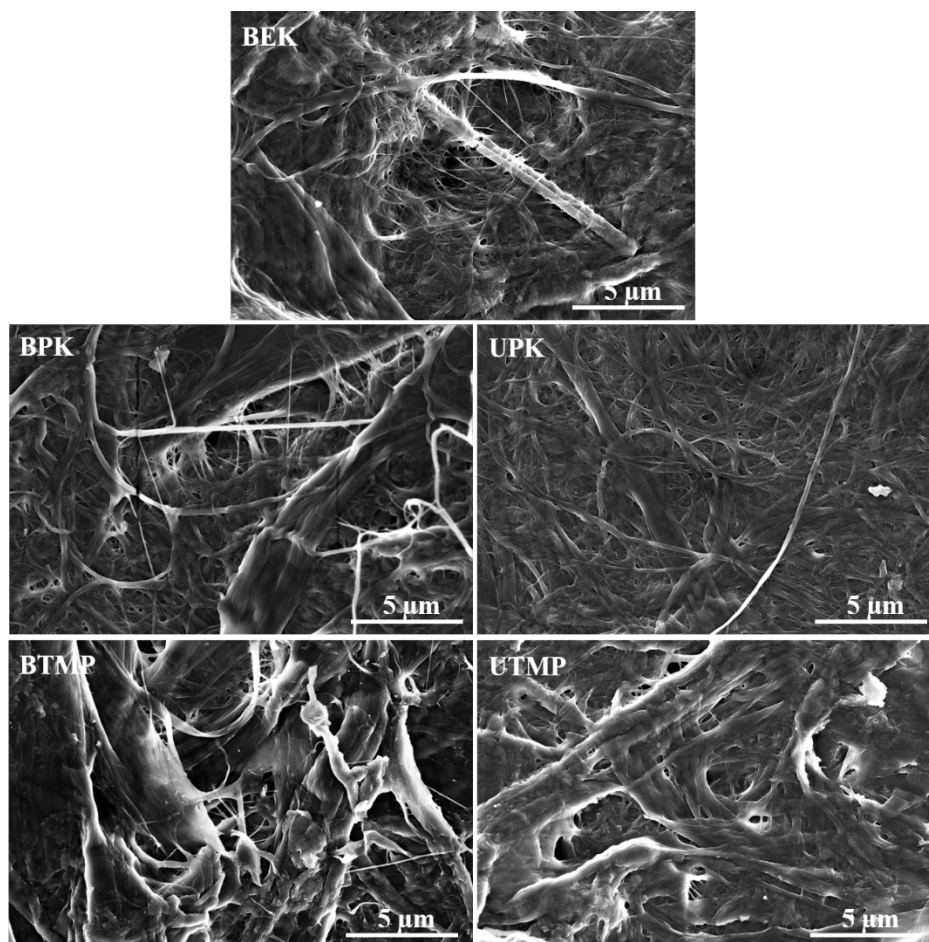


**Figure 3:** Micrographs of the composite films from bleached eucalyptus kraft pulp (BEK) (top), bleached (BPK) and unbleached (UPK) radiata pine kraft pulp (middle panel), bleached (BTMP) and unbleached (UTMP) radiata pine thermomechanical pulp (bottom panel) showing the fibre dimensions.

### 3.5.2.3. Surface characterisation

Figure 4 shows the optical profilometry images of the surface of the blank films and their height profiles. The height profile of the images on the horizontal centre line (white dashed line) shows that the bleached and unbleached thermomechanical pulp films demonstrate more variation in height. The height variation of BEK, BPK and UPK does not exceed 15 μm, whereas BTMP and UTMP surfaces show height up to 20 and 25 μm respectively. The larger difference in height in the TMP films signifies presence of thick fibres giving rise to a rougher surface. While the SEM images provides higher resolution micrographs with qualitative information about the fibre size,

the height data in the profilometry images gives a good understanding about the surface topography of the films over a larger area.

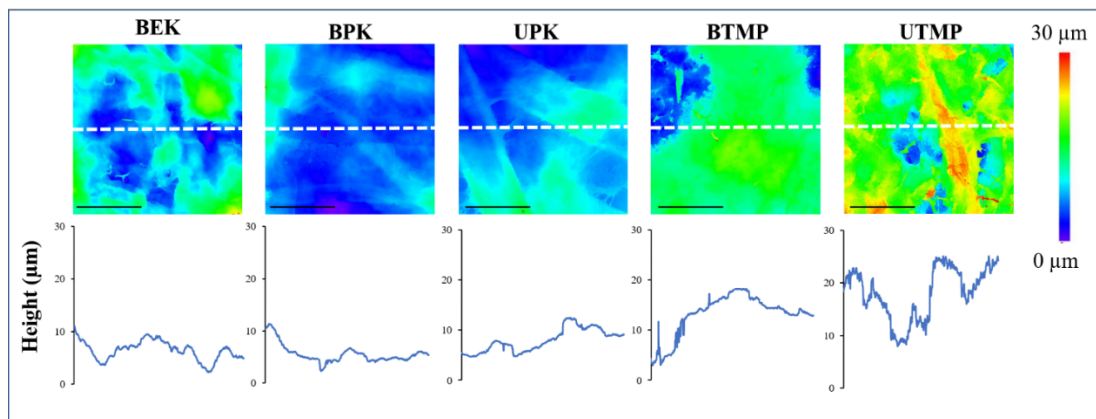


**Figure 4:** Optical profilometry images of the surface of blank films (no bismuth) (top panel) and the height profiles of the surface along the horizontal centre line shown (bottom panel). The scale bars indicate 50  $\mu\text{m}$ .

#### 3.5.2.4. Aspect Ratio

**Table 2:** Average aspect ratio values calculated from the gel point determined using the EMT and CN empirical equations

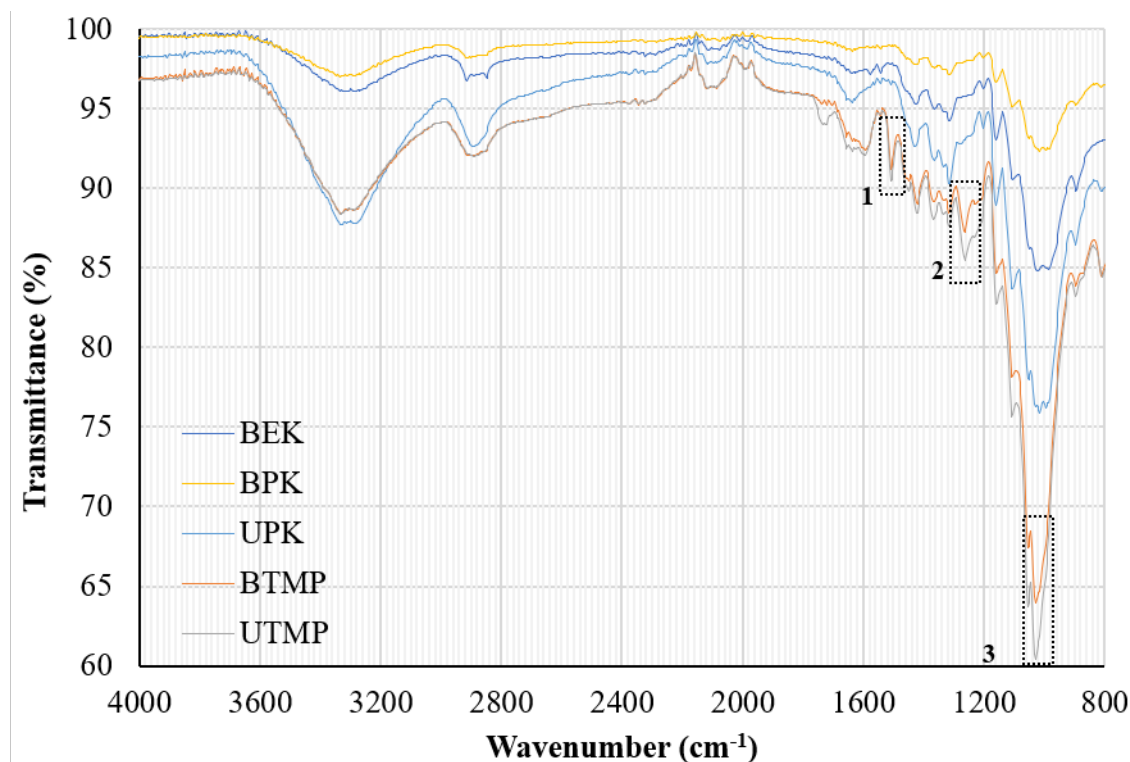
Type of pulp	Gel point, $C_c$ (wt%)	Aspect Ratio	
		EMT	CN
BEK	0.222	109	127
BPK	0.150	137	155
UPK	0.119	157	174
BTMP	1.110	43	57
UTMP	0.824	51	66

Table 2 shows the aspect ratios of the fibres studied using the EMT and CN theories. It is clear that the kraft pulp (BEK, BPK, UPK) have lower gel point and higher aspect ratio compared to the thermomechanical pulp (BTMP and UTMP). The gel point is the lowest concentration at which the fibres in the suspension can form a continuous network and the aspect ratio is the ratio of length to diameter of each of the fibres, both giving us an indication of the fibre dimensions. The kraft pulp has significantly higher aspect ratio, indicating they are much easier to fibrillate. Similar result was also reported by Peltola *et al.* [29]. On the other hand, the aspect ratio for TMP is quite low. Gunawardhana *et al.* reported that TMP is much less responsive to fibrillation treatment and even energy-intensive treatments of up to 200,000 kWh/tonne fibre can only change

the aspect ratio to 120 approximately and reduce the fibre diameter to 40nm [21]. In comparison, with BEK a fibrillation treatment of only 3542 kWh/tonne is sufficient to achieve an aspect ratio of 102 and fibre diameter of 31 nm. In fact, 40,000 kWh/tonne will result in aspect ratio and fibre diameter of 229 and 12nm respectively [30]. In this paper, the refining treatment is equivalent to 7000 kWh/tonne fibre. Softwood fibres are longer than hardwood fibres [22], which could be the reason behind slightly higher aspect ratio of BPK than BEK.

### 3.5.2.5. FTIR analysis

Figure 5 shows the FTIR spectra of the bismuth complex loaded composite films prepared using the different kinds of pulp. FTIR analysis of both the blank and Bi-loaded films were performed. They do not show any change in peaks irrespective of the presence or absence of the complex, since a low level of loading (1 wt%) has been studied here. Thus, the spectrum for the Bi-loaded composites only are shown in the figure for simplicity and the spectra of the blank films are shown in figure S2. There are a few strong peaks for the bleached and unbleached thermomechanically treated pulp films (BTMP and UTMP), which are missing in the kraft pulp ones. The peaks at  $1510\text{ cm}^{-1}$  (labelled as 1) represent the aromaticity, at  $1260\text{ cm}^{-1}$  (labelled as 2) represent the alkyl aryl group, and the peaks at  $1020\text{ cm}^{-1}$  (labelled as 3) represent the aliphatic ether in the lignin.



**Figure 5:** FTIR spectrum of the Bi-complex loaded films prepared from bleached eucalyptus kraft pulp (BEK), bleached (BPK) and unbleached (UPK) radiata pine kraft pulp and bleached (BTMP)

and unbleached (UTMP) radiata pine thermomechanical pulp showing the difference in chemical composition

Thermomechanical treated pulp has around 38% cellulose and quite high lignin content of 30% approximately, along with the highest level of extractives. Bleached and unbleached kraft pulp from softwood or hardwood, on the other hand, has high cellulose content (78-79%), around 20% hemicellulose and low lignin and extractives content [28]. The large amounts of lignin present in the thermomechanically treated pulp is evident from the FTIR results.

### 3.5.2.6. ICP-OES analysis

**Table 3:** Actual bismuth complex content of the composite films analysed from ICP-OES analysis

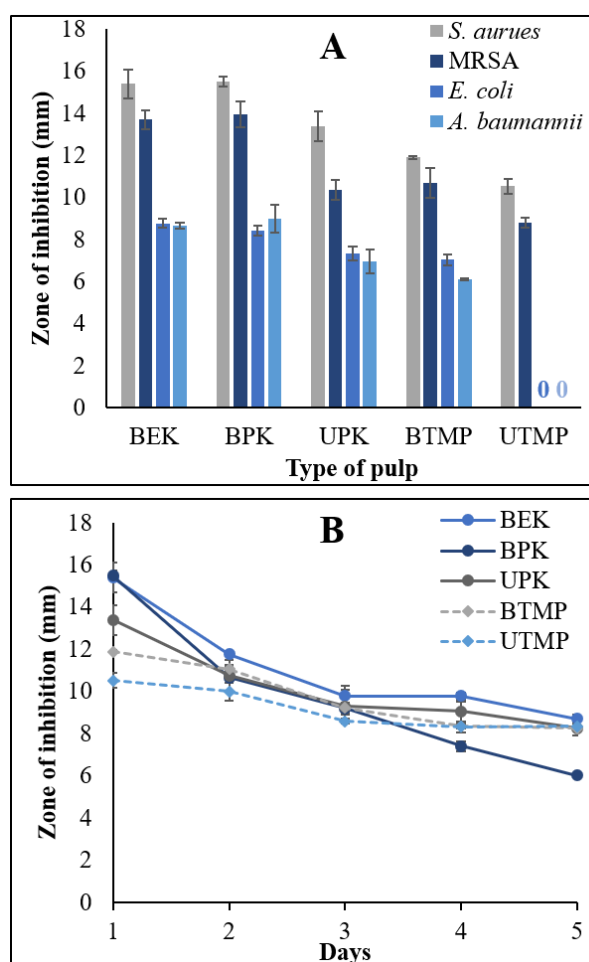
Type of pulp	Actual Bi-complex content (wt%) (g of Bi complex/g composite film)
BEK	0.78±0.01
BPK	0.82±0.01
UPK	1.09±0.19
BTMP	1.10±0.03
UTMP	1.04±0.03

Table 3 shows the actual amount of bismuth complex in the composites determined using ICP-OES analysis. It can be clearly seen that the bleached kraft pulps have slightly lower bismuth complex than targeted, similar to our previous work [25]. It can be speculated that the highly hydrophobic nature of the complex results in loss of the complex while preparation of the films. On the other hand, the unbleached kraft pulp and the thermomechanically treated pulp contains the targeted amount within the standard error limits. Kraft pulp has very low levels of lignin, and bleaching removes any residual lignin. Lignin, being a complex organic polymer containing phenol groups, forms hydrophobic interactions with the bismuth complex, resulting in higher additive retention in the composites. Similarly, the lignin in the unbleached kraft pulp, although in small quantities, helps in the bismuth complex retention in the composites. The lignin-free bleached kraft pulp, containing mainly hydrophilic cellulose, does not have a hydrophobic interaction with the complex, resulting in more loss of the complex.

### 3.5.3. Antibacterial properties

Figure 6 shows the zones of inhibition of the bismuth complex loaded composites prepared from different types of pulp. Figure 6(A) shows that the composites have larger zones of inhibitions and appears to be more susceptible to the Gram-positive bacteria (*S. aureus* and MRSA) compared

to the Gram-negative ones (*E. coli* and *A. baumannii*). This is consistent with our previous work with bismuth complex-MFC composites [25]. Gram-negative bacteria are harder to kill due to its lipopolysaccharide membrane, which is absent in Gram-positive bacteria. Larger zones of inhibition typically indicate a low minimum inhibitory concentration and hence somewhat higher relative susceptibility, but this is often debatable and is thought to be dependent on a number of other factors [31]. However, the complex has been shown to be selectively more active on the Gram-negative bacteria when prepared in hydrogel form and dispersed in a bacterial broth in our previous work [32]. This difference in behaviour from the disk diffusion test and the broth suspension is not yet understood.



**Figure 6:** The zones of inhibition of the bismuth loaded composites of bleached eucalyptus kraft pulp (BEK), bleached (BPK) and unbleached (UPK) radiata pine kraft pulp and bleached (BTMP) and unbleached (UTMP) radiata pine thermomechanical pulp against different bacteria after 24 hours (A) and against *S. aureus* over a period of 5 days (B). There was no zone observed where it is labelled with a zero (0) in the graph.

The bleached kraft pulp films (both BEK and BPK) have similar and large zones of inhibition, followed by the unbleached kraft pulp and then the thermomechanically treated pulps. However, the unbleached thermomechanical pulp composite do not inhibit the growth of both the Gram-negative bacteria. It is interesting that although the BEK and BPK showed higher zone of inhibition, they showed lower bismuth content than the target loading according to the ICP-OES analysis. The larger zones of inhibition for the bleached kraft pulp could potentially be due to higher leaching ability of the bismuth complex. Figure 6(B) shows the antibacterial activity of the composites over a period of 5 days against the Gram-positive bacteria *S. aureus*. The zone of inhibition decreases with each day due to the loss of the bismuth complex that has leached out into the agar. Similar behaviour was also observed in our previous work [25].

#### 3.5.4. Release behaviour

Figure 7 shows the percentage of bismuth complex leached out into the water with respect to the total amount of bismuth complex present in the composites. The bleached kraft softwood pulp (BPK) shows the highest amount of complex leached into the water, followed by similarly treated hardwood pulp (BEK). The bismuth complex is a highly hydrophobic complex, and has been suggested to exist in a polymeric form [7]. It is likely that the complex is weakly bonded with the bleached kraft pulp. The kraft pulp contains mainly cellulose and hemicellulose, which are hydrophilic polymers. The complex is sustained in the matrix only by physical entrapment within the fibre network. This could have resulted in lower loading of the bismuth complex than the target loading in these composites presented in Table 3. This also explains the higher release behaviour of the complex into the agar plates resulting in relatively larger zones of inhibition in Figure 6. On the other hand, the thermomechanical pulp contains a large amount of lignin, which forms a hydrophobic interaction with the complex. The behaviour of lignin in TMP forming higher adhesion with co-polymer PLA in composites was also reported previously [29].

The highest leachability of BPK explains its loss of antibacterial activity over time. Lesser amount of the bismuth complex diffuses out from unbleached kraft pulp and the bleached and unbleached thermomechanical pulp. The unbleached thermomechanical pulp (UTMP) leaches the least and hence the accessibility of the complex for the bacteria is reduced explaining the reduced antibacterial effectiveness. The lower accessibility of the complex in UTMP reduces its effectiveness against the hard-to-treat Gram-negative bacteria.

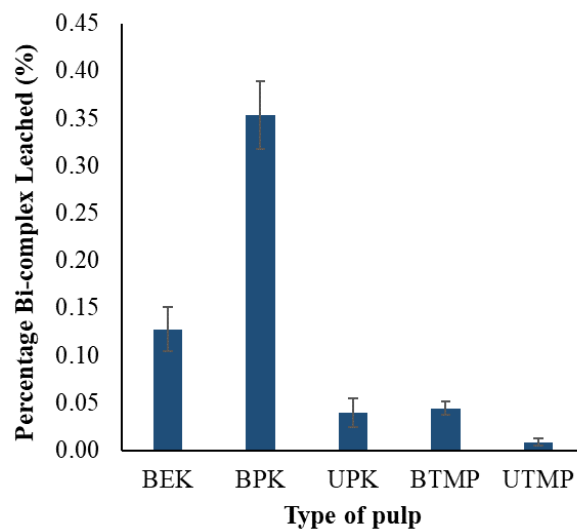


**Figure 7:** The percentage of Bi-complex released into water from composite films of bleached eucalyptus kraft pulp (BEK), bleached (BPK) and unbleached (UPK) radiata pine kraft pulp and bleached (BTMP) and unbleached (UTMP) radiata pine thermomechanical pulp. The bars represent the percentage of bismuth complex present in the leachate after 24 hours with respect to the mass of the complex contained in the composites. The error bars represents the standard deviation.

### 3.5.5. Water vapor transmission rate

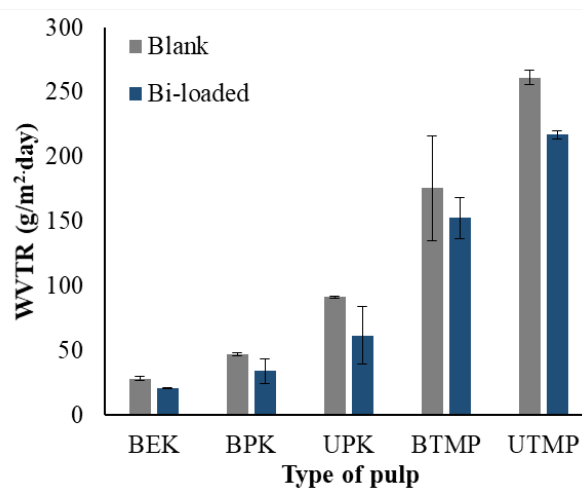


**Figure 8:** The water vapor transmission rate (WVTR) of the films prepared from bleached eucalyptus kraft pulp (BEK), bleached (BPK) and unbleached (UPK) radiata pine kraft pulp and bleached (BTMP) and unbleached (UTMP) radiata pine thermomechanical pulp with and without the bismuth complex at 23°C and 50% relative humidity. The error bars indicate standard deviations.

Figure 8 shows the water vapor transmission rate of the films prepared from the different types of pulp. It is very clear that the kraft pulp films (20-91 g/m<sup>2</sup>.day) have better water vapour barrier performance to water vapor compared to the thermomechanical films (153-261 g/m<sup>2</sup>.day). The chemically treated pulp are more easily refined and when subjected to similar refining treatments, the kraft pulp undergo more fibrillation than the thermomechanical pulp. This can be verified from the SEM images showing thinner fibre diameter for the kraft pulp. The thin fibres form a dense network held together by strong hydrogen bonding. This dense network increases the tortuosity making it harder for small water vapor molecules to pass through. The strong hydrogen bonding also results in stronger films.

WVTR is reported to be dependent on the material density [33], which was higher for BEK (0.80 and 0.81 g/cm<sup>3</sup>) compared to BPK (0.66 and 0.68 g/cm<sup>3</sup>), as presented in Table 1. Thus, since both BEK and BPK are bleached kraft pulp, the difference in density could be the reason for the variation in water vapor transmission rate. With decrease in density, the films have a more open network structure and thus gives rise to an increased pore volume. Moreover, softwood fibres are long and thick and hardwood fibres being short and thin. Thus, softwood fibres need coarser refiner plates to break them down [22]. The fibres in BPK might not be as fibrillated as BEK which might have resulted in the variation in density and water vapor barrier performance. The films from bleached pulp (BPK and BTMP) shows better barrier performance than its unbleached counterpart (UPK and UTMP). Other studies have shown that the WVTR for bleached hardwood kraft pulp, unrefined or refined using valley beater and homogeniser, is lower than the unbleached pulp [34]. In our previous study, composites prepared by spraying technique showed increase in water vapor permeability on addition on bismuth complex [25]. Interestingly herein, the addition of bismuth complex decreases the transmission rate. The large bismuth complex particles seem to fill in the pores when vacuum was applied during sheet formation. The WVTR of a common packaging material, low density polyethylene, has been reported to be in the range of 16-23 g/m<sup>2</sup>/day [35]. The WVTR of cellulose nanofibres (CNF) and acylated CNF has been reported to be 234 g/m<sup>2</sup>/day and 167 g/m<sup>2</sup>/day respectively [36]. For a packaging application, a low WVTR is desired. Thus, based on the barrier properties, the kraft pulp is a better choice for preparation of bismuth complex loaded packaging material.

### **3.5.6. Mechanical properties**

The mechanical properties of the films from the different pulp with and without the bismuth complex are shown in Figure 9. The films from the kraft pulp have significantly higher tensile index and thus are stronger than the films from the thermomechanical pulp. Unrefined BEK has a tensile index of 30 Nm/g [30] which has been improved to 78±8 Nm/g. The mechanical

properties were reported to be independent of the lignin content up to 14% lignin by Rojo et al [33], which explains the similar mechanical properties of BPK and UPK. Beyond that level, high lignin content interferes significantly with the bonding between fibres. Mechanical treatment results in low strength pulp nonetheless [13], resulting in weaker films. The presence of large amounts of lignin in TMP limits the extent of fibrillation, resulting in larger fibre diameter and thereby weak films [28]. The addition of the bismuth complex does not have any detrimental effect on the tensile index of the films. However, the Young Modulus decreases implying that the films becomes slightly more elastic when the bismuth complex is present.

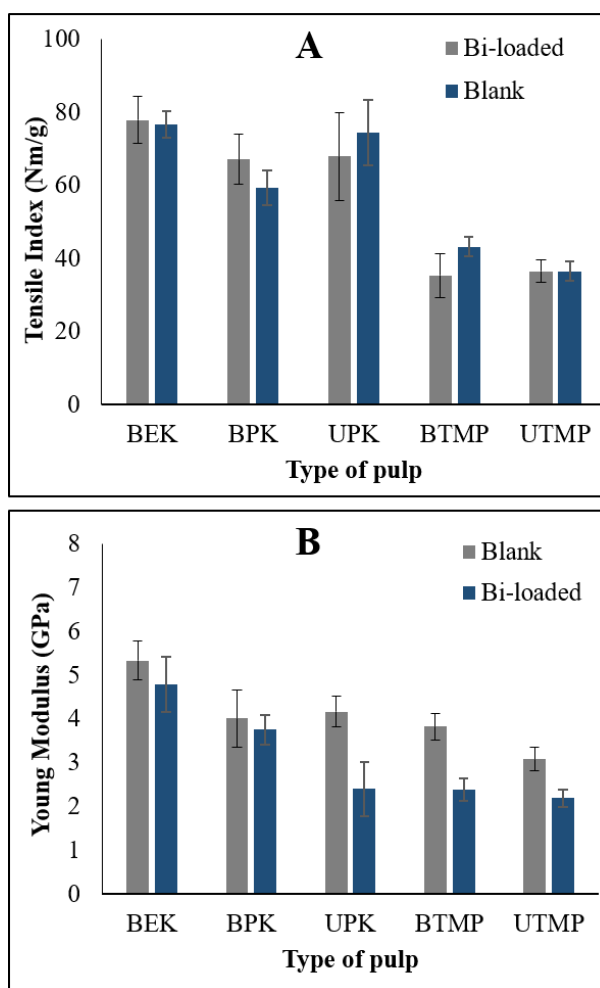


**Figure 9:** Mechanical properties from tensile testing for composite films from bleached eucalyptus kraft pulp (BEK), bleached (BPK) and unbleached (UPK) radiata pine kraft pulp and bleached (BTMP) and unbleached (UTMP) radiata pine thermomechanical pulp with and without bismuth complex loading expressed as an average tensile index (A) and Young modulus (B). Error bars represent 95% confidence interval.

### 3.6. Conclusion

MFC were prepared from bleached hardwood (eucalyptus) kraft pulp, bleached and unbleached softwood (radiata pine) kraft pulp, and bleached and unbleached thermomechanical pulp. Bisphosphinato bismuth complex loaded (1 wt%) MFC composites were prepared and characterised to understand their performance as active packaging material. The objective of this paper was to optimise the most suitable type of lignocellulosic matrix for such applications. We have seen that the performance of the composite material is determined by two controlling factors, viz. the interaction of the bismuth complex with the matrix phase and the physical dimensions of the fibres. While the leaching properties and the antibacterial activity is directly related to the bonding between the bismuth complex and the carrier matrix, the mechanical and barrier properties are linked to the extent of fibrillation. The weak interaction of the complex with the hydrophilic matrix in the bleached kraft pulp composites makes it more available to be released and kill the bacteria in the surrounding environment. The kraft pulps are most easily fibrillated and so produced the lowest diameter fibres, when refined to the same extent. This results in a more compact structure with strong hydrogel bond, thereby have low water vapor permeability and high tensile strength. Thus, the bleached kraft pulp appears to be a great choice in terms of barrier performance, mechanical properties and the antibacterial properties. Although the higher release in these composites results in better antibacterial performance, the loss of bismuth complex remains a drawback. Hardwood or softwood does not make a significant difference in the composite properties for packaging applications. The presence of the bismuth complex improves the barrier performance and does not have any significant detrimental effect on the tensile index. Thus, the bismuth complex can be used as the antibacterial agent in such lignocellulosic active packaging material. To utilise bismuth complex-MFC composite films as active packaging material, it is important to understand the material performance using the different kinds of pulp that is available in the paper mills. This paper provides a good understanding of that to help choose the best carrier matrix for the complex making it easier to translate the production in paper mills.

### 3.7. Acknowledgements

The authors acknowledge the financial support from Monash University and The National Health and Medical Research Council (APP1139844). The authors would like to acknowledge the use of the facilities in the Monash Centre for Electron Microscopy. The authors would like to thank Dr. Thilina Gunawardhana for his assistance in obtaining the pulp from different mills. Maisha Maliha would like to acknowledge the Australian Government for the Research Training Program (RTP) Scholarship.

**3.8. References**

1. McKeen, L.W., *Introduction to Use of Plastics in Food Packaging*, in *Plastic Films in Food Packaging*. 2013, William Andrew Publishing: Oxford. p. 1-15.
2. Appendini, P. and J.H. Hotchkiss, *Review of antimicrobial food packaging*. *Innovative Food Science & Emerging Technologies*, 2002. **3**(2): p. 113-126.
3. Patra, M., G. Gasser, and N. Metzler-Nolte, *Small organometallic compounds as antibacterial agents*. *Dalton Transactions*, 2012. **41**(21): p. 6350-6358.
4. Lemire, J.A., J.J. Harrison, and R.J. Turner, *Antimicrobial activity of metals: mechanisms, molecular targets and applications*. *Nature Reviews Microbiology*, 2013. **11**: p. 371.
5. Pal, C., et al., *BacMet: antibacterial biocide and metal resistance genes database*. *Nucleic acids research*, 2014. **42**(Database issue): p. D737.
6. Philip, A., M. Werrett, and B. Madleen, *Antibacterial Bismuth Complexes*. 2016: Australia.
7. Werrett, M., et al., *Bismuth Phosphinates in Bi-Nanocellulose Composites and their Efficacy towards Multi-Drug Resistant Bacteria*. *Chemistry- A European Journal*, 2018.
8. Yu, H.Y., et al., *Fabrication of multifunctional cellulose nanocrystals/poly(lactic acid) nanocomposites with silver nanoparticles by spraying method*. *Carbohydr Polym*, 2016. **140**: p. 209-19.
9. Oun, A.A., S. Shankar, and J.W. Rhim, *Multifunctional nanocellulose/metal and metal oxide nanoparticle hybrid nanomaterials*. *Crit Rev Food Sci Nutr*, 2020. **60**(3): p. 435-460.
10. Garusinghe, U.M., et al., *Nanocellulose-montmorillonite composites of low water vapour permeability*. *Colloids and Surfaces A: Physicochemical and Engineering Aspects*, 2018. **540**: p. 233-241.
11. Lavoine, N., et al., *Active bio-based food-packaging: Diffusion and release of active substances through and from cellulose nanofiber coating toward food-packaging design*. *Carbohydr Polym*, 2016. **149**: p. 40-50.
12. Balea, A., et al., *Industrial Application of Nanocelluloses in Papermaking: A Review of Challenges, Technical Solutions, and Market Perspectives*. *Molecules*, 2020. **25**(3): p. 526.
13. Biermann, C.J., *Handbook of Pulping and Papermaking*. 1996, San Diego: San Diego: Elsevier Science & Technology.
14. Ang, S., V. Haritos, and W. Batchelor, *Cellulose nanofibers from recycled and virgin wood pulp: A comparative study of fiber development*. *Carbohydr Polym*, 2020. **234**: p. 115900-115900.

15. Jonoobi, M., et al., *Different preparation methods and properties of nanostructured cellulose from various natural resources and residues: a review*. Cellulose, 2015. **22**(2): p. 935-969.
16. Dankovich, T.A. and D.G. Gray, *Bactericidal paper impregnated with silver nanoparticles for point-of-use water treatment*. Environ Sci Technol, 2011. **45**(5): p. 1992-8.
17. Bideau, B., et al., *Mechanical and antibacterial properties of a nanocellulose-polypyrrole multilayer composite*. Mater Sci Eng C Mater Biol Appl, 2016. **69**: p. 977-84.
18. Krol, L.F., et al., *Microfibrillated cellulose-SiO<sub>2</sub> composite nanopapers produced by spray deposition*. Journal of Materials Science, 2015. **50**(11): p. 4095-4103.
19. Yan, J., et al., *Antibacterial activity of silver nanoparticles synthesized In-situ by solution spraying onto cellulose*. Carbohydr Polym, 2016. **147**: p. 500-8.
20. Ma, P., et al., *Influence of TEMPO-mediated oxidation on the lignin of thermomechanical pulp*. Bioresour Technol, 2012. **118**: p. 607-10.
21. Gunawardhana, T., et al. *Development of cellulose nanofibre quality with mechanical energy: Effect of starting material*. in *16th Fundamental Research Symposium, Oxford*. 2017.
22. Chauhan, V.S., et al., *Effect of separate and mixed refining of hardwood and softwood pulps on paper properties*. Journal of Korea Technical Association of the Pulp and Paper Industry, 2011. **43**(4): p. 1-10.
23. Pickering, K.L., M.G.A. Efendy, and T.M. Le, *A review of recent developments in natural fibre composites and their mechanical performance*. Composites Part A: Applied Science and Manufacturing, 2016. **83**: p. 98-112.
24. Huber, T., et al., *A critical review of all-cellulose composites*. Vol. 47. 2012.
25. Maliha, M., et al., *Bismuth phosphinate incorporated nanocellulose sheets with antimicrobial and barrier properties for packaging applications*. Journal of Cleaner Production, 2019. **246**.
26. Varanasi, S., R. He, and W. Batchelor, *Estimation of cellulose nanofibre aspect ratio from measurements of fibre suspension gel point*. Cellulose, 2013. **20**(4): p. 1885-1896.
27. Raj, P., et al., *Effect of cationic polyacrylamide on the processing and properties of nanocellulose films*. Journal of Colloid and Interface Science, 2015. **447**: p. 113-119.
28. Spence, K.L., et al., *The effect of chemical composition on microfibrillar cellulose films from wood pulps: mechanical processing and physical properties*. Bioresour Technol, 2010. **101**(15): p. 5961-8.

29. Peltola, H., E. Laatikainen, and P. Jetsu, *Effects of physical treatment of wood fibres on fibre morphology and biocomposite properties*. *Plastics, rubber & composites*, 2011. **40**(2): p. 86-92.
30. Ang, S., V. Haritos, and W. Batchelor, *Effect of refining and homogenization on nanocellulose fiber development, sheet strength and energy consumption*. *Cellulose*, 2019. **26**(8): p. 4767-4786.
31. Cooper, K.E., *Chapter 1 - The Theory of Antibiotic Inhibition Zones*, in *Analytical Microbiology*, F. Kavanagh, Editor. 1963, Academic Press. p. 1-86.
32. Maliha, M., et al., *Biocompatibility and selective antibacterial activity of a bismuth phosphinato-nanocellulose hydrogel*. *Cellulose*, 2021.
33. Rojo, E., et al., *Comprehensive elucidation of the effect of residual lignin on the physical, barrier, mechanical and surface properties of nanocellulose films*. *Green Chemistry*, 2015. **17**(3): p. 1853-1866.
34. Spence, K.L., et al., *A comparative study of energy consumption and physical properties of microfibrillated cellulose produced by different processing methods*. *Cellulose*, 2011. **18**(4): p. 1097-1111.
35. Rodionova, G., et al., *Surface chemical modification of microfibrillated cellulose: improvement of barrier properties for packaging applications*. *Cellulose*, 2011. **18**(1): p. 127-134.
36. Nair, S.S., et al., *High performance green barriers based on nanocellulose*. *Sustainable Chemical Processes*, 2014. **2**(1): p. 23.

THIS PAGE HAS BEEN INTENTIONALLY LEFT BLANK

---

## **CHAPTER 4**

**BIOCOMPATIBILITY AND SELECTIVE ANTIBACTERIAL ACTIVITY OF A BISMUTH  
PHOSPHINATO-NANOCELLULOSE HYDROGEL**

---

---

THIS PAGE HAS BEEN INTENTIONALLY LEFT BLANK

**PREFACE**

In the previous two chapters, the utility of the complex in nanocellulose composite sheets for packaging applications was explored. In this chapter, a very different type of carrier matrix has been considered for a biomedical application where infection control is crucial. This chapter aims to address the third research objective of this thesis. Nanocellulose hydrogel loaded with the *bis*-phosphinato bismuth (III) complex was proposed as an antimicrobial wound care material as an alternative to Ag-based hydrogels most commonly studied or commercially produced. This chapter studies how the bismuth complex affects the rheological properties of the hydrogel and its suitability for spreading on wounds in terms of its physical properties. Antibacterial performance and biocompatibility of different concentrations of the bismuth complex are studied, to establish a possible safe formulation of the Bi-complex loaded nanocellulose hydrogel for future preclinical studies.

THIS PAGE HAS BEEN INTENTIONALLY LEFT BLANK

---

**CHAPTER 4: BIOCOMPATIBILITY AND SELECTIVE ANTIBACTERIAL  
ACTIVITY OF A BISMUTH PHOSPHINATO-NANOCELLULOSE  
HYDROGEL**

<b>4.1. Abstract</b> .....	137
<b>4.2. Keywords</b> .....	138
<b>4.3. Introduction</b> .....	138
<b>4.4. Materials and Methods</b> .....	140
4.4.1. Chemicals and Materials .....	140
4.4.2. Preparation Method.....	140
4.4.2.1. Bismuth complex synthesis.....	140
4.4.2.2. Preparation of Bi-nanocellulose hydrogel.....	141
4.4.3. Morphology.....	141
4.4.4. Rheology .....	141
4.4.5. <i>In-vitro</i> biocompatibility .....	142
4.4.5.1. Cytotoxicity Assay .....	142
4.4.5.2. Live-dead assay .....	142
4.4.5.3. Cell Morphology .....	143
4.4.5.4. Statistical Analysis.....	143
4.4.6. Antibacterial Activity.....	143
4.4.6.1. Time-kill Assay.....	143
4.4.6.2. Bacterial cell morphology .....	144
4.4.6.3. Internal Quality Control .....	144
4.4.7. Hydrogel quality check .....	144
<b>4.5. Results and Discussion</b> .....	145
4.5.1. Morphology.....	145
4.5.2. Rheology .....	145
4.5.3. <i>In-vitro</i> biocompatibility .....	148
4.5.3.1. Cytotoxicity Assay .....	148
4.5.3.2. Live-dead Assay.....	149
4.5.3.3. Cell Morphology .....	150
4.5.4. Antibacterial activity.....	152

4.5.4.1.	Time-kill Assay .....	152
4.5.4.2.	Bacterial cell morphology .....	155
4.5.4.3.	Internal Quality Control.....	157
4.5.5.	Hydrogel Quality check.....	157
<b>4.6.</b>	<b>Conclusion .....</b>	<b>158</b>
<b>4.7.</b>	<b>Acknowledgements .....</b>	<b>159</b>
<b>4.8.</b>	<b>References.....</b>	<b>159</b>

**BIOCOMPATIBILITY AND SELECTIVE ANTIBACTERIAL ACTIVITY OF A BISMUTH PHOSPHINATO-NANOCELLULOSE HYDROGEL**

Maisha Maliha<sup>1</sup>, Rajini Brammananth<sup>2</sup>, Jennifer Dyson<sup>3,4</sup>, Ross L. Coppel<sup>2</sup>, Melissa Werrett<sup>5,6</sup>, Philip C. Andrews<sup>5,6</sup>, Warren Batchelor<sup>1\*</sup>

<sup>1</sup>*Bioresource Processing Research Institute of Australia (BioPRIA), Department of Chemical Engineering, Monash University, VIC 3800, Australia*

<sup>2</sup>*Department of Microbiology, Monash University, VIC 3800, Australia*

<sup>3</sup>*Monash Institute of Medical Engineering (MIME), Monash University, VIC 3800, Australia*

<sup>4</sup>*Department of Biochemistry and Molecular Biology, Monash Biomedicine Discovery Institute, Monash University, VIC 3800, Australia*

<sup>5</sup>*School of Chemistry, Monash University, VIC 3800, Australia*

<sup>6</sup>*Centre to Impact AMR, Monash University, VIC 3800, Australia*

Corresponding author email: warren.batchelor@monash.edu

**4.1. Abstract**

Antimicrobial hydrogels are of immense value in wound care applications. However, the rapid rise of antimicrobial resistance has made it necessary to look for new antimicrobial additives for such materials. In this study, a novel antimicrobial hydrogel for wound care applications has been developed. The material combines TEMPO-oxidized nanocellulose hydrogel with a new class of antimicrobial agent, phenyl *bis*-phosphinato bismuth (III) complex. The hydrogel was characterized using scanning electron microscope (SEM) imaging to show the overall distribution of the complex particles within the nanocellulose hydrogel matrix phase. The rheological properties of the bismuth loaded hydrogel are comparable to commercial over-the-counter burn hydrogels and behave like true gels. Activity of the different concentrations of the complex was studied against a range of medically important bacteria and mammalian fibroblast cells. Bismuth complex target loading of 9 µg/g showed bactericidal activity against *Acinetobacter baumannii* and *Pseudomonas aeruginosa* and bacteriostatic effect against MRSA and VRE, while having no toxic effect on mammalian fibroblast cells. However, *E. coli* was less susceptible to this concentration comparatively. Our study has identified a range of bismuth complex loading levels for the material at which the additive appears to be safe and active. This study is a step towards the design of a biocompatible and renewable hydrogel containing a safe antimicrobial additive, which has an excellent safety margin to pathogenic bacteria

over mammalian cells and would appear to be a promising material for active wound dressing applications.

## 4.2. Keywords

Nanocellulose, Bismuth, Hydrogel, Antibacterial, Fibroblasts, *In-vitro* cytotoxicity

## 4.3. Introduction

Skin is the largest organ of the human body, protecting all internal organs. Trauma to the skin breaches this protective layer and exposes internal structures to the risk of infection and other forms of damage. The repair of skin in which the integrity of this layer is restored involves three phases: inflammation, proliferation of various cell types, and tissue remodeling. The initial inflammatory phase involves the action of preformed proteins and resident and migratory cells to sterilise the area of the wound in preparation for a proliferative phase in which subcutaneous and dermal cells proliferate to generate new skin layers including new blood vessels. Finally, the newly generated tissues are remodeled to regenerate the various layers of the skin and to integrate with the pre-existing tissues on either side of the wound. Disruption in any one phase of repair can jeopardise the satisfactory completion of the process [1]. A large number of factors including infection can affect wound healing and control of infection is a pre-requisite for satisfactory wound healing [2, 3]. Bacterial infection in burn wounds complicates their management and in the worst cases can lead to the death of patient [4]. Technologies to deal with wound management include artificial skin for grafting, aids to skin regeneration and wound closure, and infection control by various exogenous materials and dressings [5]. A large number of wound dressings have been developed, both from natural and synthetic materials [6]. Active wound dressings that deliver drugs or contains antibacterial agents are commonly used to minimise risk of infection [4]. Bacteria are constantly evolving and developing increased resistance to antibiotics and disinfectants and appropriate dressings need to be developed to account for this. In addition, wound dressing materials need to be biocompatible and non-toxic to host cells [7].

Hydrogel-based wound dressings are some of the most promising materials for wound care and healing due to their “tissue-like” structure and excellent biocompatibility [8]. The frequency of application of hydrogels in wound dressings has increased due to its ability to provide a moist environment to assist in the wound healing process [4]. Moisture helps with dermis repair and removal of dead cells, thus aiding in healing. Moreover, the moisture provides a cooling effect on the wound, reducing pain. Pain is also reduced due to the non-adherent nature of hydrogels preventing

sticking to the wound when dressings are removed [9]. Hydrogels have the ability to absorb the wound exudates and are also permeable to oxygen, making the properties of hydrogels further advantageous for wound dressing [10].

Hydrogels are three-dimensional structures of crosslinked polymers. For biomedical applications, physically cross-linked hydrogels are preferred as they avoid the use of chemical crosslinking agents or organic solvents, thus minimizing the risks and toxicity associated with those [8]. One such material is nanocellulose hydrogel, which is crosslinked by hydrogen bonding and is a promising material for biomedical applications [11]. The surface chemistry of nanocellulose has been studied and reported to be suitable for wound dressing applications [12]. Cellulose-based hydrogels studied for wound dressing applications are usually bacterial cellulose. Nanocellulose-based wound care products, such as Biofill, Gengiflex and XCell, are also based on bacterial cellulose (BC) [13, 14]. Bacterial cellulose (BC) and wood-based cellulose has the same chemical structure with the same sugar molecule forming the polymer. However, BC is a weak hydrogel and is hard to modify to other forms [6], and the large scale production of bacterial cellulose remains a challenge [14]. There has been limited research exploring the application of wood-based nanocellulose in wound dressings. Hakkarainen, Koivuniemi *et al* studied the use of wood-based nanocellulose as wound dressing for burns in patients [6], leading to the first wood-based nanocellulose hydrogel, recently launched to the European market as a wound care product by UPM-Kymmene Corporation [15]. Of relevance to this study, the effect of antimicrobials combined with wood-based nanocellulose hydrogels is yet to be investigated.

In this study, wood-based nanocellulose hydrogel incorporating a metal-based antimicrobial agent has been studied. Silver nanoparticles and silver-based compounds are common antimicrobial additives used for wound dressing applications. These have been studied as antimicrobial agents in hydrogels assembled with both synthetic polymers [10, 16-22] and natural polymers [4, 23, 24]. Bacterial cellulose hydrogel has also been impregnated with silver nanoparticles and the material displays antibacterial activity against both Gram-positive and Gram-negative bacteria [25]. However, due to the overuse of silver in a large number of products, bacterial resistance towards silver has become a major concern [26-28]. It has also been reported that silver compounds, such as silver nitrate and the most commonly used silver sulfadiazine, can have a toxic effect in the human body [4, 26, 29-32]. Furthermore, there are concerns about a build-up of silver in the environment and a desire to restrict its widespread use because of toxicity to various organisms, including humans [33].

Researchers have shown that bismuth compounds and complexes possess antibacterial activity [33-37]. In addition, bismuth compounds, such as bismuth *subsalicylate* (Pepto-Bismol) and colloidal bismuth subcitrate (De-Nol) have been used for treating gastrointestinal disorders [38-40]. Moreover, bismuth and its compounds, unlike other heavy metals, are low in toxicity [36] [40]. In this study, a Bi (III) complex with phosphinate ligands,  $\text{BiPh}(\text{OP}(=\text{O})\text{Ph}_2)_2$  is studied as an additive to a wound dressing hydrogel. While the antibacterial activity of this hydrophobic complex [33] as well as the production of bismuth-nanocellulose composite sheets as an antimicrobial packaging material [41] has been previously studied, the suitability of its incorporation into a hydrogel matrix for wound healing purposes is not known.

The aim of this study is to combine the new organobismuth complex, phenyl bismuth *bis*(diphenylphosphinato), into a nanocellulose hydrogel matrix to impart antibacterial properties to the hydrogel. The antibacterial properties of the hydrogel towards some of the medically important bacteria that commonly infect wounds has been studied. The rheological properties of the hydrogel were investigated and compared to commonly used commercial burn hydrogels. Moreover, biocompatibility of the hydrogel with mammalian fibroblast cells was studied to understand the overall safety of the composite.

#### **4.4. Materials and Methods**

##### **4.4.1. Chemicals and Materials**

Bleached Eucalyptus Kraft (BEK) pulp was obtained from Australian paper, Maryvale. 2,2,6,6-Tetramethylpiperidine-1-oxyl (TEMPO) and NaBr were obtained from Sigma-Aldrich. 12 w/v% Sodium hypochlorite (NaOCl) was purchased from Thermo Fisher Scientific. Triphenyl bismuth ( $\text{BiPh}_3$ ) was prepared using the standard Grignard method [42] and diphenyl phosphinic acid was purchased from Sigma-Aldrich. NaOH and HCl were purchased from Merck and Univar, and diluted as required. Dulbecco's modified Eagle medium (DMEM) was purchased from Gibco. MTS reagent was purchased from Promega, Australia. Calcein, AM and Propidium iodide was obtained from Life technologies, Australia.

##### **4.4.2. Preparation Method**

###### **4.4.2.1. Bismuth complex synthesis**

Phenyl bismuth *bis*(diphenylphosphinato) was prepared according to Andrews *et al* [33]. Triphenyl bismuth and diphenyl phosphinic acid were mixed in the ratio of 1:2 in ethanol and heated at reflux

for 24 hours. The reaction mixture was then filtered, and the insoluble phenyl bismuth *bis*(diphenylphosphinato) was isolated as a white powder.

#### **4.4.2.2. Preparation of Bi-nanocellulose hydrogel**

BEK pulp was oxidised by TEMPO-mediated oxidation as described by Isogai *et al* [43]. TEMPO (0.4 g) and NaBr (2.5 g) were mixed with water to which a suspension containing 25 dry grams of BEK pulp was added. This 3 L reaction mixture was initiated using 75 mL NaOCl added dropwise while being continuously stirred using an overhead stirrer. The NaOCl was pre-adjusted to pH 10 using 36 % HCl. The reaction mixture was also maintained at pH 10 through the dropwise addition of 0.5 M NaOH. The oxidation was carried out for 2 hours. The oxidised fibres were then dewatered and washed several times using vacuum filtration. The TEMPO-oxidised cellulose nanofibres thus obtained were then dispersed in deionised water to a concentration of 2 wt% and passed through the high-pressure homogeniser (GEA Niro Soavi Homogeniser Panda) at 1000 bar with one pass. Fibres produced similarly have been reported to have diameters in the range of 3-4 nm [44].

The desired mass of bismuth complex was dispersed in DI water using a dispermat at a speed of 6000 rpm for 15-25 minutes to ensure uniform dispersing of the complex. The dispersion was mixed with the 2 wt% nanocellulose (NC) hydrogels in 1:1 ratio and dispersed using the dispermat at 4000 rpm for 5 minutes. The Bi-NC hydrogel thus obtained had 0.1 wt% bismuth complex with respect to mass of hydrogel and was stored at 4° C for further analysis. Blank hydrogel was prepared by mixing 2 wt % hydrogel with DI water in 1:1 ratio.

#### **4.4.3. Morphology**

The bismuth distribution in the hydrogel was analysed using Scanning Electron Microscope (SEM) imaging. The hydrogel was air-dried on a silicon chip secured using carbon tape. The hydrogel film was coated with a thin conducting layer of iridium. SEM imaging was done using the FEI Magellan 400 FEG SEM using an accelerating voltage of 5 keV and spot size 2.

#### **4.4.4. Rheology**

Rheological tests were done using Anton Paar MCR302 rheometer with the 1-degree cone and plate geometry. The analysis was done at 25 °C. Oscillatory strain sweep was performed at a constant frequency of 1 Hz at shear strains ranging from 0.01 to 100 %.

#### **4.4.5. *In-vitro* biocompatibility**

##### **4.4.5.1. Cytotoxicity Assay**

The cytotoxicity assay was performed according to modified ISO 10993-5. Mouse fibroblast L929 cells were cultured in Dulbecco's Modified Eagle's Medium (DMEM) containing 10 % (v/v) fetal bovine serum (FBS) and 1% antibiotics (penicillin, streptomycin) in a humidified incubator at 37 °C and 5 % CO<sub>2</sub>. 10,000 cells/well were seeded into 96 well plates in DMEM medium and incubated for 24±1 hour to form a monolayer. The media was removed and cells washed with PBS. Fresh media mixed with the hydrogel samples was incubated with the cells. The 0.1 wt% hydrogel (containing 1000 µg Bi-complex/g hydrogel) was first dispersed in DMEM to contain 20 wt% hydrogel using a vortex mixture. This mixture was pipetted to further ensure homogenous distribution and then serially diluted with DMEM to test concentrations of 100, 50, 25, 12, 9, 6, 3, and 1 µg/g of the bismuth complex (rounded to the nearest whole number). The control cells were incubated with either fresh DMEM (negative control) or fresh DMEM containing 10% dimethyl sulfoxide (DMSO) to induce cell death (positive control). A similar set of experiments was undertaken using 0.1 wt% silver sulfadiazine loaded nanocellulose hydrogel in the same concentration range as the Bi-complex. DMEM containing 20 wt% blank nanocellulose hydrogel or commercial hydrogels were also tested. These were the two non-active over-the counter hydrogels, Solosite® and Solugel®, and silver-based active hydrogel, Silvasorb® and are referred to as commercial hydrogel **1**, commercial hydrogel **2** and commercial hydrogel **3** respectively in the paper. Cell viability was assessed after 24 hours of treatment by MTS assay. The treatment media was replaced by MTS stock solution, when tetrazolium compound MTS is converted to formazan by viable cells. After 1 hour of incubation in the dark, the absorbance was recorded using a Thermo Scientific Multiskan Spectrum plate reader at 490 nm and using the software SkanIt RE 2.4.2. The absorbance was corrected by subtracting the background absorbance, i.e. DMEM only in TCPS (tissue culture polystyrene) and was normalised against the negative control, i.e. the untreated cells grown on TCPS with fresh DMEM media, to express the absorbance in percentage of viability relative to the negative control. Four independent sets of experiments were performed with triplicates of each samples every time.

##### **4.4.5.2. Live-dead assay**

The live-dead assay was performed in a 96 well plate seeded with 10,000 cells/well and allowed to form a monolayer for 24±1 hour in 37 °C and 5 % CO<sub>2</sub> condition. Cells were treated with media mixed with the hydrogel samples (with the same concentrations achieved by serial dilution as

described above in section 2.5.1) and incubated for 24 hours. The staining solution was prepared by mixing 6 drops of propidium iodide (PI) and 2  $\mu\text{L}$  of Calcein AM to 3mL PBS. The treatment media was replaced by staining solution and incubated in the dark for 30 minutes. Live-dead imaging was performed using the fluorescent microscope Nikon Eclipse Ts2 at 560 nm and 470 nm for Calcein AM and PI respectively.

#### **4.4.5.3. Cell Morphology**

A monolayer of L929 cell line in a 96 well plate seeded with 10,000 cells/ well was treated with different concentrations of the bismuth complex in a similar way as above in section 2.5.1, and incubated at 37 °C and 5 % CO<sub>2</sub> condition for 24 hours. The morphology of the cells was observed using light microscopy using the microscope Nikon Eclipse Ts2.

#### **4.4.5.4. Statistical Analysis**

The MTS assay results were statistically analysed by one-way analysis of variance (ANOVA), followed by Tukey's post hoc test to compare selected pairs of data using GraphPad Prism 8.0.2. Tests with p-values <0.05 were considered to be statistically significant.

### **4.4.6. Antibacterial Activity**

#### **4.4.6.1. Time-kill Assay**

Different amounts of 0.1 wt% Bi-loaded hydrogel was mixed with 5 mL of diluted overnight culture (1 in 100,000) of a specific bacterium such as to achieve concentrations of 12  $\mu\text{g}$ , 9  $\mu\text{g}$ , 6  $\mu\text{g}$  and 3  $\mu\text{g}$  of bismuth complex per gram of the broth (assuming density of broth as 1g/ml). The time-kill assay of these different concentrations was performed against *Acinetobacter baumannii* (C403/ATCC17978), *Pseudomonas aeruginosa* (ATCC27853), *Escherichia coli* (G102), MRSA (M118797, methicillin-resistant *Staphylococcus aureus*) and Vancomycin-resistant *enterococcus* (M846910). Luria-Bertani (LB) media and LB agar plates were used for growing each of the bacterial line. The culture was spread on agar plate at the beginning of the experiment for time zero count. A vortex shaker was used to ensure proper mixing of the hydrogel with the broth. The suspension was kept in an incubator at 37 °C at 200 rpm shaking for 24 hr and samples were aliquoted out after 4, 8, 12 and 24 hours. 20  $\mu\text{L}$  of the sample was plated on agar plates and the number of viable cells was determined by the colony counting technique. Each time point was analysed in triplicate, and each experiment was done three times.

#### 4.4.6.2. Bacterial cell morphology

The morphology of bacterial cells after being treated was studied using SEM. The Bi-loaded hydrogel was mixed with 5 mL of diluted overnight culture (1 in 100,000) of *P. aeruginosa*, as described above, to obtain concentrations of 12 µg and 9 µg of bismuth complex per gram of the broth. These, along with a control, were incubated for 24 hr at 37 °C. The treated culture was then centrifuged at 2000 rpm for 30 minutes at 4 °C. The supernatant was discarded and the pelleted cells were used for SEM sample preparation. The cells were washed with PBS and fixed using 2.5 % glutaraldehyde and 2 % paraformaldehyde for 1 hour at room temperature. The fixed cells were then washed with fresh sodium cacodylate buffer and post-fixed with 1 % osmium tetroxide in cacodylate buffer. The cells were then washed with milli-Q water and incubated on coverslips coated with 0.1 % polyethyleneimine for 45 minutes. The coverslips were immersed in water to get rid of the unadhered cells, and treated with increasing concentrations of ethanol for dehydration. The coverslip was then critically point dried, mounted on SEM stub and coated with a thin conducting layer of gold. The SEM imaging was performed using FEI Nova NanoSEM.

#### 4.4.6.3. Internal Quality Control

Quality control tests were done to evaluate the reliability and reproducibility of the antibacterial test results. Blinded experimental repeats of the time-kill assays were performed against MRSA (M118797, methicillin-resistant *Staphylococcus aureus*) and *Acinetobacter baumannii* (C403/ATCC17978). One sample contained the Bi-loaded hydrogel to achieve a concentration of 9 µg/g and another one contained the same amount of blank hydrogel as the control. The samples were analysed at 4 and 24 hours and each time point was analysed in triplicate. The experiment was performed in the same way as before, except the test and the blank (control) samples were blinded.

#### 4.4.7. Hydrogel quality check

Bismuth content analysis were carried out using a PerkinElmer Avio 200 Inductively Coupled Plasma-Optical Emission Spectrometer (ICP-OES), measuring Bi at 223.06 nm. Known masses from different batches of Bi-loaded hydrogels were ashed in a muffle furnace, wherein the temperature was ramped to and maintained at 600 °C for 3 hours. The ash was then digested in concentrated nitric acid and diluted using 3 % nitric acid. The elemental bismuth content was analysed and used to determine the bismuth complex content. Each batch of hydrogel was tested in triplicate and the mean mass of the bismuth complex per gram of hydrogel was reported.

## 4.5. Results and Discussion

### 4.5.1. Morphology

Figure 1(a) and (b) shows the SEM images of the same area of the Bi-loaded hydrogel films. The secondary electron image in Figure 1(a) shows the surface morphology only. In the back-scattered electron image (BSE) in Figure 1(b), the bright structures indicate the presence of higher atomic number element, which is bismuth. The main point of interest in these images is the distribution of the bismuth complex.

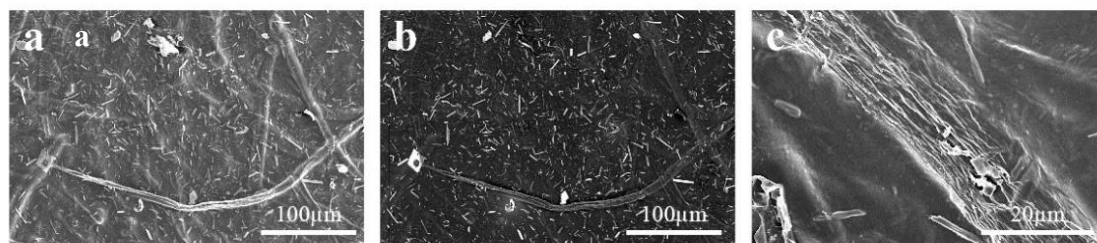


**Figure 1:** SEM image of air-dried Bi-NC hydrogel. (a) Secondary electron image (b) Back-scattered electron image of the same area (c) secondary electron image showing a nanofiber bundle

The bismuth particles have been shown to be well distributed within the nanocellulose fibres. Few bundles of fibres were observed, which is more closely shown in Figure 1(c). Those bundles that were present could be due to only having a single pass in the homogeniser in preparation of the gel. Better fibrillation can be achieved by more extensive mechanical treatment, although this would only be worthwhile if it led to a more active gel or was needed to satisfy regulatory requirements. Despite the presence of the bundles, the BSE image in Figure C1 in supplementary data shows that the bismuth complex particles are sitting in between the nanofibres in the fibre bundle.

### 4.5.2. Rheology

To understand how the physical properties of the hydrogel are altered upon incorporation of the bismuth complex, its rheological properties were assessed. The complex viscosity plot shown in Figure 2 indicates that the viscosity profile of the Bi-loaded hydrogel is similar to that of the blank hydrogel, showing a clear yield point for both and thereby suggesting the shear thinning behaviour of the hydrogel is retained. The dynamic strain sweep in Figure 3 shows the elastic modulus  $G'$  (solid-like properties) and the viscous modulus  $G''$  (liquid-like properties). For hydrogels, the elastic modulus should be higher than the viscous modulus [45], which is consistent with our results. A rise

of the zero-shear complex viscosity and storage modulus was observed with Bi-complex loading, suggesting the presence of the bismuth complex does not negatively affect the inter-fibre network. Although it has previously been observed that bismuth particles interfere with fibre-fibre bonding and upset the mechanical properties of nanocellulose paper [41], the opposite is evident here. Figures 2 and 3 also show the complex viscosity and the modulus of two commercially available over-the-counter non-active wound hydrogels.

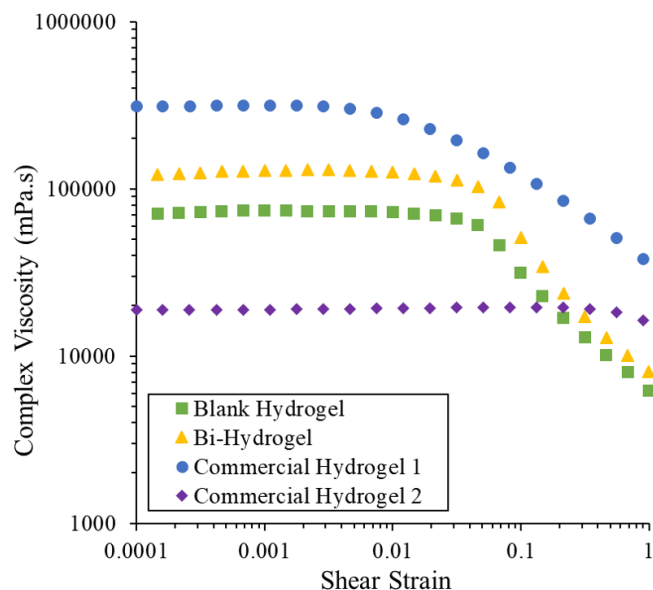


**Figure 2:** Viscosity profile of blank hydrogel and bismuth-complex loaded hydrogel compared to commercial wound hydrogel

The rheological analysis show that the incorporation of bismuth does not affect the viscoelastic properties of the hydrogel and that the hydrogel behaves like a true gel. The blank nanocellulose hydrogel and the Bi-NC hydrogel showed  $G'$  higher than  $G''$  at low shear strains and showed a linear viscoelastic region (LVR). These hydrogels have more solid-like properties at these strains and the  $G'$  and  $G''$  remains independent of the change in strain. Beyond a certain strain, the viscous behaviour starts to take over. This is the critical strain beyond which the viscosity changes with shear and behaves like a non-Newtonian fluid. Thus, these can be used as free-flowing gels and have the capacity to be packaged in tubes as soft solids having an entangled fibrous network. The high zero shear viscosity tells us about the stability and the solid-like behaviour of the hydrogel during storage suggesting there is little possibility of sedimentation or phase separation. The higher elastic modulus and the zero-shear viscosity after the addition of the bismuth complex indicates stronger network formation. It can be speculated that the bismuth complex particles are taking part in the physical chain

entanglement. Hence due to these particles being able to arrange themselves within the network, the material becomes less flexible and stiffer increasing the shear force required for the material to start flowing. The loss factor,  $\tan \delta$ , can be calculated as the ratio of the loss modulus to storage modulus and was found to be 0.15 for both the blank hydrogel and the Bi-hydrogel in the LVR. Moreover, the viscoelastic behaviour of the Bi-nanocellulose hydrogel studied here is comparable to commercial burn hydrogels as its elastic modulus and zero shear viscosity lies in the range of commercial brands investigated. Also, the critical strain for both the blank and Bi-complex loaded nanocellulose hydrogel is 0.068 and lies in between the range of the two commercial ones (0.003 and 0.347 for commercial hydrogel **1** and **2**, respectively). The yield point represents the ease of squeezing the gel out of a tube and the shear-thinning behaviour predicts the spreadability on shear forces for topical applications. These properties are important aspects for potential commercial translation. However, if required, the rheological properties of our Bi-hydrogel composites can be altered by changing the cellulose content of the hydrogel, as reported by Mendoza *et al* [45].

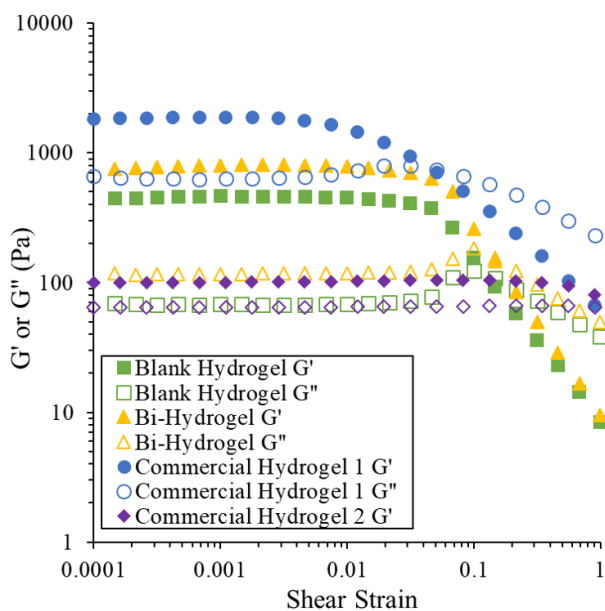


**Figure 3:** Dynamic strain sweep of blank hydrogel and bismuth-complex loaded hydrogel compared to commercial wound hydrogel

### 4.5.3. *In-vitro* biocompatibility

#### 4.5.3.1. Cytotoxicity Assay

To determine whether the bismuth hydrogels are cytotoxic, several approaches were undertaken. Firstly, an MTS assay was employed to determine the viability of mouse fibroblast L929 cells that had been incubated with bismuth hydrogels, and the percentage cell viability determined relative to untreated cells i.e. cells grown in DMEM only. Statistical analysis was carried out using a 1-way ANOVA and a post-hoc Tukey's test. Figure 4 shows a concentration-dependent effect of bismuth hydrogels on the viability of L929 cells. Generally, cell viability was unaffected by lower bismuth concentrations in the hydrogel, however, reduced cell viability was observed at higher concentrations. At bismuth complex concentrations greater than 12  $\mu\text{g/g}$ , the mean normalised cell viability relative to the untreated control cells is below 20 %, indicating a cytotoxic effect of the complex as per the requirements of ISO 10993-5 standard. The standard identifies any medical device or material that leads to cell viability less than 70 % as cytotoxic. At concentrations  $\leq 12 \mu\text{g/g}$ , the mean normalised cell viability was 70 % or greater, demonstrating a dose response curve for viability. Supporting this contention, at bismuth complex concentrations  $\leq 12 \mu\text{g/g}$ , the mean normalised cell viability was not statistically different to that of untreated cells. This type of dose-dependent phenomenon was also seen with the silver sulfadiazine loaded hydrogel. Viability was significantly reduced when cells were cultured on high concentrations of silver in a dose-dependent manner. For example, concentrations  $\leq 6 \mu\text{g/g}$ , silver sulfadiazine were not cytotoxic. We compared the toxicity of the blank nanocellulose hydrogel to commercial hydrogels in Figure 4B. Commercial hydrogel 1 and 2 are non-antibacterial products. Commercial hydrogel 3 is a silver based antimicrobial hydrogel, that releases silver ions. The silver content of this hydrogel was studied using ICP-OES analysis and it was found to contain  $3.81 \pm 0.40 \mu\text{g/g}$  of equivalent silver sulfadiazine ( $1.15 \pm 0.12 \mu\text{g/g Ag}^+$ ). The silver content is well below the toxic limit observed herein. Surprisingly, all three of the commercial hydrogels showed a degree of cellular toxicity with viability counts far below 70 %. Nonetheless, these products are in clinical use and this suggests that *in-vitro* experiments may differ from a real-life scenario. There are a number of possible reasons for this. Monolayers of cells have only 15 % of cell contact as the cell density is lower than 1 % compared to normal skin tissue and extracellular content is very much different in the culture dish. Moreover, *in-vitro* experiments only deal with one cell type, in our case the fibroblast, and cell-cell interactions between different cell types in skin tissue is not taken into consideration [46]. Skin tissue does not only consist of fibroblasts, but a number of different kinds of cells in various layers of skin including keratinocytes, Langerhans cells, melanocytes and vascular

networks of blood vessels, sebaceous glands, nerves and many proteins like collagen [47]. These along with the difficulty in understanding the reaction of the tissue to a foreign material or stress situation results in the difference in behaviour of cells in isolated cultures compared to when in the organism. Thus, it is difficult to extrapolate the *in-vitro* effects to *in-vivo* performance [48]. Moreover, the commercial hydrogels contain a range of other components (preservatives like parabens, imidazolidinyl urea etc.), some of which could also be the cause of the *in-vitro* cytotoxicity [49, 50].

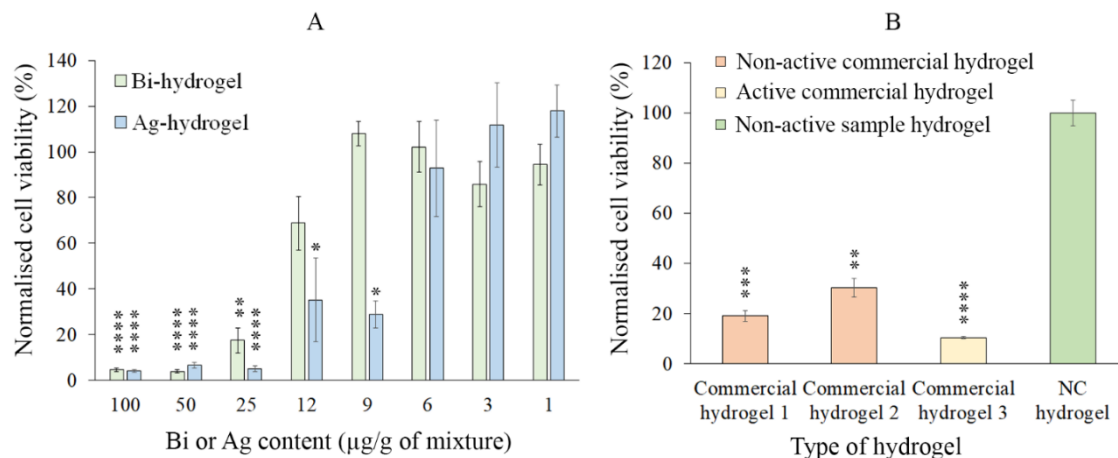


**Figure 4:** Viability of L929 cells after treatment with (A) nanocellulose hydrogels loaded with the indicated target concentrations of Bi-complex (green) or Ag-compound (blue) and (B) the indicated commercial hydrogel and blank nanocellulose hydrogel, determined by MTS assay. Percentage viability normalised over no treatment DMEM control. The data presented are expressed as mean  $\pm$  standard error of mean of technical triplicates from four independent sets of biological replicates. The number of asterisks over the bars show the level of significance of the data when compared with no treatment control. \* represents  $p \leq 0.05$ , \*\* represents  $p \leq 0.01$ , \*\*\* represents  $p \leq 0.001$  and \*\*\*\* represents  $p \leq 0.0001$ .

#### 4.5.3.2. Live-dead Assay

As an alternative approach for evaluating the potential cytotoxicity of bismuth-loaded hydrogels, a live-dead assay was undertaken. This assay employs two fluorescent probes - propidium iodide (PI) and calcein AM. PI is a red fluorescent nucleic acid stain that is only able to pass through the compromised membranes of non-viable cells, resulting in red nuclear fluorescence in dying or dead cells. Calcein AM is a cell membrane permeant fluorogenic substrate that is hydrolysed by active esterase in viable cells, resulting in a green cytosolic fluorescence in live cells. Figure 5 shows the L929 cells incubated with hydrogels loaded with various bismuth complex concentrations and stained

with PI and calcein AM. Notably, at bismuth concentrations  $\geq 12$   $\mu\text{g/g}$  the majority of cells were positive for PI indicating a cytotoxic affect, however,  $\leq 9$   $\mu\text{g/g}$  most of the cells were positive for calcein and negative for PI suggesting lower bismuth concentrations do not significantly compromise cellular viability of this particular cell line. In control studies, the L929 cells were incubated with either the blank nanocellulose hydrogel (NC-gel) lacking bismuth, or DMEM cell culture media, and both conditions were associated with high levels of cell viability.

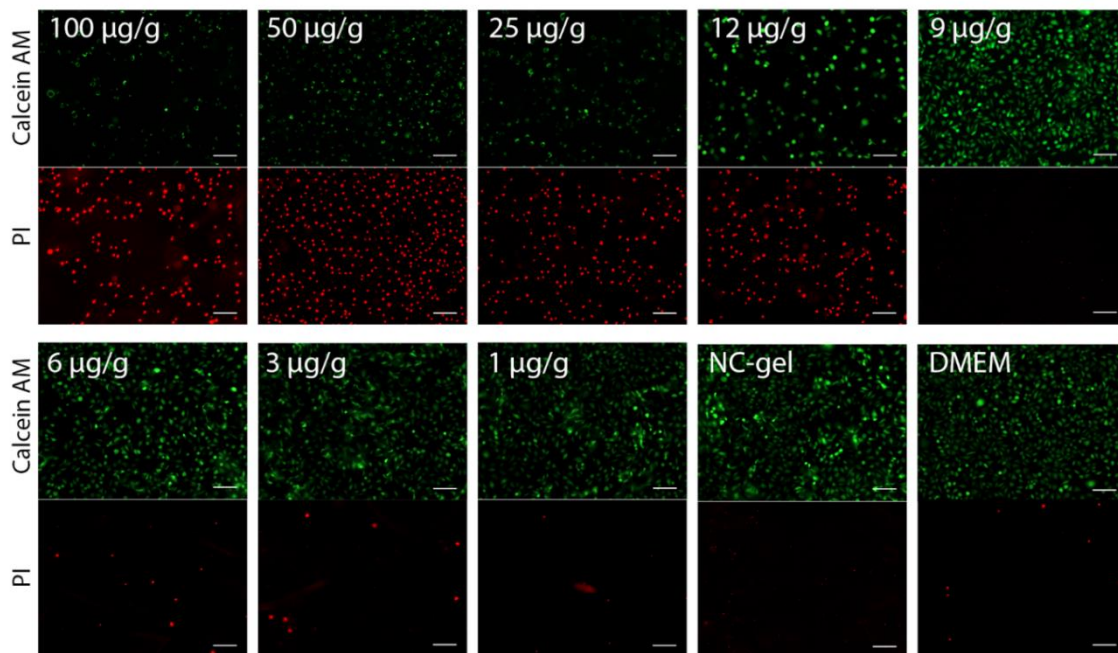


**Figure 5:** Live-dead staining of L929 cells after 24 hours of incubation with the indicated target concentration of the bismuth complex in nanocellulose hydrogel, the blank nanocellulose hydrogel (NC-gel) or DMEM culture media only. The green and red fluorescence show live and dead/dying cells respectively. Scale bar represents 100  $\mu\text{m}$ .

#### 4.5.3.3. Cell Morphology

Cell health and viability is intimately linked to cell morphology. Indeed, the induction of cell death is associated with distinct morphological events including cell shrinkage, plasma membrane blebbing and fragmentation. We examined the effect of increasing concentrations of the bismuth complex on the morphology of L929 cells (Figure 6). Notably, a significant change in cell morphology indicating the induction of cell death was apparent at bismuth treatment concentrations above 9  $\mu\text{g/g}$ , which is consistent with our observations in the cytotoxicity assays. At higher bismuth complex concentrations, the cells appeared smaller and more circular compared to the control cells cultured

with a blank hydrogel (NG-gel) or in DMEM media. In addition, some cells displayed blebbing of the peripheral membrane (Figure 6 see inset at 25  $\mu\text{g/g}$  Bi-complex treatment). Following treatment with lower concentrations of the bismuth complex (9  $\mu\text{g/g}$ ), the cell size appeared unaffected, and the cell morphology was spindle shaped, similar to the control cells (NC-gel and DMEM). Thus, at or below bismuth complex concentrations of 9  $\mu\text{g/g}$ , the presence of the complex in the hydrogel does not appear to affect the cell morphology.

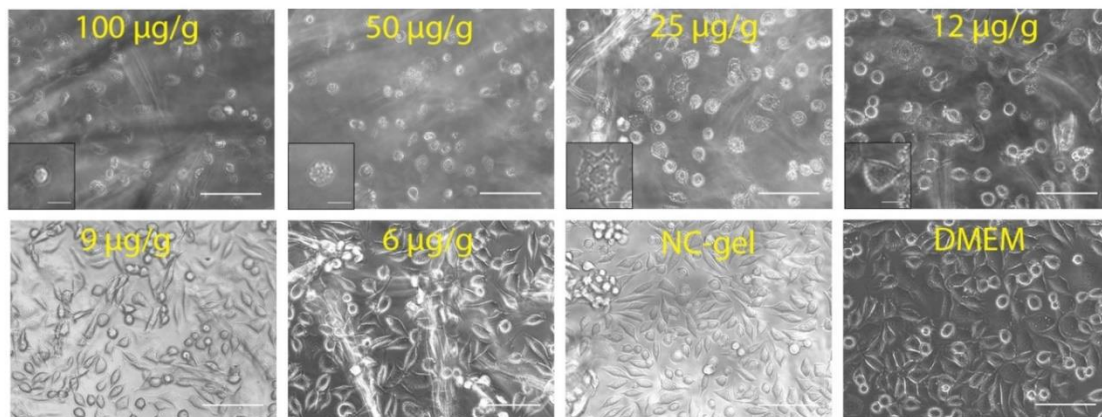


**Figure 6:** Light microscopy of L929 cells after 24 hours of incubation with the indicated target concentration of the bismuth complex in nanocellulose hydrogel, or blank nanocellulose hydrogel (NC-gel) without the bismuth complex or DMEM media only. Scale bar represents 100  $\mu\text{m}$  in the images and 20  $\mu\text{m}$  in the inset.

The process of wound healing is highly regulated and complex, and involves a variety of cell types including immune cells, fibroblasts and keratinocytes. Upon tissue injury, fibroblasts migrate into the wound and deposit extracellular matrix proteins such as collagen that is required for filling the injured site with newly synthesised tissue. As fibroblasts play a critical role in wound repair, it is important to evaluate the interactions of the cells with wound dressing materials, including potential cytotoxic effects [51] [52]. As per the ISO standard 10993-5, the cytotoxicity of the bismuth-loaded nanocellulose hydrogels was evaluated via assessing the cell viability of the murine fibroblast cell line L929. In addition, cytotoxicity was evaluated qualitatively via live-dead cell staining and morphological analysis. It is not clear how predictive the murine L929 cell line is of human fibroblast viability, but it is a widely employed cell line for cytotoxicity analysis and allows comparisons to other compounds. The vehicle, which is the pure nanocellulose hydrogel had no adverse effect on the fibroblast cells. The effect on cell viability of the bismuth-loaded gel was assessed using the MTS assay, live dead assay and the morphology of the mammalian cells. These experiments showed that

at higher bismuth concentrations, the proportion of dead cells is increased, and hence viability is lower and the cell morphology deviates from normal. 12  $\mu\text{g/g}$  was the highest concentration of bismuth complex which did not significantly reduce cell viability as determined by the MTS assay. However, in the live-dead assay and the morphology study, the cells showed no difference compared to controls at or below 9  $\mu\text{g/g}$  loading of the bismuth complex. Further assays would be required to unequivocally demonstrate the safe bismuth loading for cells. However, results herein show that target concentrations of 9  $\mu\text{g/g}$  bismuth complex appear to be well tolerated by the cells *in-vitro*. Similar *in-vitro* studies have shown that silver nanoparticles concentrations of 1.7  $\mu\text{g/ml}$ , 5  $\mu\text{g/ml}$  and 10  $\mu\text{g/ml}$  have reduced viability on human epidermal keratinocytes [53], rat liver cells [54] and stem cells [55] respectively. Argyria occurs at levels greater than 2  $\mu\text{g/g}$  [56]. *In-vivo* studies have also shown that silver nanoparticle exposure can affect different organs in mammals including liver and bile duct when ingested [31]. Skin contact (porcine skin) causes swelling, increased size of epidermal layer of skin, inflammation and greyish color at concentration of 3.4 and 34  $\mu\text{g/ml}$  [53]. It has been reported that many topical silver containing commercial products contain silver nanoparticles higher than 15  $\mu\text{g/g}$  [57]. Despite this, many silver-based hydrogel products are already approved in the commercial market. The limited safety data for the novel Bi-based hydrogel suggests it is worthy of further investigation as a potentially safe new material for wound management. However, further animal testing is imperative to better understand its clinical efficacy and effects on living organisms. The findings with approved commercial hydrogels tested herein tells us that these *in-vitro* performance differ significantly from a real-life scenario, thus suggesting that expanded biocompatibility assays will be required to adequately extrapolate to use *in vivo*.

#### **4.5.4. Antibacterial activity**

##### **4.5.4.1. Time-kill Assay**

Time-kill assays were performed to understand the effect of concentration of the bismuth-complex loading at the safe concentrations established in the previous section 3.3 against some common and significant wound pathogens. The time-kill kinetics in Figure 7 shows that the Bi-loaded hydrogel is bactericidal within 4 hours at 12 and 9  $\mu\text{g/g}$  against the Gram-negative bacteria *A. baumannii*, rapidly eradicating bacterial colonies. However, the lower bismuth content (6 and 3  $\mu\text{g/g}$ ) remained bacteriostatic over the 24-hour test period. When tested against *P. aeruginosa* (also Gram negative), bactericidal activity is observed within 8-12 hours at 12 and 9  $\mu\text{g/g}$ . At 6  $\mu\text{g/g}$ , bactericidal activity is observed over the first 12 hours, after which slow regrowth occurred. With the minimum loading of 3  $\mu\text{g/g}$ , the bismuth complex was only able to slow down bacterial growth. Representative plates

for *P. aeruginosa* are shown in Figure C2. Interestingly, with the Gram-positive methicillin resistant strain of *Staphylococcus aureus* (MRSA) and Vancomycin-resistant *Enterococcus* (VRE), the trend observed was quite different. Bacteriostatic effects were observed upon treatment with 12, 9 or 6  $\mu\text{g/g}$  of the complex up to 12 hours for MRSA and 24 hours for VRE. With MRSA, regrowth was observed at the above-mentioned concentrations after 12 hours, with the regrowing rate and the final level of colony forming units being lower than the control after 24 hours. With treatment of 3  $\mu\text{g/g}$ , MRSA remained slow growing throughout the tested period. There was no reduction in bacterial colonies at any of the treatment concentrations (or times), thus indicating less activity of these hydrogels against these Gram-positive bacterial strains. Interestingly, the concentration dependency of *E. coli* was different to all the other bacteria tested, including the other Gram-negative ones. Important to note is that blank hydrogel (i.e. no bismuth additive) leads to a growth curve similar to medium alone and is shown in Figure C3 in the supplementary information. Therein, the tests were done in hydrogel-broth mixture containing 20 % w/w of the blank hydrogel or the Bi-loaded hydrogel.

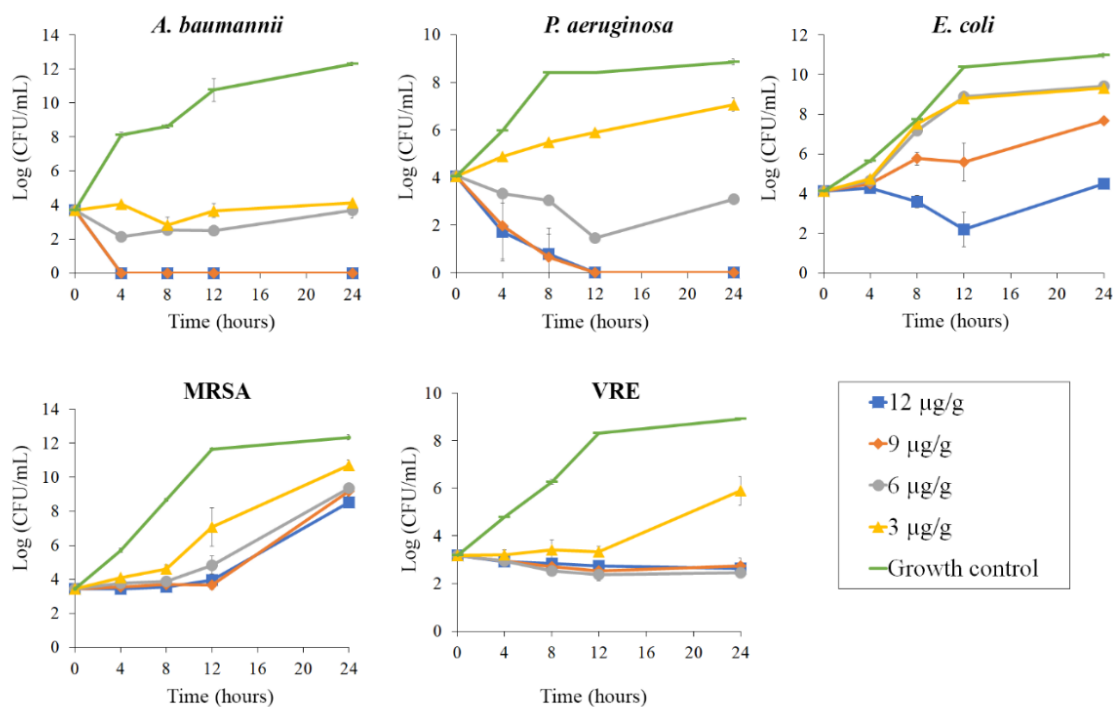


**Figure 7:** Time-kill kinetics of the Bi-NC hydrogel at indicated target concentration of the bismuth complex against the Gram-negative bacterial strains of *A. baumannii*, *P. aeruginosa* and *E. coli* and the Gram-positive strains of MRSA and VRE for 24 hours period. The values expressed represent mean  $\pm$  standard deviation ( $n=3$ ). All measurements were done in triplicate and all data included except for the following three instances where two replicates were in agreement and one was an

outlier, which was excluded: *A. baumannii* at 6 and 3  $\mu\text{g/g}$  at 12 hours and *P. aeruginosa* at 6 $\mu\text{g/g}$  at 12 hours

*P. aeruginosa* and *A. baumannii* have been identified as critical priority pathogens, followed by *E. coli*, VRE and MRSA as a high priority pathogens by the World Health Organization [58]. These are responsible for the most common bacterial infections in burns [59, 60]. Around 12 % of infections following burns are caused by *A. baumannii*, of which 99, 60 and 87 % are resistant to ceftazidime, imipenem and ciprofloxacin respectively. *P. aeruginosa* infections, which comprise 16 % of the total cases, have more than 35 % of strains resistant to ceftazidime and imipenem. *S. aureus* still being the most common causative agent giving rise to 20 % of all burn infections with 68 % being methicillin resistant but susceptible to glycopeptides [59]. Infection from both *S. aureus* and *P. aeruginosa* are known to interfere with epithelization significantly, having a serious effect on the healing process [61]. Burn patients are at very high risk of MRSA infection, and combinations of infection control strategies are needed [62]. The bismuth complex loaded hydrogels studied herein showed rapid killing of the entire bacterial population of *P. aeruginosa* and *A. baumannii* at target concentrations of 12 and 9  $\mu\text{g/g}$  within less than 24 hr. However, with MRSA and VRE bacteriostatic effects were observed at these concentrations, followed by regrowth of MRSA after 12 hours. Regrowth phenomena are common in time-kill studies [63]. Mathematical models suggest these phenomena are indicative of adaptation and rapid evolution, which may be due to the presence of susceptible and resistant sub-populations within a bacterial strain.[64].

Paradoxically, the bismuth containing hydrogels appear more active against Gram-negative bacteria. This is surprising because previous research with bismuth compounds has shown the opposite and found them more active against Gram positive bacteria [33, 36, 41]. The reasons for this are presently unknown however it may reflect improved availability of the complex for bacteria within a hydrogel matrix. This selectivity in the current formulation will limit its utility if a broad-spectrum agent is desired. However, this selectivity for target bacteria is commonly found among commercial hydrogels. A silver-based wound hydrogel containing 55 ppm of AgCl is not active against *P. aeruginosa* but is active against most Gram-positive bacteria [57]. The silver-based commercial hydrogel, Silvasorb®, has a broader spectrum of action eliminating MRSA in 3 hours, VRE in 2 hours and *E. coli* in 6 hours. Studies also suggests that it kills *P. aeruginosa* within 24 hours, which is also true for our bismuth-NC hydrogel [65]. Broad spectrum antimicrobials have the benefit of being active against a range of bacteria, but have greater risks of selecting resistance genes. Narrow-spectrum antimicrobial agents may be preferred for treatment of skin infections, urinary tract

infections and other non-life-threatening cases [66]. It is encouraging that the current bismuth-hydrogel formulation targets two Gram-negative bacteria, a group that is generally more resistant and has fewer therapeutic options for treatment. However, *E. coli* showed to be an exception to this trend. In spite of being a Gram-negative bacterium, the bismuth complex was not successful in showing bactericidal activity at any concentrations tested. For Gram-negative bacteria, the permeability barrier by the cell wall is an important factor and depends on the efflux mechanism of a particular bacterial species and physicochemical properties of the antimicrobial agent [67]. The bismuth-phosphinato antimicrobial agent studied herein is hydrophobic and present as large needle shaped particles in the hydrogel [41]. Hydrophobic compounds are generally transported into the cells of Gram-negative bacteria by passive diffusion. The structure of the outer membrane of *Pseudomonas* and *Acinetobacter* species are similar to most Gram-negative bacteria, except enterobacteria like *E. coli* [67]. Species of *Acinetobacter* and *Pseudomonas* also showed higher permeability and more susceptibility than *E. coli* to large hydrophobic antibiotics like novobiocin, and erythromycin [68]. Moreover, *E. coli* has greater sensitivity to small molecule antibiotics compared to other Gram-negative ones. So the higher susceptibility of the more problematic bacterial species to the bismuth complex can be advantageous [60]. Reports indicate that *A. baumannii* uses hydrophobic compounds as growth nutrients and thus has a unique pathway for transport of hydrophobic substances into the cells [69]. This transport pathway may explain the rapid bactericidal effect the Bi-complex had on *A. baumannii* within only 4 hours. The concentration dependent activity of the hydrogel does suggest that higher concentrations of the bismuth complex may induce a bactericidal or sustained bacteriostatic effect for *E. coli*, MRSA and VRE. However, higher concentrations were not tested due to reduced mammalian cell viability.

#### **4.5.4.2. Bacterial cell morphology**

The hydrogel loaded with the bismuth complex is shown to have an effect on bacterial viability by time-kill kinetics. *P. aeruginosa* was taken as a model bacterium for this study, and bactericidal concentrations of 12 and 9  $\mu\text{g/g}$  were studied. Untreated cells served as the control, which shows smooth surfaces on the rod-shaped bacterial cells, with no visible cell damage shown in Figure 8 (a-b). Figure 8(c) shows the appearance of the cells after being treated with Bi-loaded hydrogels at 12  $\mu\text{g/g}$  of the bismuth complex in the broth, with the cell surface having an uneven texture. Fibrous features formed on the exterior of the cells along with debris build-up around them. Figure 8(b) and (d) show the bacterial cells at the same magnification, clearly showing the difference in number of bacterial cells after being treated with Bi-loaded hydrogel with concentration of 9  $\mu\text{g/g}$  of the bismuth

complex compared to the control. Figure 9 shows the structure of a single bacterial cell to illustrate the morphological changes to individual cells after exposure to Bi-loaded hydrogels. The treated cells show obvious shape malformation, indicating possible disruption of the cell wall and/or loss of membrane integrity. When treated at 12  $\mu\text{g/g}$ , intracellular material was observed to be leaking out of the cells, likely by formation of membrane bound vesicles. Overall, the cells show severe shape distortion and a crumpled surface after being treated, which supports the findings from the time-kill assay.

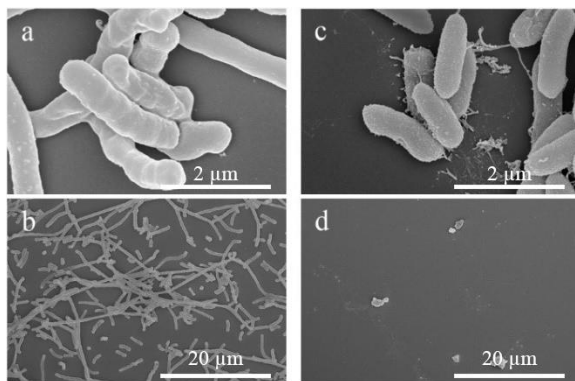


**Figure 8:** SEM images of untreated *P. aeruginosa* cells (a-b), and treated with Bi-NC hydrogel with bismuth complex concentrations of 12  $\mu\text{g/g}$  (c) and 9  $\mu\text{g/g}$  (d).

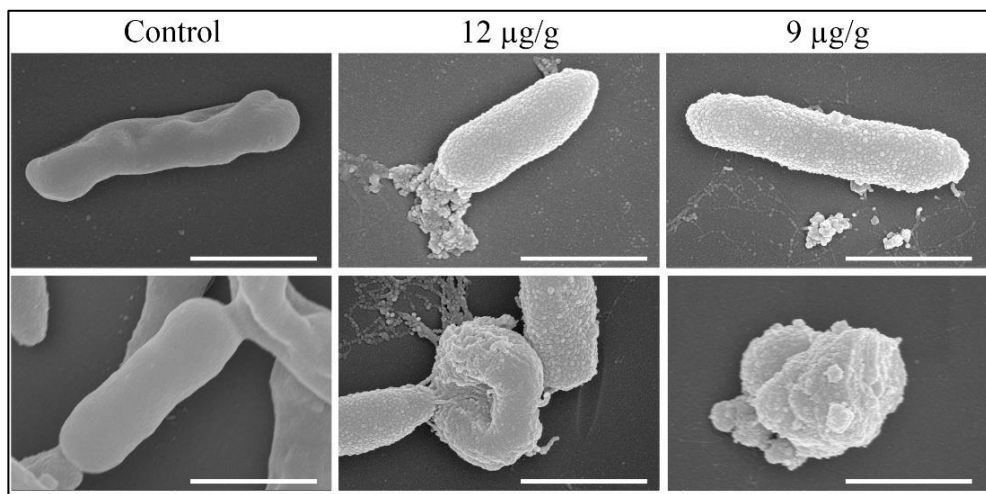


**Figure 9:** SEM images of a single *P. aeruginosa* cell with no treatment (control), and treated with Bi-NC hydrogel with bismuth complex concentrations of 12  $\mu\text{g/g}$  and 9  $\mu\text{g/g}$ . Scale bar represents 1  $\mu\text{m}$ .

#### 4.5.4.3. Internal Quality Control

Quality control tests were done to evaluate the reliability and reproducibility of the antibacterial test results. Blinded experimental repeats of the time-kill assays were performed using one Gram-positive (MRSA) and one Gram-negative (*A. baumannii*) bacteria in a different laboratory using a different batch of hydrogel. This was done to verify that the difference in activity towards these two classes of bacteria is reproducible, so one of each kind of bacteria was chosen. There were also some differences in the bacterial population in the blinded experiments in Figure C4 compared to the original time-kill assay. This was true for both the 9 µg/g and the control growth curves. The control curve showed less growth in the blinded experiments. For instance, after 24 hours MRSA showed 9 CFU/mL in the blinded experiment as opposed to 12 CFU/mL with the original time-kill assay. This could be because the interlaboratory repeatability of bacterial cell count using the CFU method is poor [70]. However, the aim of this research was not to prove the interlaboratory reproducibility of the growth curve, but to show that the effect of the bismuth complex on the bacterial population compared to an untreated control at the same conditions is reproducible. The bacterial count showed similar fold reduction when treated with 9 µg/g Bi-complex compared to the control in the blinded repeats. For example, for MRSA, the ratio of the log CFU/mL of the control to the 9 µg/g at 4 hours was 1.32 and 1.61 and at 24 hours was 1.56 and 1.35 for the blinded experiment and the original experiment respectively. So, the bismuth complex was able to achieve a similar fold reduction. With the *A. baumannii*, the entire bacterial population was killed in 4 hours, similar to the original assay. The interlaboratory reproducibility of the antibacterial activity proven from this study demonstrates the stability and reliability of the antibacterial activity of Bi-complex loaded hydrogels.

#### 4.5.5. Hydrogel Quality check

The 0.1 wt% hydrogel was tested to verify the actual loading of the bismuth complex to account for all losses during the various stages of hydrogel preparation. It was found that the hydrogel contained  $0.08 \pm 0.01$  wt% of the bismuth complex, reported as batch 1 in Table C1. It is important to note that the actual bismuth content is somewhat lower than the target concentration. For applications like this, it is critical to ensure that the active agent concentration is consistent and predictable. A quality check study was performed to understand the bismuth complex content in different batches of hydrogels produced. The actual bismuth complex content of three more different batches of the bismuth-loaded hydrogel were tested, as shown in Table C1. The average  $\pm$  standard deviation of the bismuth complex content in the four batches of hydrogels was  $0.081 \pm 0.002$  wt%, showing that a consistent loading was achieved.

The studies reported here identify a bismuth complex loading of 9  $\mu\text{g/g}$  as the most appropriate concentration for further study. Concentrations of 12 and 9  $\mu\text{g/g}$  do not show much difference in antibacterial activity to the most bacterial strains tested. The cytotoxicity assays suggest there is a measurable deleterious effect on fibroblasts at 12  $\mu\text{g/g}$  and above compared to the DMEM control. Lower concentrations do not decrease cellular proliferation or viability of the fibroblast line tested. From this comparison, a target concentration of 9  $\mu\text{g/g}$  is identified as the optimum concentration, showing toxicity to prokaryotic bacterial cells (of Gram-negative type in particular) along with having no adverse effect on mammalian cells. According to the ICP-OES analysis the actual bismuth complex content is slightly, yet consistently, lower than the target loading. The optimised target concentration of 9  $\mu\text{g/g}$  (9.375  $\mu\text{g/g}$  in 3 decimal places) is calculated to contain 7.5  $\mu\text{g/g}$ . The actual bismuth content quality check must be performed prior to commercial production. The bismuth complex is highly hydrophobic and tends to stick to beaker walls and other surfaces during the Bi-loaded hydrogel preparation resulting in lower than the target loading. This makes it difficult to synthesize a hydrogel with such low concentration at laboratory scale. Once incorporated into a nanocellulose matrix, the complex particles are intertwined by the fibres which protect them from coming out onto the surfaces. Moreover, the limitation of *in-vitro* tests is that the sample must be diluted in media and it is this treatment mixture of sample and media that is delivered to the cells. Therefore, the bismuth content in the treatment mixture and the prepared (neat) hydrogel will be different. Hence, a single batch of hydrogel was prepared for which the actual bismuth content was measured. The Bi-hydrogel was diluted to study the effect of different concentrations of the complex. Future work should include testing a 9 $\mu\text{g/g}$  loaded nanocellulose hydrogel on an *in-vivo* skin model. Since the pure nanocellulose hydrogel was shown to be non-toxic, the toxic effect in the bismuth-loaded hydrogels was solely due to the bismuth complex content which has been optimised in this paper. Thus, nanocellulose hydrogel loaded with a target concentration of 9  $\mu\text{g/g}$  bismuth complex is the most appropriate concentration for further study as antibacterial wound dressing that can lessen the bioburden, thereby reducing the probability of wounds becoming infected. In addition, the highly hydrated nature of the hydrogel can promote wound healing.

#### **4.6. Conclusion**

The potential of phenyl *bis*-diphenylphosphinato bismuth (III) complex loaded nanocellulose hydrogels for wound care applications has been investigated. Morphological studies using SEM show a well-distributed complex in the hydrogel matrix. The rheological properties show the hydrogel behaves like true gels and is comparable to commercial burn hydrogels sold in tubes. This highlights

the suitability of our material in terms of ease of storage and application. An extensive study to optimise the loading of the bismuth complex in the hydrogel was done. It was shown there is a dose-dependent effect on both the antibacterial properties as well as the toxicity toward mammalian fibroblast cells. The study herein gives a detailed understanding of the host-cell safety and antibacterial activity of different levels of the bismuth complex in the hydrogel matrix. The optimum target concentration of 9  $\mu\text{g/g}$  was established to have a selective toxicity towards bacteria over mammalian cells. This study demonstrates that these hydrogels can be promising candidates as antimicrobial wound gels when the bismuth complex is used at safe but active levels. This opens opportunities for formulation of a renewable, safe and active wound care hydrogel using a new class of antibacterial agent to address the issue of rising antimicrobial resistance. Moreover, the bactericidal behaviour of the complex towards the Gram-negative bacterial strains, *A. baumannii* and *P. aeruginosa*, at concentrations safe to host cells is promising, given therapeutics for treatment of infections caused by these bacteria are limited [60]. The antibacterial selectivity towards the different bacterial strains suggests its usefulness in specific clinical utility over a broad-spectrum antibacterial material. This might be advantageous over silver wound gels, which are generally broad-spectrum antibacterial materials [57]. However, our study here is limited to *in-vitro* experiments of the biocompatibility and antibacterial effect. The *in-vitro* results presented in this paper provides a useful preliminary screening to optimise Bi-nanocellulose hydrogel formulation and future *in-vivo* studies on animal models is required using hydrogel loaded with the optimised level of bismuth complex for regulatory purposes. An infected wound model is highly recommended to understand not only the biocompatibility and antibacterial activity of the composite hydrogel, but also to understand the healing properties of the hydrogel.

#### **4.7. Acknowledgements**

The authors thank Monash University and The National Health and Medical Research Council (APP1139844) for financial support. The authors would like to acknowledge the use of the facilities in the Monash Centre for Electron Microscopy and Ramaciotti Centre for Cryo-Electron Microscopy. The authors would like to thank Dr. Simon Crawford for his assistance. Maisha Maliha would like to acknowledge the Australian Government for the Research Training Program (RTP) Scholarship.

#### **4.8. References**

1. Agyingi, E., S. Maggelakis, and D. Ross, *The Effect of Bacteria on Epidermal Wound Healing*. Mathematical Modelling of Natural Phenomena, 2010. **5**(3): p. 28-39.

2. Jones, V., J. Grey, and K. Harding, *Wound dressings*. British Medical Journal, 2006. **332**(7544): p. 777.
3. Caló, E. and V.V. Khutoryanskiy, *Biomedical applications of hydrogels: A review of patents and commercial products*. European Polymer Journal, 2015. **65**: p. 252-267.
4. Rattanaeuengsrikul, V., N. Pimpha, and P. Supaphol, *Development of Gelatin Hydrogel Pads as Antibacterial Wound Dressings*. Macromolecular Bioscience, 2009. **9**(10): p. 1004-1015.
5. Ashtikar, M. and M. Wacker, *Nanopharmaceuticals for wound healing –Lost in translation?* Vol. 129. 2018.
6. Hakkarainen, T., et al., *Nanofibrillar cellulose wound dressing in skin graft donor site treatment*. Journal of Controlled Release, 2016. **244**: p. 292-301.
7. Basu, A., et al., *Ion-crosslinked wood-derived nanocellulose hydrogels with tunable antibacterial properties: Candidate materials for advanced wound care applications*. Carbohydrate Polymers, 2018. **181**: p. 345-350.
8. Kamoun, E.A., E.-R.S. Kenawy, and X. Chen, *A review on polymeric hydrogel membranes for wound dressing applications: PVA-based hydrogel dressings*. Journal of Advanced Research, 2017. **8**(3): p. 217-233.
9. Basu, A., et al., *On the use of ion-crosslinked nanocellulose hydrogels for wound healing solutions: Physicochemical properties and application-oriented biocompatibility studies*. Carbohydrate Polymers, 2017. **174**: p. 299-308.
10. Singh, R. and D. Singh, *Radiation synthesis of PVP/alginate hydrogel containing nanosilver as wound dressing*. Official Journal of the European Society for Biomaterials, 2012. **23**(11): p. 2649-2658.
11. De France, K., T. Hoare, and E. Cranston, *Review of Hydrogels and Aerogels Containing Nanocellulose*, in *Chem. Mat.* 2017. p. 4609-4631.
12. Chinga-Carrasco, G. and K. Syverud, *Pretreatment-dependent surface chemistry of wood nanocellulose for pH-sensitive hydrogels*. Journal of Biomaterials Applications, 2014. **29**(3): p. 423-432.
13. Laçin, N.T., *Development of biodegradable antibacterial cellulose based hydrogel membranes for wound healing*. International Journal of Biological Macromolecules, 2014. **67**(Supplement C): p. 22-27.
14. Czaja, W., et al., *Microbial cellulose—the natural power to heal wounds*. Biomaterials, 2006. **27**(2): p. 145-151.
15. *Finland : UPM's FibDex, a wood-based innovation for wound care, receives regulatory approval and CE mark*. 2019: Mena Report.

16. Resmi, R., et al., *Synthesis and characterization of silver nanoparticle incorporated gelatin-hydroxypropyl methacrylate hydrogels for wound dressing applications*. Journal of Applied Polymer Science, 2017. **134**(10).
17. González-Sánchez, M.I., et al., *Silver nanoparticle based antibacterial methacrylate hydrogels potential for bone graft applications*. Materials Science and Engineering: C, 2015. **50**: p. 332-340.
18. Bardajee, G.R., Z. Hooshyar, and H. Rezanezhad, *A novel and green biomaterial based silver nanocomposite hydrogel: Synthesis, characterization and antibacterial effect*. Journal of Inorganic Biochemistry, 2012. **117**: p. 367-373.
19. Tyliczszak, B., et al., *Preparation and cytotoxicity of chitosan-based hydrogels modified with silver nanoparticles*. Colloids and Surfaces B: Biointerfaces, 2017. **160**: p. 325-330.
20. Abou-Yousef, H. and S. Kamel, *High efficiency antimicrobial cellulose-based nanocomposite hydrogels*. Journal of Applied Polymer Science, 2015. **132**(31).
21. Valle, H., et al., *Antibacterial activity and cytotoxicity of hydrogel-nanosilver composites based on copolymers from 2-acrylamido-2-methylpropanesulfonate sodium*. Journal of Applied Polymer Science, 2014. **131**(3).
22. Thomas, V., et al., *A versatile strategy to fabricate hydrogel–silver nanocomposites and investigation of their antimicrobial activity*. Journal of Colloid And Interface Science, 2007. **315**(1): p. 389-395.
23. Hebeish, A., et al., *Development of CMC hydrogels loaded with silver nano-particles for medical applications*. Carbohydrate Polymers, 2013. **92**(1): p. 407-413.
24. Babu, V.R., et al., *Development of semi-interpenetrating carbohydrate polymeric hydrogels embedded silver nanoparticles and its facile studies on E. coli*. Carbohydrate Polymers, 2010. **81**(2): p. 196-202.
25. Maneerung, T., S. Tokura, and R. Rujiravanit, *Impregnation of silver nanoparticles into bacterial cellulose for antimicrobial wound dressing*. Carbohydrate Polymers, 2008. **72**(1): p. 43-51.
26. Maillard, J.-Y. and P. Hartemann, *Silver as an antimicrobial: facts and gaps in knowledge*. Critical Reviews in Microbiology, 2013. **39**(4): p. 373-383.
27. Silver, S., *Bacterial silver resistance: molecular biology and uses and misuses of silver compounds*. FEMS Microbiology Reviews, 2003. **27**(2): p. 341-353.
28. Gunawan, C., et al., *Widespread and Indiscriminate Nanosilver Use: Genuine Potential for Microbial Resistance*. ACS nano, 2017. **11**(4): p. 3438.

29. Barros-Velázquez, J., *Industrial Applications: Regulatory Issues and Life Cycle Assessment of Food Packaging*, in *Antimicrobial Food Packaging*. 2015, Elsevier.
30. Cushen, M., et al., *Nanotechnologies in the food industry – Recent developments, risks and regulation*. Trends in Food Science & Technology, 2012. **24**(1): p. 30-46.
31. Stensberg, M.C., et al., *Toxicological studies on silver nanoparticles: challenges and opportunities in assessment, monitoring and imaging*. Nanomedicine (Lond), 2011. **6**(5): p. 879-98.
32. Restuccia, D., et al., *Chapter 16 - Industrial Applications: Regulatory Issues and Life Cycle Assessment of Food Packaging*. 2016, Elsevier Inc. p. 215-227.
33. Werrett, M., et al., *Bismuth Phosphinates in Bi-Nanocellulose Composites and their Efficacy towards Multi-Drug Resistant Bacteria*. Chemistry- A European Journal, 2018.
34. Luqman, A., et al., *The Importance of Heterolepticity in Improving the Antibacterial Activity of Bismuth(III) Thiolates*. European Journal of Inorganic Chemistry, 2016. **2016**(17): p. 2738-2749.
35. Svoboda, T., et al., *NCN Chelated Organoantimony(III) and Organobismuth(III) Phosphinates and Phosphites: Synthesis, Structure and Reactivity*. European Journal of Inorganic Chemistry, 2010. **2010**(33): p. 5222-5230.
36. Kotani, T., et al., *Antibacterial Properties of Some Cyclic Organobismuth(III) Compounds*. Antimicrobial Agents and Chemotherapy, 2005. **49**(7): p. 2729.
37. Domenico, P., et al., *Activities of Bismuth Thiols against Staphylococci and Staphylococcal Biofilms*. Antimicrobial Agents and Chemotherapy, 2001. **45**(5): p. 1417.
38. Briand, G.G. and N. Burford, *Bismuth Compounds and Preparations with Biological or Medicinal Relevance*. Chemical Reviews, 1999. **99**(9): p. 2601-2658.
39. Barry, N.P.E. and P.J. Sadler, *Exploration of the medical periodic table: towards new targets*. Chem. Commun., 2013. **49**(45): p. 5106-5131.
40. Suzuki, H. and Y. Matano, *Chapter 1 - Introduction*, in *Organobismuth Chemistry*, Y. Matano, Editor. 2001, Elsevier Science: Amsterdam. p. 1-20.
41. Maliha, M., et al., *Bismuth phosphinate incorporated nanocellulose sheets with antimicrobial and barrier properties for packaging applications*. Journal of Cleaner Production, 2019. **246**.
42. Barton, D.H.R., et al., *Pentavalent organobismuth reagents. Part vi. Comparative migratory aptitudes of aryl groups in the arylation of phenols and enols by pentavalent bismuth reagents*. Tetrahedron, 1986. **42**(12): p. 3111-3122.
43. Saito, T., et al., *Cellulose nanofibers prepared by TEMPO-mediated oxidation of native cellulose*. Biomacromolecules, 2007. **8**(8): p. 2485.

44. Fukuzumi, H., et al., *Transparent and High Gas Barrier Films of Cellulose Nanofibers Prepared by TEMPO-Mediated Oxidation*. *Biomacromolecules*, 2009. **10**(1): p. 162-165.
45. Mendoza, L., et al., *Gelation mechanism of cellulose nanofibre gels: A colloids and interfacial perspective*. *Journal of Colloid and Interface Science*, 2018. **509**(Supplement C): p. 39-46.
46. Hartung, T. and G. Daston, *Are In Vitro Tests Suitable for Regulatory Use?* *Toxicological Sciences*, 2009. **111**(2): p. 233-237.
47. Shpichka, A., et al., *Skin tissue regeneration for burn injury*. *Stem Cell Research & Therapy*, 2019. **10**(1): p. 94.
48. Ghallab, A., *In vitro test systems and their limitations*. *EXCLI journal*, 2013. **12**: p. 1024-1026.
49. Güzel Bayülken, D. and B. Ayaz Tüylü, *In vitro genotoxic and cytotoxic effects of some paraben esters on human peripheral lymphocytes*. *Drug Chem Toxicol*, 2019. **42**(4): p. 386-393.
50. Spindola, D.G., et al., *In vitro cytotoxicity of chemical preservatives on human fibroblast cells*. *Braz. J. Pharm. Sci*, 2018. **54**(1).
51. Tschumperlin, D.J., *Fibroblasts and the Ground They Walk On*. *Physiology*, 2013. **28**(6): p. 380-390.
52. Wiegand, C., et al., *Effect of non-adhering dressings on promotion of fibroblast proliferation and wound healing in vitro*. *Scientific Reports*, 2019. **9**(1): p. 4320.
53. Samberg, M.E., S.J. Oldenburg, and N.A. Monteiro-Riviere, *Evaluation of silver nanoparticle toxicity in skin in vivo and keratinocytes in vitro*. *Environmental health perspectives*, 2010. **118**(3): p. 407-413.
54. Hussain, S.M., et al., *In vitro toxicity of nanoparticles in BRL 3A rat liver cells*. *Toxicology in Vitro*, 2005. **19**(7): p. 975-983.
55. Braydich-Stolle, L., et al., *In vitro cytotoxicity of nanoparticles in mammalian germline stem cells*. *Toxicological sciences : an official journal of the Society of Toxicology*, 2005. **88**(2): p. 412-419.
56. Khattak, A.Z., et al., *A randomized controlled evaluation of absorption of silver with the use of silver alginate (Algidex) patches in very low birth weight (VLBW) infants with central lines*. *Journal of Perinatology*, 2009. **30**(5): p. 337.
57. Lee, Y., et al., *Time-kill Kinetics of a Novel Antimicrobial Silver Wound Gel Against Select Wound Pathogens*. *Wounds*, 2015. **27**(12): p. 336-46.

58. *Prioritization of pathogens to guide discovery, research and development of new antibiotics for drug resistant bacterial infections, including tuberculosis*. 2017: Geneva: World Health Organization.
59. Thabet, L., et al., *Bacteriological profile and antibiotic resistance of bacteria isolates in a burn department*. La Tunisie medicale, 2008. **86**(12): p. 1051-1054.
60. Norbury, W., et al., *Infection in Burns*. Surgical infections, 2016. **17**(2): p. 250-255.
61. Pastar, I., et al., *Epithelialization in Wound Healing: A Comprehensive Review*. Advances in Wound Care, 2014. **3**(7): p. 445-464.
62. Andrade, C., et al., *Methicillin-resistant Staphylococcus aureus: An assessment of environmental contamination in a burn center*. American Journal of Infection Control, 2009. **37**(6): p. 515-517.
63. Sim, J.-H., et al., *In vitro antibacterial and time-kill evaluation of phosphane-gold(I) dithiocarbamates, R<sub>3</sub>PAu[S<sub>2</sub>CN(iPr)CH<sub>2</sub>CH<sub>2</sub>OH] for R = Ph, Cy and Et, against a broad range of Gram-positive and Gram-negative bacteria*. Gold Bulletin, 2014. **47**(4): p. 225-236.
64. Tam, V.H., A.N. Schilling, and M. Nikolaou, *Modelling time-kill studies to discern the pharmacodynamics of meropenem*. Journal of Antimicrobial Chemotherapy, 2005. **55**(5): p. 699-706.
65. Castellano, J.J., et al., *Comparative evaluation of silver-containing antimicrobial dressings and drugs*. International Wound Journal, 2007. **4**(2): p. 139-140.
66. Melander, R.J., D.V. Zurawski, and C. Melander, *Narrow-Spectrum Antibacterial Agents*. MedChemComm, 2018. **9**(1): p. 12-21.
67. Zgurskaya, H.I., C.A. López, and S. Gnanakaran, *Permeability Barrier of Gram-Negative Cell Envelopes and Approaches To Bypass It*. ACS infectious diseases, 2015. **1**(11): p. 512-522.
68. Plésiat, P. and H. Nikaido, *Outer membranes of gram-negative bacteria are permeable to steroid probes*. Mol Microbiol, 1992. **6**(10): p. 1323-33.
69. Borneleit, P. and H.P. Kleber, *The Outer Membrane of Acinetobacter: Structure-Function Relationships*, in *The Biology of Acinetobacter: Taxonomy, Clinical Importance, Molecular Biology, Physiology, Industrial Relevance*, K.J. Towner, E. Bergogne-Bérézin, and C.A. Fewson, Editors. 1991, Springer US: Boston, MA. p. 259-271.
70. Beal, J., et al., *Robust estimation of bacterial cell count from optical density*. Commun Biol, 2020. **3**(1): p. 512.

---

## **CHAPTER 5**

**BISMUTH PHOSPHINATO INCORPORATED ANTIBACTERIAL FILTER PAPER  
FOR DRINKING WATER DISINFECTION**

---

THIS PAGE HAS BEEN INTENTIONALLY LEFT BLANK

## PREFACE

This chapter demonstrates the use of the *bis*-phosphinato bismuth (III) complex in nanocellulose for water disinfection purpose. It utilises the knowledge learnt in the previous chapters about the leaching behaviour of the complex and the effect of the fibre dimensions and sheet preparation techniques to propose the design of two water filtration techniques. This study reveals important aspects about the antibacterial activity of the bismuth (III) complex. The complex is unable to instantly deactivate bacteria but has the capacity to inhibit biofilm growth on surfaces. This chapter addresses the fourth research objective.

THIS PAGE HAS BEEN INTENTIONALLY LEFT BLANK

**CHAPTER 5: BISMUTH PHOSPHINATO INCORPORATED ANTIBACTERIAL  
FILTER PAPER FOR DRINKING WATER DISINFECTION**

<b>5.1. Abstract.....</b>	<b>171</b>
<b>5.2. Keywords .....</b>	<b>172</b>
<b>5.3. Introduction.....</b>	<b>172</b>
<b>5.4. Materials and methods .....</b>	<b>173</b>
5.4.1. Materials .....	173
5.4.2. Preparation of MFC coating on filter paper .....	174
5.4.3. Preparation of NFC membrane .....	174
5.4.4. Physical properties .....	175
5.4.4.1. Grammage measurement.....	175
5.4.4.2. Flux properties .....	175
5.4.4.3. SEM imaging .....	175
5.4.5. Pore properties .....	175
5.4.6. Antibacterial performance.....	176
5.4.6.1. Bacterial filtration: MFC Coated Filters .....	176
5.4.6.2. Bacterial filtration: NFC membrane.....	176
5.4.7. Bismuth complex leaching.....	176
5.4.8. Cytotoxicity of filtrate.....	176
5.4.9. Anti-biofilm properties of the membrane .....	177
5.4.9.1. Attachment of bacteria.....	177
5.4.9.2. Mature biofilm .....	177
<b>5.5. Results and discussion .....</b>	<b>178</b>
5.5.1. Physical properties .....	178
5.5.1.1. Grammage and flux properties.....	178
5.5.1.2. SEM imaging .....	178
5.5.2. Pore properties .....	179
5.5.3. Antibacterial performance.....	181
5.5.3.1. Bacterial filtration: MFC Coated Filters .....	181
5.5.3.2. Bacterial filtration: NFC membranes .....	184
5.5.4. Bismuth complex leaching.....	185
5.5.5. Cytotoxicity of filtrate.....	186
5.5.6. Anti-biofilm properties of the membrane .....	187

5.5.6.1.	Initial Attachment of bacteria .....	187
5.5.6.2.	Mature biofilm .....	188
<b>5.6.</b>	<b>Conclusion .....</b>	<b>189</b>
<b>5.7.</b>	<b>Acknowledgement.....</b>	<b>190</b>
<b>5.8.</b>	<b>Reference .....</b>	<b>190</b>

## BISMUTH PHOSPHINATO INCORPORATED ANTIBACTERIAL FILTER PAPER FOR DRINKING WATER DISINFECTION

Maisha Maliha<sup>1</sup>, Benjamin Tan<sup>1</sup>, Karmen Wong<sup>1</sup>, Simin Miri<sup>1</sup>, Rajini Brammananth<sup>2</sup>, Ross Coppel<sup>2</sup>, Melissa Werrett<sup>3,4</sup>, Philip C. Andrews<sup>3,4</sup>, Warren Batchelor<sup>1\*</sup>

<sup>1</sup>*Bioresource Processing Research Institute of Australia (BioPRIA), Department of Chemical Engineering, Monash University, VIC 3800, Australia*

<sup>2</sup>*Department of Microbiology, Monash University, VIC 3800, Australia*

<sup>3</sup>*School of Chemistry, Monash University, VIC 3800, Australia*

<sup>4</sup>*Centre to Impact AMR, Monash University, VIC 3800, Australia*

Corresponding author email: warren.batchelor@monash.edu

### 5.1. Abstract

Lack of safe drinking water is a major concern, mainly in the developing countries. Consequently, there is a significant and immediate need for affordable technologies to provide clean drinking water. In this paper, two approaches for drinking water disinfection using nanocellulose and the antimicrobial phenyl *bis*-diphenylphosphinato bismuth (III) complex is studied. The first approach investigates the deactivation of bacteria when contaminated water percolates through a filter paper with a microfibrillated cellulose (MFC) coating containing Bi-complex. The antibacterial activity was studied by filtering bacterial broth of *Staphylococcus aureus* and analysing the live bacteria in the filtrate. The filter composites did not show any sign of instantaneous killing of bacteria, irrespective of the Bi-complex loading or base paper substrate. However, the effluent demonstrated drastic reduction in bacterial population after resting at 37°C. Bacteria was completely eradicated 24 hours after passing through 5 wt% and 10 wt% Bi-coated filters and thus they can be used for purification of storage water. The second approach uses a Bi-complex loaded nanofibrillated cellulose (NFC) membrane. Herein, complete and immediate exclusion of bacteria was achieved in the NFC membrane when bacterial broth was passed through it at 1 bar. The 2.5 wt% Bi-loaded membrane can significantly minimise the risk of biofilm formation, even after 4 days of contact with bacterial broth. The Bi-complex concentration in the filtrate (130.6±1.9 ppb) from the 2.5 wt% Bi-loaded microfilter was shown to be within the non-toxic (to murine fibroblast cells) concentration range. This study outlines the proof of concept of two sustainable prototypes for stored or immediate drinking water purification.

## 5.2. Keywords

Nanocellulose, bismuth, filter, water purification, antibacterial

## 5.3. Introduction

Water is one of the most essential elements for survival. Contaminated drinking water can lead to water borne diseases such as cholera, diarrhoea, and typhoid [1]. While 71 % of the global population has easy access to safe drinking water, the remaining 29 % (785 million people) do not. With a large number of people drinking water contaminated with faeces, the annual death toll due to diarrhoea is estimated to be 485000 [1, 2]. This is mainly in developing countries, where poverty and lack of basic facilities deny people access to safe drinking water [2]. Thus, there is significant demand for affordable technologies that can provide clean drinking water. Currently, drinking water purification treatments include boiling, chlorination and UV treatment. However, these can be expensive and time-consuming [3]. Moreover, adding chemicals, such as chlorine, can raise concerns about toxicity [4]. A low-cost water filtration system with an antimicrobial coating could be one potential solution since such filters can be easy to operate, affordable, portable and can be used in remote areas with little or no energy consumption [5, 6]. Low cost materials for water filters include ceramics, polymeric membranes, and polyurethane and fibre-based materials [6]. We have developed and studied composite cellulosic materials as potential antimicrobial water filters and purifiers. The natural fibre cellulose, the most abundant biopolymer on earth, is biodegradable, renewable, inexpensive and non-toxic [7, 8].

Antimicrobial filters for water purification have been studied using a range of metal-based antimicrobial agents including silver [3, 9-12], copper [3, 5], and zinc [3, 13]. Silver is the most popular antimicrobial agent used as a water disinfectant in established domestic water filters, ceramic filters, or added as a silver suspension to drinking water [14]. Examples of commercial water treatment systems using silver include MARATHON<sup>®</sup> and Aquapure<sup>®</sup> [15]. Although these filters are known for being effective and low cost, the use of silver still presents a potential risk to human health and the environment [6]. Studies have shown that silver nanoparticles wash out of these filters into the drinking water [6, 9]. Since silver is not an essential element for humans, a maximum concentration of 0.1 mg/L in drinking water has been recommended as a safe limit with a total lifetime oral intake of 10 g [14]. A number of *in-vivo* studies have shown that continuous oral exposure to silver nanoparticles can lead to toxic effects to tissues and organs like the liver, kidney, brain, to even death [14]. Moreover, the release of the nanoparticles from the water treatment systems limits the lifetime of their efficacy. [15] Another major concern is that the extensive use of silver across a large variety of products has led to resistance to silver in bacterial genes. [16-18] Bacterial resistance has also been reported for other metals of interest,

such as copper and zinc [19]. As a result, there is a constant and growing demand for new, alternative and safe antimicrobial agents and materials. In this paper we report the study of an organobismuth complex, phenyl *bis*-diphenylphosphinato bismuth (III), in cellulosic material for its potential in water purification. Bismuth, as bismuth subsalicylate (Pepto-Bismol) and colloidal bismuth subcitrate (De-Nol), is commonly used for the treatment of gastrointestinal illness caused by the Gram-negative bacterium *Helicobacter pylori* [20-22]. Beyond this application, there are many other reports of bismuth complexes having antibacterial properties [23-27] while displaying relatively low levels of toxicity to human cells [26]. This complex has been reported to be barely soluble in water [23, 28], which builds the basis for the hypothesis of minimal wash out into the drinking water.

In this paper, two approaches for drinking water disinfection have been studied. The first approach is to explore the deactivation of bacteria in water after passing through the microfibrillated cellulose (MFC) -bismuth complex coated filter paper. Herein, the objective is to make an antibacterial coating with bismuth phosphinato on paper filters to develop a cheap water purification system for bacteria-free water that is capable of being driven by gravity filtration. The effect of the different types of base filter papers and varying bismuth loading in the coating on the antibacterial and leaching properties has been studied. Subsequently, a study was performed to evaluate the lethal effect of the composite on the bacteria over time for storage water. The second approach focuses on the size-exclusion principle by nanofibrillated cellulose (NFC) membrane. However, biofouling is a major problem for such filtration systems, and the role of the bismuth complex was to impart antibiofilm functionalities to the membrane.

## **5.4. Materials and methods**

### **5.4.1. Materials**

Advantec filter papers No. 2 and Whatman filter papers No. 1 were purchased from Interpath Services Pty Ltd and Pacific Laboratory Pty Ltd, respectively. Microfibrillated Cellulose (MFC) purchased from DAICEL Chemical Industries Limited, Japan (grade Celish KY-100G) was used as the nanocellulose matrix. This has been characterised to have an aspect ratio of 142 and an average fibre diameter of 70 nm [29, 30]. Phenyl *bis*-diphenylphosphinato bismuth (III) was prepared according to Werrett et al [23]. The growth medium (Dulbecco's modified Eagle medium or DMEM) and the MTS reagent were purchased from Gibco and Promega, Australia respectively.

### 5.4.2. Preparation of MFC coating on filter paper

A suspension of 2 wt% MFC and varying amounts of phenyl *bis*-diphenylphosphinato bismuth (III) complex in deionised water was made. The suspension was mixed using a hand blender and then a disintegrator, where a small propeller running at 3000 revolutions separates the fibres from each other. *Bis*-phosphinato bismuth-MFC coating was made on base sheets by spraying the suspension onto purchased Whatman and Adventec filter papers, and pre-prepared MFC base sheets. The coatings were made with target loadings of 0, 2.5, 5 and 10 wt% Bi complex with respect to mass of MFC in the suspension for Adventec, which are denoted as A-M0-S, A-M2.5-S, A-M5-S and A-M10-S. The coatings on Whatman filter paper and MFC sheet were made using a target loading of 5 wt% of Bi-complex loading and are referred to as W-M5-S and M-M5-S, respectively. The uncoated base-sheets Adventec, Whatman and MFC sheets are denoted as A, W and M, respectively. The suspension was sprayed at 200 bar using a Professional Wagner spray system (Model number 117) fitted with a spray tip of 517 type from a height of  $40 \pm 1$  cm to the conveyor belt. The base sheets were travelling on the conveyor operated at a speed of  $3.24 \pm 0.2$  cm/s. The parameters used were in accordance with Shanmugam et al. [31]. The apparatus setup is as described in our previous work. [28] After spraying, the coating was let to dry at room temperature for 24 hours. The MFC base sheets were made as described in Shanmugam et al. using 1.5 wt% MFC suspension sprayed with conveyor speed of  $0.52 \pm 0.2$  cm/s [31].

### 5.4.3. Preparation of NFC membrane

To achieve size exclusion, it is important for the pores in the membrane to be exceptionally small to entrap any passing bacteria in the liquid. This was achieved by further fibrillation of the MFC using high pressure homogeniser. The 2 wt% MFC suspension was prepared as described above and passed through the small orifice in GEA Niro Soavi Homogeniser at a pressure of 1000 bar for 1 pass. The produced nanofibrillated cellulose (NFC) suspension was then mixed with the phenyl *bis*-diphenylphosphinato bismuth (III) complex, and standalone handsheets of 60 gsm were prepared having the same bismuth complex loading. These will be referred to as N0-F, N2.5F, N5-F, N10-F for the 0, 2.5, 5 and 10 wt% Bi-complex loading. The sheets were prepared using the British handsheet maker according to the TAPPI standards T205. The suspension was diluted, and 600 g of 0.2 wt% suspension was poured into the handsheet maker over a GE Whatman 541 Hardened Ashless filter paper placed on top of a 150-mesh. The filter paper was to ensure minimum fibre loss during the vacuum filtration process. The sheet was then peeled from the filter paper and pressed for 5 mins under 3 bar pressure, followed by another 2 minutes using dry blotters.

#### **5.4.4. Physical properties**

##### **5.4.4.1. Grammage measurement**

The coated sheets were dried at 105 °C for at least 4 hours, and the dry weight was measured. The ratio of dry weight to area gives the grammage.

##### **5.4.4.2. Flux properties**

The flux of the coated filters was studied using a Merck Millipore dead-end stirred cell, model UFSC40001. A 76 mm diameter filter paper sample was placed at the bottom of the cell, secured by O-ring, and 100 mL of ultrapure water (milli-Q) water was held in the cell. The water was allowed to pass through the sample at a gauge pressure of 1 bar provided by a compressed air gas cylinder. The effluent water was collected in a container on a balance, and the flow rate or flux was obtained as the slope of a change in mass vs. time plot.

##### **5.4.4.3. SEM imaging**

The uncoated filter paper base-sheets, coated MFC surface and NFC membrane were analysed with the use of scanning electron microscopy (SEM) with FEI Magellen 400 FEGSEM. The accelerating voltage and current used were 5 kV and 25 pA, respectively. The samples were cut and mounted onto a metal stub using carbon tape. The samples were then coated with a thin layer of electrically-conductive Iridium metal.

#### **5.4.5. Pore properties**

The pore size distribution and total porosity of the composites were investigated using Micromeritics Autopore IV 9500 series. The MFC coating layer was tested separately, by peeling off the coating from the Advantec filters. The NFC membranes were analysed as prepared. The MFC coating layer and NFC membranes were cut into squares and degassed at 50 °C for 24 h prior to characterization. The volume of mercury intruded into sample pores was recorded at increasing pressures (up to 60,000 psia or 4137 bar) to an immersed sample in mercury. Around 0.2 g of a sample was weighed in a penetrometer with 3 mL stem volume for examination. The volume of mercury intruded into pores was converted to equivalent pore sizes using the instrument software. Measurement of nitrogen adsorption-desorption isotherms were calculated by Brunauer–Emmett–Teller (BET) method using Micromeritics 3FLEX-nitrogen porosimetry. An additional pressure transducer was supplied in this instrument for Krypton as the analysis adsorptive. Samples were degassed for 24 h at 105 °C before operating in Micromeritics 3FLEX.

### **5.4.6. Antibacterial performance**

#### **5.4.6.1. Bacterial filtration: MFC Coated Filters**

The antibacterial properties of the filter composites were tested by filtering a diluted (1 in 10<sup>4</sup>) overnight culture of *S. aureus* through the composite and analysing the effluent for live bacteria. *S. aureus* was grown in Lysogeny broth (LB). The filter paper samples were folded in a conical shape, and diluted LB broth containing *S. aureus* was made to pass through the cone. 1 mL of the broth was transferred into the cone held above an Eppendorf tube to facilitate gravity-driven filtration. The filtrate was then streaked out on the agar plate and incubated at 37 °C for 18-20 hours. After incubation, the agar plates were visually inspected to determine the number of colony forming units per mL (CFU/mL) in a dilute suspension of bacteria. The filtrate was also analysed in the same way after storing it at either 37 °C or 4 °C for 24 hours.

#### **5.4.6.2. Bacterial filtration: NFC membrane**

The bacteria removal efficiency was tested by filtering 5 mL of a diluted (1 in 10<sup>4</sup>) overnight bacterial broth of *S. aureus* using a Millipore dead-end stirred cell at 1 bar. The filtrate was then analysed for the determination of CFU/mL as described previously.

### **5.4.7. Bismuth complex leaching**

The bismuth complex release in the effluent was analysed by the dead end stirred cell at 1 bar as described above. The MFC coated filter papers and the NFC membranes with (different loadings of) the bismuth complex were used for this study. The effluent water was collected and analysed with inductively coupled plasma-mass spectroscopy (ICP-MS). Analysis was performed with Perkin Elmer NexION 2000-C ICP-MS to determine the amount of the bismuth complex that had leached into the filtrate.

### **5.4.8. Cytotoxicity of filtrate**

The cytotoxicity of the filtrate was tested using the filtrate from 10 wt% Bi-loaded NFC membrane (N10-F) against murine fibroblast cells (L929). The filtrate was diluted with DMEM media to obtain different bismuth complex concentrations. 10,000 cells were cultured in growth media (DMEM containing 10 % (v/v) fetal bovine serum (FBS) and 1 % penicillin and streptomycin) in a 96 well plate for 24 hours at 37 °C and 5 % CO<sub>2</sub> humidified incubator. The monolayer of cells was then treated by replacing the media with the different concentrations of the Bi-complex filtrate-media mixture and incubated for 24 hours. The negative and positive controls were treated with growth media and 10 % dimethyl sulfoxide (DMSO), respectively. The

cytotoxicity was determined using MTS assay. The treatment media was replaced by MTS reagent diluted in DMEM and incubated in dark for 1 hour. The absorbance at 490 nm was measured using Thermo Scientific Multiskan Spectrum plate reader and normalised against the negative control. The experiment was performed in four biological replicates with technical triplicates.

#### **5.4.9. Anti-biofilm properties of the membrane**

##### **5.4.9.1. Attachment of bacteria**

1 cm squares of the membranes (N0-F, N2.5-F, N5-F, N10-F) were cut using a laser cutter and placed in a sterile 12 well plate. 1 mL of diluted overnight cultures (1 in 100) was added to the samples and incubated for 24 hours in 37 °C at static conditions to allow biofilm to grow. After 24 hours, the samples were washed with 1×PBS three times to wash away all planktonic bacteria cells and studied for the presence of attached bacteria by SEM imaging. The bacteria were fixed with 2.5 % glutaraldehyde in 0.1 M PBS buffer (pH 7.4) for 24 hours at room temperature. The samples were washed 3 times with PBS and subsequently dehydrated with graded series of ethanol concentrations (10 %, 30 %, 60 %, 70 %, 80 % and 90 %) for 5 min. and absolute ethanol for 15 min . The dehydrated samples were dried at room temperature and mounted onto a stub. The samples were sputter coated with iridium metal and observed under a scanning electron microscope (SEM). Samples were imaged on FEI Magellen 400 FEGSEM.

##### **5.4.9.2. Mature biofilm**

The experiment was done as described in section 2.9.1, except the biofilm was allowed to grow for 4 days to assess the ability of the membranes to inhibit formation of a mature biofilm. The bacterial broth was changed to a fresh bacterial broth (1 in 100 diluted overnight culture) after every 24 hours to ensure there is enough growing bacteria in contact with the membrane. After 4 days of treatment, the samples were washed with PBS 3 times and prepared for SEM imaging as described above.

## 5.5. Results and discussion

### 5.5.1. Physical properties

#### 5.5.1.1. Grammage and flux properties

**Table 1:** Properties of coated filter papers: grammage and flux measured

Base Sheet	Active layer (grammage)	Target Bi-complex content wt% (g Bi complex/g active layer)	Sample Code	Flux (LMH)
Advantec 117±4	MFC, Sprayed, 40±7	10	A-M10-S	65
	MFC, Sprayed, 33±2	5	A-M5-S	112
	MFC, Sprayed, 36±0	2.5	A-M2.5-S	290
	MFC, Sprayed, 29±4	0	A-M0-S	555
	None	No second layer	A	1275
Whatman 83±1 gsm	MFC, Sprayed, 36±1	5	W-M5-S	120
	None	No second layer	W	1298
MFC, sprayed 67±1 gsm	MFC, Sprayed, 40±5	5	M-M5-S	45
	None	No second layer	M	88
None	NFC, Filtered 86±2	10	N10-F	3.76
	NFC, Filtered 79±3	5	N5-F	3.42
	NFC, Filtered 74±1	2.5	N2.5-F	1.56
	NFC, Filtered 78±3	0	N0-F	1.30

The average coating grammage is 36 g/m<sup>2</sup>. Table 01 shows that the flux remarkably decreases when coated when compared to the uncoated filter papers. With increase in the bismuth content in the coating, the flux decreases. This could be the result of the variation in coating grammage or the bismuth complex might have increased the hydrophobicity at the surface of the coating. The flux of the NFC membranes were remarkably low, compared to the MFC coated filters. This was expected since the NFC membranes were prepared with further fibrillated nanocellulose, resulting in very low porosity material. This can be confirmed using the results from SEM imaging and the pore size analysis.

#### 5.5.1.2. SEM imaging

Figure 1 shows the surface morphology of the filters at different magnifications. The uncoated surfaces or base sheets (Figure 1 a-b) shows coarse fibres at very low magnifications. On the other

hand, the MFC coated side and the NFC membrane shows fibrillated cellulose. The NFC membranes were prepared using homogenised nanocellulose, which resulted in thinner fibres. The average fibre diameter of the unhomogenised fibres has been reported to be 70 nm and 1 pass homogenisation at 1000 bar reduces it to 30 nm [30]. Images at higher magnification (d and f) show the bismuth complex within the fibres marked by the red arrows. The complex particles are needle-like in shape, and the size and dispersibility properties have been reported in our previous work [28]. The coated side of the filter (d) shows the nanofibres are arranged in an open network resulting in interfibrous pores shown by the blue arrows. These irregularly shaped pores appear to be a few microns in size and will be further discussed in the pore analysis. This is evident in the micrograph (f), showing a more compact and visibly non-porous structure.

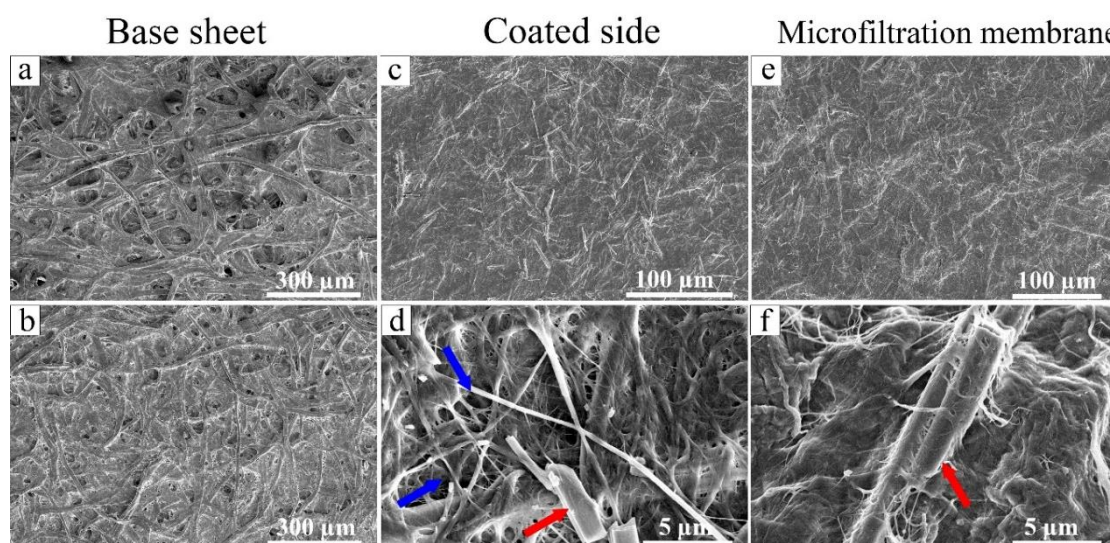


**Figure 1:** SEM image of the base sheets Advantec (a) and Whatman (b), the 5 wt% Bi-complex loaded coated side on Advantec (A-M5-S) (c-d) and the 5 wt% Bi-loaded NFC membranes (N5-F) (e-f) at two different magnifications

### 5.5.2. Pore properties

To further study the pore size of the filters, mercury porosimetry was carried out. Figure 2 shows the pore size distribution of the MFC coated filters (green lines) and NFC membranes (blue lines). The coated filters (A-M5-S and A-M0-S) shows a broad log differential intrusion peak in the range of 40 to 4000 nm, which lies in the size range of *S. aureus* bacteria (red highlighted area). This results in the high flux and bacterial permeability of these filters. On the other hand, the NFC membranes (N0-F and N5-F) showed narrow sharp peaks between 0-20 nm and no significant pores in the larger size range. This, along with the SEM images, explains the low porosity and total intrusion volume of the NFC membranes compared to the coating layer, as shown in Table 2. The large porosity of A-M5-S and A-M0-S compared to N5-F and N0-F can be partly attributed

to the use of a spraying method for sheet preparation also, while the vacuum filtration created a more packed structure and less porosity in the membranes.

The addition of the Bi-complex has an opposite effect on pore size for the MFC coated filters and the NFC membranes. The addition of the bismuth complex resulted in lower porosity in the NFC membranes. In the MFC coated filters, although the modal pore size range is the same, the addition of the bismuth complex in the coating layer shows larger numbers of the pores and thus higher porosity compared to the blank nanocellulose coating layer. This could be due to the preparation method. The NFC membranes were prepared using vacuum filtration followed by pressing, which could have potentially forced the bismuth complex to fill in the pores within the nanocellulose network as opposed to spraying followed by evaporative drying in the coating layer. The spraying process is done at 2 wt%, compared to the 0.2 wt% used in filtration. The higher solids content produces a more flocculated structure with larger pores between the flocs.

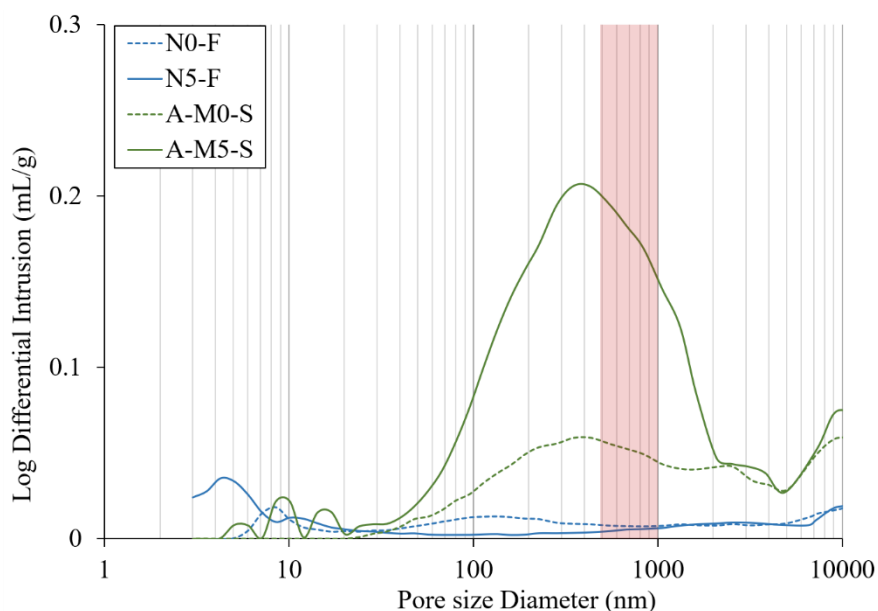


**Figure 2:** Pore size distribution of the blank and 5 wt% Bi-loaded NFC membranes (N0-F and N5-F) and coating (A-M0-S and A-M5-S). The highlighted area shows the size range of *S. aureus* bacteria.

Brunauer–Emmett–Teller (BET) specific surface area of N5-F and A-M5-S are 66 % and 70 % higher than samples N0-F and A-M0-S, respectively. The higher specific surface area in these bismuth complex loaded filters compared to the blank ones can be explained by the added surface from the complex particles.

**Table 2:** Pore properties of the MFC coated filters and NFC membranes

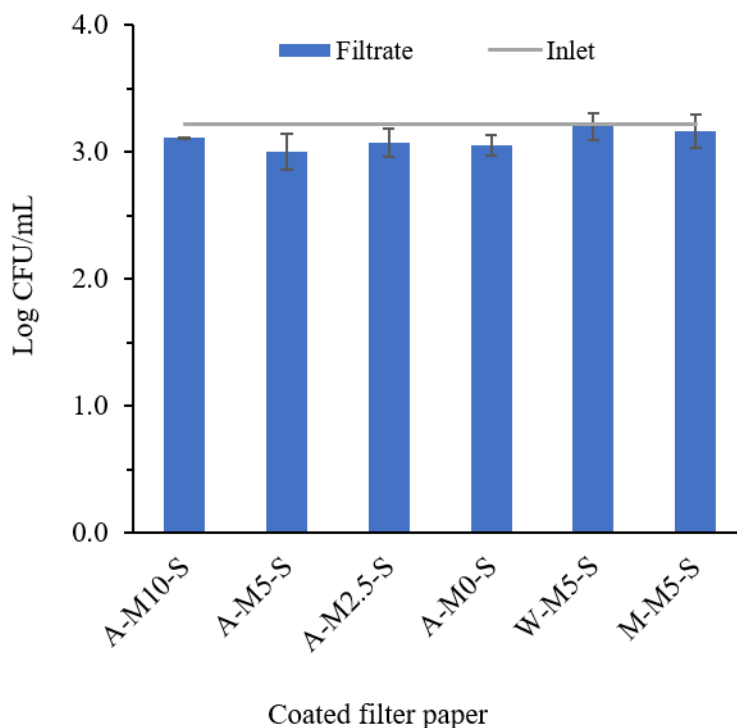
Sample	BET Surface area (m <sup>2</sup> /g)	Total intrusion volume (mL/g)	Porosity (%) (Mercury porosimetry)
N0-F	0.28	0.5468	4.07
N5-F	0.83	0.3528	2.67
A-M0-S	0.44	1.2407	17.25
A-M5-S	1.47	1.2410	25.8

### 5.5.3. Antibacterial performance

Various research has proposed antibacterial filter paper designs, but the antibacterial effectiveness has not been analysed by filtration in most studies and have been limited to disk diffusion [3]. The antibacterial activity of the MFC coated filters and NFC membranes was studied by filtering a bacterial broth, simulating contaminated water containing approximately 10<sup>3</sup> CFU/ml of *S. aureus* bacteria. The MFC coated filters have high flux and so was tested using gravity filtration. On the other hand, NFC membranes were tested using a pressure-driven microfiltration system.

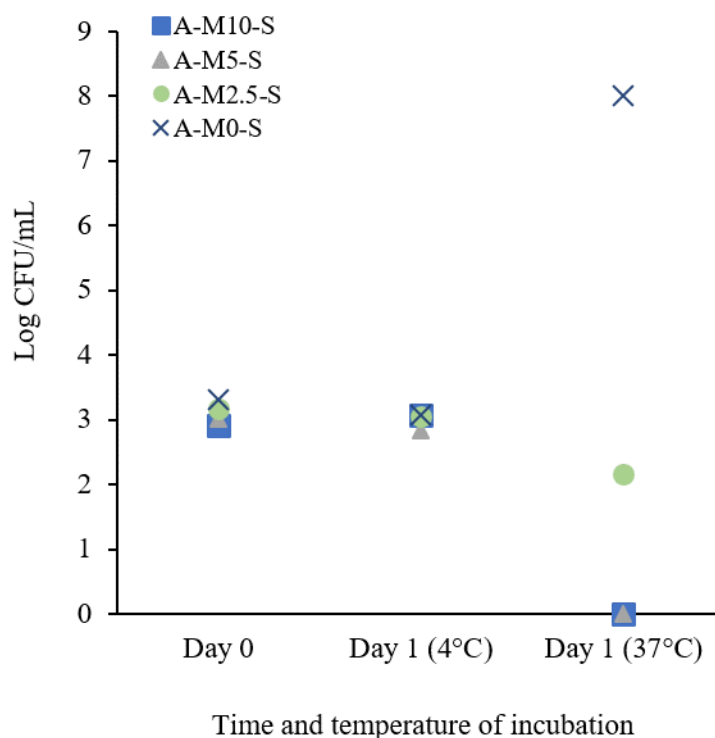
#### 5.5.3.1. Bacterial filtration: MFC Coated Filters

Figure 3 shows there is no observable effect on the bacterial count after passing through the MFC coated filter, irrespective of the Bi-loading in the coating. Thus, the loading of the complex in the coating does not affect the bacteria. This contradicts with other trends reported previously for silver- [9] and copper- [5] nanoparticle based filters by filtration techniques, where a higher loading resulted in more reduction of the bacteria immediately. It can also be observed that changing the base sheet also does not seem to facilitate the bacterial reduction. The purpose of this experiment was to understand if the bacteria could be rapidly inactivated as it passed through the Bi-coated filter. It is evident that there is no instantaneous killing effect of the bismuth coated filters on the bacterial population.



**Figure 3:** Logarithmic bacterial colony count of *S. aureus* in the filtrate after passing through the composite filters (error bars show standard deviations, n=3)

However, when the coated side of the filter was wetted with *S. aureus* bacterial suspension and placed in contact with an agar plate, the bismuth-coated filters showed inhibition of bacterial growth as shown in Figure S1. The bacteria in the Bi-coated filters did not show any growth (Figures S1a, S1b, and S1d), whereas the ones with no Bi-complex produced a lawn (Figure S1c and S1e). This demonstrates that the filters provide antibacterial activity. MFC sheets loaded with the same bismuth complex have been previously shown to be antibacterial against *S. aureus* [28]. Thus, although there is evidence to suggest the Bi-MFC coated filters exhibit antimicrobial activity, the effect does not appear to be instantaneous contact-killing and hence does not show an immediate effect upon filtration. The filtration residence time was not sufficient for the bisphosphinato bismuth (III) complex to demonstrate bactericidal activity against *S. aureus*. Therefore, the filtrate from the Advantec coated filters (A-M0-S, A-M2.5-S, A-M5-S, A-M10-S) were stored for 24 hours and analysed again to understand its potential for stored water purification. The result for storage temperatures of 4 °C and 37 °C are shown in Figure 4.



**Figure 4:** Logarithmic bacterial colony count of *S. aureus* in the filtrate after passing through the composite filters with Advantec at different loadings in different storage conditions showing the reduction in bacterial growth when stored at 37 °C for 24 hours

Filtered samples stored at 4 °C did not show any significant bacterial reduction between day 0 and day 1. However, after storing at 37 °C, 100 % bacterial reduction was observed for the filtrates from A-M10-S and A-M5-S filters (10 wt% and 5 wt% Bi-complex coated on Advantec filter). In addition, a 1 log reduction in bacterial count was observed for the filtrate from A-M2.5-S filter (2.5 wt% Bi-complex coated on Advantec filter). With sample A-M0-S (bismuth complex is absent in the coating), bacterial growth was observed with the formation of a bacterial lawn. Representative plates are shown in Figure S2. Hence, we can conclude the antibacterial action of the Bi-loaded coatings, against *S. aureus*, to be time and temperature dependent.

We wanted to understand if leached bismuth complex was causing the reduction in bacteria upon leaving the filtrate standing over 24 hours. The filtrate was centrifuged at 14,000 rpm for 30 minutes and the supernatant discarded. This would remove any bismuth complex that might have leached out of the filter coating and was present in the filtrate in soluble form. The cell pellet was then resuspended in fresh nutrient media and grown overnight. It was found that the bacteria grew into a lawn. This supports that the time-dependent killing observed here is due to the dissolved bismuth complex in the filtrate leached out of the filter paper. These results have been summarised in Figure 5 (a).

### 5.5.3.2. Bacterial filtration: NFC membranes

Pressure-driven microfiltration of a bacterial suspension through the NFC membranes demonstrated that the filtrate is free of bacteria. There were no bacterial colonies formed when the filtrate was plated onto agar plates for the blank NFC membranes (N0-F) and those loaded with the bismuth complex (N2.5-F, N5-F and N10-F). Thus, these membranes were able to exclude the entire bacterial population from the filtrate with all bacterial cells being trapped in the pores of the nanocellulose membrane. An illustration of the experiment along with a representative plate displaying no bacterial growth in the filtrate is shown in the Figure 5(b).

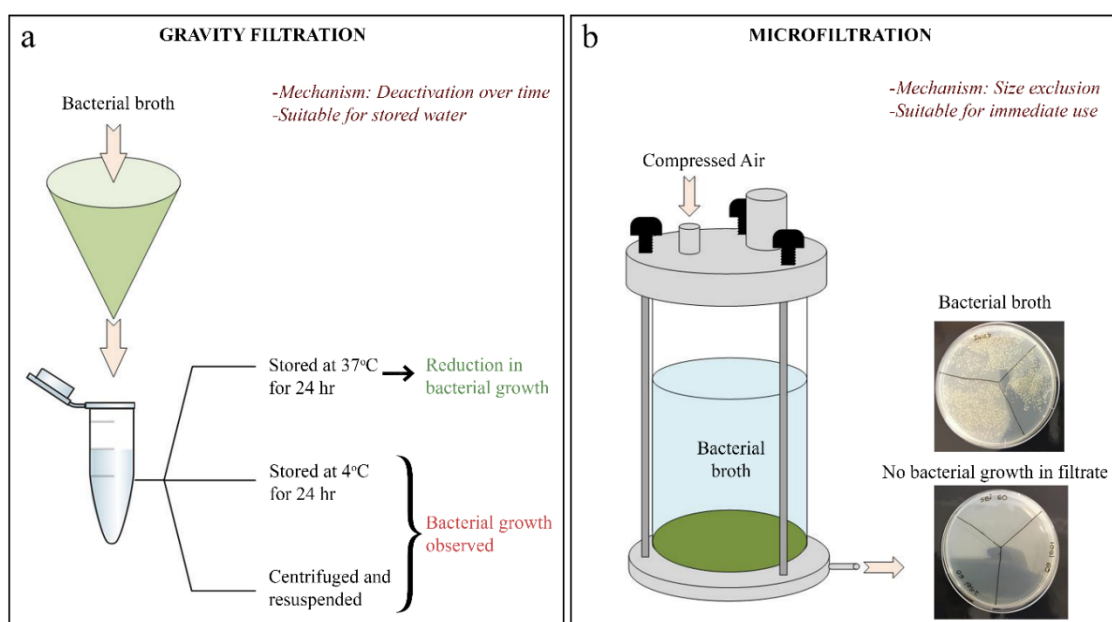


**Figure 5:** Schematic presentation of the filtration set up for the MFC coated filter papers and for the NFC microfiltration membranes. The results from the gravity filtration test using Bi-MFC coated filter papers, with antibacterial activity observed for stored water at 37 °C (a), Microfiltration setup with a representative plate showing colony count of *S. aureus* in the inlet liquid and the filtrates after passing through the NFC membranes with no bacterial presence (b).

*Staphylococci* are round-shaped bacteria with sizes ranging from 0.5 to 1.5  $\mu\text{m}$ , with *S. aureus* strain reported to be up to 1  $\mu\text{m}$  [32]. It is evident that the small bacteria can pass through the pores of the MFC coated filters. However, the NFC membranes were able to exclude the bacteria from the filtrate. This is a result of two effects. Firstly, homogenisation of MFC to NFC reduces the fibre diameter. The thinner fibres form more hydrogen bonds creating smaller pores, lower porosity and flux and thereby resulting in successful trapping of bacteria. Secondly, the spraying process produces a more open structure for the same material resulting in passing of bacteria through it. So, both the homogenisation and the method of sheet preparation has an effect on the

filtration properties and is more clearly understood in Figure S3. It shows that sheets made with unhomogenised fibres by either vacuum filtration (M0-F) or spraying (M0-S) do not trap the bacteria. Moreover, a fibrillated NFC sheet made by spraying (N0-S) is also not able to trap the bacteria.

#### 5.5.4. Bismuth complex leaching

It is important to understand the release behaviour of the biocide from the coating to assess the long-term effectiveness of the system as well as to analyse the suitability of the filtrate for safe consumption. Table 03 shows the bismuth complex content in the filtrate leached from the MFC coated filters and NFC membranes.

**Table 3:** Bismuth complex concentration in the filtrate from the MFC coated Advantec filter paper and the NFC membranes.

Bi- complex loading (wt%)	Bi-complex Concentration (ppb) (Mean $\pm$ St. dev)	
	MFC Coated filters	NFC membranes
10	23.5 $\pm$ 8.0	805.7 $\pm$ 41.1
5	33.7 $\pm$ 4.3	535.1 $\pm$ 37.9
2.5	38.6 $\pm$ 5.1	130.6 $\pm$ 1.9

It was found that bismuth is present in the filtrate after filtering water through both the MFC coated filters and the NFC membranes. This is due to the fibrous nature of the coating, where the fibre bundles swell exposing the bismuth complex to dissolve into the filtrate. The MFC coated filters allow significantly lower levels of leaching compared to the microfiltration membranes. The NFC membranes have very low flux, which provides a higher time in contact, thereby allowing more bismuth to leach out when filtering. The presence of the bismuth complex in the filtrate from the NFC membranes also means that it can provide protection against subsequent bacterial contamination and growth. However, the concern for drinking bismuth-containing water still remains.

Silver containing filters have been reported to release about 48 ppb of Ag NP and 1.8 ppm of Ag ions with a single pass of 100 mL water [9]. Papers with copper as antibacterial agents demonstrated washing out of about 200 ppb after passing through 250 mL of water. The leached out copper concentration ranged from 600 ppb to 100 ppb in the filtrate when the water volume was varied between 100 mL to 2 L [5]. These are well below the limits set by WHO/EPA to be safe for drinking water. The safe drinking standard of bismuth based compounds has not yet been

established. The complex was reported to have no toxicity to mammalian COS7 cells upto 500 ppb as solid powders [23]. Hence a study on the cytotoxicity of the filtrate on mammalian cells was performed and the results discussed in section 3.7.

The amount of biocidal additive in the membrane influences the longevity of the antibacterial membrane. The migration of the biocide to kill the bacteria is important, which also comes with the drawback of the leaching of the biocide into water [33]. So, the amount of Bi-complex retained in the membrane after filtering water (250 mL) through it was analysed and shown in Figure S4. Known mass of used and fresh (unused) membrane were ashed in a muffle furnace at 600°C and then dissolved in concentrated nitric acid. This was analysed using a Perkin-Elmer Avio 200 ICP-OES (inductively coupled plasma-optical emission spectroscopy).

The actual bismuth content in the used membranes were not found to be significantly lower than the fresh/unused membranes, which is in line with the very small amount of bismuth in the filtrate. For the 10 wt% Bi-loaded NFC membrane, the used membrane showed some decrease in the bismuth content but this can be accounted for by the larger error bar. Hence the loss in bismuth content following filtration treatment was found to be negligible. The Bi-retention in the membrane can provide an indication of how long the membrane will effectively retain its antifouling properties.

#### **5.5.5. Cytotoxicity of filtrate**

The safety of the filtrates was tested by *in-vitro* cytotoxicity analysis using the murine fibroblast cell line. Figure 6 reveals that the viability of the cells is greater than 70% when in direct contact with the filtrate at or below concentration of 200 ppb of the bismuth complex for 24 hours and thus it demonstrates that the filtrate does not show any significant toxicity according to the standard ISO 10993-5. Due to the very low solubility of the complex in water, higher concentrations could not be tested. From the release behaviour studies, it can be seen that the coated filter have prominently low bismuth complex leached in the filtrate. With the NFC microfiltration membranes, the 2.5 wt% Bi-loaded filters show bismuth complex concentration within the tested range herein and can be suggested to be safe. Hence the anti-biofilm properties of this membrane have been assessed to determine the overall suitability. If the 2.5 wt% Bi-loaded NFC microfiltration membrane works efficiently in inhibiting biofilm formation, it has good potential for future development.

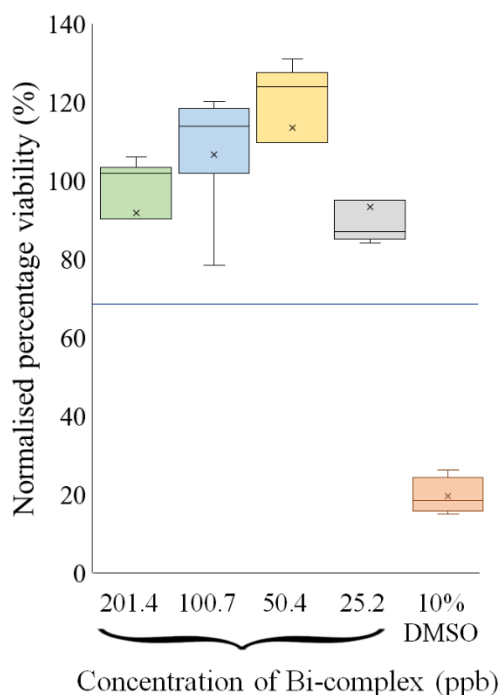


**Figure 6:** Cytotoxicity of the filtrates at different concentrations of the bismuth complex on murine fibroblast cell line expressed as a percentage of the negative control (DMEM media only, no treatment). The culture medium was diluted with the filtrate from 10 wt% Bi-loaded NFC membranes to achieve these concentrations. Culture medium containing 10% DMSO is the positive control, showing high level of toxicity. The box plot shows the interquartile range, the marker ‘×’ represents the mean and the line represents the median and the whiskers presents the range of data from independent biological replicates. The horizontal blue line shows the limit for cytotoxic material according to ISO 10993-5 (< 70%).

## 5.5.6. Anti-biofilm properties of the membrane

### 5.5.6.1. Initial Attachment of bacteria

Bacterial removal was achieved by controlling the pore size in the membranes and removing the bacteria from the filtration by size exclusion. However, fouling remains a major limitation to such filtration based systems. Different types of fouling can occur, which includes blockage of the filtration area by various size of suspended molecules and proteins and by biofouling [34]. Biofouling involves the formation of bacterial biofilm as the bacteria keeps on growing and accumulating on the membrane [33, 35]. Biofouling affects the performance of the filters by reducing the permeate flux, separation efficiency and membrane longevity [33]. The membranes can be modified to reduce the chances of biofilm formation by either preventing the attachment of bacteria to the surface or by introducing antimicrobial functionalities to the filter system [33]. Here the purpose of the bismuth complex in the NFC microfiltration membranes was to provide

the anti-biofilm properties. The results in Figure 7 illustrates that there is bacterial cells attached on the surface of the blank NFC membrane (N0-F), whereas the 2.5 wt% Bi-complex loaded one (N2.5-F) showed reduced bacterial growth on its surface.

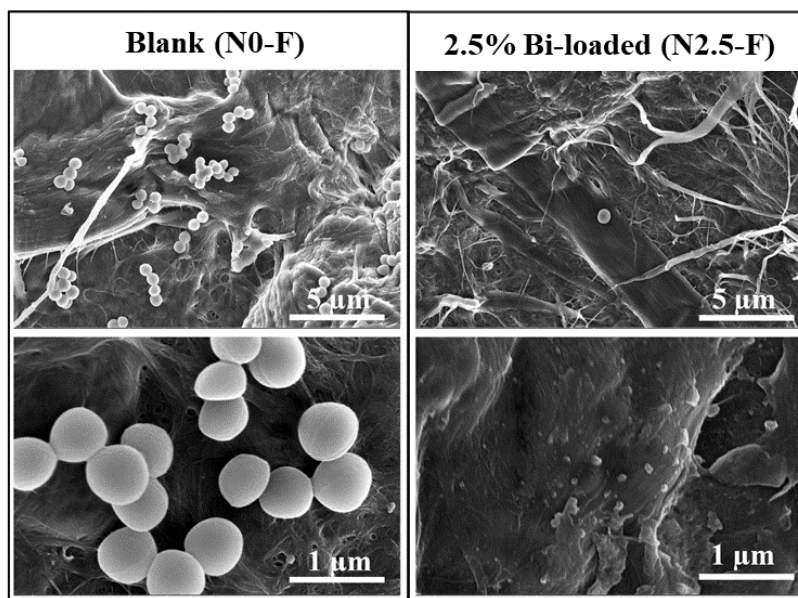


**Figure 7:** SEM image bacterial attachment on the blank NFC membrane or N0-F (left) and the 2.5 wt% Bi-loaded NFC membrane or N2.5-F (right) after 24 hours of contact showing lesser attachment on the Bi-loaded membrane.

#### 5.5.6.2. Mature biofilm

Figure 8 shows the surface of the NFC membranes after being in contact with a growing culture of *S. aureus* for 4 days for the N0-F and N2.5-F. It is very clear that the bacterial attachment and biofilm formation on the 2.5 wt% Bi-loaded membrane (N2.5-F) is significantly different to the blank NFC membrane (N0-F). There is a large number of bacterial cells on the surface of N0-F. In contrast, only a few cells could be observed on the surface of the N2.5-F membrane. Moreover, the cells on the N0-F surface look adherent to the surface rather than a loose attachment like in the N2.5-F surface. In addition, it is very clear that these large clusters of cells on N0-F are surrounded by extracellular polymeric substances (EPS) which are produced by these cells to form an established biofilm. No such film is seen with the N2.5-F surface. Hence, it is very evident that with 2.5 wt% Bi-complex loading, the bacterial attachment is significantly lower and the chance of biofilm formation is reduced over a period of 4 days in contact with growing bacterial culture.

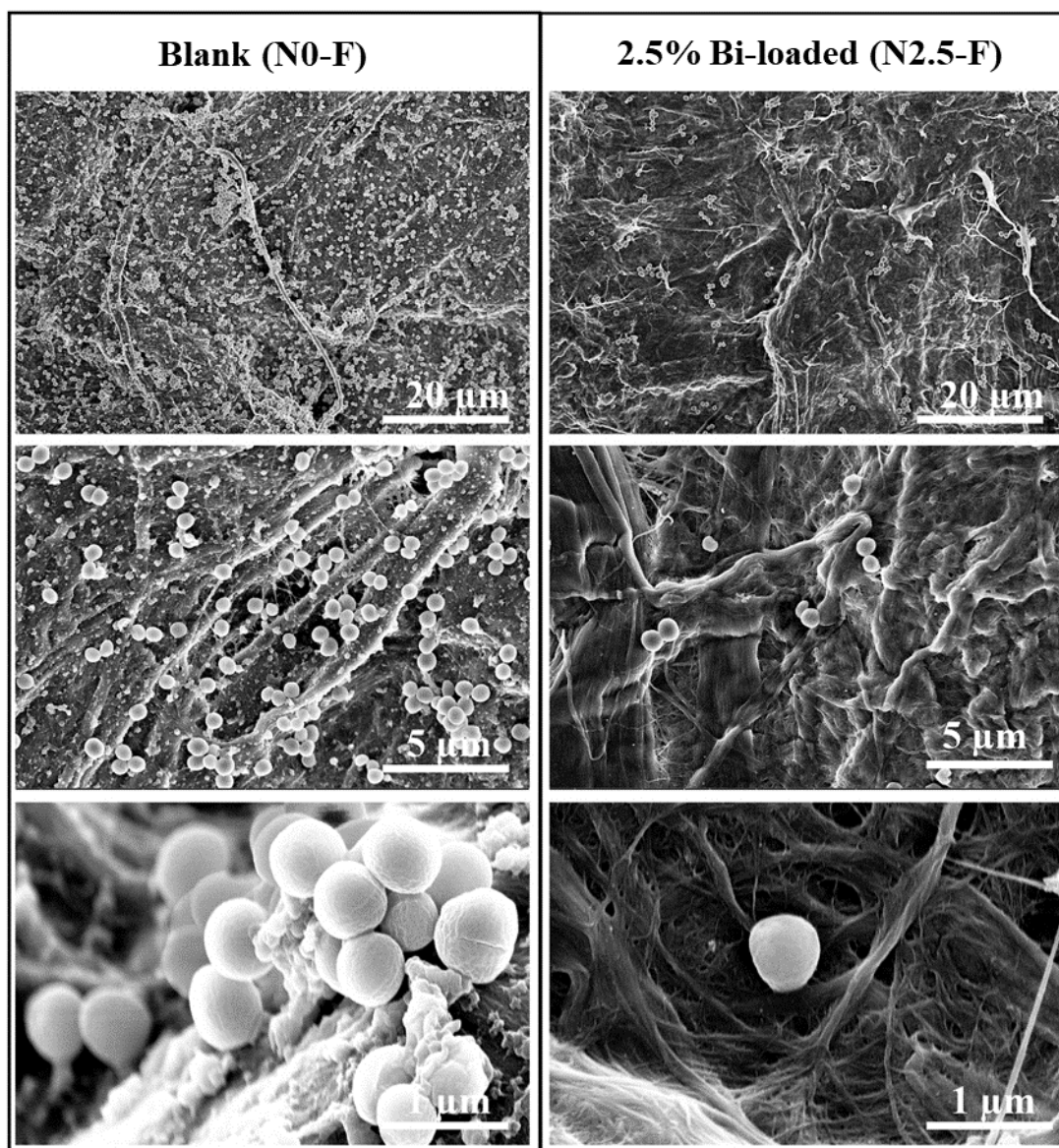


**Figure 8:** SEM image bacterial attachment on the blank NFC membrane or N0-F (left) and the 2.5 wt% Bi-loaded NFC membrane or N2.5-F (right) after 4 days of contact showing lesser attachment on the Bi-loaded NFC membrane but a mature biofilm formation on the blank NFC membrane.

## 5.6. Conclusion

Two approaches toward the development of cheap and renewable filters for point-of-use drinking water purification have been studied. Three different types of base substrates were studied for this purpose, and MFC-bismuth complex coating was made as the active layer. The results showed that there is no instantaneous antibacterial activity irrespective of the Bi-loading or base substrate. However, when the filtrate was left to rest over time, there was a drastic reduction in bacterial count. This reduction was observed to be temperature dependant, with antibacterial effectiveness

at 37 °C and not at 4 °C, and dose-dependent with larger reduction after passing through higher loading coated filters. This is due to the ppb levels of the Bi-complex leaching out into the filtrate. On the other hand, NFC membranes showed complete removal of bacteria. These filters show anti-biofilm properties when loaded with the Bi-complex even at 2.5 wt%. Thus, the results overall suggest that the coated filters can be a useful technique to disinfect stored water and can be operated by simple gravity filtration. This can be useful in developing countries in tropical region where the temperature is warm. The NFC membranes can be used for immediate use, with the limitation being requirement of a pressurised filtration system. The paper provides the proof-of-concept of two different approaches for drinking water purification for applications in different scenarios. These MFC coated filters with *bis*-phosphinato bismuth (III) complex can be a promising approach to develop a cheap and easy-to-use water purification system for storage water rather than immediate use. However, the second approach depending on the size exclusion principle can serve as an immediate drinking water purification technique. Future studies on optimising the filter design could include reducing the filtration layer thickness to increase the flux of the NFC membranes along with providing the barrier. Moreover, studies with larger volumes of water is necessary to understand its robustness over large filtration volumes and over multiple filtrations. Feasibility of large scale production of the membrane by vacuum filtration also needs to be considered. This study provides the basis for future filter paper design using nanocellulose-bismuth phosphinato composites.

### 5.7. Acknowledgement

This work was supported by The National Health and Medical Research Council (APP1139844). The authors would like to acknowledge the use of the facilities at the Monash Centre for Electron Microscopy and the Monash Institute of Medical Engineering. Maisha Maliha also wish to acknowledge the Australian Government for the Research Training Program (RTP) Scholarship.

### 5.8. Reference

1. *Drinking Water*. World Health Organization, Geneva 2019 [cited 2019 8 July 2019]; Available from: <https://www.who.int/en/news-room/fact-sheets/detail/drinking-water>.
2. *Water for life : making it happen*, in *WHO/UNICEF Joint Monitoring Programme 2005*. 2005, World Health Organization, Geneva.
3. Jain, S., et al., *Enhanced antibacterial profile of nanoparticle impregnated cellulose foam filter paper for drinking water filtration*. *Carbohydrate Polymers*, 2018. **202**: p. 219-226.
4. Thompson, T., et al., *Chemical safety of drinking-water: Assessing priorities for risk management*, in *World Heath Organization, Geneva*. 2007.

5. Dankovich, T.A. and J.A. Smith, *Incorporation of copper nanoparticles into paper for point-of-use water purification*. Water Research, 2014. **63**: p. 245-251.
6. Praveena, S. and A. Aris, *Application of Low-Cost Materials Coated with Silver Nanoparticle as Water Filter in Escherichia coli Removal*. Water Quality, Exposure and Health, 2015. **7**(4): p. 617-625.
7. Xu, Q., et al., *A facile route to prepare cellulose-based films*. Carbohydrate Polymers, 2016. **149**: p. 274-281.
8. O'Sullivan, A.C., *Cellulose: the structure slowly unravels*. Cellulose, 1997. **4**(3): p. 173-207.
9. Dankovich, T.A. and D.G. Gray, *Bactericidal paper impregnated with silver nanoparticles for point-of-use water treatment*. Environ Sci Technol, 2011. **45**(5): p. 1992-8.
10. Fernández, J.G., et al., *Development of nitrocellulose membrane filters impregnated with different biosynthesized silver nanoparticles applied to water purification*. Talanta, 2016. **146**: p. 237-243.
11. Praveena, S., K. Karuppiyah, and L. Than, *Potential of cellulose paper coated with silver nanoparticles: a benign option for emergency drinking water filter*. Cellulose, 2018. **25**(4): p. 2647-2658.
12. Reza, I., et al., *Production of antibacterial filter paper from wood cellulose*. BioResources, 2011. **6**(1): p. 891-900.
13. Huang, J., et al., *Performance of ceramic disk filter coated with nano ZnO for removing Escherichia coli from water in small rural and remote communities of developing regions.(Report)*. Environmental Pollution, 2018. **238**: p. 52.
14. *Silver as a drinking-water disinfectant*, in *Alternative drinking-water disinfectants: bromine, iodine and silver*. 2018, World Health Organization, Geneva.
15. Qu, X., P.J.J. Alvarez, and Q. Li, *Applications of nanotechnology in water and wastewater treatment*. Water research, 2013. **47**(12): p. 3931.
16. Maillard, J.-Y. and P. Hartemann, *Silver as an antimicrobial: facts and gaps in knowledge*. Critical Reviews in Microbiology, 2013. **39**(4): p. 373-383.
17. Silver, S., *Bacterial silver resistance: molecular biology and uses and misuses of silver compounds*. FEMS Microbiology Reviews, 2003. **27**(2): p. 341-353.
18. Gunawan, C., et al., *Widespread and Indiscriminate Nanosilver Use: Genuine Potential for Microbial Resistance*. ACS nano, 2017. **11**(4): p. 3438.
19. Pal, C., et al., *BacMet: antibacterial biocide and metal resistance genes database*. Nucleic acids research, 2014. **42**(Database issue): p. D737.

20. Briand, G.G. and N. Burford, *Bismuth Compounds and Preparations with Biological or Medicinal Relevance*. Chemical Reviews, 1999. **99**(9): p. 2601-2658.
21. Barry, N.P.E. and P.J. Sadler, *Exploration of the medical periodic table: towards new targets*. Chem. Commun., 2013. **49**(45): p. 5106-5131.
22. Suzuki, H. and Y. Matano, *Chapter 1 - Introduction*, in *Organobismuth Chemistry*, Y. Matano, Editor. 2001, Elsevier Science: Amsterdam. p. 1-20.
23. Werrett, M., et al., *Bismuth Phosphinates in Bi-Nanocellulose Composites and their Efficacy towards Multi-Drug Resistant Bacteria*. Chemistry- A European Journal, 2018.
24. Luqman, A., et al., *The Importance of Heterolepticity in Improving the Antibacterial Activity of Bismuth(III) Thiolates*. European Journal of Inorganic Chemistry, 2016. **2016**(17): p. 2738-2749.
25. Svoboda, T., et al., *NCN Chelated Organoantimony(III) and Organobismuth(III) Phosphinates and Phosphites: Synthesis, Structure and Reactivity*. European Journal of Inorganic Chemistry, 2010. **2010**(33): p. 5222-5230.
26. Kotani, T., et al., *Antibacterial Properties of Some Cyclic Organobismuth(III) Compounds*. Antimicrobial Agents and Chemotherapy, 2005. **49**(7): p. 2729.
27. Domenico, P., et al., *Activities of Bismuth Thiols against Staphylococci and Staphylococcal Biofilms*. Antimicrobial Agents and Chemotherapy, 2001. **45**(5): p. 1417.
28. Maliha, M., et al., *Bismuth phosphinate incorporated nanocellulose sheets with antimicrobial and barrier properties for packaging applications*. Journal of Cleaner Production, 2019. **246**.
29. Varanasi, S., R. He, and W. Batchelor, *Estimation of cellulose nanofibre aspect ratio from measurements of fibre suspension gel point*. Cellulose, 2013. **20**(4): p. 1885-1896.
30. Raj, P., et al., *Gel point as a measure of cellulose nanofibre quality and feedstock development with mechanical energy*. Cellulose (London), 2016. **23**(5): p. 3051-3064.
31. Shanmugam, K., et al., *Rapid preparation of smooth nanocellulose films using spray coating*. Cellulose, 2017. **24**(7): p. 2669.
32. Harris, L.G., S.J. Foster, and R.G. Richards, *An introduction to Staphylococcus aureus, and techniques for identifying and quantifying S. aureus adhesins in relation to adhesion to biomaterials: review*. European cells & materials, 2002. **4**: p. 39.
33. Mansouri, J., S. Harrisson, and V. Chen, *Strategies for controlling biofouling in membrane filtration systems: challenges and opportunities*. Journal of Materials Chemistry, 2010. **20**(22).
34. Cui, Z.F., Y. Jiang, and R.W. Field, *Fundamentals of Pressure-Driven Membrane Separation Processes*, in *Membrane Technology*. 2010. p. 1-18.

35. Li, Q., et al., *Antimicrobial nanomaterials for water disinfection and microbial control: potential applications and implications*. *Water Res*, 2008. **42**(18): p. 4591-602.

THIS PAGE HAS BEEN INTENTIONALLY LEFT BLANK

---

---

# **CHAPTER 6**

## **CONCLUSION**

---

---

THIS PAGE HAS BEEN INTENTIONALLY LEFT BLANK

**CHAPTER 6: CONCLUSION AND PERSPECTIVE**

**6.1. Conclusion .....198**

6.1.1. Potential of *bis*-phosphinato bismuth complex in nanocellulose materials for specific applications.....199

6.1.1.1. Active Packaging application.....199

6.1.1.2. Wound hydrogel.....200

6.1.1.3. Water purification .....200

6.1.2. Behaviour of the complex in nanocellulose materials .....201

**6.2. Perspectives .....202**

THIS PAGE HAS BEEN INTENTIONALLY LEFT BLANK

## **6.1. Conclusion**

The main goal of this doctoral thesis is to understand the utility of diphenyl *bis*-phosphinato bismuth (III) complex in nanocellulose antimicrobial materials from an engineering perspective. This was achieved by developing and characterising bismuth complex loaded nanocellulose composites and hydrogels for three different applications. This led us to understand the physico-chemical and biological behaviour of the complex in the nanocellulose matrix and the potential of using it for active packaging materials, wound dressings and water purification.

### **6.1.1. Potential of *bis*-phosphinato bismuth complex in nanocellulose materials for specific applications**

#### **6.1.1.1. Active Packaging application**

Active packaging materials containing antimicrobial agents protects the packaged product from contamination and can extend shelf life. While active packaging materials are common in recent times, the widespread use of silver and petroleum based plastic materials for this application remains an issue. Hence the potential of the *bis*-phosphinato bismuth complex-nanocellulose composites has been explored in Chapter 2 and Chapter 3. For these materials, the bismuth complex was active against bacteria as well as fungi. The commonly found lignocellulosic sources from pulp and paper mills were studied and bleached Kraft pulp (chemically treated pulp) was the most suitable. It has been shown herein that the chemical composition and the composite preparation technique both played a major role for active packaging. The leaching behaviour of the complex from the composite significantly influenced the efficacy of the composite against bacteria and fungi. Leaching was dependent on the hydrophilicity of the matrix and the interaction of the matrix phase with the dispersed phase. The barrier performance and mechanical properties were slightly lowered by the presence of the bismuth complex when the composites were prepared by spraying technique, but still remained satisfactory for use as a packaging material. Preparation using vacuum filtration improved these properties with addition of the bismuth complex. However, this technique is rather a slow process and is difficult to scale up in comparison with spraying, which is a continuous process well suited for large scale sheet production. The composites produced satisfactory properties to be used as a packaging material, however if required the barrier and mechanical properties could be improved by use of other additives.

### 6.1.1.2. Wound hydrogel

Wound infection control is very important and the potential of the *bis*-phosphinato bismuth complex for wound care applications has been studied. The complex does not interfere with the gelation of the hydrogel. The selective toxicity of the bismuth complex towards Gram-negative bacteria over Gram-positive ones was a major finding. This means that the complex is more active on the group of wound pathogens which has fewer treatment options available and hence can serve as a promising antibacterial agent for various medical applications. This dissertation explored the *in-vitro* cytotoxicity of different concentrations of the bismuth complex towards mammalian cells. At high concentrations of the complex, it induces reduced viability of the mammalian cells. This thesis showed that there was an optimised loading of *bis*-phosphinato bismuth complex loaded nanocellulose hydrogel to make it antimicrobial, while minimising toxicity to mammalian cells. This is a very early stage research and needs extensive *in-vivo* studies and clinical research for evaluating its commercial potential.

### 6.1.1.3. Water purification

Antimicrobial paper-based water filters are affordable, sustainable and easy to use technology that can be used for drinking water purification. This dissertation presents the proof of concept of two approaches of water purification using the *bis*-phosphinato bismuth complex. The bismuth complex showed no instant killing of microorganisms, but reduced bacterial load upon storage at warm temperature. It can be used as a useful technique for storage water purification in developing countries in tropical regions. Moreover, the bismuth complex loaded paper can be used as bactericidal paper strips as alternatives to chlorine-based disinfection tablets. However, this needs to be explored further. Fouling of filtration systems is a major issue. The bismuth(III) complex reduces the chances of biofilm formation, even over a period of 4 days of contact with a growing culture of bacteria. This opens up opportunities not only for drinking water filtration, but also in various other situations like industrial filtration operations, waste water treatment etc. where biofouling is a major drawback. Nanofibrillated cellulose-bismuth complex composites produced by vacuum filtration have small enough pores to trap the bacteria and thereby produce clean bacteria-free drinking water. However, the flux for this was found to be quite low. Future studies to improve the flux is required for translation into practical use and could include multilayered filter structure with a high-flux major filter media alongside a thin layer containing the bismuth complex. The pressurised dead end cell used in this thesis operates in a batch process. So, there is still a gap in understanding how much volume of water each filter can purify, the filter replacement frequency required or how long the filters resist biofilm formation. Future studies on a continuous system, with a constant flow of contaminated water being fed into a pressurised cell using a peristaltic pump is required to address this.

### 6.1.2. Behaviour of the complex in nanocellulose materials

The diphenyl *bis*-phosphinato bismuth (III) complex is a white amorphous solid. The complex is highly hydrophobic and exhibits very limited solubility. This led us to study the potency of this complex in fibrous materials. In spite of the very low solubility, the complex possesses antibacterial activity against a range of bacteria when inside these materials. The complex was found to leach out of the nanocellulose materials. However, it leached differently depending on the chemical and physical properties of the matrix, which can be controlled. This leachability controls the availability of the complex, which in turn governs the antibacterial efficacy. Chapter 3 gives us a good insight into the role of the matrix. It is important for the material to be developed from a non-continuous or fibrous matrix. Continuous materials, like plastic, do not allow the dissolution of the complex and hence is not a good choice as a carrier matrix. This has been studied by our research group by forming low density polyethylene (LDPE) composites containing the bismuth complex, which were found to have no antibacterial activity. However, this has not been included in the thesis for confidentiality reasons.

In chapter 5, it was shown that the complex is not only released out of the material to kill the bacteria but can also inhibit the formation of a bacterial biofilm on the surface. So, the complex not only kills planktonic bacterial cells but also prevents surface contamination and growth. Although this dissertation studied this from an engineering viewpoint for antifouling filtration system, this phenomena opens up opportunities for the complex to be used on other applications as well like surfaces in hospitals, or medical files and folders. This along with the toxicity studies from both chapter 4 and chapter 5 also shows prospects for using it as a surface coating on medical devices like catheters. However, careful investigation needs to be performed before doing so. While previous studies have reported the complex to be safe at 0.5 mg/mL (500ppm) to mammalian cells by *in-vitro* tests when tested as solid powders, the results presented in this thesis communicated a different behaviour. The safe level is significantly lower (9ppm) when tested dispersed in a hydrogel-media mixture (studied in chapter 4). In chapter 5, the filtrates were studied where it was shown that the complex is non-toxic at or below 200 ppb when dissolved. This was the highest concentration of filtrate tested herein and higher concentrations of filtrates could not be studied due to low solubility of the complex. Both the biocompatibility and the antibacterial behaviour were not only dose dependant but also depends on its form and availability. A few other important discoveries have been made about the bismuth(III) complex in nanocellulose materials. Firstly, it did not have an instant activity against bacteria and needed time to work on them. The antibacterial activity is time dependant as well as temperature dependant. This is important information about the complex for future studies. Secondly, not only the activity of the complex against a range of bacteria has been presented, but also a concentration

time kill study has been performed. This can serve as important data for studying its potential for other therapeutic applications beyond wound dressings. The influence of the bismuth complex and other relevant parameters on the properties of the composites are summarised in Table 1.

**Table 1:** Table showing how the different preparation parameters influences the major properties of the *bis*-phosphinato bismuth complex-nanocellulose materials

Parameter	Properties							
	Antibacterial activity	Antifungal activity	Barrier properties	Mechanical properties	Leaching behaviour	Filtration performance	Anti-biofilm properties	Cytotoxicity
Presence of Bi- complex	✓	✓	✓	✓	✓	×	✓	✓
Concentration of Bi-complex	✓	✓	✓	NS	✓	×	NS	✓
Type of the pulp/ fibre	✓	NS	✓	✓	✓	✓	NS	N/A
Composite preparation technique	NS	NS	✓	✓	NS	✓	NS	N/A

✓ = influences the property

× = does not influence the property

NS = It was not studied in this thesis

N/A = not applicable

## 6.2. Perspectives

The development and characterisation of the *bis*-phosphinato bismuth complex loaded nanocellulose materials have given us a broad perception about engineering nanocellulose-based antimicrobial materials. While the major aims of this thesis were to investigate its utility for three specific applications, the knowledge established herein gives a better understanding of such materials and shows their potential in various other applications. While this dissertation provides a better understanding of the use of the *bis*-phosphinato bismuth complex in nanocellulose materials, it has also brought up some new interesting avenues that needs further investigation.

An interesting aspect which opened up in the course of this research was the difference in nanocellulose composite properties when they are prepared by vacuum filtration and spraying. Although this was not the main aim of the thesis, this revelation is fascinating and further study on the two different sheet preparation processes will be very useful. This could involve detailed study of the internal structure of the composites, particularly the micro-agglomeration of the fibres, that could result during the sheet preparation and drying stages, and the dispersion and arrangement of the additive particles within the composites prepared by vacuum filtration and spraying.

In relation to the antifouling microfiltration NFC membranes, future studies could include a continuous filtration system with larger volume of liquid, considering a wider range of bacterial strains. This would identify the capacity and effective lifetime of the filters. Moreover, further investigation to improve the flux of such microfiltration membranes is necessary. This thesis demonstrated that a time and temperature dependant purification of water was achieved after filtering through the bismuth-coated filters. Herein, the study was undertaken at temperatures of 4 °C and 37 °C at 0 and 24 hours. This study could be extended to different temperatures and shorter time durations to open up more possibilities for practical life applications.

Although the complex was known to be non-toxic to mammalian cells, this thesis demonstrated that this property is largely dependent on the availability of the complex and previous non-toxic data were due to insolubility of the complex. It is worthwhile to investigate the cytotoxicity of the complex further in clinical setting in animal models. Further investigation of the biocompatibility and antibacterial efficacy of the complex in different forms (i.e. solid, dispersed, and soluble in water and biological fluids) is necessary for commercial translation for any application.

Overall, this thesis expands the knowledge about the utility of the *bis*-phosphinato bismuth complex and showcases the great potential of these complexes in nanocellulose based antimicrobial materials. The knowledge established herein, along with some future investigations, can lead to engineering and commercialisation of bismuth-nanocellulose based sustainable antimicrobial materials.

THIS PAGE HAS BEEN INTENTIONALLY LEFT BLANK

---

---

# **APPENDIX I**

**SUPPLEMENTARY INFORMATION**

---

---

THIS PAGE HAS BEEN INTENTIONALLY LEFT BLANK

**Supplementary Information**

**Bismuth phosphinate incorporated nanocellulose sheets with antimicrobial and barrier properties for packaging applications**

Maisha Maliha<sup>1</sup>, Megan Herdman<sup>2</sup>, Rajini Brammananth<sup>3</sup>, Michael McDonald<sup>4</sup>, Ross Coppel<sup>3</sup>,  
Melissa Werrett<sup>2</sup>, Philip Andrews<sup>2</sup>, Warren Batchelor<sup>1</sup>

<sup>1</sup>*Bioresource Processing Research Institute of Australia (BioPRIA), Department of Chemical Engineering, Monash University, VIC 3800, Australia*

<sup>2</sup>*School of Chemistry, Monash University, VIC 3800, Australia*

<sup>3</sup>*Department of Microbiology, Monash University, VIC 3800, Australia*

<sup>4</sup>*Centre for Geometric Biology, School of Biological Sciences, Monash University, VIC 3800, Australia*

Table A 1: Percentage of Experimental consistency of the different loaded Bi-MFC suspensions

Target loading of bismuth complex wt. % (g bismuth complex/g cellulose)	Experimental percentage consistency of suspension $\pm$ Standard deviation (n=3)
5.0	1.964 $\pm$ 0.033
2.5	1.986 $\pm$ 0.037
1.0	1.968 $\pm$ 0.004
0.5	1.953 $\pm$ 0.009
0.1	1.940 $\pm$ 0.019
0 (Blank)	1.925 $\pm$ 0.020

Table A 2: Basis weight and thickness of the sheets and the estimated mass of suspension sprayed on each plate

Target loading of bismuth complex wt. % (g bismuth complex/g cellulose)	Basis Weight of sheet $\pm$ Standard deviation (n=3) (g/m <sup>2</sup> )	Estimated mass of suspension sprayed on each plate (g)	Average thickness of the sheet (n=27) ( $\mu$ m)
5.0	91 $\pm$ 2	213	84 $\pm$ 8
2.5	107 $\pm$ 6	250	104 $\pm$ 9
1.0	120 $\pm$ 5	281	103 $\pm$ 5
0.5	128 $\pm$ 4	303	108 $\pm$ 4
0.1	136 $\pm$ 3	320	114 $\pm$ 3
0 (Blank)	103 $\pm$ 7	243	91 $\pm$ 2

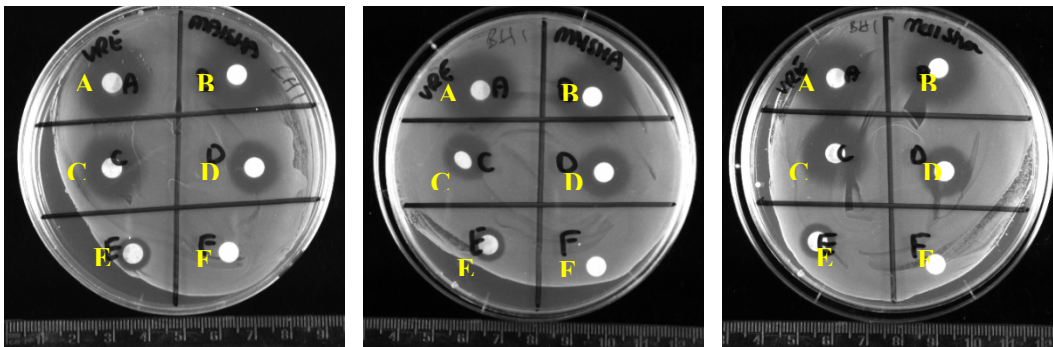


Figure A 1: Agar plate showing zone of inhibition with VRE for the differently loaded bismuth(III) phosphinato-MFC sheets- 4.37%(A), 2.10% (B), 0.94%(C), 0.39% (D), 0.07% (E) and 0% or pure MFC sheet (F)

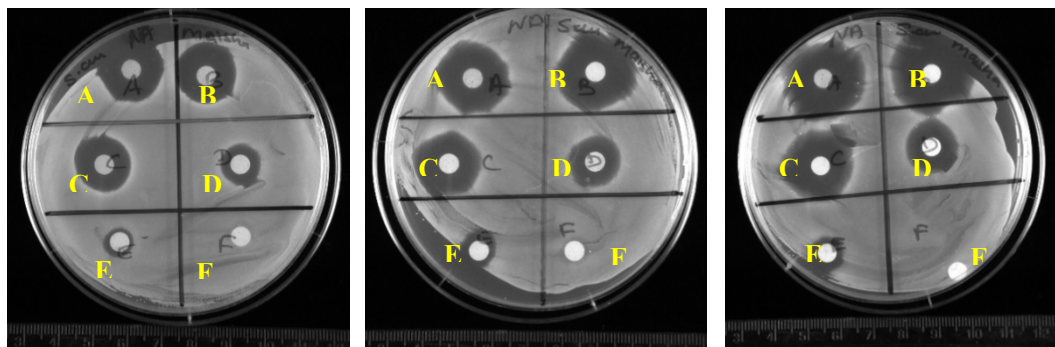


Figure A 2: Agar plate showing zone of inhibition with *S. aureus* for the differently loaded bismuth(III) phosphinato-MFC sheets- 4.37%(A), 2.10% (B), 0.94%(C), 0.39% (D), 0.07% (E) and 0% or pure MFC sheet (F)

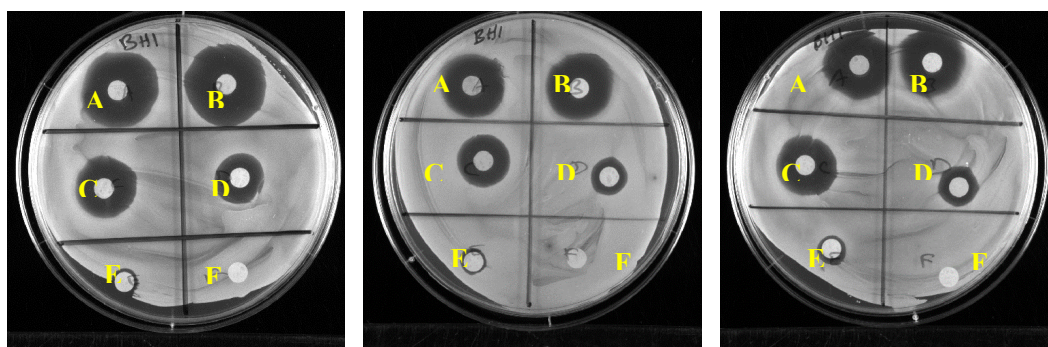


Figure A 3: Agar plate showing zone of inhibition with MRSA for the differently loaded bismuth(III) phosphinato-MFC sheets- 4.37%(A), 2.10% (B), 0.94%(C), 0.39% (D), 0.07% (E) and 0% or pure MFC sheet (F)

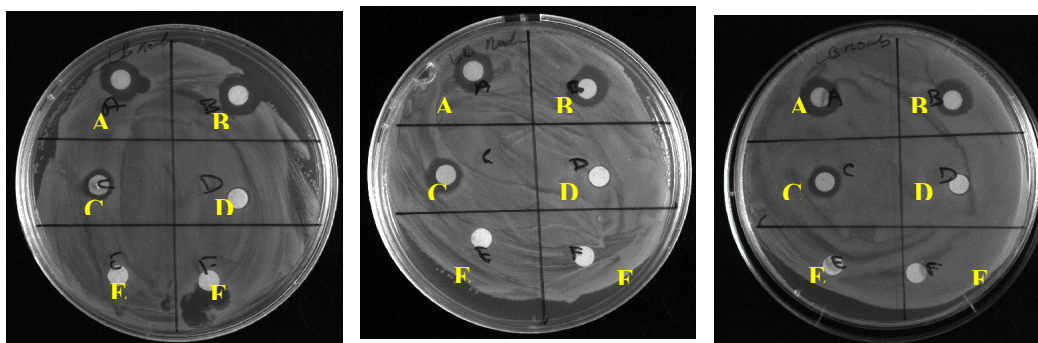


Figure A 4: Agar plate showing zone of inhibition with *E. coli* for the differently loaded bismuth(III) phosphinato-MFC sheets- 4.37%(A), 2.10% (B), 0.94%(C), 0.39% (D), 0.07% (E) and 0% or pure MFC sheet (F)

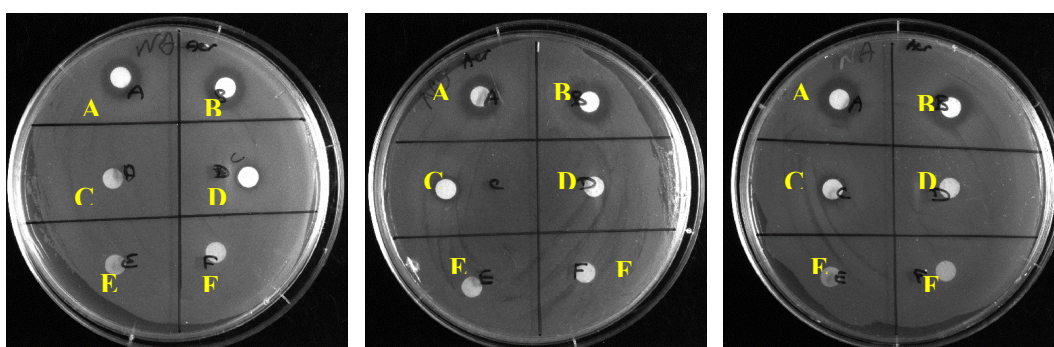


Figure A 5: Agar plate showing zone of inhibition with *P. aeruginosa* for the differently loaded bismuth(III) phosphinato-MFC sheets- 4.37%(A), 2.10% (B), 0.94%(C), 0.39% (D), 0.07% (E) and 0% or pure MFC sheet (F)



Figure A 6: Agar plate showing zone of inhibition with *C. albicans* for the differently loaded bismuth(III) phosphinato-MFC sheets- 0%(A), 0.07% (B), 0.39%(C), 0.94% (D), 2.01% (E), 4.37% (F) and 10.53 % (G)

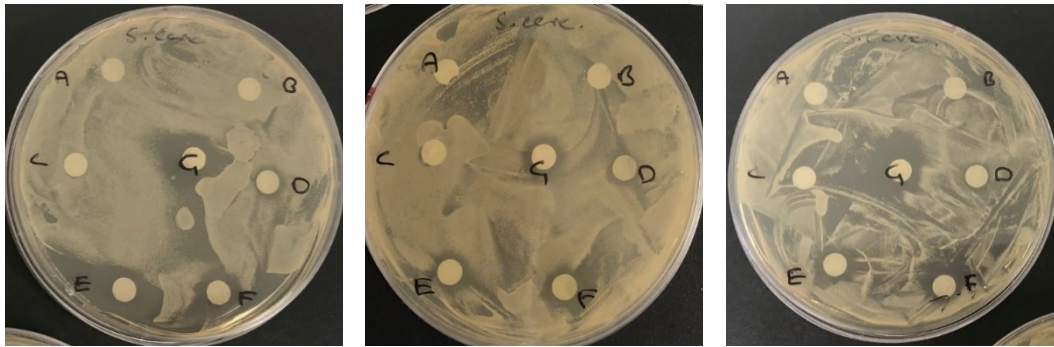


Figure A 7: Agar plate showing zone of inhibition with *S. cerevisiae* for the differently loaded bismuth(III) phosphinato-MFC sheets- 0%(A), 0.07% (B), 0.39%(C), 0.94% (D), 2.01% (E), 4.37% (F) and 10.53 %(G)



Figure A 8: : Agar plate showing zone of inhibition with *C. glabrata* for the differently loaded bismuth(III) phosphinato-MFC sheets- 0%(A), 0.07% (B), 0.39%(C), 0.94% (D), 2.01% (E), 4.37% (F) and 10.53 %(G)

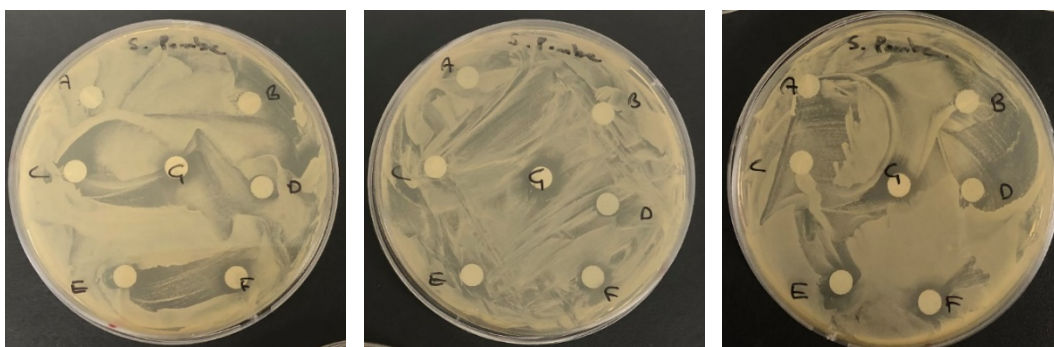


Figure A 9: : Agar plate showing zone of inhibition with *S. pombe* for the differently loaded bismuth(III) phosphinato-MFC sheets- 0%(A), 0.07% (B), 0.39%(C), 0.94% (D), 2.01% (E), 4.37% (F) and 10.53 %(G)

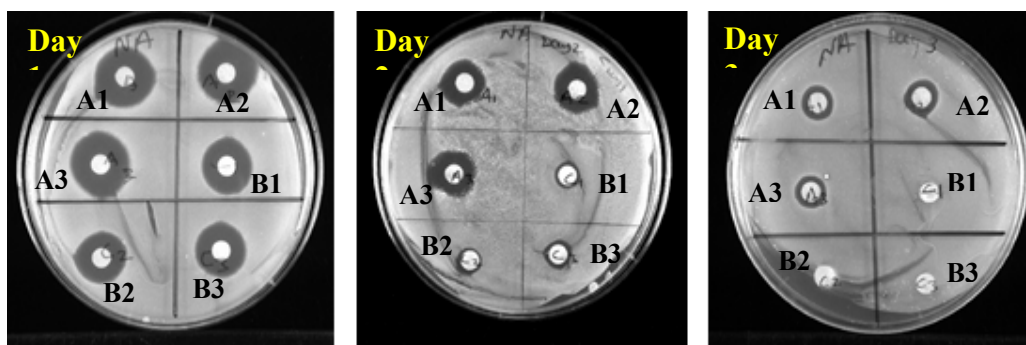


Figure A 10: Agar plate showing zone of inhibition with *S. epidermidis* for 4.37% (A1, A2, A3) and 0.94% (B1, B2, B3) loaded sheets from the over-time experiment

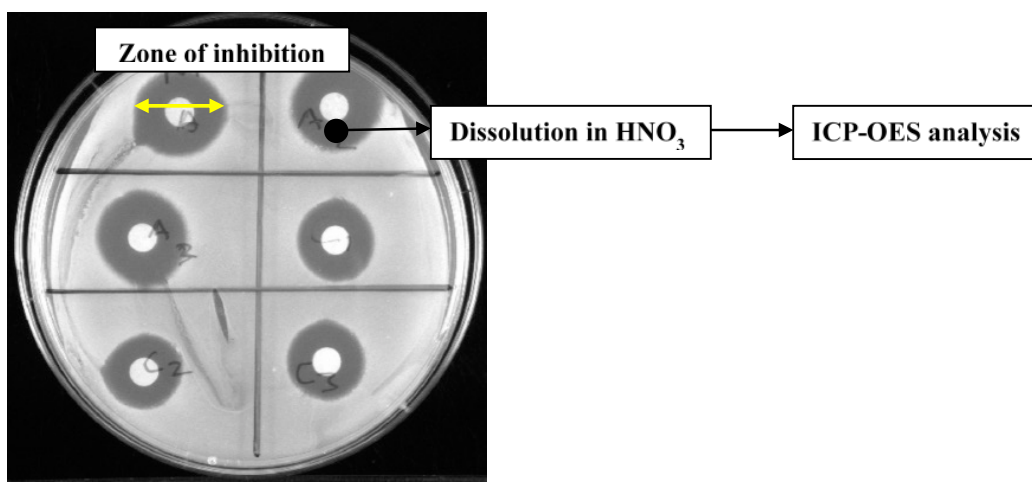


Figure A 11: Representative agar plate showing zone of inhibition and analysis of the agar by ICP-OES

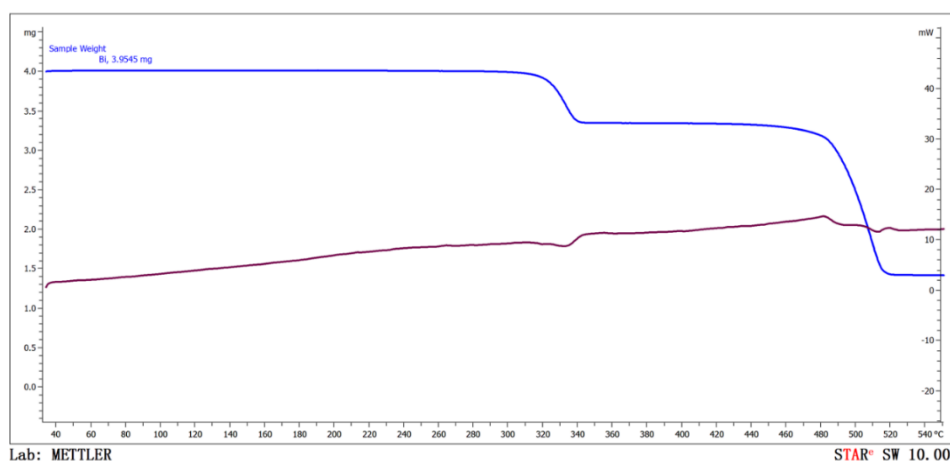


Figure A12: TGA (blue) and DSC (maroon) traces from heating the phenyl bismuth bis(diphenylphosphinato) complex at a rate of 10 °C/minute. The vertical axes show the mass loss (mg) on the left and heat flow (mW) on the right. The horizontal axis shows the temperature (°C).

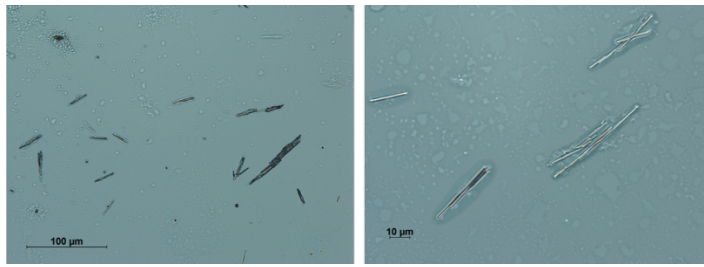


Figure A 13: Optical image of the bismuth complex

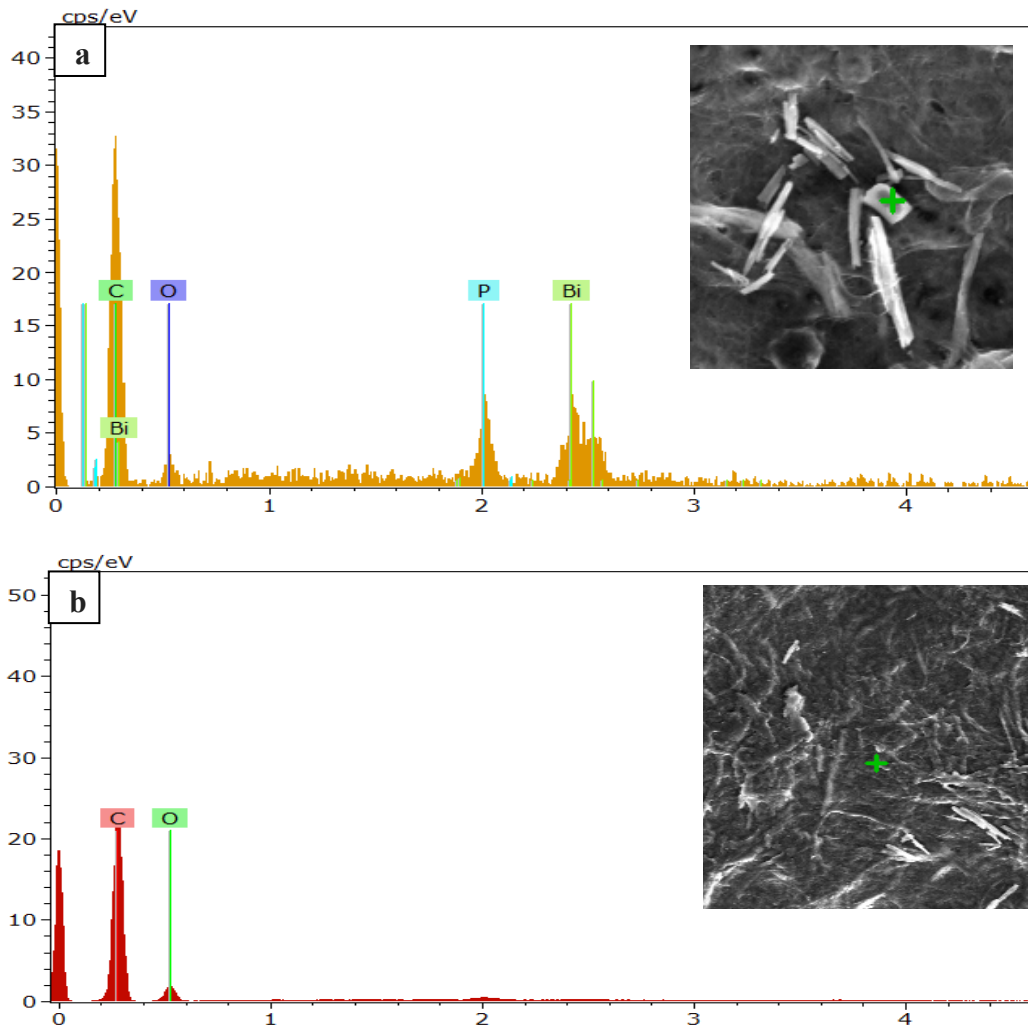


Figure A 14: EDX point analysis of bismuth(III) phosphinato-MFC sheet on the particle (a) and on the cellulose surface (b)

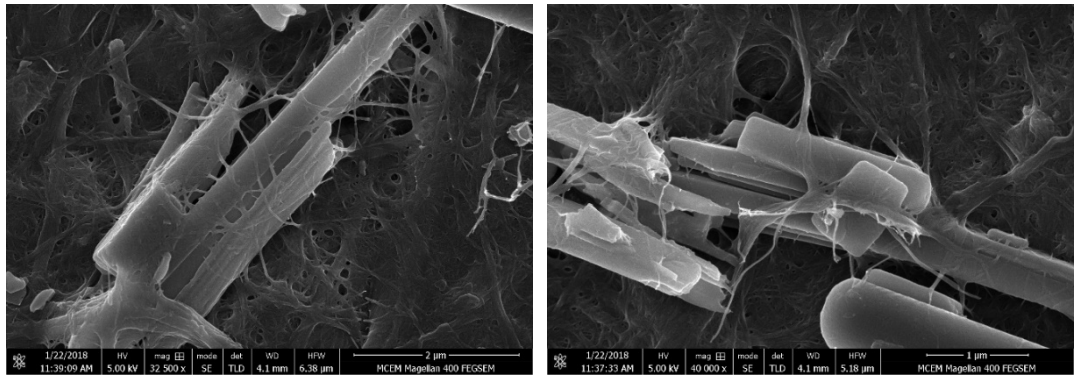


Figure A 15: SEM images of the surface of 4.37 wt.% Bi-MFC composite at high magnification showing the bismuth particles tangled within the fibres

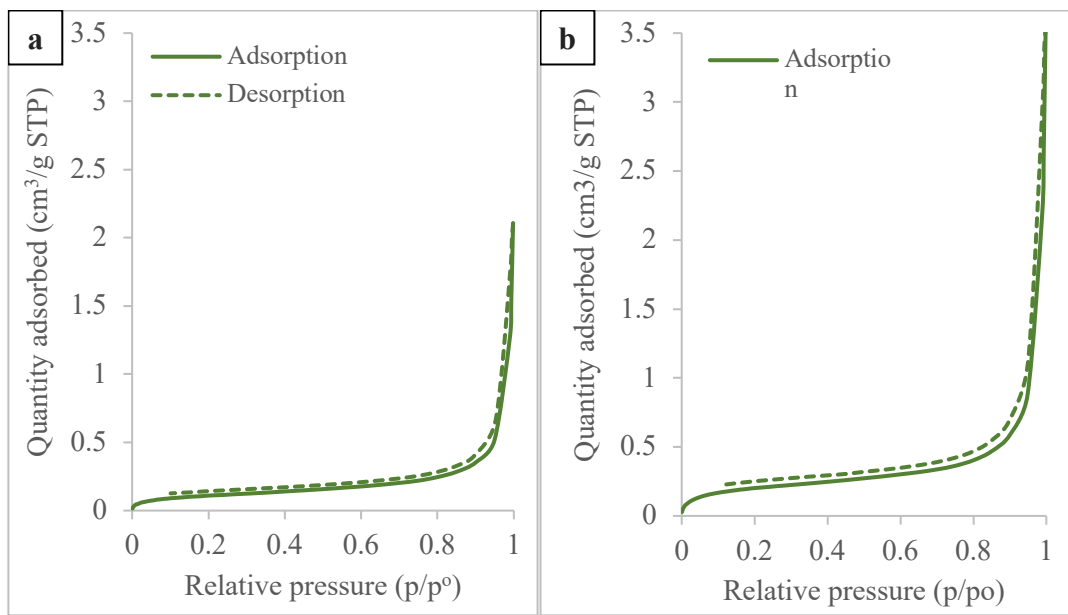


Figure A 16: BET isotherm plot of pure MFC sheet (a) and 2.10 wt.% Bi-MFC composite (b) from nitrogen adsorption- desorption

THIS PAGE HAS BEEN INTENTIONALLY LEFT BLANK

**Supplementary Information****The effect of pulp type on the barrier and antimicrobial performance of microfibrillar lignocellulosic bismuth-based active packaging material**

Maisha Maliha<sup>1</sup>, Rajini Brammananth<sup>2</sup>, Ross L. Coppel<sup>2</sup>, Melissa Werrett<sup>3</sup>, Philip Andrews<sup>3</sup>,  
Warren Batchelor<sup>1\*</sup>

<sup>1</sup>*Bioresource Processing Research Institute of Australia (BioPRIA), Department of Chemical Engineering, Monash University, VIC 3800, Australia*

<sup>2</sup>*Department of Microbiology, Monash University, VIC 3800, Australia*

<sup>3</sup>*School of Chemistry, Monash University, VIC 3800, Australia*

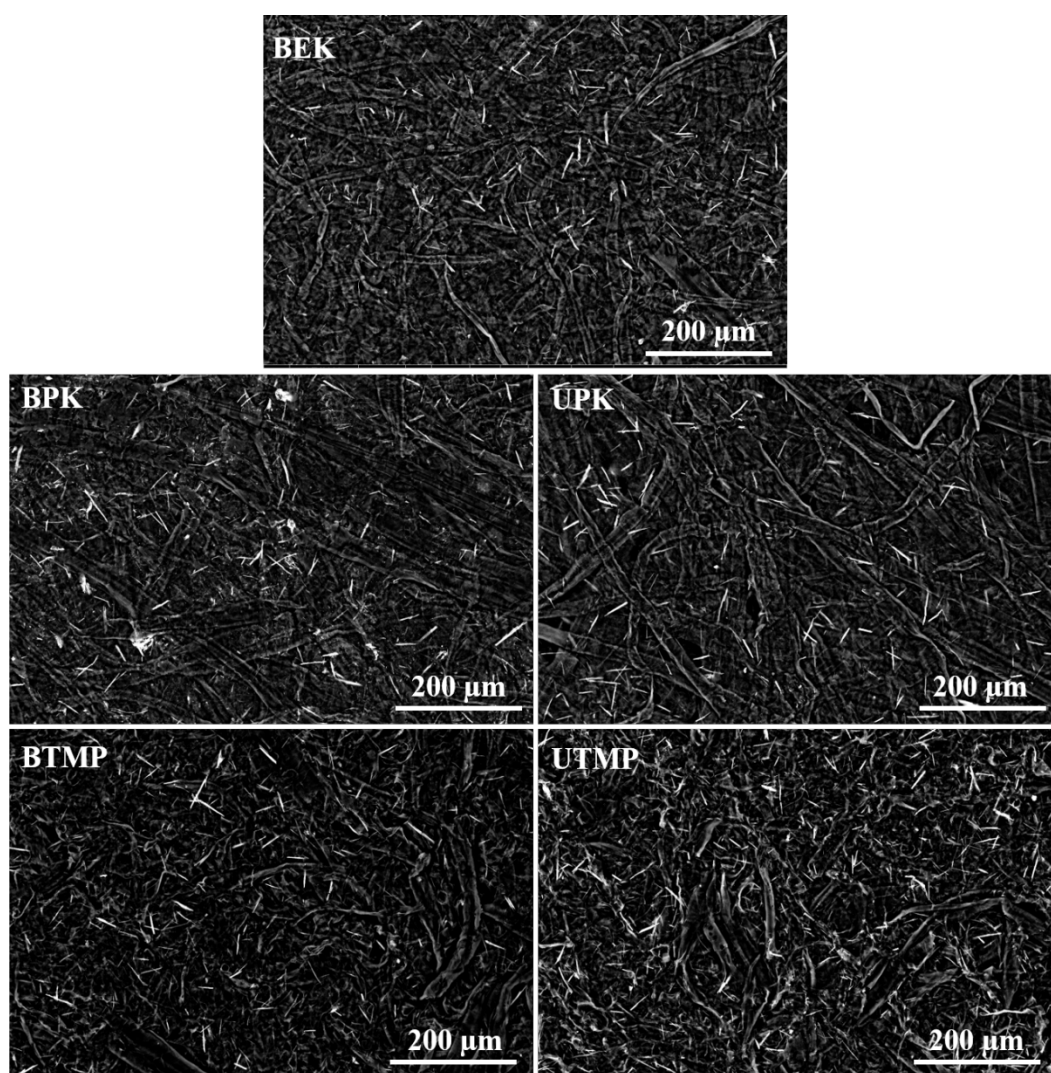


Figure B 1: Back-scattered electron (BSE) images of the composite films from bleached eucalyptus kraft pulp (BEK) (top), bleached (BPK) and unbleached (UPK) radiata pine kraft pulp (middle panel), bleached (BTMP) and unbleached (UTMP) radiata pine thermomechanical pulp (bottom panel). The bismuth with higher atomic number than carbon, nitrogen or oxygen appears

brighter in BSE images. The bright needle-shaped Bismuth complex appears to be well distributed within all the composite films.

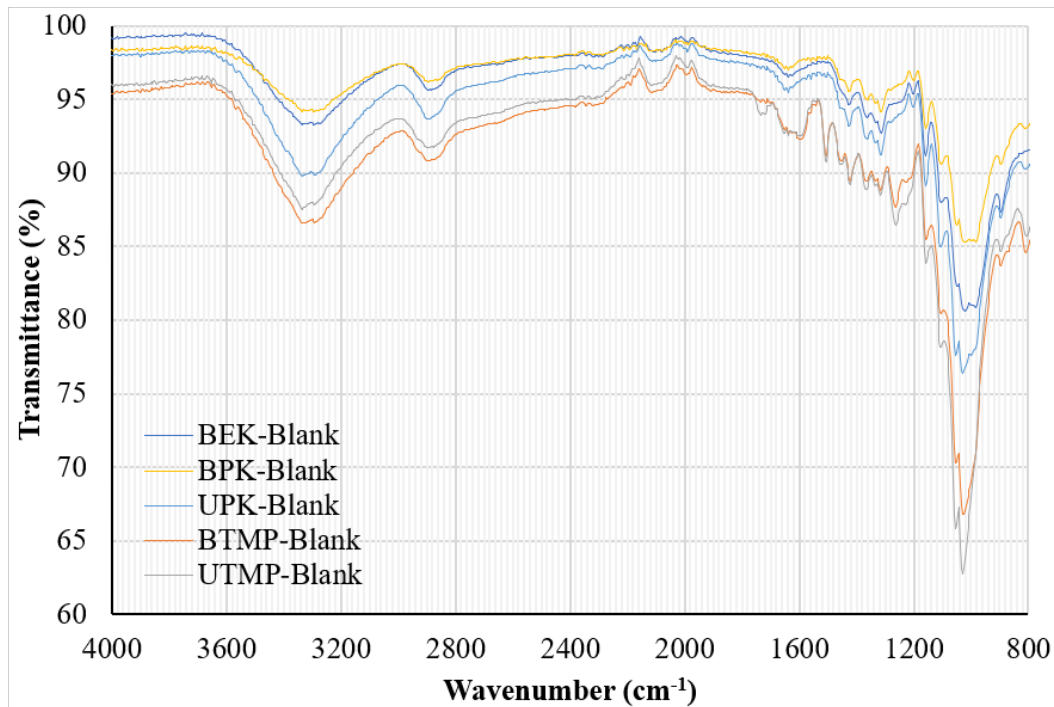


Figure B 2: FTIR spectrum of the blank films (no bismuth loading) prepared from bleached eucalyptus kraft pulp (BEK), bleached (BPK) and unbleached (UPK) radiata pine kraft pulp and bleached (BTMP) and unbleached (UTMP) radiata pine thermomechanical pulp showing the difference in chemical composition

### Supplementary Information

#### **Biocompatibility and Selective Antibacterial Activity of a Bismuth Phosphinato-Nanocellulose Hydrogel**

Maisha Maliha<sup>1</sup>, Rajini Brammananth<sup>2</sup>, Jennifer Dyson<sup>3,4</sup>, Ross L. Coppel<sup>2</sup>, Melissa Werrett<sup>5,6</sup>, Philip C. Andrews<sup>5,6</sup>, Warren Batchelor<sup>1\*</sup>

<sup>1</sup>*Bioresource Processing Research Institute of Australia (BioPRIA), Department of Chemical Engineering, Monash University, VIC 3800, Australia*

<sup>2</sup>*Department of Microbiology, Monash University, VIC 3800, Australia*

<sup>3</sup>*Monash Institute of Medical Engineering (MIME), Monash University, VIC 3800, Australia*

<sup>4</sup>*Department of Biochemistry and Molecular Biology, Monash Biomedicine Discovery Institute, Monash University, VIC 3800, Australia*

<sup>5</sup>*School of Chemistry, Monash University, VIC 3800, Australia*

<sup>6</sup>*Centre to Impact AMR, Monash University, VIC 3800, Australia*

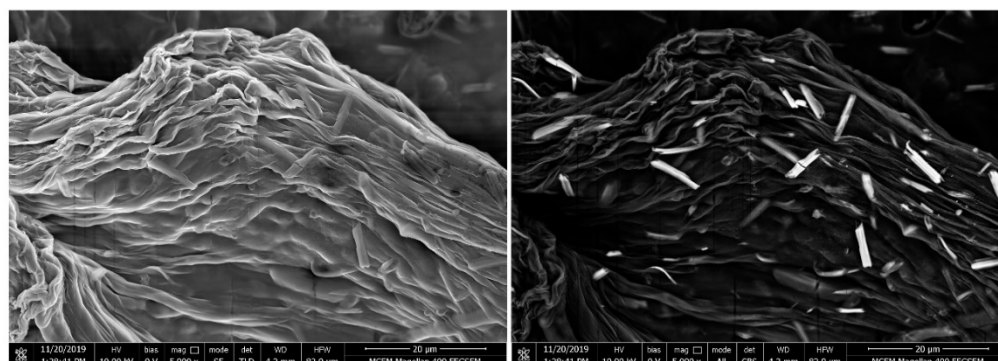


Figure C 1: SE and BSE image of air dried hydrogel showing presence of bismuth particles in between fibres in fibre bundles

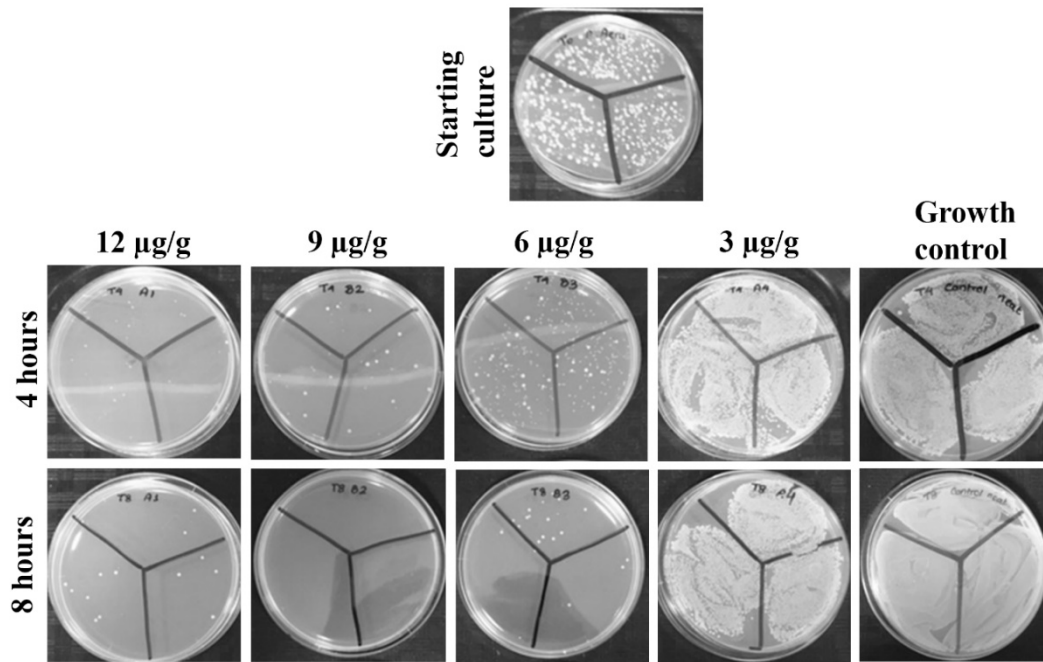


Figure C 2: Representative plates from the time-kill assay against *P. aeruginosa*

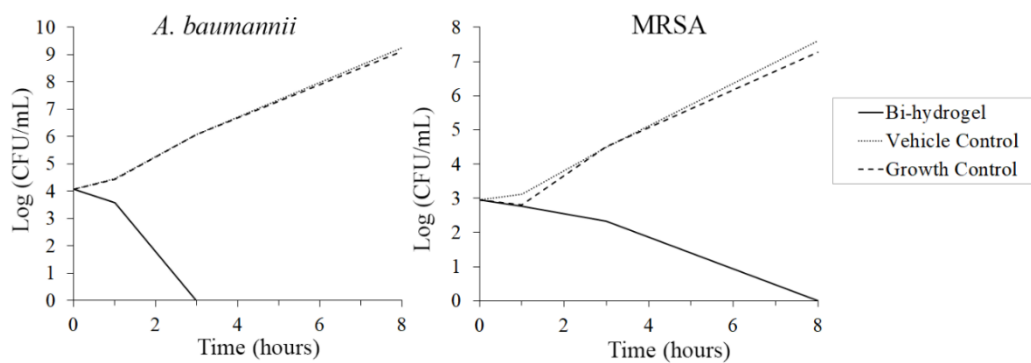


Figure C 3: Log of CFU/mL of the bismuth phosphinate loaded hydrogels with *A. baumannii* and MRSA for 8 hours period analysed at 1, 3, 5 and 8 hours performed in triplicates

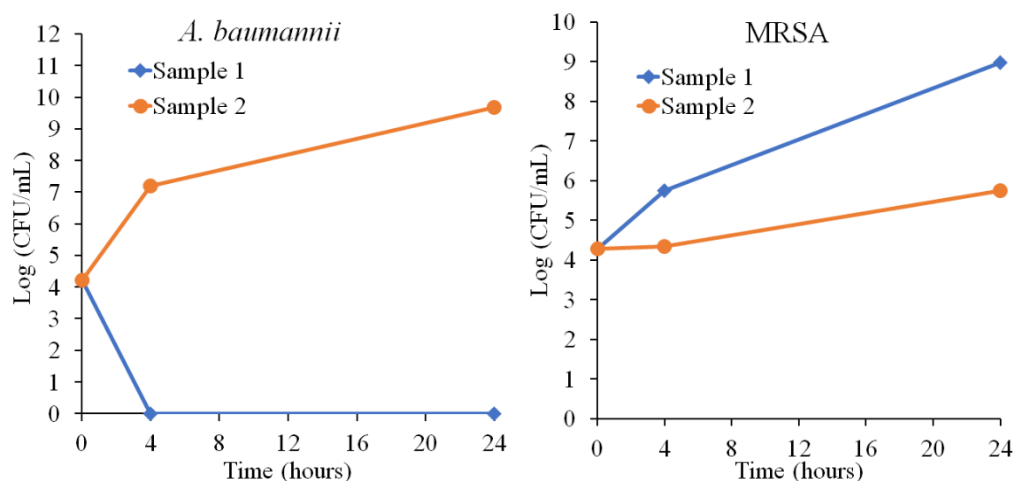


Figure C 4: Log of CFU/mL of the blinded time-kill assay of the hydrogels with the broth containing either 9 $\mu$ g/g (test) or 0 $\mu$ g/g (control) of bismuth phosphinato complex concentration with *A. baumannii* and MRSA analysed at 4 hours and 24 hours. Sample 1 was test and control for *A. baumannii* and MRSA respectively and vice versa.

Table C 1: Actual Bi-complex content in different batches of hydrogel expressed as mean  $\pm$  standard deviation (n=3)

Batch No.	Percentage of actual Bi-complex content (g Bi complex/ g hydrogel)
1	0.079 $\pm$ 0.008
2	0.083 $\pm$ 0.002
3	0.080 $\pm$ 0.002
4	0.082 $\pm$ 0.005

THIS PAGE HAS BEEN INTENTIONALLY LEFT BLANK

**Supplementary Information****Bismuth phosphinato incorporated antibacterial filter paper for drinking water disinfection**

Maisha Maliha<sup>1</sup>, Benjamin Tan<sup>1</sup>, Karmen Wong<sup>1</sup>, Simin Miri<sup>1</sup>, Rajini Brammananth<sup>2</sup>, Ross Coppel<sup>2</sup>, Melissa Werrett<sup>3,4</sup>, Philip Andrews<sup>3,4</sup>, Warren Batchelor<sup>1</sup>

<sup>1</sup>Bioresource Processing Research Institute of Australia (BioPRIA), Department of Chemical Engineering, Monash University, VIC 3800, Australia

<sup>2</sup>Department of Microbiology, Monash University, VIC 3800, Australia

<sup>3</sup>School of Chemistry, Monash University, VIC 3800, Australia

<sup>4</sup>Centre to Impact AMR, Monash University, VIC 3800, Australia

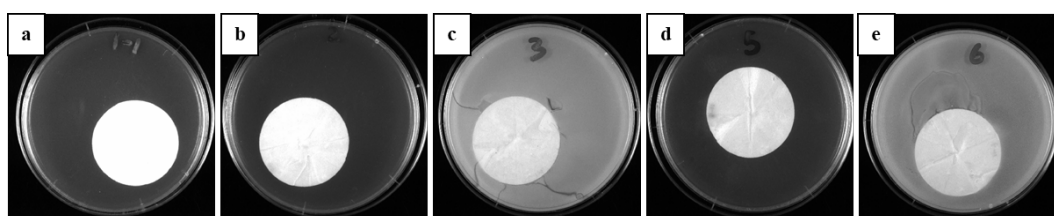


Figure D 17: Qualitative antifouling test of the wetted side of the filter composites using (a) 5% Bi-coated advantec filter or A-M5-S (b) 2.5%-Bi-coated advantec filter or A-M2.5-S (c) 0% Bi-coated advantec filter or A-M0-S (d) 5%-Bi-coated whatman filter or W-M5-S (e) 0%-Bi-coated whatman filter or W-M0-S

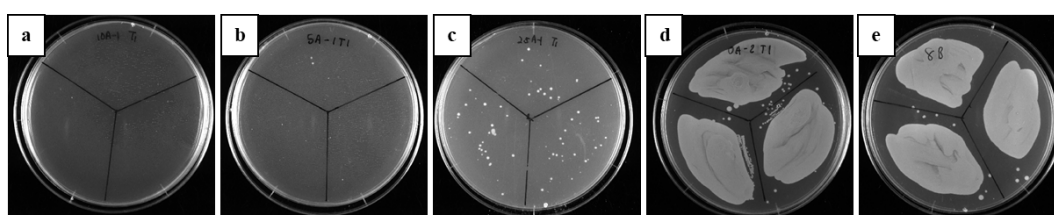


Figure D 18: Representative plates showing the time-kill study of the bacterial filtrate after 24 hours of incubation at 37°C after filtering through MFC coated advantec filters containing (a) 10%Bi-complex, (b) 5%Bi-complex, (c) 2.5% Bi-complex and (d) 0% Bi-complex and (e) the starting culture

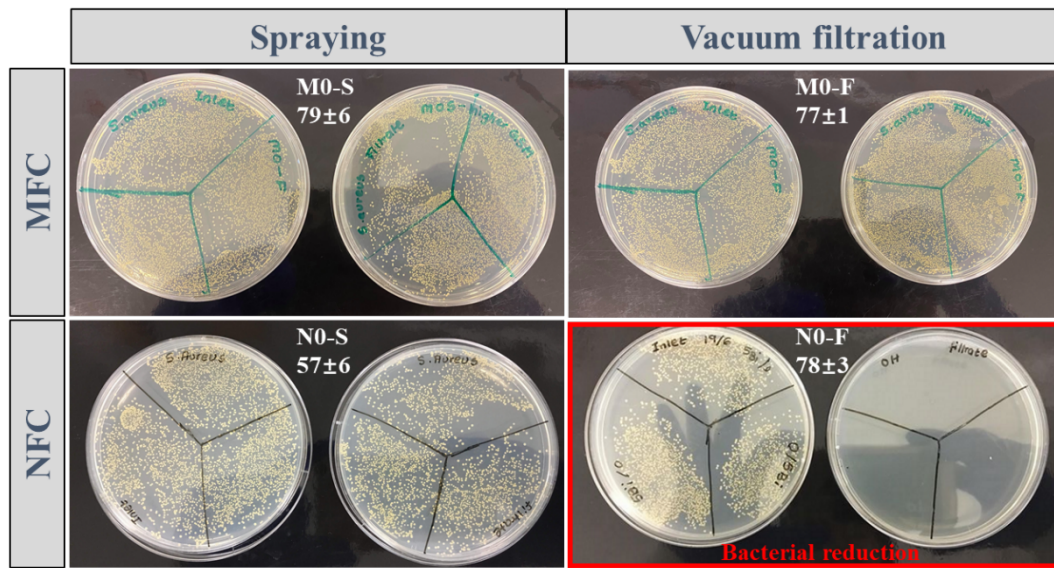


Figure D 19: Representative plates showing the bacterial colonies in the inlet (left plate in each pair) and the filtrate (right plate in each pair) from showing only NFC sheets produced by vacuum filtration (N0-F) shows reduction in bacterial colonies. Here the number represents the average grammage  $\pm$  standard deviation.

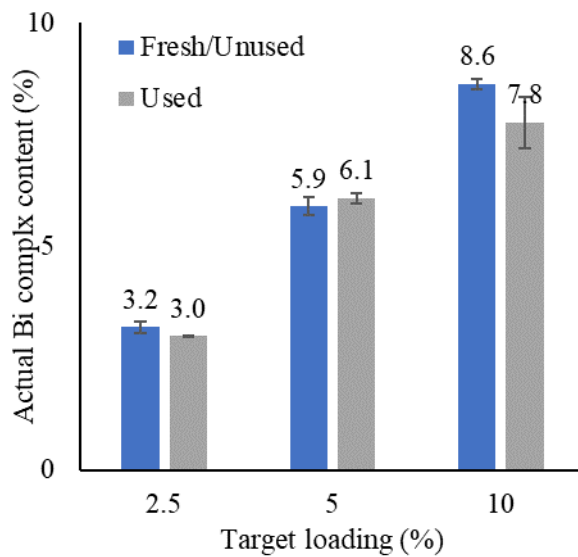


Figure D 20: Bi-complex content in fresh/unused handsheet and after filtration of milli-Q water (250 mL) at 1 bar.

---

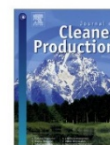
## **APPENDIX II**

**PUBLICATIONS INCLUDED IN THESIS IN THEIR PUBLISHED FORMAT**

---

---

THIS PAGE HAS BEEN INTENTIONALLY LEFT BLANK



## Bismuth phosphinate incorporated nanocellulose sheets with antimicrobial and barrier properties for packaging applications

Maisha Maliha<sup>a</sup>, Megan Herdman<sup>b</sup>, Rajini Brammananth<sup>c</sup>, Michael McDonald<sup>d</sup>, Ross Coppel<sup>c</sup>, Melissa Werrett<sup>b</sup>, Philip Andrews<sup>b</sup>, Warren Batchelor<sup>a,\*</sup>

<sup>a</sup> Bioresource Processing Research Institute of Australia (BioPRIA), Department of Chemical Engineering, Monash University, VIC, 3800, Australia

<sup>b</sup> School of Chemistry, Monash University, VIC, 3800, Australia

<sup>c</sup> Department of Microbiology, Monash University, VIC, 3800, Australia

<sup>d</sup> Centre for Geometric Biology, School of Biological Sciences, Monash University, VIC, 3800, Australia

### ARTICLE INFO

#### Article history:

Received 11 April 2019  
Received in revised form  
16 September 2019  
Accepted 22 October 2019  
Available online 24 October 2019

Handling Editor: M.T. Moreira

#### Keywords:

Nanocellulose  
Bismuth  
Antimicrobial  
Packaging  
Barrier

### ABSTRACT

The incorporation of an organobismuth complex into a nanocellulose matrix to develop a free-standing antimicrobial barrier material was investigated. The non-toxic complex, phenyl bismuth bis(diphenylphosphinato) was used as the additive to impart antimicrobial properties to nanocellulose sheets for the development of paper-based renewable and biodegradable active packaging material. A spraying technique was used to prepare sheets with different loadings of the organobismuth complex and its effects on antimicrobial and barrier properties were studied. Morphological studies of the sheets revealed the overall distribution of the complex throughout the nanocellulose matrix, with occasional clustering behaviour on the surface. Water vapour permeability of the paper sheets increased very slightly with loading of the bismuth complex, but remained in the range acceptable for packaging materials. The physical and mechanical properties of the sheets were also affected by the addition of the bismuth complex in the structure, and hence a trade-off needs to be made between the loading level and the material performance for commercialization. The composite sheets were able to inhibit the growth of bacteria and fungi, including strains of multidrug resistant bacteria. Moreover, the paper showed continued release of the bismuth complex over time with effective lifetime depending on the loading. In summary, this paper describes the preparation and characterization of a sustainable and ecofriendly antimicrobial composite paper, using a poorly soluble bismuth complex dispersed into a nanocellulose matrix, which shows the potential to be used as an active packaging material.

© 2019 Elsevier Ltd. All rights reserved.

### 1. Introduction

Packaging plays a vital role for most products in terms of consumer safety. Conventional packaging serves only as a barrier layer between the product and the environment and shields it from oxygen, water vapour and other contaminants (Pereira De Abreu et al., 2012). Demand for quality assurance and product safety of sensitive items such as food and medical products has led to the emergence of high-value active packaging material that offers enhanced protection (Lavoine et al., 2015; Inamuddin, 2016). Active packaging has the ability to either interact with the product or alter the environment enclosed within the packaging. Examples include

incorporating compounds that can absorb and remove oxygen, ethylene or moisture, or have antimicrobial properties (Pereira De Abreu et al., 2012). The latter offers better protection by inhibiting the microbial contamination of the products reducing the risk of deterioration. It can also inhibit contamination of the packaging surface, thus reducing microbial cross-contamination from the packaging. This is an effective strategy with proven improvements in product protection and quality (Appendini and Hotchkiss, 2002; Pereira De Abreu et al., 2012). Antimicrobial active packaging can be obtained by incorporating or immobilizing antibacterial and antifungal agents into the material (Lavoine et al., 2015; Amini et al., 2016; Lavoine et al., 2016).

The use of metal-based antimicrobial agents, in the form of nanoparticles and compounds, has been increasing (Patra et al., 2012; Barry and Sadler, 2013; Dizaj et al., 2014). This is due to metals often showing greater efficacy and resilience to bacterial

\* Corresponding author.

E-mail address: [warren.batchelor@monash.edu](mailto:warren.batchelor@monash.edu) (W. Batchelor).

resistance than the organic compounds. (Lemire et al., 2013). Metals such as silver, gold, arsenic, bismuth, antimony, copper, mercury, platinum, palladium, ruthenium, and cobalt, and their compounds have shown antimicrobial activity (Abd-El-Aziz et al., 2017; Alvarez-Paino et al., 2017). This includes inorganic compounds, organometallic complexes, metal organic frameworks and metal nanoparticles (Patra et al., 2012; Barry and Sadler, 2013; Abd-El-Aziz et al., 2017). Of them, silver has been the most popular metal used as an antimicrobial additive in materials (Dankovich and Gray, 2011; Haider and Kang, 2015; Huang et al., 2015; Amini et al., 2016; Carbone et al., 2016; Xiong et al., 2016). Silver nanoparticles have been studied as composites with synthetic and natural polymers, such as cellulose, chitosan, gelatine, chitin, and collagen (Martinez-Abad et al., 2012; Xiong et al., 2016; Yan et al., 2016). Silver is also used in various commercial products, including packaging materials, clothing, and healthcare and personal care products. This widespread use of silver has raised concerns about its toxicity for various organisms including humans and environmental accumulation (Barros-Velázquez, Stensberg, Wei et al., 2011; Cushen et al., 2012). The most severe toxic effect of long-term silver exposure to humans is the condition of blue coloration of the skin, known as argyria. Other harmful effects of soluble silver include damage to liver, kidney and blood cells (Drake and Hazelwood, 2005; Maillard and Hartemann, 2013). Silver nanoparticles can enter the human body through gastrointestinal absorption from food contact materials (e.g. silver based food-packaging) as well as through the respiratory tract (Cushen et al., 2012). The maximum safe level of lifetime silver intake is only 10 g as declared by the World Health Organization (Cao, 2017). Studies have shown that silver nanoparticles can migrate into food from silver-based food-packaging materials (Huang et al., 2011; Echegoyen and Nerin, 2013). It has also been reported that the concentration of silver released into food from a commercial packaging material can exceed the regulatory limits set for food contact materials after 24 days of storage (Pezzuto et al., 2015). This suggests there is a necessity to develop new active packaging materials, with more attention to safety and health concerns. In addition, the prolonged use of silver has raised the risk of induction of silver resistance in bacteria (Silver, 2003; Maillard and Hartemann, 2013; Gunawan et al., 2017), a scenario common for many other metal-based antimicrobials (Pal et al., 2014). As a result, it has been suggested that silver-based antimicrobials be regulated by governments and reserved for medical uses only (Crocetti, 2013). Accordingly, there is a need for a new generation of antimicrobial compounds for use in active packaging for food, medical supplies and other sensitive products.

The purpose of this study is to investigate a poorly soluble bismuth complex as an active species for packaging applications. Many bismuth complexes have been reported to possess antibacterial activity (Domenico et al., 2001; Kotani et al., 2005; Svoboda et al., 2010; Luqman et al., 2016; Andrews et al., 2018). Bismuth has a long history of being used for treating intestinal disorders. Pepto-Bismol (BSS or bismuth subsalicylate) and De-Nol (CBS or colloidal bismuth subcitrate) are used for gastrointestinal treatments, for example traveller's diarrhoea, and are effective agents against the bacteria *Helicobacter pylori* (Briand and Burford, 1999; Suzuki and Matano, 2001; Barry and Sadler, 2013). It is proposed that bismuth works by binding to proteins with metal binding sites, e.g. thiol (cysteine) rich protein structures (Keogan and Griffith, 2014). Unlike other heavy metals, bismuth displays a low level of toxicity in humans and is non-carcinogenic (Kotani et al., 2005). Although it is a heavy metal in the pnictide (Gp 15) family, where toxicity is assumed to increase with molecular weight, bismuth is unique in its comparatively low-toxicity (Suzuki and Matano, 2001). In this paper, a new class of organobismuth complex,

phenyl bismuth bis(diphenylphosphinato), has been chosen as the active agent. This has been reported to have little or no toxicity to mammalian cells and has significantly low solubility in water (Andrews et al., 2018). As a result, in the context of packaging, the risks of migration into the product or into the environment is also greatly reduced.

The technical challenge for applications in active packaging lies in the choice of material that is suitable for use in supporting the antimicrobial agents. In this regard, polymers have been widely used as the carrier matrix for antimicrobial agents to improve their stability and activity due to their macromolecular properties (Alvarez-Paino et al., 2017). The most studied materials for antimicrobial films are petroleum based polymers, e.g. polyethylene, polypropylene, polystyrene and polyethylene terephthalate (Martinez-Abad et al., 2012; Alvarez-Paino et al., 2017). The packaging industry is also mainly dependent on petroleum-based polymers (Inamuddin, 2016). Environmental accumulation of plastics, and the resulting impact from plastic pollution, have driven interest in the use of biodegradable polymers such as polylactic acid (PLA), polyglycolic acid (PGA), and more importantly renewable natural biopolymers such as cellulose, starch, chitosan, alginate, and collagen (Alvarez-Paino et al., 2017). Of them, cellulose is the most abundant, is biodegradable and renewable, as well as inexpensive and non-toxic (O'Sullivan, 1997; Xu et al., 2016). However, while cellulose fibres can be formed into strong and stiff paper-based packaging, the barrier properties are inferior to that of petroleum-based polymers. This limitation can be overcome by breaking down cellulose-containing materials into microfibrils or bundles of microfibrils. The product, which is generally known as nanocellulose, has excellent strength and greatly improved barrier properties when compared to conventional paper (Siró and Plackett, 2010; Lavoine et al., 2012; Kumar et al., 2014). Nanocellulose is unique due to its hydrophilicity, biocompatibility and large surface area in addition to all the attributes of nanostructured materials (Klemm et al., 2005; Klemm et al., 2011). Nanocellulose films also provide a porous structure for antimicrobial agents to attach to, both physically and chemically (Lin and Dufresne, 2014), making nanocellulose a promising material for active packaging applications. Nanocellulose suspensions can be converted to sheets and films by various methods such as vacuum filtration (Varanasi and Batchelor, 2013), casting (Kumar et al., 2014), spraying (Beneventi et al., 2014; Krol et al., 2015; Beneventi et al., 2016) or coated on a substrate/base paper (Lavoine et al., 2015; Kumar et al., 2017).

The objective of this study was to incorporate a new class of organobismuth complex, phenyl bismuth bis(diphenylphosphinato), into a nanocellulose matrix for the development of cleaner antimicrobial sheets for active packaging applications. Antimicrobial performance and physical, mechanical and barrier properties of the free-standing nanocellulose paper sheets were thoroughly studied to demonstrate the hypothesis that these materials can potentially serve as an active barrier layer as standalone sheets or as coatings on other materials.

## 2. Materials and method

### 2.1. Materials

Microfibrillated Cellulose (MFC) purchased from DAICEL Chemical Industries Limited, Japan (grade Celish KY-100G) was used as the nanocellulose matrix. The MFC used was characterized in previous work by Varanasi et al. to have a mean diameter of 73 nm and an aspect ratio of 147 (Varanasi et al., 2012). Phenyl bismuth bis(diphenylphosphinato) was prepared according to Andrews et al. (Andrews et al., 2018). Triphenyl bismuth and

diphenyl phosphinic acid were mixed in the ratio of 1:2 in ethanol and heated at reflux for 24 h. The reaction mixture was then filtered, and the insoluble phenyl bismuth bis(diphenylphosphinato) was isolated as a white powder. Following filtration, the complex was washed with hot ethanol to remove all unreacted chemicals and the by-product benzene, after which no further purification was required.

All analytical data matches that previously reported for the phenyl bismuth bis(diphenylphosphinato) complex (as shown in Scheme 1). The complex is sparingly soluble in water and the solubility as reported is 16.3 kg of water required to dissolve 1 g complex. The complex was also previously reported to have limited solubility in organic solvents like ethanol, dichloromethane, tetrahydrofuran, toluene, and dimethyl sulfoxide (DMSO). Moreover, preliminary toxicity results has been reported previously and it was shown that the complex has no toxic effect on mammalian COS-7 cells at a concentration of 0.5 mg/mL (Andrews et al., 2018).

## 2.2. MFC suspension preparation

Phenyl bismuth bis(diphenylphosphinato) was dispersed in small amounts of water using a magnetic stirrer and mixed with the MFC. This was then diluted to make a suspension of 2 wt% MFC and mixed with a hand blender, followed by disintegration. In the disintegrator, the suspension is contained in a 3 L vessel and a small propeller running at 3000 revolutions, which separates the fibres from each other. The suspensions were made with varying amount of the bismuth complex. The suspensions were made with target loadings of 5, 2.5, 1.0, 0.5, and 0.1 wt% of the bismuth complex with respect to the mass of cellulose fibres in the suspension. Thus, the composition was 2 g fibre and 0.1 g, 0.05 g, 0.02 g, 0.01 g or 0.002 g of the bismuth complex in 100 g of the 5, 2.5, 1.0, 0.5, and 0.1 wt% suspensions respectively, the remaining being DI water. The experimental consistency of the suspensions are given in Table S1 in the supplementary information. The suspensions were sprayed immediately without any time delay to ensure no settling of the particles, thus confirming uniform dispersion in the suspensions.

## 2.3. Sheet preparation

Bismuth(III) phosphinato-MFC composites were prepared using a spraying technique as described by Shanmugam et al. (Shanmugam et al., 2017). The composites were made using the suspensions described with target loadings of 5, 2.5, 1.0, 0.5, and 0.1 wt% of the bismuth. The consistency of the fibres in the suspension was kept constant throughout. The MFC suspension was sprayed onto square stainless steel plates moving on a variable speed conveyor set at  $1 \pm 0.2$  cm/s as shown in Fig. 1. The suspension was sprayed using a Professional Wagner spray system (Model number 117) at 200 bar from a height of  $30 \pm 1$  cm. A 517 type spray tip was used. After spraying, the MFC on the plates was dried at ambient temperature of 25 °C under constraint at the edges until

the sheets separated from the plate and started to roll off at the edges. The sheets were then peeled from the plates and stored in a controlled temperature and humidity condition maintained at 23 °C and 50% relative humidity.

## 2.4. Characterization

### 2.4.1. ICP-OES analysis

Weighed samples of the sheets were ashed using a muffle furnace in crucibles. During ashing, the temperature was ramped to 600 °C over 3 h and maintained at this temperature for a further 3 h. Above 100 °C all moisture, and at about 525 °C all cellulose, is removed. The inorganic complex decomposes at about 330 °C. The bismuth-based residue left in the crucible was dissolved in small quantities of concentrated nitric acid and diluted. This was then analysed using Perkin-Elmer Avio 200 ICP-OES (inductively coupled plasma-optical emission spectrometry). The concentration of the elemental bismuth in the sample solution was analysed by ICP-OES, and back calculated to the amount of bismuth complex in the paper. Each sheet was analysed in triplicate and reported as percentage of the mean mass of the bismuth complex per gram of dry paper  $\pm$  standard deviation.

### 2.4.2. Bi-complex characterization

The hydrodynamic diameter of the particles was estimated using dynamic light scattering (DLS) using a Nanobrook Omni Particle Size Analyser (Brookhaven Instruments) with a dilute suspension of 0.02 wt% Bi-complex in Milli-Q water.

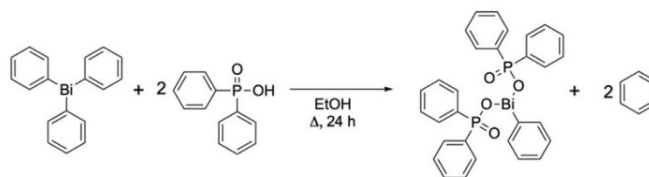
### 2.4.3. SEM imaging

Scanning Electron Microscope (SEM) imaging of the bismuth(III) phosphinato-MFC sheets was performed using the FEI Nova NanoSEM 450 FEG SEM and FEI Magellan 400 FEG SEM using an accelerating voltage of 5 keV and spot size 2 to study the morphology and distribution of the bismuth complex in the sheets. The samples were prepared by cutting a small piece of the composite sheet and mounting it onto a metal stub secured properly using carbon tape. The samples were coated with a thin conducting layer of Iridium metal.

## 2.5. Material performance

### 2.5.1. Antimicrobial test

The antibacterial and antifungal activities of differently loaded bismuth(III) phosphinato-MFC sheets were measured using disk diffusion assays. The Gram-positive bacteria, viz. *Staphylococcus aureus* (*S. aureus*), *Vancomycin-resistant enterococcus* (VRE), and *Methicillin-resistant Staphylococcus aureus* (MRSA) and Gram-negative bacteria viz. *Escherichia coli* (*E. coli*) and *Pseudomonas aeruginosa* (*P. aeruginosa*) were examined. The fungi used for the tests were the non-pathogenic model organisms *Saccharomyces cerevisiae* YJM789 and *Schizosaccharomyces pombe* H-, which are



Scheme 1. Chemical reaction for the synthesis of phenyl bismuth bis(diphenylphosphinato).

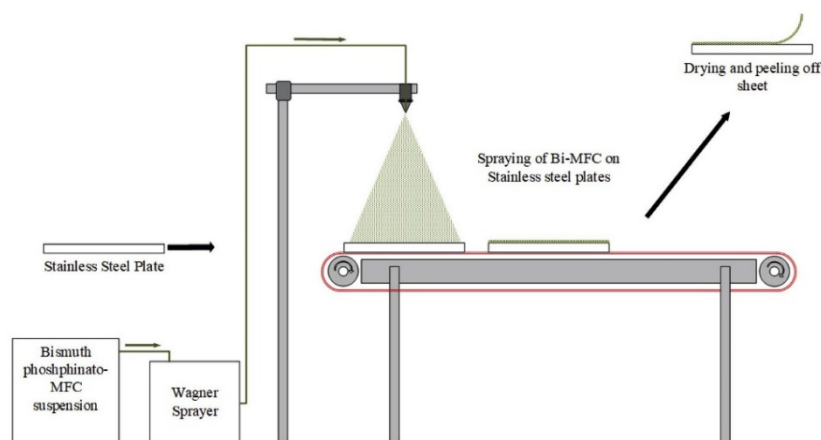


Fig. 1. Experimental Setup for lab scale spraying of the bismuth (III) phosphinato-MFC suspension onto stainless steel plates.

known for their multidrug resistance (Kawashima et al., 2012), as well as the pathogenic species, *Candida albicans* SC5314 and *Candida glabrata* BG99. *C. albicans* SC5314 is a pathogenic and virulent strain often used in lab and genomic studies (Hua et al., 2009). *C. glabrata* BG99 is the lab model for the third most common cause of fungal infection in humans (Fidel et al., 1999). The growth media Lysogeny broth (LB) was used for the bacteria *S. aureus*, *E. coli* and *P. aeruginosa* and Brain Heart Infusion (BHI) was used for *VRE* and *MRSA*. The LB or BHI agar plates were inoculated with 100  $\mu$ l of the specific stationary phase bacteria. CSM plates were inoculated with 100 ml of a stationary phase overnight culture of the yeasts. The composite sheet was cut into discs of 6 mm using a standard hole punch, which were placed on the agar plate that had already been spread with the microbial culture. All strains were incubated at 37 °C for 24 h except for *S. cerevisiae*, *S. pombe* and *C. glabrata*, which were incubated at 30 °C. For the samples that inhibited the growth of the microorganism, a clear zone was observed. The plates were then photographed and the diameter of the zone of inhibition was measured. These tests were performed in triplicate for each type of test microorganism.

#### 2.5.2. Duration of antimicrobial action

The bismuth(III) phosphinato-MFC sheets were tested to investigate the activity of the antimicrobial paper over time. The Gram-positive bacterium *Staphylococcus epidermidis* was chosen for this analysis because it is a part of human microbiota. *S. epidermidis* is the most dominant species of bacteria in human skin and mucosal surfaces, and are carried by healthy people (Fey and Olson, 2010). The zone of inhibition experiment was done in the same way as for the other bacterial strains. After 24 h, the discs were transferred aseptically to a new fresh agar plate inoculated with the same bacterial strain and incubated for another 24 h. This was repeated until no visible zone of inhibition was observed. Furthermore, the agar around the disks in each of these plates were analysed for presence of any bismuth. This was done by scooping out some agar samples, dissolving it in nitric acid and then analysing the bismuth concentration by ICP-OES.

#### 2.5.3. Physical and mechanical properties

The mass of the sheets per unit area was measured after drying the sheet in an oven at 105 °C to determine the grammage. The tensile index and Young's Modulus were measured using an Instron tensile tester (model 5965). The papers were cut into 15 mm width strips and conditioned before the test at 23 °C and 50% relative humidity for 24 h. The span tested was 50 mm with a constant strain rate of 10 mm/min. Five replicates were measured for each test. The pore size distribution and porosity were determined by mercury porosimetry using Micromeritics Autopore IV. The sheets were cut into 8 mm squares and degassed for 24 h at 100 °C in the sample holder. The measurements were done in a penetrometer (Model 14, 3 cc). The surface area and pore shape were determined by physisorption of nitrogen gas at 77 K using a Micromeritics 3Flex.

#### 2.5.4. Water vapour permeability

The water vapour transmission rate of the bismuth (III) phosphinato-MFC sheets were measured at 23 °C and 50% relative humidity by following ASTM E96, using the desiccant method (E96/E96M-16 2016). The sheets were pre-dried in an oven at 105 °C for at least 4 h. Cups complying with the standard were filled with dried desiccant, calcium chloride, and sealed with the test sample. This arrangement was kept in the test condition chamber and the variation in mass of the permeability cups over time was recorded. The rate of change in mass quantifies the water vapour transmission rate (WVTR). The WVTR was then normalized by the thickness of the paper to determine water vapour permeability (WVP). The thickness of the composite sheets was measured using a L&W thickness tester. A number of readings were taken for each sheet, and the mean thickness was calculated.

### 3. Results and discussion

#### 3.1. Characterisation

##### 3.1.1. ICP-OES analysis

ICP-OES was used to quantify the actual amount of bismuth complex present in the sheets. Table 1 shows the mean percentage

**Table 1**  
Percentage of phenyl bismuth bis(diphenylphosphinato) from ICP-OES analysis for the different loaded Bi-MFC composites.

Target loading of bismuth complex wt. % (g bismuth complex/g cellulose)	Mean actual percentage of bismuth complex wt. % from ICP $\pm$ standard deviation (g bismuth complex/g dry paper)
0.1	0.07 $\pm$ 0.01
0.5	0.39 $\pm$ 0.05
1.0	0.94 $\pm$ 0.02
2.5	2.10 $\pm$ 0.05
5.0	4.37 $\pm$ 0.07

of bismuth complex to dry paper determined using ICP-OES analysis, along with the standard deviation ( $n=3$ ). The results were found to be close to the expected values. However, the minor difference could be accounted for by loss of the complex while preparing the suspension or due to sticking of the complex within the spray system. The maximum loss (30%) was observed for 0.1 wt% loading which could mean that a larger proportion of the complex was lost on the surfaces in contact with the suspension at low loadings than at high loadings of 5.0 wt% (13% loss), with the 1.0 wt% (6% loss) being an outlier. In this instance the preparation of the composites was done in small laboratory scale, with a much greater surface to volume ratio than would be the case in large scale production. When scaling this up to a large-scale production, these losses would be expected to be minimal.

### 3.1.2. Bi-complex characterization

The bismuth(III) phosphinato complex precipitates from the reaction as long thin needles, as shown in the optical image of the bismuth complex alone in Fig. S13. The particle size of the dispersed phase plays a significant role in the properties of composite materials. Due to the particles being non-spherical, light/laser scattering techniques do not define the actual dimensions of the particles. However, scattering techniques can be used to measure the hydrodynamic diameter of an equivalent sphere of the particle that has the same diffusion coefficient. The hydrodynamic diameter of the particle was found to be  $1.25 \pm 0.18 \mu\text{m}$ , with a polydispersity index of  $0.33 \pm 0.04$ . The complex is stable up to a temperature of  $300^\circ\text{C}$ , found by TGA (Fig. S12). The melting point and the decomposition point of the complex is  $300^\circ\text{C}$  and  $330^\circ\text{C}$  respectively and has been reported previously as well (Andrews et al., 2018).

### 3.1.3. SEM imaging

Scanning Electron Microscope (SEM) was used to study the distribution of the complex within the microfibrillated cellulose fibres. Secondary electron (SE) imaging was done to obtain surface information of the 4.37 wt% Bi-MFC composite as shown in Fig. 2. It

is clear from the images that nanofibers form a highly entangled network, and the cylindrical inorganic complex particles are present on the surface entangled within the MFC fibres. It is evident that the particles vary in size and are arranged in random orientation with occasional clustering at different regions on the surface. The dimensions of randomly selected particles on the surface were measured, and the particle size distribution is as illustrated in Fig. 3(a). The smallest particle was 525 nm, and the largest one detected was  $13.3 \mu\text{m}$ .

The shape of the particles can be observed to be cylindrical needle-shaped from Fig. 2. For such a form, a simple parameter, aspect ratio, can be used to describe the shape. The aspect ratio, the ratio of the width to length of the particle, has been measured from SEM images and the aspect ratio distribution curve is shown in Fig. 3(b). Fig. 4 shows the secondary electron image and its corresponding energy-dispersive X-ray (EDX) mapping of the same bismuth (III) phosphinato-MFC composite. This, along with Fig. S14 showing the EDX point analysis of the composite, confirms the presence of bismuth at the cylindrical needle-like structures. Moreover, it also shows that not only are the particles present on the surface, but that they are also buried inside the material (as indicated by arrows in Fig. 4). This phenomenon of the particles being embedded deeper under the surface has also been supported by the back scattered electron images (BSE) in Fig. 5. The high atomic number of bismuth, compared to carbon, oxygen and hydrogen found in the cellulose, means that the bismuth complex appears much brighter in the BSE images. The bright needle-like structures in the BSE images indicate the presence of the bismuth (III) phosphinato complex. BSE imaging in Fig. 5 was done in areas where not many cylindrical particles could be spotted with secondary electron imaging, but it was found that bismuth was present in those areas. A BSE image taken at low magnification, in Fig. 6, shows that the bismuth (III) phosphinato structures can be seen throughout the space indicating that the inorganic complex is well distributed throughout the matrix.

Although the secondary images show some clustering of the complex, the BSE images and EDX mapping give clear evidence of

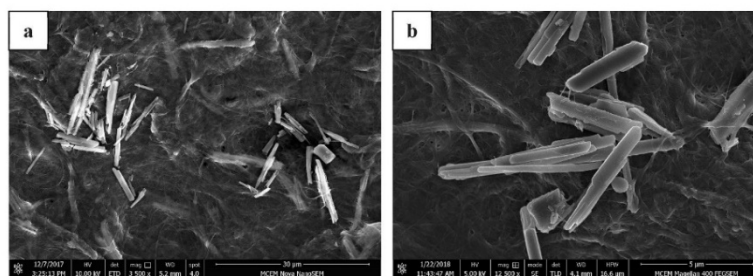


**Fig. 2.** SEM images of the surface of 4.37 wt% Bi-MFC composite at different magnifications: (a)  $\times 3500$  (b)  $\times 12500$ .

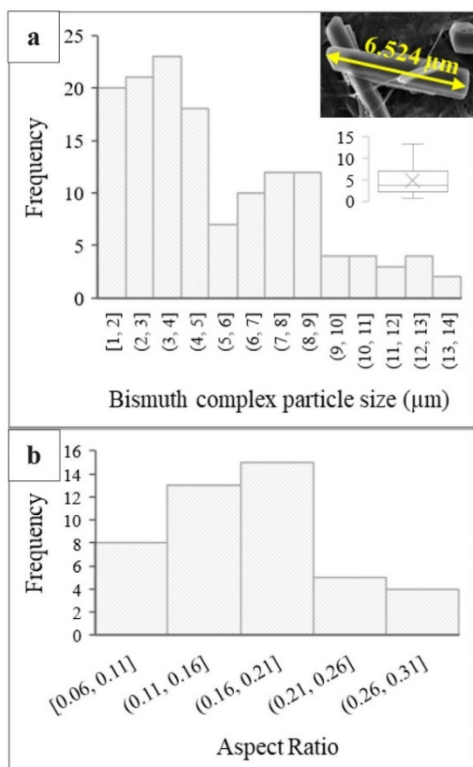


Fig. 3. (a): Particle length distribution ( $n = 140$ ) and (b) Aspect ratio distribution ( $n = 40$ ) of bismuth (III) phosphinato complex on the surface of 4.37 wt% Bi-MFC sheet.

the particles being buried under the surface and that there is an overall even distribution of the particles within the matrix. The fact

that the particles are entrapped within the fibres also mean that the particles are well secured within the matrix, and this along with the insolubility of the complex should limit the release of bismuth out of the material, thereby minimizing the risks of environmental accumulation. Fig. S15 shows the entanglement of the Bi-complex within the nanocellulose fibres. This suggests that the bismuth complex is quite securely held within the composite structure.

3.2. Material performance

3.2.1. Antibacterial activity

The disk diffusion assays show that sheets with higher bismuth complex loadings produce greater zones of inhibition. The agar plates for the zones of inhibition is shown in Fig. S1-S5 in the supplementary information and the results summarized in Fig. 7. Fig. 7 shows that the Gram-negative bacteria, *P. aeruginosa* and *E. coli*, are less susceptible to the Bi-MFC composite, as evidenced by smaller zones of inhibition, compared to the Gram-positive bacteria. The composites provided little or no inhibition of Gram-negative bacteria at loadings below 0.94 wt%. In contrast, Gram-positive bacteria showed evidence of growth inhibition even at the lowest levels of bismuth loading tested, which is 0.07 wt%. These observations agree with previous work that showed that the bismuth (III) complex is more active against Gram-positive bacteria than Gram-negative strains (Kotani et al., 2005; Luqman et al., 2016; Andrews et al., 2018). Gram-negative bacteria are in general harder to kill or inhibit as these cells are surrounded by an outer membrane of lipopolysaccharide, which is absent in Gram-positive bacteria. This extra outer membrane in Gram-negative bacteria acts as a permeability barrier to antibiotics and bactericidal agents, making attack more difficult (Tegos et al., 2002). Fig. 7 also shows that the increase in effectiveness with increased loadings becomes less pronounced for higher loadings and the antibacterial activity seems to reach a plateau beyond 2.10 wt %, as observed by the trends for *E. coli*, *P. aeruginosa* and MRSA.

The results also showed the bismuth-loaded composites were as effective against the drug-resistant form of *S. aureus*, i.e. MRSA as it was to the more sensitive strain of this medically-important bacterium. MRSA is very difficult to treat by most antibiotics and is a major problem in the hospital system (Patra et al., 2012). Silver-resistance has been reported in 33 strains of MRSA (Loh et al., 2009). We examined a limited set of MRSA strains in this study but it raises the possibility that these bismuth-based materials could potentially replace silver-based ones. Based on the results, it was demonstrated that bismuth (III) phosphinato loaded sheets are

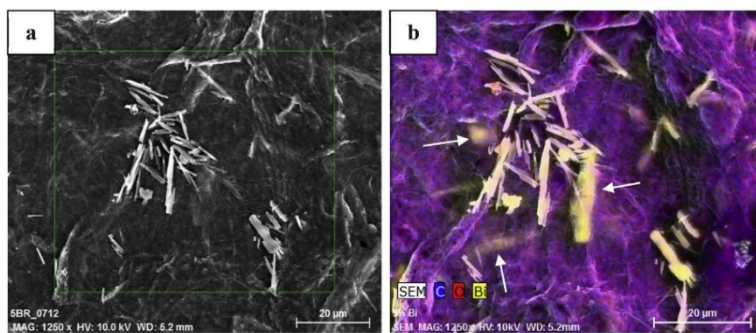


Fig. 4. SEM images of the 4.37 wt% Bi-MFC composite using (a) secondary electron imaging (b) EDX mapping of the selected area.

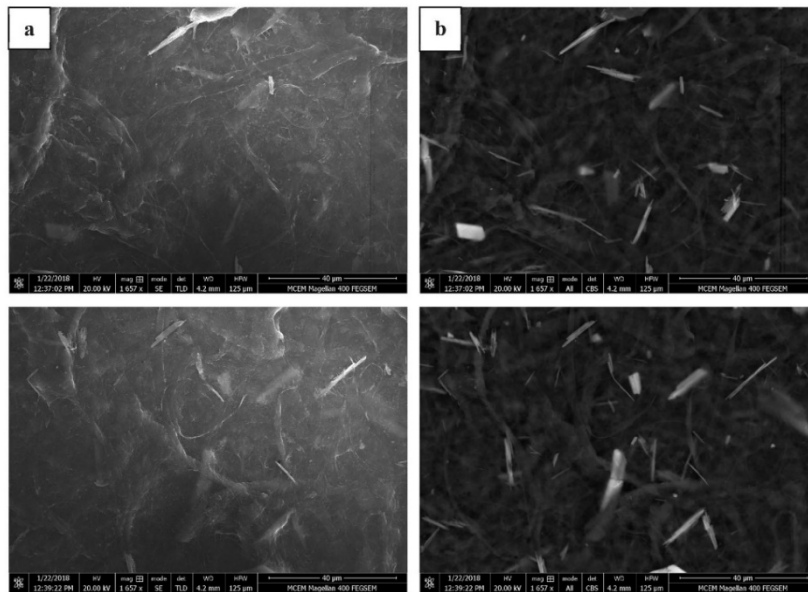


Fig. 5. SEM images of the 4.37 wt% Bi- MFC sheets using (a) secondary electron imaging and their corresponding (b) Back scattered electron imaging.

active against the Gram-positive bacteria and to a lesser extent the Gram-negative bacteria.

Previous research showed bacterial nanocellulose-silver nanoparticle composite with 1.01 wt% loading produced small zones of inhibition against *E. coli*, *S. aureus* and *P. aeruginosa*, with all results being below 8 mm (Wu et al., 2014). When compared to bismuth composites, with a similar loading of 0.94 wt%, the zones of inhibitions were 8.7 mm, 17 mm and 7 mm respectively. Also, it was reported that silver sulfadiazine loaded nanocellulose sheets with 0.43 wt% loading produced a 9 mm zone of inhibition against VRE

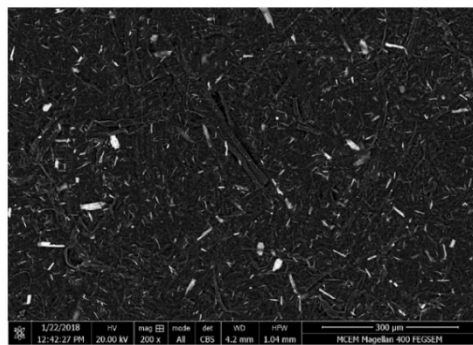


Fig. 6. Back scattered electron image of the 4.37 wt% Bi- MFC sheet at low magnification (x200).

(Andrews et al., 2018). Whereas in Fig. 7, we can observe that bismuth composites with a much lower loading of 0.072 wt% produced an 8 mm diameter zone of inhibition against the same bacteria. Based on the zones of inhibition, it can be inferred that the bismuth loaded nanocellulose composites have an equal or greater activity than similar composites loaded with silver-based

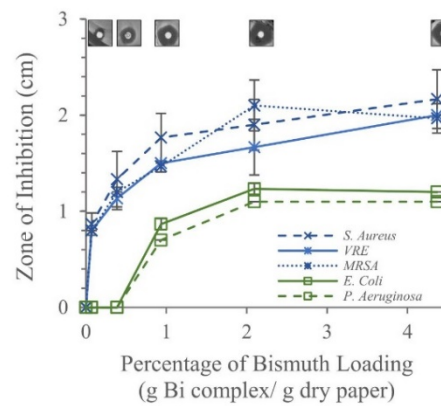


Fig. 7. Effect of bismuth complex loading on zone of inhibition with different bacteria from disk diffusion assay and the top images show their picture representation against *S. aureus*

**Table 2**  
Antifungal activity of the Bi-MFC composites determined by the zone of inhibition assay.

Percentage of bismuth loading (g Bi complex/g dry paper)		0	0.07	0.39	0.94	2.01	4.37	10.53
Test Fungus								
<i>S. pombe</i>		–	–	–	±	±	+	++
<i>S. cerevisiae</i>		–	–	–	+	++	++	++
<i>C. glabrata</i>		–	–	–	±	±	±	+
<i>C. albicans</i>		–	–	–	+	++	++	++
–	no inhibition							
±	not clear/inconclusive							
+	clear zone of 0.6–0.8 cm							
++	clear zone greater than 0.8 cm							

antibacterial agents.

3.2.2. Antifungal activity

It was found that the bismuth (III) phosphinato loaded composites were effective against several fungi species, including the pathogenic *C. glabrata* and *C. albicans*. The zone of inhibition on the fungal plates were similar in size to that observed for *P. aeruginosa* and *E.coli*, suggesting a lower level of inhibition but one that may still prove useful to control contamination of products inside the packaging. Table 2 shows the zones of inhibition of the composites against fungal species. Some of the fungal species were hard to grow evenly across the plate, which made visual assessment difficult, as shown in Figs. S6–S9 in the supplementary information. However, close examination and measurement of the halo allowed an objective comparison of the effect of the composite on all of the yeasts. Since the results for *C. glabrata* were inconclusive for all samples tested, further experiments were done with a higher composite loading of 10.53 wt% and a zone in the range 0.6 cm–0.8 cm was observed. On the other hand, for *C. albicans*, a zone of inhibition was observed even at the low loading of 0.94 wt%. Overall, this composite is shown to be effective not only on bacteria but also on some pathogenic fungi strains.

3.2.3. Duration of antimicrobial action

It was observed that the activity of the bismuth(III) phosphinato-MFC composites decreased with time for both 0.94 wt% and 4.37 wt% Bi-loaded samples, illustrated by the decreasing zone of inhibition with time in Fig. 8(a) and Fig. S10, which was performed in triplicates. The 0.94 wt% and 4.37 wt% loaded sheets remained active for 3 and 5 days respectively. Also, the zone of

inhibition was greater for the 4.37 wt% sheets at all times due to presence of higher amounts of active complex shown in Fig. 8(b). Exhausted composites were further analysed by ICP-OES, and the final bismuth content was found to be 0.15 wt% and 0.04 wt% (g of Bi-complex/g dry paper) for the 4.37 wt% and 0.94 wt% original composites respectively after 5 days of agar testing. Thus, the complex will eventually leach out of the composite to work on the bacteria when in contact with it, but remains securely held within the fibres while being transported or handled.

3.2.4. Physical and mechanical properties

The pure MFC sheet and all the composites are white and opaque, with no visible difference among them to the naked eye. Fig. 9 shows the physical appearance of the composites. The sheets are satisfactorily homogenous in terms of thickness and basis weight, as reported in Table S2 in the supplementary information. It was observed that the addition of the Bi-complex into MFC affects the mechanical strength of the sheets formed. The tensile index for the pure MFC sheet was found to be 76.5 ± 5.8 Nm/g. However, with only 0.07 wt% Bi-complex additive added to the composite, the tensile index dropped to 55.8 ± 1.0 Nm/g. On a higher loading of 4.37 wt%, the tensile index further dropped to 40.0 ± 1.5 Nm/g. These values are comparable to the mechanical strength of similar MFC sheets, which were reported to be in the range 45–104 Nm/g (Beneventi et al., 2016). Similar trends were observed for the Young's modulus, which were 8.4 ± 0.4 GPa, 7.6 ± 0.3 GPa and 5.4 ± 0.3 GPa for 0 wt%, 0.07 wt% and 4.37 wt% Bi-loaded composites, respectively. The Young's modulus of pure MFC has been reported by various researchers to be up to 6 GPa (Gabr et al., 2013). It can be suggested that the Bi-complex particles interferes with the

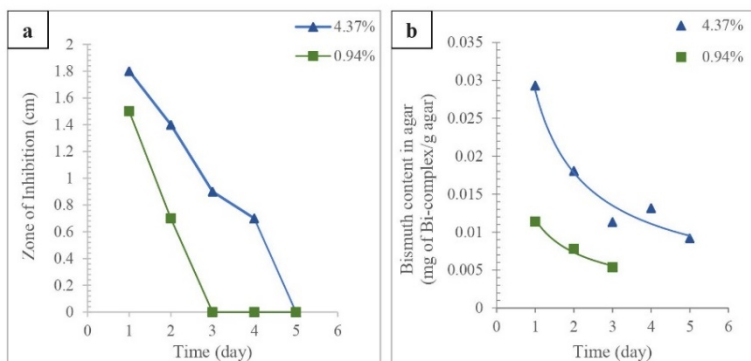


Fig. 8. (a) Zone of inhibition and (b) the amount of bismuth leached out into agar in the zone of inhibition for the 4.37 wt% and 0.94 wt% loaded bismuth sheets with time.

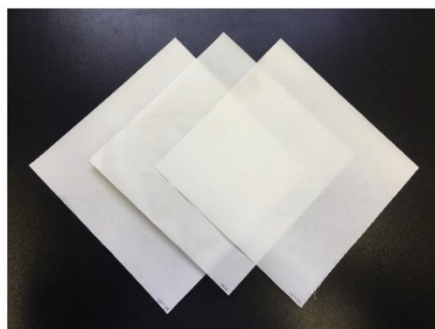


Fig. 9. Physical appearance of the 0.39 wt%, 0.94 wt% and 2.10 wt% bismuth (III) phosphinato-MFC sheets (left to right).

inter-fibre bonding, which has been recognised to directly impact the mechanical properties of such composites (Sehaqui et al., 2010). At higher loadings, any agglomerated hydrophobic cluster can thus result in poor bonding between the cellulose chains. A similar effect was reported for high loading of nanoclay in MFC composites (Gabr et al., 2013; Garusinghe et al., 2018).

The pore structure analysis was done, where the 2.10 wt% Bi-MFC composite was chosen as it was the closest to the pure MFC sheet in terms of grammage. Fig. 10 shows bimodal distribution of pore size in both the pure MFC sheet and the Bi-MFC composite. The modal pore size range did not seem to change much with the addition of bismuth complex. However, there seems to be significantly higher number of smaller pores as well as slightly more larger pores for the Bi-loaded composite than the pure MFC sheet, hence also explaining the rise in overall porosity reported in Table 3. The increased number of pores, along with the added surface from the bismuth particles, explains the rise in BET surface area for the Bi-MFC composite as reported in Table 3. The shape of the adsorption-desorption isotherm obtained from physisorption of nitrogen, in Fig. S16, also tells us the material has slit-shaped

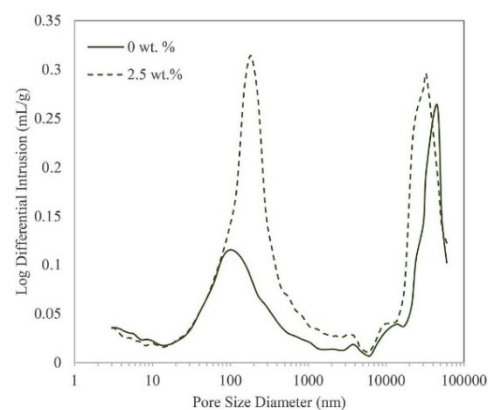


Fig. 10. Pore size distribution for pure MFC sheet and Bi-MFC composite.

Table 3  
Pore properties of the pure MFC sheet and Bi-MFC composite.

Property	Pure MFC	2.10 wt % Bi-MFC composite
Porosity (%)	19.3	28.9
Total intrusion volume (mL/g)	0.2357	0.3678
BET surface area (m <sup>2</sup> /g)	0.4112 ± 0.0011	0.7552 ± 0.0020

pores, rather than cylindrical ones, according to the IUPAC classification of porous materials (Allothman, 2012).

### 3.2.5. Water vapour permeability

Packaging materials must be able to act as a barrier to the entry of water vapour in order to protect packaged goods from contamination and degradation. Molecule migration across a polymer film depends on the adsorption and desorption ability of the molecule on the surface and particularly on the rate of molecule diffusion across the film (Nair et al., 2014). The dense network of the microfibrillated cellulose fibres creates small pores across the surface of the MFC sheets and increases the mean free path that the water molecule has to travel to reach the other end, i.e. it increases the tortuosity of travel as compared to normal cellulose.

However, with addition of the bismuth complex, the WVP was observed to increase slightly as shown in Fig. 11. The SEM images and EDX mapping confirmed the even distribution of the complex throughout the material, with evidence of them being distributed under the surface. It was also observed that the particles were large, with the largest observed dimension of 13 μm. It can be proposed that arrangement of some of the particles with its largest dimension parallel to the diffusion pathway allowed water vapour molecules to follow a more direct path rather than a tortuous path. This resulted in minor reductions in the WVP performance. Increasing the loading from 0.07 wt% to 2.10 wt % did not significantly alter WVP performance. Surprisingly, increasing the loading to 4.37 wt% showed a significant increase. It can be proposed that beyond a certain loading, the particles become interconnected due to aggregation of the hydrophobic complexes. It is possible that at this point the percolation threshold might have been reached, creating a conducting pathway that increases the WVP. It has been reported

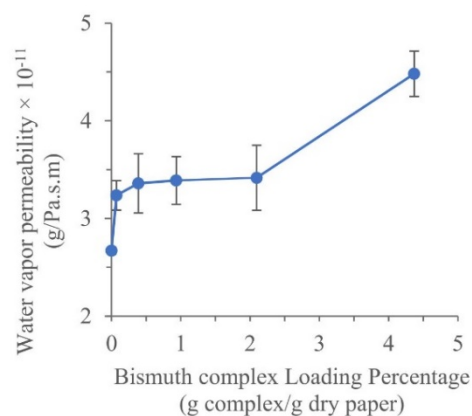


Fig. 11. Effect of bismuth complex loading on the water vapour permeability of the phenyl bismuth bis(diphenylphosphinato) functionalized MFC.

**Table 4**  
Literature comparison of WVP of common packaging materials with Bi-MFC composites.

Film	WVP $\times 10^{-11}$ (g/m.Pas)	Relative Humidity (%)	Temperature (°C)	Reference
<i>Experimental sheets</i>				
Pure MFC sheet	2.67	0–50%	23	–
Bi-MFC composites	3.23–4.48	0–50%	23	–
<i>Synthetic Films</i>				
HDPE	0.002	0–100	27.6	Bourlieu et al. (2009)
LDPE	0.014	–	27.6	
PP	0.010	–	25	
PVC	0.041	–	27.6	
PSs	0.5	0–100	25	(Aulin and Lindstrom)
<i>Biobased Films</i>				
Cellulose derivatives	9.2–11	0–85%	21	Park and Chinnan (1995)
Chitosan	13	76.2	25	Rhim and Ng (2007)

that diffusion across a material with embedded tubular particles increases with an increase in concentration of the particles within, and the most significant change occurs near the percolation threshold (Grekhov et al., 2013; Likhomanova et al., 2015). The barrier properties are dependent on a number of factors, which include the size and shape of the additive agent, its distribution as well as the total amount present in the structure (Garusinghe et al., 2018). All these parameters have been studied to support the hypothesis. However, the effect of the complex was very minor and permeability was still in the range of  $10^{-11}$  when compared to the WVP of commercial plastic based packaging materials, which are within  $10^{-12}$  to  $10^{-13}$  range (Aulin and Lindstrom, Bourlieu, Guillard et al., 2009).

Table 4 compares the values of WVP for various packaging materials. The published data were obtained using different testing conditions and so are not exactly comparable to our values without considering the relative humidity and temperature. A higher relative humidity gives higher permeability values for a test sample. However, these values provide an indication of the Bi-MFC sheets performance with respect to commercial packaging materials. The WVP values of the bismuth-based sheets are not as low as those for synthetic films, but further modifications may be possible to arrive at similar performance levels. Additionally, of course, the bismuth-impregnated material has the advantage of being antimicrobial against some of the medically important microorganisms. However, to be used as a packaging material for food packaging applications in particular, further investigation with food pathogens will be required. Moreover, the antimicrobial additive will get used up during its application, thereby losing its effectiveness over time and ensuring that the material is recyclable and biodegradable. The biodegradability and renewability of nanocellulose further makes this material a sustainable and eco-friendly product that not only safeguards public health but also protects the environment throughout its life cycle.

This material can be the answer to a number of environmental issues from a broad cleaner production perception. It has the antimicrobial and barrier properties for use as a packaging material along with

- being a safer alternative to silver-based material, addressing all the issues of overuse of silver, viz. environmental accumulation, cytotoxicity and induction of resistance in bacteria
- while using a biodegradable and renewable natural polymer as the matrix

#### 4. Conclusion

The study investigated the preparation of bismuth-based nanocellulose composites on a laboratory scale using a spraying

system for the development of a biodegradable and renewable active packaging material. The composites prepared in this study have antimicrobial properties against some of the most medically-important bacteria and fungi, along with the virtue of having activity at relatively low loadings. There is a clear dose effect on the performance of these sheets. In addition, the composites have reasonable barrier performance against water vapour, with the bismuth complex not having any significant effect on the barrier performance unless present at relatively high levels. The physical and mechanical properties are also affected by the addition of the complex, but were still in expected range within the scope of study. Bismuth-based nanocellulose composites have potential to serve as a cleaner antimicrobial barrier material and can potentially replace silver-based packaging material. However, a proper understanding of the loading and its corresponding material properties needs to be fully understood, and this paper provides a fair direction for doing so.

#### Acknowledgements

We would like to thank Kirubanandan Shanmugam (BioPRIA) for assistance with sheet preparation. The authors thank Monash University and The National Health and Medical Research Council (APP1139844) for financial support. The authors would like to acknowledge the use of the facilities in the Monash Centre for Electron Microscopy. Maisha Maliha and Megan Herdman would like to acknowledge the Australian Government for the Research Training Program (RTP) Scholarship.

#### Appendix A. Supplementary data

Supplementary data to this article can be found online at <https://doi.org/10.1016/j.jclepro.2019.119016>.

#### References

- E96/E96M-16, 2016. A Standard Test Methods for Water Vapor Transmission of Materials. ASTM International West, Conshohocken, PA.
- Abd-El-Aziz, A.S., Agatemor, C., Etkin, N., 2017. Antimicrobial resistance challenged with metal-based antimicrobial macromolecules. *Biomaterials* 118, 27–50.
- Alotman, Z., 2012. A review: fundamental aspects of silicate mesoporous materials. *Materials* 5 (12), 2874–2902.
- Alvarez-Paino, M., Munoz-Bonilla, A., Fernandez-Garcia, M., 2017. Antimicrobial polymers in the nano-world. *Nanomaterials (Basel)* 7 (2).
- Amini, E., Azadfallah, M., Layeghi, M., Talaei-Hassanloui, R., 2016. Silver-nanoparticle-impregnated cellulose nanofiber coating for packaging paper. *Cellulose* 23 (1), 557–570.
- Andrews, P.C., Werrett, M., Herdman, M., Brammananth, R., Garusinghe, U., Batchelor, W., Crellin, P., Coppel, R., 2018. In: Bismuth Phosphinates in Bionanocellulose Composites and Their Efficacy towards Multi-Drug Resistant Bacteria. Chemistry, Weinheim an der Bergstrasse, Germany.
- Appendini, P., Hotchkiss, J.H., 2002. Review of antimicrobial food packaging. *Innov. Food Sci. Emerg. Technol.* 3 (2), 113–126.

- Aulin, C. and T. Lindstrom Biopolymer Coatings for Paper and Paperboard. *Biopolymers – New Materials for Sustainable Films and Coatings*.
- Barros-Velázquez, J. *Industrial Applications: Regulatory Issues and Life Cycle Assessment of Food Packaging*. Antimicrobial Food Packaging, Elsevier.
- Barry, N.P.E., Sadler, P.J., 2013. Exploration of the medical periodic table: towards new targets. *Chem. Commun.* 49 (45), 5106–5131.
- Beneventi, D., Chaussy, D., Curti, D., Zolin, L., Gerbaldi, C., Penazzi, N., 2014. Highly porous paper loading with microfibrillated cellulose by spray coating on wet substrates. *Ind. Eng. Chem. Res.* 53 (27), 10982–10989.
- Beneventi, D., Zeno, E., Chaussy, D., 2016. Rapid nanopaper production by spray deposition of concentrated microfibrillated cellulose slurries. *ATIP. Association Technique de L'Industrie Papetière* 70 (2), 6–14.
- Bourlieu, C., Guillard, V., Vallès-Pamiès, B., Guilbert, S., Gontard, N., 2009. Edible moisture barriers: how to assess of their potential and limits in food products shelf-life extension? *Crit. Rev. Food Sci. Nutr.* 49 (5), 474–499.
- Briand, G.G., Burford, N., 1999. Bismuth compounds and preparations with biological or medicinal relevance. *Chem. Rev.* 99 (9), 2601–2658.
- Cao, H., 2017. *Silver Nanoparticles for Antibacterial Devices : Biocompatibility and Toxicity*. CRC Press, Taylor & Francis Group, Boca Raton.
- Carbone, M., Donia, D.T., Sabbatella, G., Antiochia, R., 2016. Silver nanoparticles in polymeric matrices for fresh food packaging. *J. King Saud Univ. Sci.* 28 (4), 273–279.
- Crocetti, G., 2013. Save the nano-silver for where it's needed. *Chain-reaction* 117, 16.
- Cushen, M., Kerry, J., Morris, M., Cruz-Romero, M., Cummins, E., 2012. Nanotechnologies in the food industry – recent developments, risks and regulation. *Trends Food Sci. Technol.* 24 (1), 30–46.
- Dankovich, T.A., Gray, D.G., 2011. Bactericidal paper impregnated with silver nanoparticles for point-of-use water treatment. *Environ. Sci. Technol.* 45 (5), 1992–1998.
- Dizaj, S.M., Lotfipour, F., Barzegar-Jalali, M., Zarrintan, M.H., Adibkia, K., 2014. Antimicrobial activity of the metals and metal oxide nanoparticles. *Mater. Sci. Eng. C* 44, 278–284.
- Domenico, P., Baldassarri, L., Schoch, P.E., Kaehler, K., Sasatsu, M., Cunha, B.A., 2001. Activities of bismuth thiols against staphylococci and staphylococcal biofilms. *Antimicrob. Agents Chemother.* 45 (5), 1417.
- Drake, P.L., Hazelwood, K.J., 2005. Exposure-related health effects of silver and silver compounds: a review. *Ann. Occup. Hyg.* 49 (7), 575–585.
- Echegeyev, Y., Nerin, C., 2013. Nanoparticle release from nano-silver antimicrobial food containers. *Food Chem. Toxicol.* 62, 16–22.
- Fey, P.D., Olson, M.E., 2010. Current concepts in biofilm formation of *Staphylococcus epidermidis*. *Future Microbiol.* 5 (6), 917–933.
- Fidel Jr., P.L., Vazquez, J.A., Sobel, J.D., 1999. *Candida glabrata*: review of epidemiology, pathogenesis, and clinical disease with comparison to *C. albicans*. *Clin. Microbiol. Rev.* 12 (1), 80–96.
- Gabr, M.H., Phong, N.T., Abdelkareem, M.A., Okubo, K., Uzawa, K., Kimpara, I., Fujii, T., 2013. Mechanical, thermal, and moisture absorption properties of nano-clay reinforced nano-cellulose biocomposites. *Cellulose* 20 (2), 819–826.
- Garusinghe, U.M., Varanasi, S., Raghuvanshi, V.S., Garnier, G., Batchelor, W., 2018. Nanocellulose-montmorillonite composites of low water vapour permeability. *Colloid. Surf. Physicochem. Eng. Asp.* 540, 233–241.
- Grekhov, A.M., Eremin, Y.S., Dibrov, G.A., Volkov, V.V., 2013. Percolation of composite poly(vinyltrimethylsilane) membranes with carbon nanotubes. *Pet. Chem.* 53 (8), 549–553.
- Gunawan, C., Marquis, C.P., Amal, R., Sotiriou, G.A., Rice, S.A., Harry, E.J., 2017. Widespread and indiscriminate nanosilver use: genuine potential for microbial resistance. *ACS Nano* 11 (4), 3438.
- Haider, A., Kang, I.K., 2015. Preparation of silver nanoparticles and their industrial and biomedical applications: a comprehensive review. *Adv. Mater. Sci. Eng.* 2015, 1–16.
- Hua, X., Yuan, X., Mitchell, B.M., Lorenz, M.C., O'Day, D.M., Wilhelmus, K.R., 2009. Morphogenic and genetic differences between *Candida albicans* strains are associated with keratomycosis virulence. *Mol. Vis.* 15, 1476–1484.
- Huang, Y., Chen, S., Bing, X., Gao, C., Wang, T., Yuan, B., 2011. Nanosilver migrated into food-simulating solutions from commercially available food fresh containers. *Packag. Technol. Sci.* 24 (5), 291–297.
- Huang, J.-Y., Li, X., Zhou, W., 2015. Safety assessment of nanocomposite for food packaging application. *Trends Food Sci. Technol.* 45 (2), 187–199.
- Inamuddin, 2016. *Green Polymer Composites Technology : Properties and Applications*. Chapman and Hall/CRC, Boca Raton, UNITED KINGDOM.
- Kawashima, S.A., Takemoto, A., Nurse, P., Kapoor, T.M., 2012. Analyzing fission yeast multidrug resistance mechanisms to develop a genetically tractable model system for chemical biology. *Chem. Biol.* 19 (7), 893–901.
- Keogan, D., Griffith, D., 2014. Current and potential applications of bismuth-based drugs. *Molecules* 19 (9), 15258.
- Klemm, D., Heublein, B., Fink, H.-P., Bohn, A., 2005. Cellulose: fascinating biopolymer and sustainable raw material. *Angew. Chem. Int. Ed.* 44 (22), 3358–3393.
- Klemm, D., Kramer, F., Moritz, S., Lindström, T., Ankerlors, M., Gray, D., Dorris, A., 2011. Nanocelluloses: a new family of nature-based materials. *Angew. Chem. Int. Ed.* 50 (24), 5438–5466.
- Kotani, T., Nagai, D., Asahi, K., Suzuki, H., Yamao, F., Kataoka, N., Yagura, T., 2005. Antibacterial properties of some cyclic organobismuth(III) compounds. *Antimicrob. Agents Chemother.* 49 (7), 2729.
- Krol, L.F., Beneventi, D., Alloin, F., Chaussy, D., 2015. Microfibrillated cellulose-SiO<sub>2</sub> composite nanopapers produced by spray deposition. *J. Mater. Sci.* 50 (11), 4095–4103.
- Kumar, V., Bollström, R., Yang, A., Chen, Q., Chen, G., Salminen, P., Bousfield, D., Toivakka, M., 2014. Comparison of nano- and microfibrillated cellulose films. *Cellulose* 21 (5), 3443–3456.
- Kumar, V., Koppolu, V.R., Bousfield, D., Toivakka, M., 2017. Substrate role in coating of microfibrillated cellulose suspensions. *Cellulose* 24 (3), 1247–1260.
- Lavoine, N., Desloges, I., Dufresne, A., Bras, J., 2012. Microfibrillated cellulose - its barrier properties and applications in cellulosic materials: a review. *Carbohydr. Polym.* 90 (2), 735–764.
- Lavoine, N., Desloges, I., Manship, B., Bras, J., 2015. Antibacterial paperboard packaging using microfibrillated cellulose. *J. Food Sci. Technol.* 52 (9), 5590–5600.
- Lavoine, N., Guillard, V., Desloges, I., Gontard, N., Bras, J., 2016. Active bio-based food-packaging: diffusion and release of active substances through and from cellulose nanofiber coating toward food-packaging design. *Carbohydr. Polym.* 149, 40–50.
- Lemire, J.A., Harrison, J.J., Turner, R.J., 2013. Antimicrobial activity of metals: mechanisms, molecular targets and applications. *Nat. Rev. Microbiol.* 11, 371.
- Likhomanova, P.A., Tronin, I.V., Grekhov, A.M., Eremin, Y.S., 2015. Modeling of particle diffusion in heterogeneous structure near to the percolation threshold. *Physics Procedia* 72, 42–46.
- Lin, N., Dufresne, A., 2014. Nanocellulose in biomedicine: current status and future prospect. *Eur. Polym. J.* 59, 302–325.
- Loh, J.V., Percival, S.L., Woods, E.J., Williams, N.J., Cochrane, C.A., 2009. Silver resistance in MRSA isolated from wound and nasal sources in humans and animals. *Int. Wound J.* 6 (1), 32–38.
- Luqman, A., Blair, V.L., Brammananth, R., Crellin, P.K., Coppel, R.L., Andrews, P.C., 2016. The importance of heterolepticity in improving the antibacterial activity of bismuth(III) thiolates. *Eur. J. Inorg. Chem.* 2016 (17), 2738–2749.
- Maillard, J.-Y., Hartemann, P., 2013. Silver as an antimicrobial: facts and gaps in knowledge. *Crit. Rev. Microbiol.* 39 (4), 373–383.
- Martinez-Abad, A., Lagaron, J.M., Ocio, M.J., 2012. Development and characterization of silver-based antimicrobial ethylene-vinyl alcohol copolymer (EVOH) films for food-packaging applications. *J. Agric. Food Chem.* 60 (21), 5350–5359.
- Nair, S.S., Zhu, J., Deng, Y., Ragauskas, A.J., 2014. High performance green barriers based on nanocellulose. *Sustain. Chem. Process.* 2 (1), 23.
- O'Sullivan, A.C., 1997. Cellulose: the structure slowly unravels. *Cellulose* 4 (3), 173–207.
- Pal, C., Bengtsson-Palme, J., Rensing, C., Kristiansson, E., Larsson, D.G.J., 2014. BacMet: antibacterial biocide and metal resistance genes database. *Nucleic Acids Res.* 42 (Database issue), D737.
- Park, H.J., Chinnan, M.S., 1995. Gas and water vapor barrier properties of edible films from protein and cellulosic materials. *J. Food Eng.* 25 (4), 497–507.
- Patra, M., Gasser, G., Metzler-Nolte, N., 2012. Small organometallic compounds as antibacterial agents. *Dalton Trans.* 41 (21), 6350–6358.
- Pereira De Abreu, D.A., Cruz, J.M., Paseiro Losada, P., 2012. Active and intelligent packaging for the food industry. *Food Rev. Int.* 28 (2), 146–187.
- Pezzuto, A., Losasso, C., Mancini, M., Gallochio, F., Piovesana, A., Binato, G., Gallina, A., Marangon, A., Mioni, R., Favretti, M., Ricci, A., 2015. Food safety concerns deriving from the use of silver based food packaging materials. *Front. Microbiol.* 6, 1109–1109.
- Rhim, J.-W., Ng, P.K.W., 2007. Natural biopolymer-based nanocomposite films for packaging applications. *Crit. Rev. Food Sci. Nutr.* 47 (4), 411–433.
- Sehaqui, H., Liu, A., Zhou, Q., Berglund, L.A., 2010. Fast preparation procedure for large, flat cellulose and cellulose/inorganic nanocomposite structures. *Biomacromolecules* 11 (9), 2195–2198.
- Shanmugam, K., Varanasi, S., Garnier, G., Batchelor, W., 2017. Rapid preparation of smooth nanocellulose films using spray coating. (Report/Author abstract). *Cellulose* 24 (7), 2669.
- Silver, S., 2003. Bacterial silver resistance: molecular biology and uses and misuses of silver compounds. *FEMS (Fed. Eur. Microbiol. Soc.) Microbiol. Rev.* 27 (2), 341–353.
- Siró, I., Plackett, D., 2010. Microfibrillated cellulose and new nanocomposite materials: a review. *Cellulose* 17 (3), 459–494.
- Stensberg, M.C., Wei, Q., McLamore, E.S., Porterfield, D.M., Wei, A., Sepulveda, M.S., 2011. Toxicological studies on silver nanoparticles: challenges and opportunities in assessment, monitoring and imaging. *Nanomedicine* 6 (5), 879–898.
- Suzuki, H., Matano, Y., Matano, Y., 2001. Chapter 1 - Introduction A2 - Suzuki, Hitomi. *Organobismuth Chemistry*. Elsevier Science, Amsterdam, pp. 1–20.
- Svoboda, T., Jambor, R., Ruzicka, A., Padelkova, Z., Erben, M., Dostal, L., 2010. NCN chelated organoantimony(III) and organobismuth(III) phosphinates and phosphites: synthesis, structure and reactivity. *Eur. J. Inorg. Chem.* 2010 (33), 5222–5230.
- Tegos, G., Stermitz, F.R., Lomovskaya, O., Lewis, K., 2002. Multidrug pump inhibitors uncover remarkable activity of plant antimicrobials. *Antimicrob. Agents Chemother.* 46 (10), 3133.
- Varanasi, S., Batchelor, W.J., 2013. Rapid preparation of cellulose nanofiber sheet. *Cellulose* 20 (1), 211–215.
- Varanasi, S., Chiam, H., Batchelor, W., 2012. Application and interpretation of zero and short-span testing on nanofiber sheet materials. *Nord. Pulp Pap. Res. J.* 27 (2), 343–351.
- Wu, J., Zheng, Y., Song, W., Luan, J., Wen, X., Wu, Z., Chen, X., Wang, Q., Guo, S., 2014. In situ synthesis of silver-nanoparticles/bacterial cellulose composites for slow-released antimicrobial wound dressing. *Carbohydr. Polym.* 102, 762.
- Xiong, Z.C., Zhu, Y.J., Chen, F.F., Sun, T.W., Shen, Y.Q., 2016. One-step synthesis of silver nanoparticle-decorated hydroxyapatite nanowires for the construction of

highly flexible free-standing paper with high antibacterial activity. *Chemistry* 22 (32), 11224–11231.

Xu, Q., Chen, C., Rosswurm, K., Yao, T., Janaswamy, S., 2016. A facile route to prepare cellulose-based films. *Carbohydr. Polym.* 149, 274–281.

Yan, J., Abdelgawad, A.M., El-Naggar, M.E., Rojas, O.J., 2016. Antibacterial activity of silver nanoparticles synthesized in-situ by solution spraying onto cellulose. *Carbohydr. Polym.* 147, 500–508.

Cellulose  
<https://doi.org/10.1007/s10570-021-03835-5>



ORIGINAL RESEARCH

## Biocompatibility and selective antibacterial activity of a bismuth phosphinato-nanocellulose hydrogel

Maisha Maliha · Rajini Brammananth · Jennifer Dyson · Ross L. Coppel ·  
Melissa Werrett · Philip C. Andrews · Warren Batchelor

Received: 9 November 2020 / Accepted: 16 March 2021  
© The Author(s), under exclusive licence to Springer Nature B.V. 2021

**Abstract** Antimicrobial hydrogels are of immense value in wound care applications. However, the rapid rise of antimicrobial resistance has made it necessary to look for new antimicrobial additives for such materials. In this study, a novel antimicrobial hydrogel for wound care applications has been developed. The material combines TEMPO-oxidized nanocellulose hydrogel with a new class of antimicrobial agent, phenyl *bis*-phosphinato bismuth (III) complex. The hydrogel was characterized using scanning electron microscope imaging to show the overall distribution of the complex particles within the nanocellulose hydrogel matrix phase. The rheological properties of the bismuth loaded hydrogel are comparable to commercial over-the-counter burn hydrogels and behave like

true gels. Activity of the different concentrations of the complex was studied against a range of medically important bacteria and mammalian fibroblast cells. Bismuth complex target loading of 9 µg/g showed bactericidal activity against *Acinetobacter baumannii* and *Pseudomonas aeruginosa* and bacteriostatic effect against MRSA and VRE, while having no toxic effect on mammalian fibroblast cells. However, *Escherichia coli* was less susceptible to this concentration comparatively. Our study has identified a range of bismuth complex loading levels for the material at which the additive appears to be safe and active. This study is a step towards the design of a biocompatible and renewable hydrogel containing a safe antimicrobial additive, which has an excellent safety margin to pathogenic bacteria over mammalian cells and would appear to be a promising material for active wound dressing applications.

**Supplementary Information** The online version contains supplementary material available at <https://doi.org/10.1007/s10570-021-03835-5>.

M. Maliha · W. Batchelor (✉)  
Department of Chemical Engineering, Bioresource  
Processing Research Institute of Australia (BioPRIA),  
Monash University, Clayton, VIC 3800, Australia  
e-mail: warren.batchelor@monash.edu

R. Brammananth · R. L. Coppel  
Department of Microbiology, Monash University,  
Clayton, VIC 3800, Australia

J. Dyson  
Monash Institute of Medical Engineering (MIME),  
Monash University, Clayton, VIC 3800, Australia

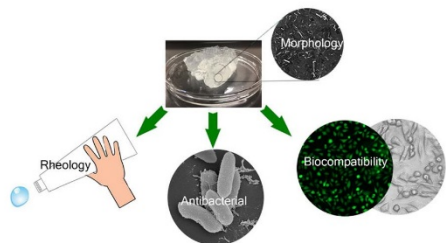
J. Dyson  
Department of Biochemistry and Molecular Biology,  
Monash Biomedicine Discovery Institute, Monash  
University, Clayton, VIC 3800, Australia

M. Werrett · P. C. Andrews  
School of Chemistry, Monash University, Clayton,  
VIC 3800, Australia

M. Werrett · P. C. Andrews  
Centre To Impact AMR, Monash University, Clayton,  
VIC 3800, Australia

Published online: 29 March 2021

Springer

**Graphic abstract**

**Keywords** Nanocellulose · Bismuth · Hydrogel · Antibacterial · Fibroblasts · In-vitro cytotoxicity

**Introduction**

Skin is the largest organ of the human body, protecting all internal organs. Trauma to the skin breaches this protective layer and exposes internal structures to the risk of infection and other forms of damage. The repair of skin in which the integrity of this layer is restored involves three phases: inflammation, proliferation of various cell types, and tissue remodeling. The initial inflammatory phase involves the action of preformed proteins and resident and migratory cells to sterilise the area of the wound in preparation for a proliferative phase in which subcutaneous and dermal cells proliferate to generate new skin layers including new blood vessels. Finally, the newly generated tissues are remodeled to regenerate the various layers of the skin and to integrate with the pre-existing tissues on either side of the wound. Disruption in any one phase of repair can jeopardise the satisfactory completion of the process (Agyingi et al. 2010). A large number of factors including infection can affect wound healing and control of infection is a pre-requisite for satisfactory wound healing (Caló and Khutoryanskiy 2015; Jones et al. 2006). Bacterial infection in burn wounds complicates their management and in the worst cases can lead to the death of patient (Rattanaeuengsrikul et al. 2009). Technologies to deal with wound management include artificial skin for grafting, aids to skin regeneration and wound closure, and infection control by various exogenous materials and dressings (Ashtikar and Wacker 2018). A large number of

wound dressings have been developed, both from natural and synthetic materials (Hakkarainen et al. 2016). Active wound dressings that deliver drugs or contains antibacterial agents are commonly used to minimise risk of infection (Rattanaeuengsrikul et al. 2009). Bacteria are constantly evolving and developing increased resistance to antibiotics and disinfectants and appropriate dressings need to be developed to account for this. In addition, wound dressing materials need to be biocompatible and non-toxic to host cells (Basu et al. 2018).

Hydrogel-based wound dressings are some of the most promising materials for wound care and healing due to their “tissue-like” structure and excellent biocompatibility (Kamoun 2017). The frequency of application of hydrogels in wound dressings has increased due to its ability to provide a moist environment to assist in the wound healing process (Rattanaeuengsrikul et al. 2009). Moisture helps with dermis repair and removal of dead cells, thus aiding in healing. Moreover, the moisture provides a cooling effect on the wound, reducing pain. Pain is also reduced due to the non-adherent nature of hydrogels preventing sticking to the wound when dressings are removed (Basu et al. 2017). Hydrogels have the ability to absorb the wound exudates and are also permeable to oxygen, making the properties of hydrogels further advantageous for wound dressing (Singh and Singh 2012).

Hydrogels are three-dimensional structures of crosslinked polymers. For biomedical applications, physically cross-linked hydrogels are preferred as they avoid the use of chemical crosslinking agents or organic solvents, thus minimizing the risks and toxicity associated with those (Kamoun 2017). One such material is nanocellulose hydrogel, which is crosslinked by hydrogen bonding and is a promising material for biomedical applications (De France et al. 2017). The surface chemistry of nanocellulose has been studied and reported to be suitable for wound dressing applications (Chinga-Carrasco and Syverud 2014). Cellulose-based hydrogels studied for wound dressing applications are usually bacterial cellulose. Nanocellulose-based wound care products, such as Biofill, Gengiflex and XCell, are also based on bacterial cellulose (BC) (Czaja et al. 2006; Laçin 2014). Bacterial cellulose (BC) and wood-based cellulose has the same chemical structure with the same sugar molecule forming the polymer. However,

## Cellulose

BC is a weak hydrogel and is hard to modify to other forms (Hakkarainen et al. 2016), and the large scale production of bacterial cellulose remains a challenge (Czaja et al. 2006). There has been limited research exploring the application of wood-based nanocellulose in wound dressings. Hakkarainen, Koivuniemi et al. studied the use of wood-based nanocellulose as wound dressing for burns in patients (Hakkarainen et al. 2016), leading to the first wood-based nanocellulose hydrogel, recently launched to the European market as a wound care product by UPM-Kymmene Corporation (Finland: UPM's FibDex, a wood-based innovation for wound care, receives regulatory approval and CE mark 2019). Of relevance to this study, the effect of antimicrobials combined with wood-based nanocellulose hydrogels is yet to be investigated.

In this study, wood-based nanocellulose hydrogel incorporating a metal-based antimicrobial agent has been studied. Silver nanoparticles and silver-based compounds are common antimicrobial additives used for wound dressing applications. These have been studied as antimicrobial agents in hydrogels assembled with both synthetic polymers (Abou-Yousef and Kamel 2015; Bardajee et al. 2012; González-Sánchez et al. 2015; Resmi et al. 2017; Singh and Singh 2012; Thomas et al. 2007; Tyliszczak et al. 2017; Valle et al. 2014) and natural polymers (Babu et al. 2010; Hebeish et al. 2013; Rattanaeuengsrikul et al. 2009). Bacterial cellulose hydrogel has also been impregnated with silver nanoparticles and the material displays antibacterial activity against both Gram-positive and Gram-negative bacteria (Maneerung et al. 2008). However, due to the overuse of silver in a large number of products, bacterial resistance towards silver has become a major concern (Gunawan et al. 2017; Maillard and Hartemann 2013; Silver 2003). It has also been reported that silver compounds, such as silver nitrate and the most commonly used silver sulfadiazine, can have a toxic effect in the human body (Restuccia et al. 2016; Maillard and Hartemann 2013; Rattanaeuengsrikul et al. 2009; Stensberg et al. 2011). Furthermore, there are concerns about a build-up of silver in the environment and a desire to restrict its widespread use because of toxicity to various organisms, including humans (Werrett et al. 2018).

Researchers have shown that bismuth compounds and complexes possess antibacterial activity (Domenico et al. 2001; Kotani et al. 2005; Luqman et al.

2016; Svoboda et al. 2010; Werrett et al. 2018). In addition, bismuth compounds, such as bismuth *subsalicylate* (Pepto-Bismol) and colloidal bismuth subcitrate (De-Nol) have been used for treating gastrointestinal disorders (Barry and Sadler 2013; Briand and Burford 1999; Suzuki and Matano 2001). Moreover, bismuth and its compounds, unlike other heavy metals, are low in toxicity (Kotani et al. 2005) (Suzuki and Matano 2001). In this study, a Bi (III) complex with phosphinate ligands,  $\text{BiPh}(\text{OP}(=\text{O})\text{Ph}_2)_2$  is studied as an additive to a wound dressing hydrogel. While the antibacterial activity of this hydrophobic complex (Werrett et al. 2018) as well as the production of bismuth-nanocellulose composite sheets as an antimicrobial packaging material (Maliha et al. 2019) has been previously studied, the suitability of its incorporation into a hydrogel matrix for wound healing purposes is not known.

The aim of this study is to combine the new organobismuth complex, phenyl bismuth *bis*(diphenylphosphinato), into a nanocellulose hydrogel matrix to impart antibacterial properties to the hydrogel. The antibacterial properties of the hydrogel towards some of the medically important bacteria that commonly infect wounds has been studied. The rheological properties of the hydrogel were investigated and compared to commonly used commercial burn hydrogels. Moreover, biocompatibility of the hydrogel with mammalian fibroblast cells was studied to understand the overall safety of the composite.

## Materials and methods

### Chemicals and materials

Bleached Eucalyptus Kraft (BEK) pulp was obtained from Australian paper, Maryvale. 2,2,6,6-Tetramethylpiperidine-1-oxyl (TEMPO) and NaBr were obtained from Sigma-Aldrich. 12 w/v% Sodium hypochlorite (NaOCl) was purchased from Thermo Fisher Scientific. Triphenyl bismuth ( $\text{BiPh}_3$ ) was prepared using the standard Grignard method (Barton et al. 1986) and diphenyl phosphinic acid was purchased from Sigma-Aldrich. NaOH and HCl were purchased from Merck and Univar, and diluted as required. Dulbecco's modified Eagle medium (DMEM) was purchased from Gibco. MTS reagent

was purchased from Promega, Australia. Calcein, AM and Propidium iodide was obtained from Life technologies, Australia.

#### Preparation method

##### *Bismuth complex synthesis*

Phenyl bismuth *bis*(diphenylphosphinato) was prepared according to Andrews et al. (Werrett et al. 2018). Triphenyl bismuth and diphenyl phosphinic acid were mixed in the ratio of 1:2 in ethanol and heated at reflux for 24 h. The reaction mixture was then filtered, and the insoluble phenyl bismuth *bis*(diphenylphosphinato) was isolated as a white powder.

##### *Preparation of bi-nanocellulose hydrogel*

BEK pulp was oxidised by TEMPO-mediated oxidation as described by Isogai et al. (Saito et al. 2007). TEMPO (0.4 g) and NaBr (2.5 g) were mixed with water to which a suspension containing 25 dry grams of BEK pulp was added. This 3 L reaction mixture was initiated using 75 mL NaOCl added dropwise while being continuously stirred using an overhead stirrer. The NaOCl was pre-adjusted to pH 10 using 36% HCl. The reaction mixture was also maintained at pH 10 through the dropwise addition of 0.5 M NaOH. The oxidation was carried out for 2 h. The oxidised fibres were then dewatered and washed several times using vacuum filtration. The TEMPO-oxidised cellulose nanofibres thus obtained were then dispersed in deionised water to a concentration of 2 wt% and passed through the high-pressure homogeniser (GEA Niro Soavi Homogeniser Panda) at 1000 bar with one pass. Fibres produced similarly have been reported to have diameters in the range of 3–4 nm (Fukuzumi et al. 2009).

The desired mass of bismuth complex was dispersed in DI water using a dispermat at a speed of 6000 rpm for 15–25 min to ensure uniform dispersing of the complex. The dispersion was mixed with the 2 wt% nanocellulose (NC) hydrogels in 1:1 ratio and dispersed using the dispermat at 4000 rpm for 5 min. The Bi-NC hydrogel thus obtained had 0.1 wt% bismuth complex with respect to mass of hydrogel and was stored at 4 °C for further analysis. Blank hydrogel

was prepared by mixing 2 wt% hydrogel with DI water in 1:1 ratio.

#### Morphology

The bismuth distribution in the hydrogel was analysed using Scanning Electron Microscope (SEM) imaging. The hydrogel was air-dried on a silicon chip secured using carbon tape. The hydrogel film was coated with a thin conducting layer of iridium. SEM imaging was done using the FEI Magellan 400 FEG SEM using an accelerating voltage of 5 keV and spot size 2.

#### Rheology

Rheological tests were done using Anton Paar MCR302 rheometer with the 1-degree cone and plate geometry. The analysis was done at 25 °C. Oscillatory strain sweep was performed at a constant frequency of 1 Hz at shear strains ranging from 0.01 to 100%.

#### In-vitro biocompatibility

##### *Cytotoxicity assay*

The cytotoxicity assay was performed according to modified ISO 10993-5. Mouse fibroblast L929 cells were cultured in Dulbecco's Modified Eagle's Medium (DMEM) containing 10% (v/v) fetal bovine serum (FBS) and 1% antibiotics (penicillin, streptomycin) in a humidified incubator at 37 °C and 5% CO<sub>2</sub>. 10,000 cells/well were seeded into 96 well plates in DMEM medium and incubated for 24 ± 1 h to form a monolayer. The media was removed and cells washed with PBS. Fresh media mixed with the hydrogel samples was incubated with the cells. The 0.1 wt% hydrogel (containing 1000 µg Bi-complex/g hydrogel) was first dispersed in DMEM to contain 20 wt% hydrogel using a vortex mixture. This mixture was pipetted to further ensure homogenous distribution and then serially diluted with DMEM to test concentrations of 100, 50, 25, 12, 9, 6, 3, and 1 µg/g of the bismuth complex (rounded to the nearest whole number). The control cells were incubated with either fresh DMEM (negative control) or fresh DMEM containing 10% dimethyl sulfoxide (DMSO) to induce cell death (positive control). A similar set of experiments was undertaken using 0.1 wt% silver sulfadiazine loaded nanocellulose hydrogel in the same

## Cellulose

concentration range as the Bi-complex. DMEM containing 20 wt% blank nanocellulose hydrogel or commercial hydrogels were also tested. These were the two non-active over-the counter hydrogels, Solosite® and Solugel®, and silver-based active hydrogel, Silvasorb® and are referred to as commercial hydrogel 1, commercial hydrogel 2 and commercial hydrogel 3 respectively in the paper. Cell viability was assessed after 24 h of treatment by MTS assay. The treatment media was replaced by MTS stock solution, when tetrazolium compound MTS is converted to formazan by viable cells. After 1 h of incubation in the dark, the absorbance was recorded using a Thermo Scientific Multiskan Spectrum plate reader at 490 nm and using the software SkanIt RE 2.4.2. The absorbance was corrected by subtracting the background absorbance, i.e. DMEM only in TCPS (tissue culture polystyrene) and was normalised against the negative control, i.e. the untreated cells grown on TCPS with fresh DMEM media, to express the absorbance in percentage of viability relative to the negative control. Four independent sets of experiments were performed with triplicates of each samples every time.

*Live-dead assay*

The live-dead assay was performed in a 96 well plate seeded with 10,000 cells/well and allowed to form a monolayer for  $24 \pm 1$  h in 37 °C and 5% CO<sub>2</sub> condition. Cells were treated with media mixed with the hydrogel samples (with the same concentrations achieved by serial dilution as described above in “Cytotoxicity assay” section) and incubated for 24 h. The staining solution was prepared by mixing 6 drops of propidium iodide (PI) and 2 µL of Calcein AM to 3 mL PBS. The treatment media was replaced by staining solution and incubated in the dark for 30 min. Live-dead imaging was performed using the fluorescent microscope Nikon Eclipse Ts2 at 560 nm and 470 nm for Calcein AM and PI respectively.

*Cell Morphology*

A monolayer of L929 cell line in a 96 well plate seeded with 10,000 cells/ well was treated with different concentrations of the bismuth complex in a similar way as above in “Cytotoxicity assay” section, and incubated at 37 °C and 5% CO<sub>2</sub> condition for 24 h.

The morphology of the cells was observed using light microscopy using the microscope Nikon Eclipse Ts2.

*Statistical analysis*

The MTS assay results were statistically analysed by one-way analysis of variance (ANOVA), followed by Tukey’s post hoc test to compare selected pairs of data using GraphPad Prism 8.0.2. Tests with *p* values < 0.05 were considered to be statistically significant.

*Antibacterial activity**Time-kill assay*

Different amounts of 0.1 wt% Bi-loaded hydrogel was mixed with 5 mL of diluted overnight culture (1 in 100,000) of a specific bacterium such as to achieve concentrations of 12 µg, 9 µg, 6 µg and 3 µg of bismuth complex per gram of the broth (assuming density of broth as 1 g/ml). The time-kill assay of these different concentrations was performed against *Acinetobacter baumannii* (C403/ATCC17978), *Pseudomonas aeruginosa* (ATCC27853), *Escherichia coli* (G102), MRSA (M118797, methicillin-resistant *Staphylococcus aureus*) and Vancomycin-resistant *enterococcus* (M846910). Luria–Bertani (LB) media and LB agar plates were used for growing each of the bacterial line. The culture was spread on agar plate at the beginning of the experiment for time zero count. A vortex shaker was used to ensure proper mixing of the hydrogel with the broth. The suspension was kept in an incubator at 37 °C at 200 rpm shaking for 24 h and samples were aliquoted out after 4, 8, 12 and 24 h. 20 µL of the sample was plated on agar plates and the number of viable cells was determined by the colony counting technique. Each time point was analysed in triplicate, and each experiment was done three times.

*Bacterial cell morphology*

The morphology of bacterial cells after being treated was studied using SEM. The Bi-loaded hydrogel was mixed with 5 mL of diluted overnight culture (1 in 100,000) of *P. aeruginosa*, as described above, to obtain concentrations of 12 µg and 9 µg of bismuth complex per gram of the broth. These, along with a control, were incubated for 24 h at 37 °C. The treated culture was then centrifuged at 2000 rpm for 30 min at

4 °C. The supernatant was discarded and the pelleted cells were used for SEM sample preparation. The cells were washed with PBS and fixed using 2.5% glutaraldehyde and 2% paraformaldehyde for 1 h at room temperature. The fixed cells were then washed with fresh sodium cacodylate buffer and post-fixed with 1% osmium tetroxide in cacodylate buffer. The cells were then washed with milli-Q water and incubated on coverslips coated with 0.1% polyethyleneimine for 45 min. The coverslips were immersed in water to get rid of the unadhered cells, and treated with increasing concentrations of ethanol for dehydration. The coverslip was then critically point dried, mounted on SEM stub and coated with a thin conducting layer of gold. The SEM imaging was performed using FEI Nova NanoSEM.

#### Internal quality control

Quality control tests were done to evaluate the reliability and reproducibility of the antibacterial test results. Blinded experimental repeats of the time-kill assays were performed against MRSA (M118797, methicillin-resistant *Staphylococcus aureus*) and *Acinetobacter baumannii* (C403/ATCC17978). One sample contained the Bi-loaded hydrogel to achieve a concentration of 9 µg/g and another one contained the same amount of blank hydrogel as the control. The samples were analysed at 4 and 24 h and each time point was analysed in triplicate. The experiment was performed in the same way as before, except the test and the blank (control) samples were blinded.

#### Hydrogel quality check

Bismuth content analysis were carried out using a PerkinElmer Avio 200 Inductively Coupled Plasma - Optical Emission Spectrometer (ICP-OES), measuring Bi at 223.06 nm. Known masses from different batches of Bi-loaded hydrogels were ashed in a muffle furnace, wherein the temperature was ramped to and maintained at 600 °C for 3 h. The ash was then digested in concentrated nitric acid and diluted using 3% nitric acid. The elemental bismuth content was analysed and used to determine the bismuth complex content. Each batch of hydrogel was tested in triplicate and the mean mass of the bismuth complex per gram of hydrogel was reported.

## Results and discussion

### Morphology

Figure 1a and b shows the SEM images of the same area of the Bi-loaded hydrogel films. The secondary electron image in Fig. 1a shows the surface morphology only. In the back-scattered electron image (BSE) in Fig. 1b, the bright structures indicate the presence of higher atomic number element, which is bismuth. The main point of interest in these images is the distribution of the bismuth complex.

The bismuth particles have been shown to be well distributed within the nanocellulose fibres. Few bundles of fibres were observed, which is more closely shown in Fig. 1c. Those bundles that were present could be due to only having a single pass in the homogeniser in preparation of the gel. Better fibrillation can be achieved by more extensive mechanical treatment, although this would only be worthwhile if it led to a more active gel or was needed to satisfy regulatory requirements. Despite the presence of the bundles, the BSE image in Fig. S1 in supplementary data shows that the bismuth complex particles are sitting in between the nanofibres in the fibre bundle.

### Rheology

To understand how the physical properties of the hydrogel are altered upon incorporation of the bismuth complex, its rheological properties were assessed. The complex viscosity plot shown in Fig. 2 indicates that the viscosity profile of the Bi-loaded hydrogel is similar to that of the blank hydrogel, showing a clear yield point for both and thereby suggesting the shear thinning behaviour of the hydrogel is retained. The dynamic strain sweep in Fig. 3 shows the elastic modulus  $G'$  (solid-like properties) and the viscous modulus  $G''$  (liquid-like properties). For hydrogels, the elastic modulus should be higher than the viscous modulus (Mendoza et al. 2018), which is consistent with our results. A rise of the zero-shear complex viscosity and storage modulus was observed with Bi-complex loading, suggesting the presence of the bismuth complex does not negatively affect the inter-fibre network. Although it has previously been observed that bismuth particles interfere with fibre-fibre bonding and upset the mechanical properties of nanocellulose paper (Maliha et al. 2019), the opposite

Cellulose

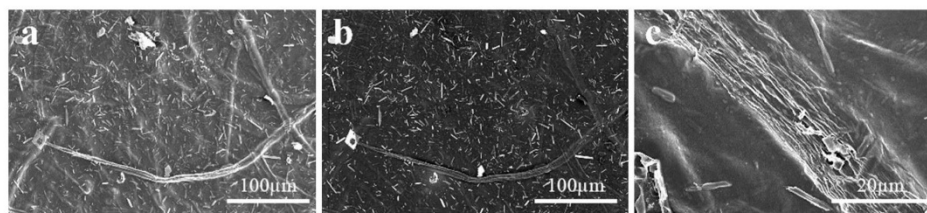


**Fig. 1** SEM image of air-dried Bi-NC hydrogel. **a** Secondary electron image **b** Back-scattered electron image of the same area **c** secondary electron image showing a nanofiber bundle

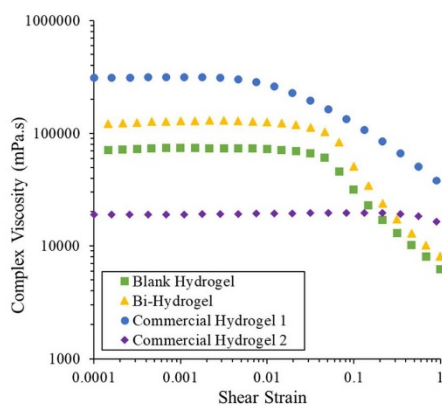


**Fig. 2** Viscosity profile of blank hydrogel and bismuth-complex loaded hydrogel compared to commercial wound hydrogel

is evident here. Figures 2 and 3 also show the complex viscosity and the modulus of two commercially available over-the-counter non-active wound hydrogels.

The rheological analysis show that the incorporation of bismuth does not affect the viscoelastic properties of the hydrogel and that the hydrogel behaves like a true gel. The blank nanocellulose hydrogel and the Bi-NC hydrogel showed  $G'$  higher than  $G''$  at low shear strains and showed a linear viscoelastic region (LVR). These hydrogels have more solid-like properties at these strains and the  $G'$  and  $G''$  remains independent of the change in strain. Beyond a certain strain, the viscous behaviour starts to take over. This is the critical strain beyond which the viscosity changes with shear and behaves like a non-Newtonian fluid. Thus, these can be used as free-flowing gels and

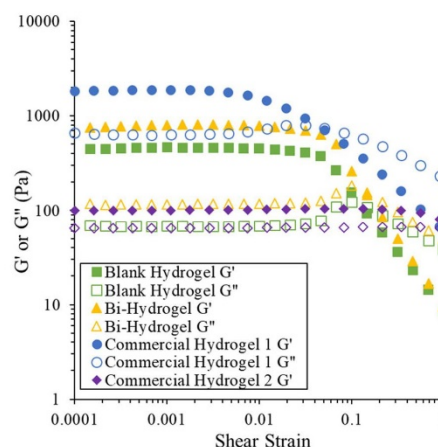


**Fig. 3** Dynamic strain sweep of blank hydrogel and bismuth-complex loaded hydrogel compared to commercial wound hydrogel

have the capacity to be packaged in tubes as soft solids having an entangled fibrous network. The high zero shear viscosity tells us about the stability and the solid-like behaviour of the hydrogel during storage suggesting there is little possibility of sedimentation or phase separation. The higher elastic modulus and the zero-shear viscosity after the addition of the bismuth complex indicates stronger network formation. It can be speculated that the bismuth complex particles are taking part in the physical chain entanglement. Hence due to these particles being able to arrange themselves within the network, the material becomes less flexible and stiffer increasing the shear force required for the material to start flowing. The loss factor,  $\tan \delta$ , can be calculated as the ratio of the loss modulus to storage modulus and was found to be 0.15 for both the blank

hydrogel and the Bi-hydrogel in the LVR. Moreover, the viscoelastic behaviour of the Bi-nanocellulose hydrogel studied here is comparable to commercial burn hydrogels as its elastic modulus and zero shear viscosity lies in the range of commercial brands investigated. Also, the critical strain for both the blank and Bi-complex loaded nanocellulose hydrogel is 0.068 and lies in between the range of the two commercial ones (0.003 and 0.347 for commercial hydrogel 1 and 2, respectively). The yield point represents the ease of squeezing the gel out of a tube and the shear-thinning behaviour predicts the spreadability on shear forces for topical applications. These properties are important aspects for potential commercial translation. However, if required, the rheological properties of our Bi-hydrogel composites can be altered by changing the cellulose content of the hydrogel, as reported by Mendoza et al. (Mendoza et al. 2018).

#### In-vitro biocompatibility

##### *Cytotoxicity assay*

To determine whether the bismuth hydrogels are cytotoxic, several approaches were undertaken. Firstly, an MTS assay was employed to determine the viability of mouse fibroblast L929 cells that had been incubated with bismuth hydrogels, and the percentage cell viability determined relative to untreated cells i.e. cells grown in DMEM only. Statistical analysis was carried out using a 1-way ANOVA and a post-hoc Tukey's test. Fig. 4 shows a concentration-dependent effect of bismuth hydrogels on the viability of L929 cells. Generally, cell viability was unaffected by lower bismuth concentrations in the hydrogel, however, reduced cell viability was observed at higher concentrations. At bismuth complex concentrations greater than 12  $\mu\text{g/g}$ , the mean normalised cell viability relative to the untreated control cells is below 20 %, indicating a cytotoxic effect of the complex as per the requirements of ISO 10993-5 standard. The standard identifies any medical device or material that leads to cell viability less than 70 % as cytotoxic. At concentrations  $\leq 12 \mu\text{g/g}$ , the mean normalised cell viability was 70 % or greater, demonstrating a dose response curve for viability. Supporting this contention, at bismuth complex concentrations  $\leq 12 \mu\text{g/g}$ , the mean normalised cell

viability was not statistically different to that of untreated cells. This type of dose-dependent phenomenon was also seen with the silver sulfadiazine loaded hydrogel. Viability was significantly reduced when cells were cultured on high concentrations of silver in a dose-dependent manner. For example, concentrations  $\leq 6 \mu\text{g/g}$ , silver sulfadiazine were not cytotoxic. We compared the toxicity of the blank nanocellulose hydrogel to commercial hydrogels in Fig. 4b. Commercial hydrogel 1 and 2 are non-antibacterial products. Commercial hydrogel 3 is a silver based antimicrobial hydrogel, that releases silver ions. The silver content of this hydrogel was studied using ICP-OES analysis and it was found to contain  $3.81 \pm 0.40 \mu\text{g/g}$  of equivalent silver sulfadiazine ( $1.15 \pm 0.12 \mu\text{g/g Ag}^+$ ). The silver content is well below the toxic limit observed herein. Surprisingly, all three of the commercial hydrogels showed a degree of cellular toxicity with viability counts far below 70 %. Nonetheless, these products are in clinical use and this suggests that in-vitro experiments may differ from a real-life scenario. There are a number of possible reasons for this. Monolayers of cells have only 15 % of cell contact as the cell density is lower than 1 % compared to normal skin tissue and extracellular content is very much different in the culture dish. Moreover, in-vitro experiments only deal with one cell type, in our case the fibroblast, and cell-cell interactions between different cell types in skin tissue is not taken into consideration (Hartung and Daston 2009). Skin tissue does not only consist of fibroblasts, but a number of different kinds of cells in various layers of skin including keratinocytes, Langerhans cells, melanocytes and vascular networks of blood vessels, sebaceous glands, nerves and many proteins like collagen (Shpichka et al. 2019). These along with the difficulty in understanding the reaction of the tissue to a foreign material or stress situation results in the difference in behaviour of cells in isolated cultures compared to when in the organism. Thus, it is difficult to extrapolate the in-vitro effects to in-vivo performance (Ghallab 2013). Moreover, the commercial hydrogels contain a range of other components (preservatives like parabens, imidazolidinyl urea etc.), some of which could also be the cause of the in-vitro cytotoxicity (Güzel Bayülken and Ayaz Tüylü 2019; Spindola et al. 2018).

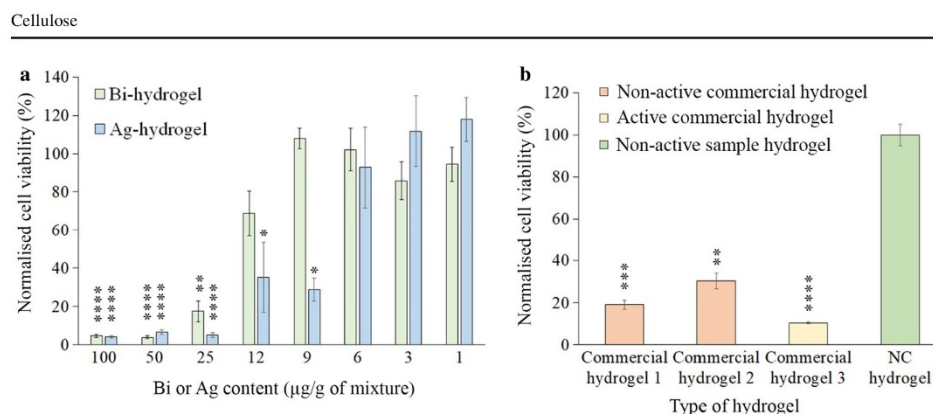


**Fig. 4** Viability of L929 cells after treatment with **a** nanocellulose hydrogels loaded with the indicated target concentrations of Bi-complex (green) or Ag-compound (blue) and **b** the indicated commercial hydrogel and blank nanocellulose hydrogel, determined by MTS assay. Percentage viability normalised over no treatment DMEM control. The data presented are expressed as mean  $\pm$  standard error of mean of technical triplicates from four independent sets of biological replicates. The number of asterisks over the bars show the level of significance of the data when compared with no treatment control. \* $p \leq 0.05$ , \*\* $p \leq 0.01$ , \*\*\* $p \leq 0.001$  and \*\*\*\* $p \leq 0.0001$

#### Live-dead assay

As an alternative approach for evaluating the potential cytotoxicity of bismuth-loaded hydrogels, a live-dead assay was undertaken. This assay employs two fluorescent probes—propidium iodide (PI) and calcein AM. PI is a red fluorescent nucleic acid stain that is only able to pass through the compromised membranes of non-viable cells, resulting in red nuclear fluorescence in dying or dead cells. Calcein AM is a cell membrane permeant fluorogenic substrate that is hydrolysed by active esterase in viable cells, resulting in a green cytosolic fluorescence in live cells. Figure 5 shows the L929 cells incubated with hydrogels loaded with various bismuth complex concentrations and stained with PI and calcein AM. Notably, at bismuth concentrations  $\geq 12$   $\mu\text{g/g}$  the majority of cells were positive for PI indicating a cytotoxic affect, however,  $\leq 9$   $\mu\text{g/g}$  most of the cells were positive for calcein and negative for PI suggesting lower bismuth concentrations do not significantly compromise cellular viability of this particular cell line. In control studies, the L929 cells were incubated with either the blank nanocellulose hydrogel (NC-gel) lacking bismuth, or DMEM cell culture media, and both conditions were associated with high levels of cell viability.

#### Cell morphology

Cell health and viability is intimately linked to cell morphology. Indeed, the induction of cell death is associated with distinct morphological events including cell shrinkage, plasma membrane blebbing and fragmentation. We examined the effect of increasing concentrations of the bismuth complex on the morphology of L929 cells (Fig. 6). Notably, a significant change in cell morphology indicating the induction of cell death was apparent at bismuth treatment concentrations above 9  $\mu\text{g/g}$ , which is consistent with our observations in the cytotoxicity assays. At higher bismuth complex concentrations, the cells appeared smaller and more circular compared to the control cells cultured with a blank hydrogel (NG-gel) or in DMEM media. In addition, some cells displayed blebbing of the peripheral membrane (Fig. 6 see inset at 25  $\mu\text{g/g}$  Bi-complex treatment). Following treatment with lower concentrations of the bismuth complex (9  $\mu\text{g/g}$ ), the cell size appeared unaffected, and the cell morphology was spindle shaped, similar to the control cells (NC-gel and DMEM). Thus, at or below bismuth complex concentrations of 9  $\mu\text{g/g}$ , the presence of the complex in the hydrogel does not appear to affect the cell morphology.

The process of wound healing is highly regulated and complex, and involves a variety of cell types

Cellulose

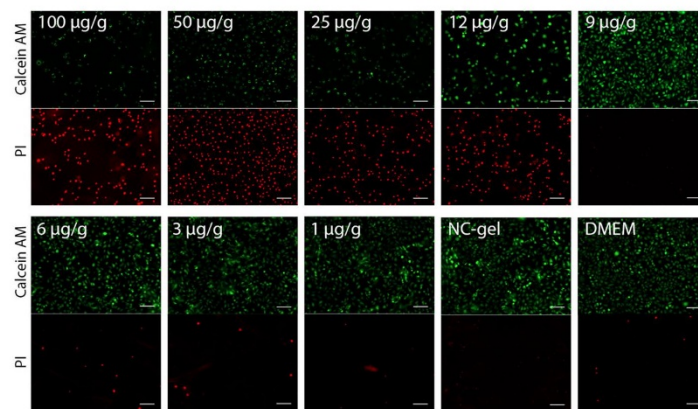


**Fig. 5** Live-dead staining of L929 cells after 24 h of incubation with the indicated target concentration of the bismuth complex in nanocellulose hydrogel, the blank nanocellulose hydrogel (NC-gel) or DMEM culture media only. The green and red fluorescence show live and dead/dying cells respectively. Scale bar represents 100  $\mu\text{m}$

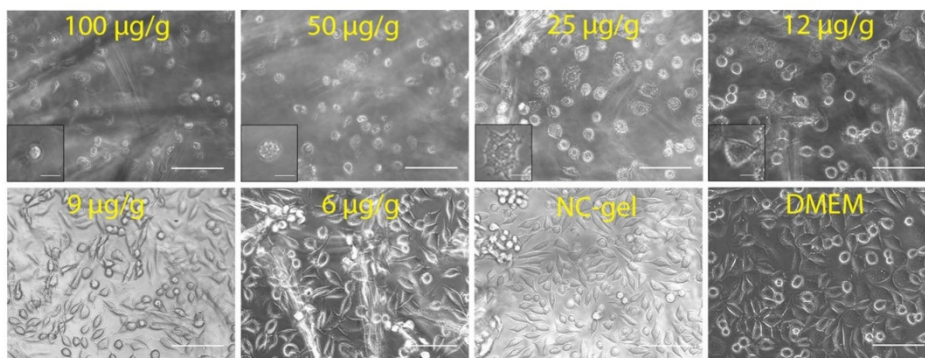


**Fig. 6** Light microscopy of L929 cells after 24 h of incubation with the indicated target concentration of the bismuth complex in nanocellulose hydrogel, or blank nanocellulose hydrogel (NC-gel) without the bismuth complex or DMEM media only. Scale bar represents 100  $\mu\text{m}$  in the images and 20  $\mu\text{m}$  in the inset

including immune cells, fibroblasts and keratinocytes. Upon tissue injury, fibroblasts migrate into the wound and deposit extracellular matrix proteins such as collagen that is required for filling the injured site with newly synthesised tissue. As fibroblasts play a critical role in wound repair, it is important to evaluate the interactions of the cells with wound dressing materials, including potential cytotoxic effects (Tschumperlin 2013) (Wiegand et al. 2019). As per

the ISO standard 10993-5, the cytotoxicity of the bismuth-loaded nanocellulose hydrogels was evaluated via assessing the cell viability of the murine fibroblast cell line L929. In addition, cytotoxicity was evaluated qualitatively via live-dead cell staining and morphological analysis. It is not clear how predictive the murine L929 cell line is of human fibroblast viability, but it is a widely employed cell line for cytotoxicity analysis and allows comparisons to other

## Cellulose

compounds. The vehicle, which is the pure nanocellulose hydrogel had no adverse effect on the fibroblast cells. The effect on cell viability of the bismuth-loaded gel was assessed using the MTS assay, live dead assay and the morphology of the mammalian cells. These experiments showed that at higher bismuth concentrations, the proportion of dead cells is increased, and hence viability is lower and the cell morphology deviates from normal. 12  $\mu\text{g/g}$  was the highest concentration of bismuth complex which did not significantly reduce cell viability as determined by the MTS assay. However, in the live-dead assay and the morphology study, the cells showed no difference compared to controls at or below 9  $\mu\text{g/g}$  loading of the bismuth complex. Further assays would be required to unequivocally demonstrate the safe bismuth loading for cells. However, results herein show that target concentrations of 9  $\mu\text{g/g}$  bismuth complex appear to be well tolerated by the cells in-vitro. Similar in-vitro studies have shown that silver nanoparticles concentrations of 1.7  $\mu\text{g/ml}$ , 5  $\mu\text{g/ml}$  and 10  $\mu\text{g/ml}$  have reduced viability on human epidermal keratinocytes (Samberg et al. 2010), rat liver cells (Hussain et al. 2005) and stem cells (Braydich-Stolle et al. 2005) respectively. Argyria occurs at levels greater than 2  $\mu\text{g/g}$  (Khattak et al. 2009). In-vivo studies have also shown that silver nanoparticle exposure can affect different organs in mammals including liver and bile duct when ingested (Stensberg et al. 2011). Skin contact (porcine skin) causes swelling, increased size of epidermal layer of skin, inflammation and greyish color at concentration of 3.4 and 34  $\mu\text{g/ml}$  (Samberg et al. 2010). It has been reported that many topical silver containing commercial products contain silver nanoparticles higher than 15  $\mu\text{g/g}$  (Lee et al. 2015). Despite this, many silver-based hydrogel products are already approved in the commercial market. The limited safety data for the novel Bi-based hydrogel suggests it is worthy of further investigation as a potentially safe new material for wound management. However, further animal testing is imperative to better understand its clinical efficacy and effects on living organisms. The findings with approved commercial hydrogels tested herein tells us that these in-vitro performance differ significantly from a real-life scenario, thus suggesting that expanded biocompatibility assays will be required to adequately extrapolate to use in vivo.

## Antibacterial activity

*Time-kill assay*

Time-kill assays were performed to understand the effect of concentration of the bismuth-complex loading at the safe concentrations established in the previous section against some common and significant wound pathogens. The time-kill kinetics in Fig. 7 shows that the Bi-loaded hydrogel is bactericidal within 4 h at 12 and 9  $\mu\text{g/g}$  against the Gram-negative bacteria *A. baumannii*, rapidly eradicating bacterial colonies. However, the lower bismuth content (6 and 3  $\mu\text{g/g}$ ) remained bacteriostatic over the 24-h test period. When tested against *P. aeruginosa* (also Gram negative), bactericidal activity is observed within 8–12 h at 12 and 9  $\mu\text{g/g}$ . At 6  $\mu\text{g/g}$ , bactericidal activity is observed over the first 12 h, after which slow regrowth occurred. With the minimum loading of 3  $\mu\text{g/g}$ , the bismuth complex was only able to slow down bacterial growth. Representative plates for *P. aeruginosa* are shown in Fig. S2. Interestingly, with the Gram-positive methicillin resistant strain of *Staphylococcus aureus* (MRSA) and Vancomycin-resistant *Enterococcus* (VRE), the trend observed was quite different. Bacteriostatic effects were observed upon treatment with 12, 9 or 6  $\mu\text{g/g}$  of the complex up to 12 h for MRSA and 24 h for VRE. With MRSA, regrowth was observed at the above-mentioned concentrations after 12 h, with the regrowing rate and the final level of colony forming units being lower than the control after 24 h. With treatment of 3  $\mu\text{g/g}$ , MRSA remained slow growing throughout the tested period. There was no reduction in bacterial colonies at any of the treatment concentrations (or times), thus indicating less activity of these hydrogels against these Gram-positive bacterial strains. Interestingly, the concentration dependency of *E. coli* was different to all the other bacteria tested, including the other Gram-negative ones. Important to note is that blank hydrogel (i.e. no bismuth additive) leads to a growth curve similar to medium alone and is shown in Fig. S3 in the supplementary information. Therein, the tests were done in hydrogel-broth mixture containing 20% w/w of the blank hydrogel or the Bi-loaded hydrogel.

*Pseudomonas aeruginosa* and *A. baumannii* have been identified as critical priority pathogens, followed by *E. coli*, VRE and MRSA as a high priority pathogens by the World Health Organization (World

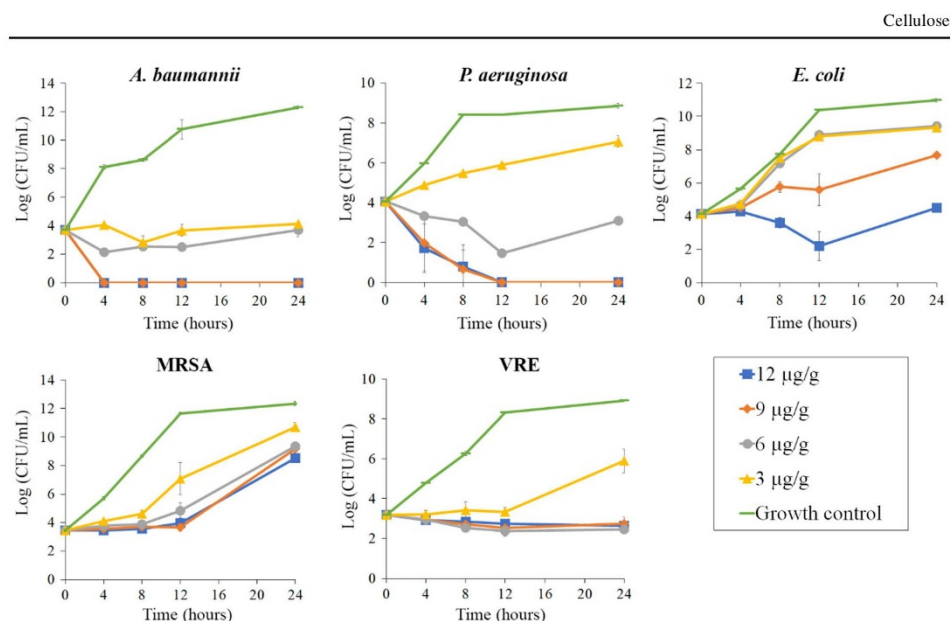


**Fig. 7** Time-kill kinetics of the Bi-NC hydrogel at indicated target concentration of the bismuth complex against the Gram-negative bacterial strains of *A. baumannii*, *P. aeruginosa* and *E. coli* and the Gram-positive strains of MRSA and VRE for 24 h period. The values expressed represent mean  $\pm$  standard deviation ( $n = 3$ ). All measurements were done in triplicate and all data included except for the following three instances where two replicates were in agreement and one was an outlier, which was excluded: *A. baumannii* at 6 and 3  $\mu\text{g/g}$  at 12 h and *P. aeruginosa* at 6  $\mu\text{g/g}$  at 12 h

Health Organization 2017). These are responsible for the most common bacterial infections in burns (Norbury et al. 2016; Thabet et al. 2008). Around 12% of infections following burns are caused by *A. baumannii*, of which 99, 60 and 87% are resistant to ceftazidime, imipenem and ciprofloxacin respectively. *P. aeruginosa* infections, which comprise 16% of the total cases, have more than 35% of strains resistant to ceftazidime and imipenem. *S. aureus* still being the most common causative agent giving rise to 20% of all burn infections with 68% being methicillin resistant but susceptible to glycopeptides (Thabet et al. 2008). Infection from both *S. aureus* and *P. aeruginosa* are known to interfere with epithelization significantly, having a serious effect on the healing process (Pastar et al. 2014). Burn patients are at very high risk of MRSA infection, and combinations of infection control strategies are needed (Andrade et al. 2009). The bismuth complex loaded hydrogels studied herein showed rapid killing of the entire bacterial population of *P. aeruginosa* and *A. baumannii* at target

concentrations of 12 and 9  $\mu\text{g/g}$  within less than 24 h. However, with MRSA and VRE bacteriostatic effects were observed at these concentrations, followed by regrowth of MRSA after 12 h. Regrowth phenomena are common in time-kill studies (Sim et al. 2014). Mathematical models suggest these phenomena are indicative of adaptation and rapid evolution, which may be due to the presence of susceptible and resistant sub-populations within a bacterial strain (Tam et al. 2005).

Paradoxically, the bismuth containing hydrogels appear more active against Gram-negative bacteria. This is surprising because previous research with bismuth compounds has shown the opposite and found them more active against Gram positive bacteria (Kotani et al. 2005; Maliha et al. 2019; Werrett et al. 2018). The reasons for this are presently unknown however it may reflect improved availability of the complex for bacteria within a hydrogel matrix. This selectivity in the current formulation will limit its utility if a broad-spectrum agent is desired. However,

this selectivity for target bacteria is commonly found among commercial hydrogels. A silver-based wound hydrogel containing 55 ppm of AgCl is not active against *P. aeruginosa* but is active against most Gram-positive bacteria (Lee et al. 2015). The silver-based commercial hydrogel, Silvasorb®, has a broader spectrum of action eliminating MRSA in 3 h, VRE in 2 h and *E. coli* in 6 h. Studies also suggests that it kills *P. aeruginosa* within 24 h, which is also true for our bismuth-NC hydrogel (Castellano et al. 2007). Broad spectrum antimicrobials have the benefit of being active against a range of bacteria, but have greater risks of selecting resistance genes. Narrow-spectrum antimicrobial agents may be preferred for treatment of skin infections, urinary tract infections and other non-life-threatening cases (Melander et al. 2018). It is encouraging that the current bismuth-hydrogel formulation targets two Gram-negative bacteria, a group that is generally more resistant and has fewer therapeutic options for treatment. However, *E. coli* showed to be an exception to this trend. In spite of being a Gram-negative bacterium, the bismuth complex was not successful in showing bactericidal activity at any concentrations tested. For Gram-negative bacteria, the permeability barrier by the cell wall is an important factor and depends on the efflux mechanism of a particular bacterial species and physicochemical properties of the antimicrobial agent (Zgurskaya et al. 2015). The bismuth-phosphinato antimicrobial agent studied herein is hydrophobic and present as large needle shaped particles in the hydrogel (Maliha et al. 2019). Hydrophobic compounds are generally transported into the cells of Gram-negative bacteria by passive diffusion. The structure of the outer membrane of *Pseudomonas* and *Acinetobacter* species are similar to most Gram-negative bacteria, except enterobacteria like *E. coli* (Zgurskaya et al. 2015). Species of *Acinetobacter* and *Pseudomonas* also showed higher permeability and more susceptibility than *E. coli* to large hydrophobic antibiotics like novobiocin, and erythromycin (Plésiat and Nikaido 1992). Moreover, *E. coli* has greater sensitivity to small molecule antibiotics compared to other Gram-negative ones. So the higher susceptibility of the more problematic bacterial species to the bismuth complex can be advantageous (Norbury et al. 2016). Reports indicate that *A. baumannii* uses hydrophobic compounds as growth nutrients and thus has a unique pathway for transport of hydrophobic substances into

the cells (Borneleit and Kleber 1991). This transport pathway may explain the rapid bactericidal effect the Bi-complex had on *A. baumannii* within only 4 h. The concentration dependent activity of the hydrogel does suggest that higher concentrations of the bismuth complex may induce a bactericidal or sustained bacteriostatic effect for *E. coli*, MRSA and VRE. However, higher concentrations were not tested due to reduced mammalian cell viability.

#### Bacterial cell morphology

The hydrogel loaded with the bismuth complex is shown to have an effect on bacterial viability by time-kill kinetics. *P. aeruginosa* was taken as a model bacterium for this study, and bactericidal concentrations of 12 and 9  $\mu\text{g/g}$  were studied. Untreated cells served as the control, which shows smooth surfaces on the rod-shaped bacterial cells, with no visible cell damage shown in Fig. 8a, b. Figure 8c shows the appearance of the cells after being treated with Bi-loaded hydrogels at 12  $\mu\text{g/g}$  of the bismuth complex in the broth, with the cell surface having an uneven texture. Fibrous features formed on the exterior of the cells along with debris build-up around them. Figure 8b and d show the bacterial cells at the same magnification, clearly showing the difference in number of bacterial cells after being treated with Bi-loaded hydrogel with concentration of 9  $\mu\text{g/g}$  of the bismuth complex compared to the control. Figure 9 shows the structure of a single bacterial cell to illustrate the morphological changes to individual cells after exposure to Bi-loaded hydrogels. The

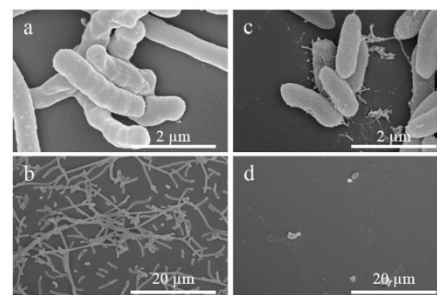


**Fig. 8** SEM images of untreated *P. aeruginosa* cells (a, b), and treated with Bi-NC hydrogel with bismuth complex concentrations of 12  $\mu\text{g/g}$  (c) and 9  $\mu\text{g/g}$  (d)

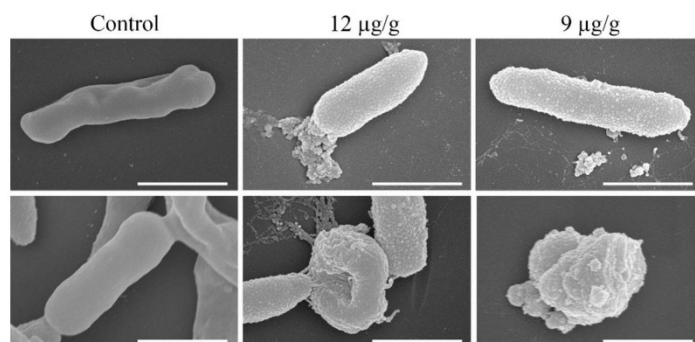


**Fig. 9** SEM images of a single *P. aeruginosa* cell with no treatment (control), and treated with Bi-NC hydrogel with bismuth complex concentrations of 12 µg/g and 9 µg/g. Scale bar represents 1 µm

treated cells show obvious shape malformation, indicating possible disruption of the cell wall and/or loss of membrane integrity. When treated at 12 µg/g, intracellular material was observed to be leaking out of the cells, likely by formation of membrane bound vesicles. Overall, the cells show severe shape distortion and a crumpled surface after being treated, which supports the findings from the time-kill assay.

#### Internal quality control

Quality control tests were done to evaluate the reliability and reproducibility of the antibacterial test results. Blinded experimental repeats of the time-kill assays were performed using one Gram-positive (MRSA) and one Gram-negative (*A. baumannii*) bacteria in a different laboratory using a different batch of hydrogel. This was done to verify that the difference in activity towards these two classes of bacteria is reproducible, so one of each kind of bacteria was chosen. There were also some differences in the bacterial population in the blinded experiments in Fig. S4 compared to the original time-kill assay. This was true for both the 9 µg/g and the control growth curves. The control curve showed less growth in the blinded experiments. For instance, after 24 h MRSA showed 9 CFU/mL in the blinded experiment as opposed to 12 CFU/mL with the original time-kill assay. This could be because the interlaboratory repeatability of bacterial cell count using the CFU method is poor (Beal et al. 2020). However, the aim of this research was not to prove the interlaboratory

reproducibility of the growth curve, but to show that the effect of the bismuth complex on the bacterial population compared to an untreated control at the same conditions is reproducible. The bacterial count showed similar fold reduction when treated with 9 µg/g Bi-complex compared to the control in the blinded repeats. For example, for MRSA, the ratio of the log CFU/mL of the control to the 9 µg/g at 4 h was 1.32 and 1.61 and at 24 h was 1.56 and 1.35 for the blinded experiment and the original experiment respectively. So, the bismuth complex was able to achieve a similar fold reduction. With the *A. baumannii*, the entire bacterial population was killed in 4 h, similar to the original assay. The interlaboratory reproducibility of the antibacterial activity proven from this study demonstrates the stability and reliability of the antibacterial activity of Bi-complex loaded hydrogels.

#### Hydrogel quality check

The 0.1 wt.% hydrogel was tested to verify the actual loading of the bismuth complex to account for all losses during the various stages of hydrogel preparation. It was found that the hydrogel contained  $0.08 \pm 0.01$  wt.% of the bismuth complex, reported as batch 1 in Table S1. It is important to note that the actual bismuth content is somewhat lower than the target concentration. For applications like this, it is critical to ensure that the active agent concentration is consistent and predictable. A quality check study was performed to understand the bismuth complex content in different batches of hydrogels produced. The actual

## Cellulose

bismuth complex content of three more different batches of the bismuth-loaded hydrogel were tested, as shown in Table S1. The average  $\pm$  standard deviation of the bismuth complex content in the four batches of hydrogels was  $0.081 \pm 0.002$  wt.%, showing that a consistent loading was achieved.

The studies reported here identify a bismuth complex loading of  $9 \mu\text{g/g}$  as the most appropriate concentration for further study. Concentrations of 12 and  $9 \mu\text{g/g}$  do not show much difference in antibacterial activity to the most bacterial strains tested. The cytotoxicity assays suggest there is a measurable deleterious effect on fibroblasts at  $12 \mu\text{g/g}$  and above compared to the DMEM control. Lower concentrations do not decrease cellular proliferation or viability of the fibroblast line tested. From this comparison, a target concentration of  $9 \mu\text{g/g}$  is identified as the optimum concentration, showing toxicity to prokaryotic bacterial cells (of Gram-negative type in particular) along with having no adverse effect on mammalian cells. According to the ICP-OES analysis the actual bismuth complex content is slightly, yet consistently, lower than the target loading. The optimised target concentration of  $9 \mu\text{g/g}$  ( $9.375 \mu\text{g/g}$  in 3 decimal places) is calculated to contain  $7.5 \mu\text{g/g}$ . The actual bismuth content quality check must be performed prior to commercial production. The bismuth complex is highly hydrophobic and tends to stick to beaker walls and other surfaces during the Bi-loaded hydrogel preparation resulting in lower than the target loading. This makes it difficult to synthesize a hydrogel with such low concentration at laboratory scale. Once incorporated into a nanocellulose matrix, the complex particles are intertwined by the fibres which protect them from coming out onto the surfaces. Moreover, the limitation of in-vitro tests is that the sample must be diluted in media and it is this treatment mixture of sample and media that is delivered to the cells. Therefore, the bismuth content in the treatment mixture and the prepared (neat) hydrogel will be different. Hence, a single batch of hydrogel was prepared for which the actual bismuth content was measured. The Bi-hydrogel was diluted to study the effect of different concentrations of the complex. Future work should include testing a  $9 \mu\text{g/g}$  loaded nanocellulose hydrogel on an in-vivo skin model. Since the pure nanocellulose hydrogel was shown to be non-toxic, the toxic effect in the bismuth-loaded hydrogels was solely due to the bismuth complex

content which has been optimised in this paper. Thus, nanocellulose hydrogel loaded with a target concentration of  $9 \mu\text{g/g}$  bismuth complex is the most appropriate concentration for further study as antibacterial wound dressing that can lessen the bioburden, thereby reducing the probability of wounds becoming infected. In addition, the highly hydrated nature of the hydrogel can promote wound healing.

## Conclusion

The potential of phenyl *bis*-diphenylphosphinato bismuth (III) complex loaded nanocellulose hydrogels for wound care applications has been investigated. Morphological studies using SEM show a well-distributed complex in the hydrogel matrix. The rheological properties show the hydrogel behaves like true gels and is comparable to commercial burn hydrogels sold in tubes. This highlights the suitability of our material in terms of ease of storage and application. An extensive study to optimise the loading of the bismuth complex in the hydrogel was done. It was shown there is a dose-dependent effect on both the antibacterial properties as well as the toxicity toward mammalian fibroblast cells. The study herein gives a detailed understanding of the host-cell safety and antibacterial activity of different levels of the bismuth complex in the hydrogel matrix. The optimum target concentration of  $9 \mu\text{g/g}$  was established to have a selective toxicity towards bacteria over mammalian cells. This study demonstrates that these hydrogels can be promising candidates as antimicrobial wound gels when the bismuth complex is used at safe but active levels. This opens opportunities for formulation of a renewable, safe and active wound care hydrogel using a new class of antibacterial agent to address the issue of rising antimicrobial resistance. Moreover, the bactericidal behaviour of the complex towards the Gram-negative bacterial strains, *A. baumannii* and *P. aeruginosa*, at concentrations safe to host cells is promising, given therapeutics for treatment of infections caused by these bacteria are limited (Norbury et al. 2016). The antibacterial selectivity towards the different bacterial strains suggests its usefulness in specific clinical utility over a broad-spectrum antibacterial material. This might be advantageous over silver wound gels, which are generally broad-spectrum antibacterial materials (Lee et al. 2015). However, our study here is limited to in-vitro experiments of the

biocompatibility and antibacterial effect. The in-vitro results presented in this paper provides a useful preliminary screening to optimise Bi-nanocellulose hydrogel formulation and future in-vivo studies on animal models is required using hydrogel loaded with the optimised level of bismuth complex for regulatory purposes. An infected wound model is highly recommended to understand not only the biocompatibility and antibacterial activity of the composite hydrogel, but also to understand the healing properties of the hydrogel.

**Acknowledgments** The authors thank Monash University and The National Health and Medical Research Council (APP1139844) for financial support. The authors would like to acknowledge the use of the facilities in the Monash Centre for Electron Microscopy and Ramaciotti Centre for Cryo-Electron Microscopy. The authors would like to thank Dr. Simon Crawford for his assistance. Maisha Maliha would like to acknowledge the Australian Government for the Research Training Program (RTP) Scholarship.

**Author contributions** Conceptualization: MM, MW, PA, WB; Methodology: MM, JD; Investigation: MM, RB; Formal analysis: MM; Writing—original draft preparation: MM; Writing—review and editing: MM, RB, JD, RLC, MW, PCA, WB; Funding acquisition: WB; Resources: JD, RC, PCA, WB; Supervision: MW, PCA, WB.

**Funding** The National Health and Medical Research Council (APP1139844).

**Data availability** <https://doi.org/10.26180/5f7b1a1262a02>.

#### Declarations

**Conflict of interest** The authors declare that they have no conflicts of interest to declare.

#### References

- Abou-Yousef H, Kamel S (2015) High efficiency antimicrobial cellulose-based nanocomposite hydrogels. *J Appl Polym Sci*. <https://doi.org/10.1002/app.42327>
- Agyingi E, Maggelakis S, Ross D (2010) The effect of bacteria on epidermal wound healing. *Math Model Nat Phenom* 5:28–39. <https://doi.org/10.1051/mmnp/20105303>
- Andrade C, Champagne S, Caruso D, Foster K, Reynolds K (2009) Methicillin-resistant *Staphylococcus aureus*: an assessment of environmental contamination in a burn center. *Am J Infect Control* 37:515–517. <https://doi.org/10.1016/j.ajic.2008.10.026>

- Ashtikar M, Wacker M (2018) Nanopharmaceuticals for wound healing: Lost in translation? *Adv Drug Deliv Rev*. <https://doi.org/10.1016/j.addr.2018.03.005>
- Babu VR, Kim C, Kim S, Ahn C, Lee YI (2010) Development of semi-interpenetrating carbohydrate polymeric hydrogels embedded silver nanoparticles and its facile studies on *E. coli*. *Carbohydr Polym* 81:196–202. <https://doi.org/10.1016/j.carbpol.2010.02.050>
- Bardajee GR, Hooshyar Z, Rezanezhad H (2012) A novel and green biomaterial based silver nanocomposite hydrogel: synthesis, characterization and antibacterial effect. *J Inorganic Biochem* 117:367–373. <https://doi.org/10.1016/j.jinorgbio.2012.06.012>
- Barry NPE, Sadler PJ (2013) Exploration of the medical periodic table: towards new targets. *Chem Commun* 49:5106–5131. <https://doi.org/10.1039/c3cc41143e>
- Barton DHR, Bhatnagar NY, Finet J-P, Motherwell WB (1986) Pentavalent organobismuth reagents. Part VI Comparative migratory aptitudes of aryl groups in the arylation of phenols and enols by pentavalent bismuth reagents. *Tetrahedron* 42:3111–3122. [https://doi.org/10.1016/S0040-4020\(01\)87378-6](https://doi.org/10.1016/S0040-4020(01)87378-6)
- Basu A, Lindh J, Ålander E, Strømme M, Ferraz N (2017) On the use of ion-crosslinked nanocellulose hydrogels for wound healing solutions: Physicochemical properties and application-oriented biocompatibility studies. *Carbohydr Polym* 174:299–308. <https://doi.org/10.1016/j.carbpol.2017.06.073>
- Basu A, Heitz K, Strømme M, Welch K, Ferraz N (2018) Ion-crosslinked wood-derived nanocellulose hydrogels with tunable antibacterial properties: Candidate materials for advanced wound care applications. *Carbohydr Polym* 181:345–350. <https://doi.org/10.1016/j.carbpol.2017.10.085>
- Beal J et al (2020) Robust estimation of bacterial cell count from optical density. *Commun Biol* 3:512. <https://doi.org/10.1038/s42003-020-01127-5>
- Borneleit P, Kleber HP (1991) The Outer Membrane of *Acinetobacter*: Structure-Function Relationships. In: Towner KJ, Bergogne-Bérézin E, Fewson CA (eds) *The Biology of Acinetobacter: Taxonomy, Clinical Importance, Molecular Biology, Physiology, Industrial Relevance*. Springer, Boston. [https://doi.org/10.1007/978-1-4899-3553-3\\_18](https://doi.org/10.1007/978-1-4899-3553-3_18)
- Braydich-Stolle L, Hussain S, Schlager JJ, Hofmann M-C (2005) vitro cytotoxicity of nanoparticles in mammalian germline stem cells. *Toxicol Sci* 88:412–419. <https://doi.org/10.1093/toxsci/kfi256>
- Briand GG, Burford N (1999) Bismuth compounds and preparations with biological or medicinal relevance. *Chem Rev* 99:2601–2658. <https://doi.org/10.1021/cr980425s>
- Caló E, Khutoryanskiy VV (2015) Biomedical applications of hydrogels: a review of patents and commercial products. *Eur Polymer J* 65:252–267. <https://doi.org/10.1016/j.eurpolymj.2014.11.024>
- Castellano JJ et al (2007) Comparative evaluation of silver-containing antimicrobial dressings and drugs. *Int Wound J* 4:139–140. <https://doi.org/10.1111/j.1742-481X.2007.00316.x>
- Chinga-Carrasco G, Syverud K (2014) Pretreatment-dependent surface chemistry of wood nanocellulose for pH-sensitive

## Cellulose

- hydrogels. *J Biomater Appl* 29:423–432. <https://doi.org/10.1177/0885328214531511>
- Cushen M, Kerry J, Morris M, Cruz-Romero M, Cummins E (2012) Nanotechnologies in the food industry: Recent developments, risks and regulation. *Trends Food Sci Technol* 24:30–46. <https://doi.org/10.1016/j.tifs.2011.10.006>
- Czaja W, Krystynowicz A, Bielecki S, Brown RM (2006) Microbial cellulose—the natural power to heal wounds. *Biomaterials* 27:145–151. <https://doi.org/10.1016/j.biomaterials.2005.07.035>
- De France K, Hoare T, Cranston E (2017) Review of hydrogels and aerogels containing nanocellulose. *Chemistry Material*. <https://doi.org/10.1021/acs.chemmater.7b00531>
- Domenico P, Baldassarri L, Schoch PE, Kaehler K, Sasatsu M, Cunha BA (2001) Activities of Bismuth Thiols against staphylococci and staphylococcal biofilms. *Antimicrob Agents Chemother* 45:1417
- Finland : UPM's FibDex, a wood-based innovation for wound care, receives regulatory approval and CE mark (2019). Mena Report
- Fukuzumi H, Saito T, Iwata T, Kumamoto Y, Isogai A (2009) Transparent and High Gas Barrier Films of Cellulose Nanofibers Prepared by TEMPO-Mediated Oxidation. *Biomacromol* 10:162–165. <https://doi.org/10.1021/bm801065u>
- Ghallab A (2013) In vitro test systems and their limitations. *EXCLI J* 12:1024–1026
- González-Sánchez MI, Pemi S, Tommasi G, Morris NG, Hawkins K, López-Cabarcos E, Prokopovich P (2015) Silver nanoparticle based antibacterial methacrylate hydrogels potential for bone graft applications. *Mater Sci Eng C* 50:332–340. <https://doi.org/10.1016/j.msec.2015.02.002>
- Gunawan C, Marquis CP, Amal R, Sotiriou GA, Rice SA, Harry EJ (2017) Widespread and Indiscriminate Nanosilver Use: Genuine Potential for Microbial Resistance. *ACS Nano* 11:3438. <https://doi.org/10.1021/acsnano.7b01166>
- Güzel Bayülken D, Ayaz Tüylü B (2019) vitro genotoxic and cytotoxic effects of some paraben esters on human peripheral lymphocytes. *Drug Chem Toxicol* 42:386–393. <https://doi.org/10.1080/01480545.2018.1457049>
- Hakkarainen T et al (2016) Nanofibrillar cellulose wound dressing in skin graft donor site treatment. *J Control Release* 244:292–301. <https://doi.org/10.1016/j.jconrel.2016.07.053>
- Hartung T, Daston G (2009) Are in vitro tests suitable for regulatory use? *Toxicol Sci* 111:233–237. <https://doi.org/10.1093/toxsci/kfp149>
- Hebeish A, Hashem M, El-Hady MMA, Sharaf S (2013) Development of CMC hydrogels loaded with silver nanoparticles for medical applications. *Carbohydr Polym* 92:407–413. <https://doi.org/10.1016/j.carbpol.2012.08.094>
- Hussain SM, Hess KL, Gearhart JM, Geiss KT, Schlager JJ (2005) In vitro toxicity of nanoparticles in BRL 3A rat liver cells. *Toxicol in Vitro* 19:975–983. <https://doi.org/10.1016/j.tiv.2005.06.034>
- Jones V, Grey J, Harding K (2006) Wound dressings. *Br Med J* 332:777
- Kamoun EA, Kenawy E-RS, Chen X (2017) A review on polymeric hydrogel membranes for wound dressing applications: PVA-based hydrogel dressings. *J Adv Res* 8:217–233. <https://doi.org/10.1016/j.jare.2017.01.005>
- Khattak AZ, Ross R, Ngo T, Shoemaker CT (2009) A randomized controlled evaluation of absorption of silver with the use of silver alginate (Algidex) patches in very low birth weight (VLBW) infants with central lines. *J Perinatol* 30:337. <https://doi.org/10.1038/jp.2009.169>
- Kotani T, Nagai D, Asahi K, Suzuki H, Yamao F, Kataoka N, Yagura T (2005) Antibacterial properties of some cyclic Organobismuth(III) compounds. *Antimicrob Agents Chemother* 49:2729. <https://doi.org/10.1128/AAC.7.2729-2734.2005>
- Laçın NT (2014) Development of biodegradable antibacterial cellulose based hydrogel membranes for wound healing. *Int J Biol Macromol* 67:22–27. <https://doi.org/10.1016/j.ijbiomac.2014.03.003>
- Lee Y, Atchley DH, Proctor CA, Smith FL, Yi S, Loftis CM, Yates KM (2015) Time-kill Kinetics of a Novel Antimicrobial Silver Wound Gel Against Select Wound Pathogens Wounds: a compendium of clinical research and practice. *Eur J Inorg Chem* 27:336–346
- Luqman A, Blair VL, Brammananth R, Crellin PK, Coppel RL, Andrews PC (2016) The importance of heterolepticity in improving the antibacterial activity of Bismuth(III) thiolates. *Eur J Inorg Chem* 2016:2738–2749. <https://doi.org/10.1002/ejic.201600076>
- Maillard J-Y, Hartemann P (2013) Silver as an antimicrobial: facts and gaps in knowledge. *Crit Rev Microbiol* 39:373–383. <https://doi.org/10.3109/1040841X.2012.713323>
- Maliha M et al (2019) Bismuth phosphinate incorporated nanocellulose sheets with antimicrobial and barrier properties for packaging applications. *J Cleaner Prod*. <https://doi.org/10.1016/j.jclepro.2019.119016>
- Maneerung T, Tokura S, Rujiravanit R (2008) Impregnation of silver nanoparticles into bacterial cellulose for antimicrobial wound dressing. *Carbohydr Polym* 72:43–51. <https://doi.org/10.1016/j.carbpol.2007.07.025>
- Melander RJ, Zurawski DV, Melander C (2018) Narrow-spectrum antibacterial agents. *Medchemcomm* 9:12–21. <https://doi.org/10.1039/C7MD00528H>
- Mendoza L, Batchelor W, Tabor RF, Garnier G (2018) Gelation mechanism of cellulose nanofibre gels: a colloids and interfacial perspective. *J Colloid Interface Sci* 509:39–46. <https://doi.org/10.1016/j.jcis.2017.08.101>
- Norbury W, Herndon DN, Tanksley J, Jeschke MG, Finnerty CC (2016) Infection in Burns. *Surg Infect* 17:250–255. <https://doi.org/10.1089/sur.2013.134>
- Pastar I et al (2014) Epithelialization in Wound Healing: A Comprehensive Review. *Adv Wound Care* 3:445–464. <https://doi.org/10.1089/wound.2013.0473>
- Plésiat P, Nikaido H (1992) Outer membranes of gram-negative bacteria are permeable to steroid probes. *Mol Microbiol* 6:1323–1333. <https://doi.org/10.1111/j.1365-2958.1992.tb00853.x>
- Rattananaruengsrikul V, Pimpha N, Supaphol P (2009) Development of gelatin hydrogel pads as antibacterial wound dressings. *Macromol Biosci* 9:1004–1015. <https://doi.org/10.1002/mabi.200900131>

- Resmi R, Unnikrishnan S, Krishnan LK, Kalliyana Krishnan V (2017) Synthesis and characterization of silver nanoparticle incorporated gelatin-hydroxypropyl methacrylate hydrogels for wound dressing applications. *J Appl Polym Sci*. <https://doi.org/10.1002/app.44529>
- Restuccia D, Salomone R, Spizzirri UG, Saija G, Ioppolo G, Parisi OL, Picci N (2016) Industrial Applications: Regulatory issues and life cycle assessment of food packaging, chap 16. Elsevier Inc. <https://doi.org/10.1016/B978-0-12-800723-5.00016-4>
- Saito T, Kimura S, Nishiyama Y, Isogai A (2007) Cellulose nanofibers prepared by TEMPO-mediated oxidation of native cellulose. *Biomacromol* 8:2485. <https://doi.org/10.1021/bm0703970>
- Samberg ME, Oldenburg SJ, Monteiro-Riviere NA (2010) Evaluation of silver nanoparticle toxicity in skin in vivo and keratinocytes in vitro. *Environ Health Perspect* 118:407–413. <https://doi.org/10.1289/ehp.0901398>
- Shpichka A et al (2019) Skin tissue regeneration for burn injury. *Stem Cell Res Therapy* 10:94. <https://doi.org/10.1186/s13287-019-1203-3>
- Silver S (2003) Bacterial silver resistance: molecular biology and uses and misuses of silver compounds. *FEMS Microbiol Rev* 27:341–353. [https://doi.org/10.1016/S0168-6445\(03\)00047-0](https://doi.org/10.1016/S0168-6445(03)00047-0)
- Sim J-H, Jamaludin NS, Khoo C-H, Cheah Y-K, Halim SNBA, Seng H-L, Tiekink ERT (2014) In vitro antibacterial and time-kill evaluation of phosphane-gold(I) dithiocarbamates,  $R_3PAu[S_2CN(iPr)CH_2CH_2OH]$  for R = Ph Cy and Et, against a broad range of Gram-positive and Gram-negative bacteria. *Gold Bull* 47:225–236. <https://doi.org/10.1007/s13404-014-0144-y>
- Singh R, Singh D (2012) Radiation synthesis of PVP/alginate hydrogel containing nanosilver as wound dressing. *Off J Eur Soc Biomater* 23:2649–2658. <https://doi.org/10.1007/s10856-012-4730-3>
- Spindola DG, Hinsberger A, Antunes VMdS, Michelin LFG, Bincoletto C, Oliveira CR (2018) In vitro cytotoxicity of chemical preservatives on human fibroblast cells. *Braz J Pharm Sci*. <https://doi.org/10.1590/s2175-97902018000100031>
- Stensberg MC, Wei Q, McLamore ES, Porterfield DM, Wei A, Sepulveda MS (2011) Toxicological studies on silver nanoparticles: challenges and opportunities in assessment, monitoring and imaging. *Nanomedicine (Lond)* 6:879–898. <https://doi.org/10.2217/nnm.11.78>
- Suzuki H, Matano Y (2001) Chapter 1: Introduction. In: Matano Y (ed) *Organobismuth Chemistry*. Elsevier, Amsterdam. <https://doi.org/10.1016/B978-044420528-5/50003-3>
- Svoboda T, Jambor R, Ruzicka A, Padelkova Z, Erben M, Dostal L (2010) NCN Chelated Organoantimony(III) and Organobismuth(III) Phosphinates and Phosphites: Synthesis Structure and Reactivity. *Eur J Inorg Chem* 2010:5222–5230. <https://doi.org/10.1002/ejic.201000746>
- Tam VH, Schilling AN, Nikolaou M (2005) Modelling time-kill studies to discern the pharmacodynamics of meropenem. *J Antimicrob Chemother* 55:699–706. <https://doi.org/10.1093/jac/dki086>
- Thabet L, Turki A, Ben Redjeb S, Messadi A (2008) Bacteriological profile and antibiotic resistance of bacteria isolates in a burn department. *Tunis Med* 86:1051–1054
- Thomas V, Yallapu MM, Sreedhar B, Bajpai SK (2007) A versatile strategy to fabricate hydrogel-silver nanocomposites and investigation of their antimicrobial activity. *J Colloid Interface Sci* 315:389–395. <https://doi.org/10.1016/j.jcis.2007.06.068>
- Tschumperlin DJ (2013) Fibroblasts and the ground they walk on. *Physiology* 28:380–390. <https://doi.org/10.1152/physiol.00024.2013>
- Tyliszczak B, Drabczyk A, Kudłacik-Kramarczyk S, Bialik-Was K, Kijkowska R, Sobczak-Kupiec A (2017) Preparation and cytotoxicity of chitosan-based hydrogels modified with silver nanoparticles. *Colloids Surf B* 160:325–330. <https://doi.org/10.1016/j.colsurfb.2017.09.044>
- Valle H, Rivas B, Fernandez M, Mondaca M, Aguilar M, Roman J (2014) Antibacterial activity and cytotoxicity of hydrogel-nanosilver composites based on copolymers from 2-acrylamido-2-methylpropanesulfonate sodium *Journal of Applied Polymer Science* 131 doi:<https://doi.org/10.1002/app.39644>
- Werrett M et al (2018) Bismuth phosphinates in Bi-nanocellulose composites and their efficacy towards multi-drug resistant bacteria chemistry- a. *Eur J*. <https://doi.org/10.1002/chem.201801803>
- World Health Organization (2017) Prioritization of pathogens to guide discovery, research and development of new antibiotics for drug resistant bacterial infections, including tuberculosis. World Health Organization, Geneva (WHO/EMP/IAU/2017.12). (Licence: CC BY-NC-SA 3.0 IGO)
- Wiegand C, Abel M, Hipler U-C, Elsner P (2019) Effect of non-adhering dressings on promotion of fibroblast proliferation and wound healing in vitro. *Sci Rep* 9:4320. <https://doi.org/10.1038/s41598-019-40921-y>
- Zgurskaya HI, López CA, Gnanakaran S (2015) Permeability barrier of gram-negative cell envelopes and approaches to bypass it *ACS. Infect Dis* 1:512–522. <https://doi.org/10.1021/acsinfectdis.5b00097>

**Publisher's Note** Springer Nature remains neutral with regard to jurisdictional claims in published maps and institutional affiliations.

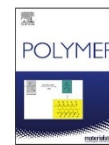
---

## **APPENDIX III**

**CO-AUTHORED PUBLICATIONS NOT INCLUDED IN THESIS**

---

THIS PAGE HAS BEEN INTENTIONALLY LEFT BLANK



## Engineering laminated paper for SARS-CoV-2 medical gowns

Laila Hossain<sup>a,b,1</sup>, Maisha Maliha<sup>a,b,1</sup>, Ruth Barajas-Ledesma<sup>a,b,1</sup>, Jinhee Kim<sup>b</sup>, Kevin Putera<sup>b</sup>, Dinesh Subedi<sup>c</sup>, Joanne Tanner<sup>a,b</sup>, Jeremy J. Barr<sup>c</sup>, Mark M. Banaszak Holl<sup>b</sup>, Gil Garnier<sup>a,b,\*</sup>

<sup>a</sup> Bioresource Processing Research Institute of Australia (BioPRIA), Australia

<sup>b</sup> Department of Chemical Engineering, Monash University, VIC, 3800, Australia

<sup>c</sup> School of Biological Sciences, Monash University, VIC, 3800, Australia

### ARTICLE INFO

#### Keywords:

Medical gown  
Virus protection  
Barrier material  
PE laminated Paper  
COVID-19  
Coating morphology

### ABSTRACT

The COVID-19 pandemic has highlighted the need for diversity in the market and alternative materials for personal protective equipment (PPE). Paper has high coatability for tunable barrier performance, and an agile production process, making it a potential substitute for polyolefin-derived PPE materials. Bleached and newsprint papers were laminated with polyethylene (PE) coatings of different thicknesses, and characterised for their potential use as medical gowns for healthcare workers and COVID-19 patients. Thicker PE lamination improved coating homogeneity and water vapour resistance. 49 GSM bleached paper with 16 GSM PE coating showed high tensile and seam strength, and low water vapour transmission rate (WVTR). Phi-X174 bacteriophage testing revealed that paper laminated with 15 GSM coating hinders virus penetration. This research demonstrates that PE laminated paper is a promising material for low cost viral protective gowns.

### 1. Introduction

In March 2020, the World Health Organisation declared the outbreak of COVID-19 to be a global pandemic. The highly infectious nature of the virus SARS-CoV-2, which causes COVID-19, has made the prevention of person-to-person transmission a critical mechanism to halt the spread of the disease. The use of personal protective equipment (PPE) is therefore vitally important [1]. Without appropriate protection from exposure to the SARS-CoV-2 virus, front-line health care workers are at great personal risk, and represent a critical transmission link to other patients and their families [2]. The rapid spread of COVID-19 and the consequential increase in demand for PPE has resulted in significant worldwide PPE shortages, including medical gowns.

Medical gowns are designed to prevent the transmission of pathogens to the wearer from an infected patient's body fluids [3,4]. These have been shown to be superior to apron-style coverings in the reduction of contamination from splashes [5,6]. According to the American Food, Drug and Cosmetic act [7], PPE used in healthcare facilities is considered to be a medical device. PPE is categorised as either a Class I (low to moderate risk) or Class II (moderate to high risk) device by the USFDA [8]. Medical gowns are classified as Class II medical devices, for which regulatory standards must be met for commercialisation [9]. According

to the AAMI PB70 standard, the four tests required for the barrier performance of medical gowns are water, hydrostatic pressure, blood penetration and virus penetration resistance [10]. Based on their performance in these tests, medical gowns are categorised from level 1 (low protection) to level 4 (high protection) [11].

In the absence of genuine and appropriate PPE, many workers have been forced to adopt makeshift solutions, such as wearing plastic garbage bags as gowns, which do not meet any of the above standards [12]. Public Health England sought to mitigate the shortage of appropriate PPE by allowing the use of reusable laboratory coats and patient gowns made of washable, woven fabrics as alternatives to disposable, non-woven gowns [13]. Many PPE manufacturers have increased or introduced the production of reusable gowns to meet the increasing demand [14–16]. However, some products only meet level 2 [17] or level 3 [18] regulatory requirements. Granzow [19] demonstrated that reusable woven fabric gowns have a lower resistance to microorganism and liquid penetration than disposable non-woven polypropylene gowns, which achieve the best liquid penetration resistance.

The global pandemic, spike in demand, and shortage of traditional PPE materials suitable for viral transmission protection has driven biopolymer researchers, virologists, and biomedical experts to collaborate and explore low cost alternative materials for medical gowns and

\* Corresponding author. Bioresource Processing Research Institute of Australia (BioPRIA), Australia.

E-mail address: [gil.garnier@monash.edu](mailto:gil.garnier@monash.edu) (G. Garnier).

<sup>1</sup> Authors contribute equally.

<https://doi.org/10.1016/j.polymer.2021.123643>

Received 9 November 2020; Received in revised form 3 March 2021; Accepted 12 March 2021

Available online 19 March 2021

0032-3861/© 2021 Elsevier Ltd. All rights reserved.

other PPE [20]. Laminated paper is a non-woven material with significant potential for use as medical gowns. The inherent properties, ubiquitous availability, low cost, and agile paper production and lamination processes make this material widely available, suitable to address the health-care criteria, and able to adapt to rapid changes in demand during a pandemic event or other emergency that results in critical PPE shortage situations. Laminated paper materials are attracting attention for their physical properties, as well as their renewability and biodegradability in many industries including packaging [21–23], superabsorbents [24–27], membranes [28,29] and biomedical [30–32]. However, the use of paper-based protective apparel has not yet been reported.

This study presents engineered and optimised laminated paper composite materials for medical gowns. Paper as the base material provides the mechanical strength, and a thin laminated coating of polyethylene acts as a barrier to increase the level of viral protection of the gowns. The effects of basis weight, laminate thickness, and combinations thereof on the composite performance were determined. The mechanical and barrier properties, viral protection, and liquid resistance of the composites were quantified. The ease of gown manufacture and performance with respect to the regulatory requirements for Level 4 medical gowns were critically evaluated. Finally, bespoke prototypes were designed and manufactured from the optimised laminated paper material, and feedback from health-care workers was sought to demonstrate the application.

## 2. Methodology

### 2.1. Materials

Polyethylene was provided by Qenos Pty Ltd. Machine glazed bleached eucalyptus paper and newsprint paper were provided by Opal, Maryvale, VIC, Australia (formerly known as Australian Paper) and Norske Skog Boyer, Australia, respectively. Anhydrous calcium chloride was purchased from Sigma Aldrich. The surfactant polysorbate 80 was purchased from Sigma-Aldrich, Australia. Whatman filter paper 602H was obtained from Bio-Strategy Pty limited Australia.

### 2.2. Preparation of laminated paper

The base sheets were coated on one or two sides with a blend of low density polyethylene (LDPE) and linear low-density polyethylene (LLDPE), referred to simply as polyethylene (PE) in this paper. Paper samples were coated at Opal Specialty Paper, VIC, Australia (formerly known as Orora) by extrusion coating. In this process, polyethylene is melted at high temperature (300 °C to 320 °C) and pressure, extruded through a slit die and laminated onto a paper substrate at high temperature through a nip roll assembly. The nip roll assembly consists of a rubber-covered pressure roll and water-cooled chill roll. The paper is fed from the rubber-covered pressure roll into the nip where lamination is achieved by pressing the polyethylene and paper layer together. The formed laminate is rapidly cooled down by water-cooled chill roll (15 °C to 30 °C) and collected by a wind-up mechanism. The sample description and composition is given in Table 1.

### 2.3. Sample thickness

The thickness of the material was measured using the L&W Micrometer (model no. 222). The sample thickness was calculated as the average of 5 random points for 5 replicates.

### 2.4. Coating defect analysis

#### 2.4.1. Fluorescence and optical imaging

Fluorescence staining was employed to detect defects in the PE coating, followed by optical microscopy in transmission and reflectance

**Table 1**

Description and composition of laminated paper materials examined in this study.

Sample code	Sample Details	
	Base sheet	Laminate
N42/10	Newsprint 42 GSM	Polyethylene 10 GSM
N51/10	Newsprint 51 GSM	Polyethylene 10 GSM
B44/0	Bleached 44 GSM	–
B44/6	Bleached 44 GSM	Polyethylene 6 GSM
B44/10	Bleached 44 GSM	Polyethylene 10 GSM
B44/15	Bleached 44 GSM	Polyethylene 15 GSM
B49/0	Bleached 49 GSM	–
B49/16	Bleached 49 GSM	Polyethylene 16 GSM
15/B49/16	Bleached 49 GSM	Double side coated with Polyethylene 15 GSM and 16 GSM

mode to visualise the overall coating morphology. In theory, the fluorescence dye should stain defects on PE coating if the nature of the defect is a hole in the coating that exposes the underlying paper. Diluted propidium iodide (PI) solution was prepared by mixing 20 µL of stock solution (10 mM) with 80 µL of deionised water, then passing through a 0.2 µm syringe filter before spraying the solution onto the coated side(s) of the sample. PI droplets on the coated surface were dried by wicking with a delicate task wipe (Kimwipe), and the surface was rinsed with deionised water to remove any residue on the coated surface before a final drying with Kimwipe. Fluorescence images of the pinhole structures were taken with the PE coated side up using a Nikon upright microscope (model DS-R12) employing a TRITC filter (Ex 540/24, DM 565, BA 605/55) with 10x objective lens. The entire surface was scanned before capturing images of the location(s) with the largest observed pinholes. Pinhole defects appeared as red spots on the sample during fluorescence imaging. Pinholes were not always visible in the optical images. Transmission (brightfield) and reflectance images were captured sequentially at the same location using the same microscope. Reflectance images were captured with a coloured filter to enhance contrast. A fine tipped marker was used to circle the pinhole location on the PE coating to direct the subsequent acquisition of topography and chemical composition information with AFM-IR.

#### 2.4.2. Atomic force microscopy – infrared spectroscopy (AFM-IR)

The AFM-IR data were collected with a Bruker NanoIR3 system. AFM images of pinholes identified during fluorescence and optical imaging were captured areas of 3 × 3 µm to 30 × 30 µm at 0.7Hz line scan rate with 100–200 pixel density on each edge using contact mode probes (Model: PR-EX-nIR2-10). Two to four height images were stitched together depending on the defect size in order to visualise the defect topography. Four IR spectra within the range 790–1850 cm<sup>-1</sup> were taken at locations of interest with 18.74% laser power, 2.9% duty cycle, and 2429 pt IR focus spot. The resonant frequency of the tip was tuned to around 265 kHz. IR imaging was performed with IR peaks unique to PE and cellulose – 1464 cm<sup>-1</sup> and 1062 cm<sup>-1</sup>, attributed to CH<sub>2</sub> wag and C–O stretch, respectively – to acquire IR maps of the PE-to-cellulose ratio on the coated surface.

### 2.5. Mechanical properties

#### 2.5.1. Tensile strength

Bare and laminated paper samples were tested for tensile strength in accordance with the TAPPI T402 standard using an Instron tensile tester

(model 5965). The samples were cut into 50 mm wide strips by laser cutter and tested at a constant strain rate of 10 mm/min. Five replicates were measured in each direction (machine direction: MD and cross direction: CD). Geometric mean tensile (GMT) was calculated by the square root of the product of the MD tensile load and CD tensile load at break.

$$\text{GMT} = \sqrt{(\text{Tensile load at MD} \times \text{Tensile load at CD})}$$

#### 2.5.2. Tear strength

Tear strength was measured following ASTM D5587-15. Rectangular samples of dimension 150 mm by 75 mm were cut by laser cutter (Epilog Laser). Following the standard, an isosceles trapezoid template of 25 mm by 102 mm was drawn for each sample. A preliminary cut 15 mm long was made at the centre of the 25 mm edge. Samples were tested using an Instron tensile tester (model 5965) at a constant strain rate of 300 mm/min. Five replicates were measured for each direction (machine direction: MD and cross direction: CD) and the arithmetic mean value is reported.

#### 2.5.3. Seam strength

Seam strength was measured following ASTM D751-19. Rectangular samples with a dimension of 50 mm by 203 mm were cut by laser cutter (Epilog Laser). The sample was folded in half with the fold parallel to the short direction of the sample. The fold was sewn in a seam (stitch type: 301) approximately 100 mm from one end using a Janome N190 sewing machine with polyester thread (Gutermann 274 yds/vgs) and a denim needle (denim needle 16; 15 × IDE). The fold was cut after seaming, and the samples unfolded at the seam or strength testing using an Instron tensile tester (model 5965) at a constant strain rate of 300 mm/min. Five replicates were measured for each direction (machine direction: MD and cross direction: CD) and the arithmetic mean value is reported. For thermofused samples, the samples were folded similarly as described for sewn samples. Then the samples were cut through the fold and thermofused by a heat sealer (Sunbeam VAC 780).

#### 2.5.4. Statistical analysis

The tensile and the seam strengths were analysed to determine the variance in the results from each type of sample, and to determine whether there were statistically significant differences between them. This was done using GraphPad Prism 8.0.2 by one-way analysis of variance (ANOVA) for the whole set of data, followed by Tukey's post hoc test to compare individual samples.

### 2.6. Barrier properties

#### 2.6.1. Water penetration

Impact penetration tests were evaluated in triplicate following the standard AATCC TM42-2017e [33]. Samples and blotting papers were conditioned at 21 °C and 50% relative humidity for at least 4 h before testing. Once conditioned, each sample was clamped under a spring clamp located at the top of a stand with an inclination of 45°. Another spring clamp with a weight of 0.5 kg was clamped at the free end of the sample. A previously weighed blotting paper was placed beneath the sample.

A funnel with a spray nozzle at the bottom was placed 0.6 m above the top of the inclined stand (measured from the middle). The nozzle had 25 holes of 1 mm diameter. 500 mL of deionised water was poured into the funnel and allowed to spray under gravity onto the sample. The weight of the blotter paper was measured immediately after the water spraying finished.

#### 2.6.2. Hydrostatic pressure

Hydrostatic pressure tests were performed in triplicate using a set up adapted from the standard AATCC TM127-2018 [34]. Samples were conditioned at 21 °C and 50% relative humidity for at least 4 h before

testing. A pre-fabricated polypropylene tube of 15 cm diameter and 100 cm height with two clear plaques at the bottom was used to conduct the tests. Each sample was inserted in between these plaques and tighten with screws. Deionised water was poured inside the tube with the sample at the bottom until leaks were observed. The height of the water in the tube was recorded.

#### 2.6.3. Water vapour transmission rate

The water vapour transmission rate (WVTR) of the samples was measured using the desiccant method according to the standard ASTM E96. The samples were dried in an oven at 105 °C for at least 4 h prior to the test. Permeability cups containing pre-dried calcium chloride were sealed with the laminated side (outside surface) of the samples facing the desiccant, and the paper side (inside surface) facing the environment. The WVTR testing was conducted at 23 °C and 50% relative humidity. The change in mass of the cups with time was recorded and plotted. The slope of the rate of change of mass was used to calculate the water vapour transmission rate.

### 2.7. Virus protection

#### 2.7.1. Preparation of phage suspension

Bacteriophage Phi-X174 was used in this assay as a model virus as it is non-pathogenic to humans. Phi-X174 was propagated using host *Escherichia coli* C ATCC 13706. The lysate was purified following the Phage-on-Tap protocol [35]. Chloroform extraction was not performed during phage purification of the lysate due to incompatibility with the test materials. The phage titre was determined by the soft agar overlay method, in which phage lysate was diluted 10 fold in bacteriophage nutrient broth [Bacto-tryptone (8.0 ± 0.1) g + Potassium chloride (5.0 ± 0.06) g + Calcium chloride (0.2 ± 0.003) g + Purified water (pH 5.3) (1 000 ± 12.5) ml] with surfactant [poly-sorbate 80 (0.1 ± 0.001 25) ml] to simulate the surface tension range for blood and body fluids.

#### 2.7.2. Penetration test

The resistance of the material to Bacteriophage Phi-X174 was studied using the standard method ISO 16604:2004 (E). Herein, Phi-X174 in liquid was used in contact with the outside surface (laminated side) of the material. 90 mm diameter sample were tested in a penetration cell of diameter 70 mm. The penetration test cell and the samples were steam sterilised at 121 °C and 214 kPa for 15 min before each test. The sample was placed within the penetration cell, and the cell was closed by torquing the bolts to 2.8 Nm each. The cell was covered with the transparent cover and mounted vertically in the apparatus for the penetration test. The cell was filled with 75 ± 2 mL of approximately 10<sup>7</sup> plaque forming units (pfu)/mL of Phi-X174 (challenge suspension) using a syringe and needle. The liquid was subjected to 0 kPa for 5 min followed by 20 kPa for 5 min. The cell was visually inspected for any sign of visible liquid penetration to the inside surface from the outside surface. At the end of the test, the challenge suspension was collected by opening the drain valve. The inside surface of the material (paper side) was washed with 5 mL of sterile nutrient broth, referred to as assay fluid. The entire surface area was brought into contact with the assay fluid by swirling the cell manually. If penetration was observed visually at any point earlier than the completion of the test, the cell was drained immediately and the assay fluid was collected and examined by viral titration using the soft agar overlay method with the media specified in the ISO 16604:2004 (E) protocol. The total number of plaques was counted. The sample passed the test if the count was less than 1 pfu/mL and vice versa. Positive and negative controls were performed using Whatman filter paper 602H and a heavy gauge polypropylene autoclavable bag material, respectively. All experiments were performed in triplicate.

Settle plates were performed to ensure there was no airborne contamination during any stage of the experiment. The agar plates containing *E. coli* C were exposed for 15–20 min at the locations of phage

titration and the penetration testing area. Material compatibility testing was performed to ensure there was no phage inactivation by the sample or the material of the penetration cell. This was done by pouring 10 mL of the phage suspension of 2200 pfu/ml onto the surface of the test material while it was in the cell. The lysate was then collected after 10 min of exposure to the sample and the cell. Phage titration was performed on this lysate as described above.

### 2.8. Ash content

The ash in the paper laminate composites were tested using the standard method TAPPI T211. Samples of known mass were combusted in an electrical muffle furnace (Model no. BT7670 Tetlow kilns & furnaces) at 525 °C for 3 h and the mass of the resulting ash was recorded. The moisture content was measured by keeping the samples of known mass in 105 °C for 4 h and recording the dried mass. The ash content was calculated as follows:

$$\text{Ash content (\%)} = \frac{\text{Weight of ash (g)}}{\text{Weight of paper sample (moisture free)(g)}} \times 100$$

## 3. Results

This study aimed to characterise laminated paper composite materials for their potential use as medical gown. The paper laminate composites were analysed by combining optical microscope and AFM-IR to detect surface composition and topographical heterogeneity of the base sheet-laminate interface, thus relating permeability to composite structure. The mechanical properties of the laminate materials, including tensile strength, seam strength and tear strength, were also analysed to quantify the effect of each layer. The materials were further tested against AAMI PB 70 for level 4 medical gowns, for which the required properties are >30 N for tensile and seam strength and >10 N

for tear strength. The barrier properties of the composites were tested against both water and a bacteriophage virus to determine the role and importance of each layer.

### 3.1. Coating morphology

Laminate integrity is key in achieving the required level of viral protection. However, the PE coating must also be as thin as possible for economic purposes, and to optimise wearer comfort. Further, analysis of the level of adhesion and the morphology of the interface can reveal a new understanding of the diffusion and barrier properties of laminated papers. Here, we combine advanced optical microscopy with AFM-IR analysis to probe and quantify the surface and interface between the layers of laminated paper.

#### 3.1.1. PE coating morphology visualised with optical microscopy and AFM-IR

The surface and interface between the layers of the laminated papers were measured through advanced optical microscopy combined with AFM-IR analysis (Fig. 1). The optical microscopy transmission (brightfield) image shows the underlying cellulose fibres while the reflectance image reveals coating morphology. Pinholes were not readily detectable in the brightfield images, but a faint hue of the dye was occasionally observed. The reflectance images show heterogeneous coating morphology across the samples. The images of the two thinnest laminate layers and base sheet thicknesses (B44/6 and B44/10) show light and dark domains, revealing higher amorphous arrangement of PE chains (dark) than the semi-crystalline domains (light), which is consistent with the AFM-IR observations (Fig. 2) [36]. Samples B44/15, B49/16 and 15/B49/16 show no distinct light and dark domains; however, an overall dense bubble morphology indicates air trapped in the melt.

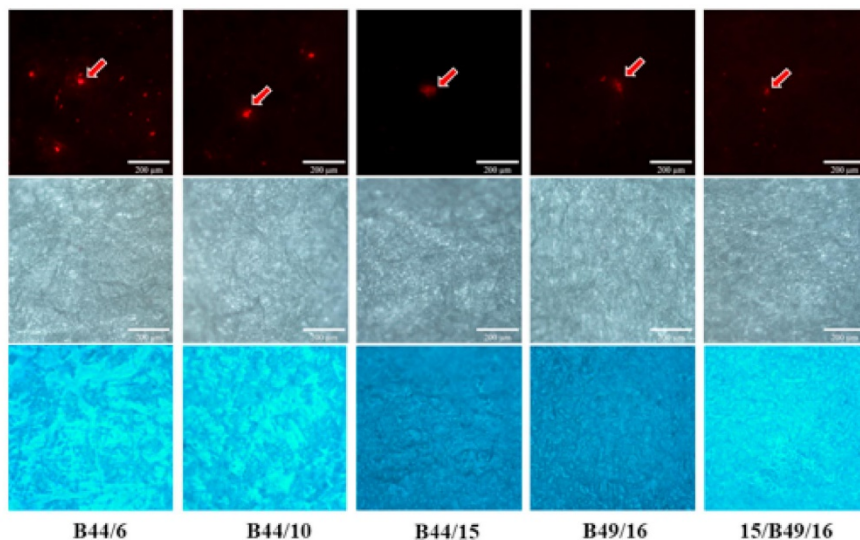


**Fig. 1.** Optical microscopy of laminate paper composites (scalebar: 200 µm) with PI staining. Fluorescence (top row), transmission (brightfield) (middle row) and reflectance with coloured filter (bottom row) images of propidium-iodide (PI) stained samples with various base sheet and laminate layer thicknesses. Fluorescence images reveal pinholes (in red), brightfield shows cellulose fibres and reflectance images highlight coating morphology. (For interpretation of the references to colour in this figure legend, the reader is referred to the Web version of this article.)

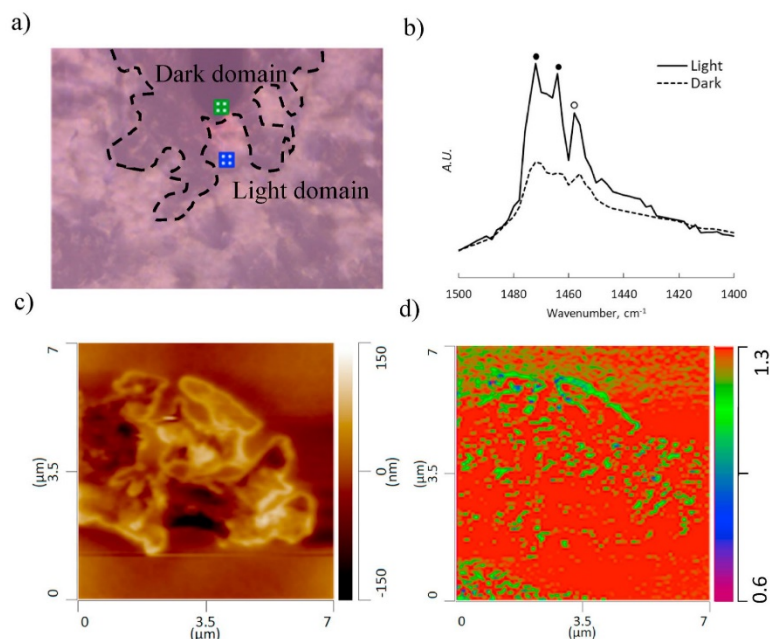


**Fig. 2.** Characterisation of the heterogeneous coating morphology of sample B44/10: a) NanoIR3 Optical microscopy view ( $375 \times 282 \mu\text{m}$ ) of the coating surface showing light and dark domains. b) AFM-IR spectrum showing the prominent  $\text{CH}_2$  bending peaks of semicrystalline PE (solid circles,  $1472 \text{ cm}^{-1}$ ,  $1464 \text{ cm}^{-1}$ ) and amorphous PE (open circle,  $1458 \text{ cm}^{-1}$ ). Dark domains have higher intensity due to semi-crystalline bands compared to the light regions, which show diminished semi-crystalline band signal intensity and similar intensity from the amorphous band. c) AFM topography map of a dark domain showing uneven surface morphology. d) PE ( $1464 \text{ cm}^{-1}$ ) to-Cellulose ( $1062 \text{ cm}^{-1}$ ) IR ratio map of region (c) showing distinct PE rich (red) and PE poor (green) areas at the edges of the uneven surface topography. (For interpretation of the references to colour in this figure legend, the reader is referred to the Web version of this article.)

### 3.1.2. Pinholes visualised with fluorescence microscopy and AFM-IR

The fluorescence and optical images of selected samples after propidium iodide staining are displayed in Fig. 1. Fluorescence images show that the thinner laminate layer has the most pinholes while the thickest base sheet shows the least. The AFM topography images reveal two types of defect morphologies for pinholes. The first morphology is a protrusion of cellulose fibres through the coating from the base sheet due to insufficient amount of coating material (Fig. 3A); the other is a crater-like defect due to uneven coating (Fig. 3b). The AFM-IR shows an increase in the cellulose signal ( $1064 \text{ cm}^{-1}$ ) peak closer to the bottom of the crater-like defect than at shallower regions, indicating a thinner layer of the polyethylene coating at the base of the crater. The protruding fibre features give an even stronger cellulose signal at  $1064 \text{ cm}^{-1}$  in addition to a deformation of the polyethylene peak ( $1464 \text{ cm}^{-1}$ ) with lowered intensity and widened base. For protrusion defects, the IR composition map of polyethylene-to-cellulose ratio revealed poor polyethylene coating (Fig. 3c). A simultaneous measurement of the relative stiffness of the material was collected by tracking the resonant frequency of the AFM tip. The protruded defect generated higher frequencies than the surrounding area, indicating that a PE poor region can introduce mechanical heterogeneity, such as domains with high relative stiffness contrast compared to that of surrounding areas due to exposed cellulose material from base sheet (Fig. 3d).

### 3.2. Mechanical properties

Achieving the required mechanical properties with paper laminate materials, particularly high tensile strength, is expected to be challenging. Here, the effect of the type and thickness of paper base-sheet and the thickness of the PE coating are analysed. The material strength must also be preserved upon gown assembly, therefore two seam options, sewn and fused, are presented and analysed here.

#### 3.2.1. Tensile strength

The mechanical properties of the laminated paper samples were expressed as the geometric mean tensile (GMT) at break point. Results are presented in Fig. 4. The dotted line represents the strength required (30N) for level 4 medical gown materials according to AAMI PB 70. All samples except the two newsprint composites meet the requirement. The newsprint composites (N42/10 and N51/10) have a lower GMT compared to those of bleached paper. These results indicate that pulp type plays an important role in governing the composite strength.

Increasing the thickness of the laminate for the same bleached base-sheet (B44/6, B44/10, B44/16) does not change the GMT significantly, nor does increasing the base sheet grammage from 44 to 49 GSM (B49/0 and B49/16). The effect of laminate thickness is also negligible when paper is coated on a single side. However, coating on both sides (15/B49/16) improves GMT significantly compared to single side coating.

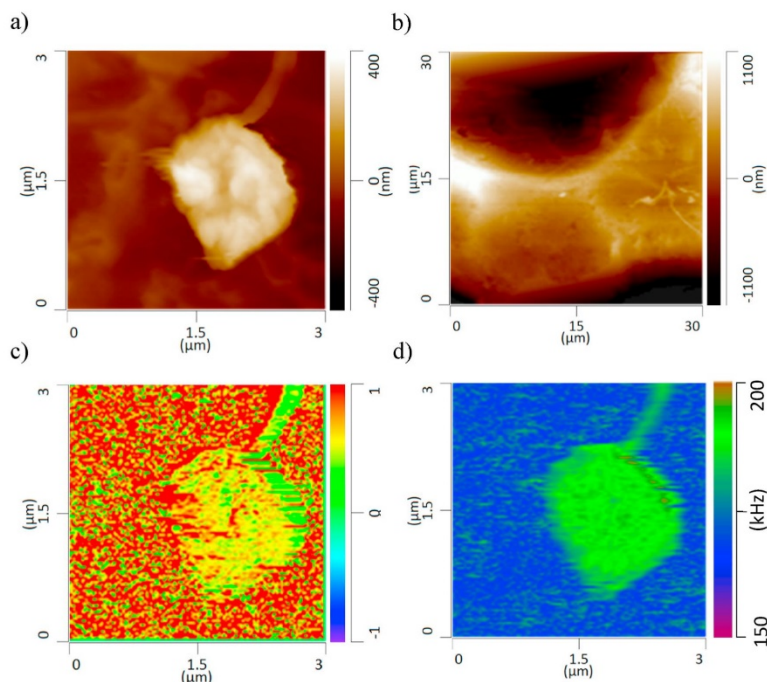


**Fig. 3.** Evidence of pinhole defect morphologies detected by AFM-IR characterization. a) An AFM topography map of a protruding defect (type 1) and b) An AFM topography map of a concave crater-like defect (type 2). c) PE (1464  $\text{cm}^{-1}$ )-to-Cellulose(1062  $\text{cm}^{-1}$ ) IR ratio map of a protruding defect in A showing reduced IR absorption of 1464  $\text{cm}^{-1}$  indicating poor PE coating on cellulose base sheet. d) PLL frequency map showing that protruding defects introduce domains with high relative stiffness contrast.

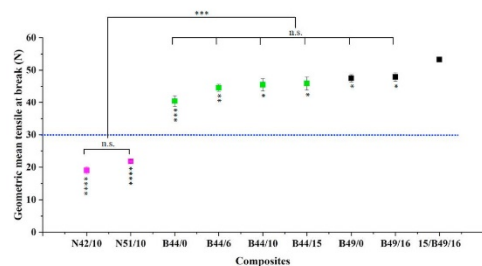


**Fig. 4.** Geometric mean tensile strength at break point for the different laminate composites. The dotted line shows the AAMI PB 70 requirement. The asterisks brackets show statistically significant differences between the indicated data points and groups. The asterisks below each data point show the level of significance when compared with 15/B49/16. Here, n.s. represents "not statistically significant", \* represents  $p \leq 0.05$ , \*\* is for  $p \leq 0.01$ , \*\*\* for  $p \leq 0.001$  and \*\*\*\* corresponds to  $p \leq 0.0001$ .

**3.2.2. Seam strength**

Seam strength was measured for both sewn and thermofused sample assemblies (Fig. 5). Slippage occurred for sewn seams at a low force for the un laminated bleached paper with a 44 GSM base sheet (B44/0).

Increasing the laminate thickness on this base sheet (B44/6, B44/10, B44/16) or increasing the base sheet grammage (B49/0) does not affect seam strength significantly. However, when higher GSM base sheets were laminated on one side (B49/16), the seam strength improved considerably. Coating the sample on both sides (15/B49/16) improves the seam strength compared to its single-sided laminated counterpart (B49/16). This material (15/B49/16) has significantly higher seam strength than the un laminated base sheets (B44/0 and B49/0) and the laminated base sheet with a lower GSM (B44/6,10,15). Therefore, it appears that both base sheet and laminate layers contribute to seam strength.

Thermofused composites did not show any difference in seam strength, irrespective of base sheet grammage, laminate thickness, or double-sided coating. Moreover, none of the thermofused composites samples meet the seam strength required (30 N) for by AAMI PB 70 for level 4 medical gowns (Fig. 5b). However, the thermofuser used here was a kitchen heat seal and thus might not have provided sufficient heat.

**3.3. Barrier properties**

Paper laminate barrier properties are important to ensure protection from the surrounding environment. Here, the effect of the thickness of paper base sheet and the thickness of the coating are evaluated.

**3.3.1. Water resistant**

The water resistance of the composites was measured through

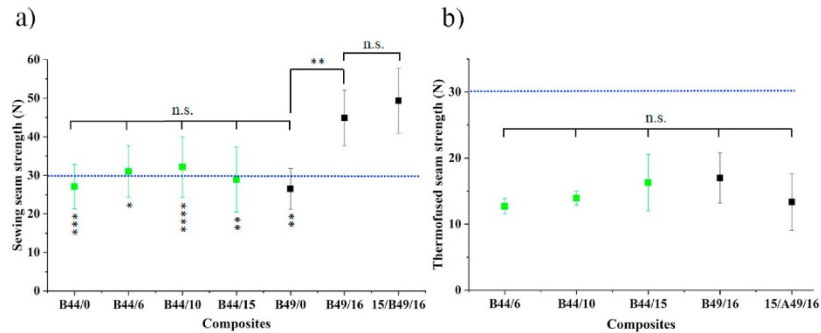


Fig. 5. Seam strength after (a) sewing and (b) thermofusing for the different laminate composites. The dotted line shows the AAMI PB 70 requirement. The asterisks brackets show statistically significant differences between data points and groups. The asterisks below each data point show the level of significance compared to 15/B49/16. Here, n.s. represents not statistically significant, \* is  $p \leq 0.05$ , \*\* shows  $p \leq 0.01$ , \*\*\* for  $p \leq 0.001$  and \*\*\*\* corresponds to  $p \leq 0.0001$ .

hydrostatic pressure and impact penetration tests with results displayed in Table S1 and Fig. 6. The hydrostatic pressure increased with increasing base sheet thickness. However, a more substantial increase was observed when the effect of the laminate was considered simultaneously. For A44/0 and A49/0, hydrostatic pressure was 24 and 37 cm, respectively. These values increased above 98 cm when a coating layer was added.

Water penetration values decreased with increasing base sheet thickness. Similar to the hydrostatic pressure tests, the greatest impact was noted when a laminate layer was included. For A44/0 and A49/0, water penetration was 0.11 and 0.06 g, respectively, decreasing to below 0.3 g when a coating layer was added.

3.3.2. Water vapour transmission rate

Materials without a PE layer showed the highest water vapour transmission rate (WVTR) (Fig. 7). WVTR values were similar for different base sheet thickness (A44/0 and A49/0). However, introducing a PE layer to the base sheet decreased the WVTR by 94% for A44/6 (31.3  $\text{g}/\text{m}^2\cdot\text{day}$ ) compared to the base sheet A44/0 (530.4  $\text{g}/\text{m}^2\cdot\text{day}$ ). Increasing the laminate layer thickness further reduced the WVTR. The lowest WVTR (2.4  $\text{g}/\text{m}^2\cdot\text{day}$ ) occurred when a laminate layer was applied to both sides of a base sheet (15/B49/16).

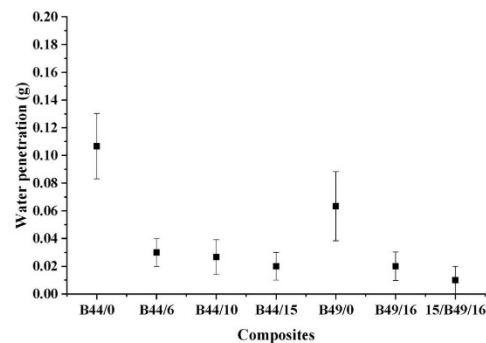


Fig. 6. Water penetration of the different samples.

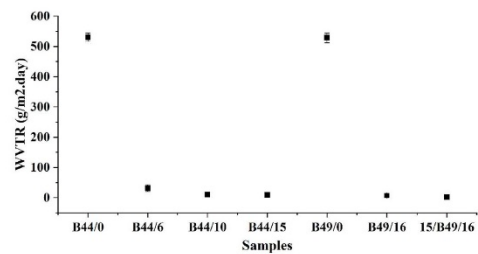


Fig. 7. Water vapour transmission rate for the different laminate composites.

3.4. Virus protection

The ability of the laminate materials to resist the penetration of viruses was tested using a surrogate virion Phi-X174 bacteriophage. The penetration of a virus suspension containing  $10^7$  pfu/mL from one side of the material to the other side was tested. Table S2 shows the resistance of the bleached paper samples coated with laminates of different thickness to virus penetration. The samples with a higher PE lamination passed the penetration tests irrespective of the paper type and base sheet grammage. The samples with low PE lamination (A44/6 and A44/10) failed the penetration test, whereas those with higher lamination (A44/15 and A49/16) could withstand a pressure of 20 kPa without allowing the virus particles to penetrate, thereby passing the test. The double coated sample (15/A49/16) also passed the test. The experimental method was validated with positive and negative controls. The positive control, which was a filter paper having a pore size of 2  $\mu\text{m}$ , provided no barrier to the virus particles. The impermeable polyethylene material, with very low wettability and a small pore size, showed no penetration of the virus suspension even under pressure.

Virus sizes usually range between 24 and 200 nm. The Phi-X174 bacteriophage tested here was reported to have an icosahedral shape with external spikes on each vertex, with a diameter of 25 nm excluding the spikes [37]. This virus particle is reported to be  $34 \pm 2$  nm in size, including the spikes [38]. The viral species causing the COVID-19 outbreak is SARS-CoV-2. SARS-CoV-2 virions are spherical in shape, also containing glycoprotein spikes, and their diameter ranges from 60

nm to 140 nm [39,40]. SARS-CoV-2 viruses are larger than the microbe tested. It is therefore concluded that materials that provides barrier to the Phi-X174 bacteriophage would also resist penetration by the SARS-CoV-2 virus.

### 3.5. Ash content

The ash content signifies the presence of inorganic residues from wood pulp, the paper making process, and paper fillers. The ash content of the newsprint (N42/10) and bleached paper (B44/10) having the same laminate coating were  $1.35 \pm 0.36\%$  and  $0.50 \pm 0.07\%$ . The ash content of the newsprint sample was significantly higher than the bleached sample. The ash content of the uncoated bleached paper (B44/0) is  $0.21 \pm 0.12\%$ , which shows that the 10 GSM coating also has some contribution to the ash.

## 4. Discussion

Paper based materials have never been reported for use as medical gowns. Thus, their prospect in this area remains poorly understood. At first, this material may seem to be an injudicious choice because of its perceived weakness, high porosity and high wicking ability. However, two events have challenged this perception. The first is the COVID crisis that has drastically limited access to typical polyolefin non-woven gown materials, which are predominantly manufactured in Asia [41,42]. In contrast, paper is manufactured on all the inhabited continents, and indeed, in most countries. The second is the advance of paper as an engineered material. Substantial progress in strength and barrier performance has been achieved in the last decade. However, commodity paper has yet to be reported as an accessible medical gown material, without the use of advanced technologies such as nanocellulose and assembling systems. This section has two objectives. The first is to investigate the property-structure relationship of laminated papers in the context of COVID-19 medical gown materials; the second is to determine if and how the current gown standard (AAMI PB 70) can be met with paper technology.

The AAMI PB 70 standard states the mechanical and barrier property requirements for medical gowns. Hence, these were studied to understand the suitability of the base sheet-laminate combination for Level 4 medical gowns, the highest level of protection. Special attention was dedicated to coating homogeneity, which was identified as a critical factor to ensure both reliability and safety of the material in COVID-19 medical gowns.

### 4.1. Material morphology

Defects in the laminate layer may compromise the barrier and mechanical function of laminated paper during use as COVID-19 surgical and isolation gowns. Due to the sub-micron size of the SARS-CoV-2 virus, a high resolution technique, namely AFM-IR, was utilised to acquire nanoscale structural and composition information regarding material defects by revealing these features with fluorescence staining. The concept is to stain the paper underneath the laminated surface with a fluorescent dye, which gives highly sensitive detection of any defects present.

Fluorescence stained regions, or pinholes, are defects which are more prevalent in composites with lower grammage base sheets, which introduces more pores in the sheet, or thinner laminate layers providing inadequate coverage over the rough paper surface. AFM-IR characterization reveals protruding (type 1) or crater like (type 2) defect morphologies with circular to ellipsoidal shapes that are 1–30  $\mu\text{m}$  on the longest axis. Samples of the lowest base sheet grammage and thinner laminate layers (B44/6) have the largest type 1 and type 2 defects. The number of defects reduces with increasing laminate layer thickness (B44/15); in addition, an increase in base sheet grammage also aids in reducing the number and size of defects. The IR absorption of type 1

defects displays stronger absorptions around  $1060\text{ cm}^{-1}$  and a reduced absorption around  $1466\text{ cm}^{-1}$ . Type 2 defects exhibit an increase in absorption around  $1060\text{ cm}^{-1}$  nearer the bottom of the crater. In addition, the relative stiffness of a type 1 defect is significantly higher than that of the surrounding material. This suggests protruding defects result from the base sheet having little to no coating while crater defects consists of regions with a thinner laminate layer with nano-holes at the bottom of the crater. Both types of defects must be mitigated as defects initiate tears and reduces barrier function, especially type 1 defects. However, mechanical and barrier test results must also be considered when determining the base sheet and laminate layer thicknesses (which determine the minimum number of defects) required for a functional yet economical medical gown.

AFM-IR analysis of light and dark domains visualised with optical microscopy reveals a heterogeneous coating morphology with distinct domains of semi-crystalline (light) and amorphous (dark) arrangement of polyethylene in materials with the lowest base sheet grammage (B44/6 and B44/10). While the nature of these domains does not indicate defects of the laminate layer, it does indicate reduced uniformity and molecular orientation, which may imply poor material function and impact laminate adhesion. Sollogoub et al. used optical microscopy to demonstrate that a substrate surface of higher roughness and lower polymer thickness had poor adhesion because the polymer had not reached the bottom of all the substrate surface irregularities due to the polymer flow being halted by crystallization or solidification [43]. Optical microscopy is thus a simple way to gauge the potential quality of laminate adhesion and to identify macroscopic coating defects.

### 4.2. Material performance

#### 4.1.1. Effect of base sheet type

Two different types of base sheets were evaluated: Newsprint paper and Bleached Kraft paper. Newsprint paper is made from softwood pulp (yellow pine) by thermomechanical pulping, which involves refining (grinding) under saturated vapour to separate the fibres from wood [44] at temperatures above the glass temperature ( $T_g$ ) of lignin. Newsprint paper retains most of its lignin and some of the hemicelluloses. In contrast, bleached Kraft paper is produced from hardwood (Eucalyptus) by chemical (Kraft) pulping, followed by bleaching. In Kraft pulping, wood chips are pre-steamed and mixed with a hot mixture of sodium hydroxide, sodium sulphide and water, which reacts with lignin to separate the cellulose fibres [45]. Around 90% of the lignin and most of the hemicelluloses are removed in this process. The chemical composition and wood polymer distribution of the two types of paper are thus significantly different. The most critically different properties are the length and therefore bonding abilities of the fibres with Pine fibres ( $L = 2\text{ mm}$  and  $D = 20\text{ }\mu\text{m}$ ) being significantly coarser than Eucalyptus fibres ( $L = 0.8\text{ mm}$ ,  $D = 8\text{ }\mu\text{m}$ ).

The base sheet type directly affects strength, measured here as the maximum tensile force at rupture [46]. Composites made from Kraft-based paper are twice as strong (GMT) as bleached newsprint (N42/10 and N51/10). This is attributed to the high lignin content in the newsprint paper, which decreases fibre-fibre bonding by the limiting hydrogen bonding ability and reducing fibre conformability, resulting in a lower GMT. Wet end chemistry is not expected to play any significant role as only retention aids and sizing agents (internal and surface for Bleached Kraft paper) are used; there are no wet/dry strengths agents. Further, the Kraft paper contains no filler while the Newsprint likely contains some  $\text{CaCO}_3$  from the recycling process. This supposition is supported by the ash content analysis, which shows that the newsprint composites (N42/10) has a higher ash content compared to the bleached Kraft paper (B44/10).

#### 4.1.2. Effect of base sheet and laminate thickness

Virus penetration of these composites is entirely dependent on the laminate thickness; base sheet type and thickness has no effect. Samples

with thin laminate show penetration of the virus suspension from the outside (laminated) surface to the inside. A lower grammage base sheet (44 GSM) can provide full protection to virus particles only when the PE layer is above 15 GSM. Granzow et al. showed that gowns made of polypropylene resist fluid strikethrough and microorganism penetration better than those made of polyester or cotton [19]. Thus, it is the polymer coating on the laminated gowns that dictate the level of virus protection. Image analysis confirms that thinner laminates have a heterogeneous coating morphology, and defects may allow virus penetration. Coating thicknesses above 15 GSM show lower coating heterogeneity and less pinhole defects. Therefore, a thicker laminate coating should provide improved virus protection.

Increasing the laminate layer or base sheet thickness does not result in a statistically significant difference in the tensile strength. This is confirmed by the similar GMT results observed for the 44 GSM base sheet composite tested at three laminate layer thickness. The laminate layer mainly contributes to the flexibility or 'drapability' of the composite, and provides a hydrophobic barrier and viral barrier.

For seam strength, sewing outperforms thermofusing. Sewn seam slippage (displacement of thread) occurs at a low force for the unlaminated bleached paper and for laminated bleached papers with lower base sheet grammage. For the 44 GSM base sheets, increasing the laminate thickness does not affect the seam strength significantly. However, the seam strength improves significantly with laminated (one side) 49 GSM base sheets. Coating the sample on both sides further increases seam strength compared to unlaminated base sheets with the same grammage (B49/O). This indicates that both the base sheet and laminate layer contribute to seam strength. For the thermofused composites, increasing the base sheet thickness or the laminate thickness does not affect the seam strength, which is universally poor.

The presence of the laminate has a conspicuous effect on the barrier properties of the composites. The hydrostatic pressure of the paper composites significantly increases when a laminate layer is added, independent of the laminate thickness. Similar results are observed for water resistance and the water vapour transmission rate of laminated samples, which confirms that the polymer coating is responsible for the permeability and hydrophobicity of these composites [47].

#### 4.1.3. Meeting standard requirements

16 GSM polyethylene lamination on a 49 GSM Kraft pulp base sheet is a suitable material for the production of Level 4 isolation gowns, as per the requirements of AAMI PB 70, providing the highest level of protection [10]. According to ASTM F3352-19, the laminated composite developed in this study meets the standard requirements for tensile and seam strength (matching or exceeding 30 N) [48]. The analysis indicates that the best combination is a 49 GSM base sheet with 16 GSM PE layer. Although the tear strength of all the laminated composites is lower than the standard requirement, this can potentially be improved by including a thin polypropylene (PP) layer between the composite base sheet and laminate layer, or with a tape or mesh at the ends, preventing crack propagation.

## 5. Conclusion

This study investigates polyethylene (PE) laminated paper as a novel material for the manufacture of disposable medical gowns meeting the stringent requirements for SARS-CoV-2 protection. Medical gowns have standards to meet in tensile strength, tear strength, seam strength, water penetration, hydrostatic pressure and viral protection.

Bleached and newsprint papers of varying basis weights were laminated with a polyethylene coating (on one or both sides). The laminated composites were characterised for coating morphology (optical microscopy and IR-AFM), mechanical properties, water resistance, water-vapour permeability and viral penetration. The performance achieved were compared to the medical gown material standards.

The water resistance of the laminated papers meets the standard requirements regardless of the laminate thickness or the base sheet grammage. The mechanical strength of the composite results from the type of paper base sheet, with bleached paper being the strongest. The virus protection is dependent on the laminate thickness; a minimum PE coating of 15 GSM is required for viral resistance, regardless of the paper base sheet. Image analysis of the laminated paper surface reveals coating heterogeneity in thinly coated laminates. A thicker coating is required for achieving a coating morphology free of defects, which is imperative for providing good viral protection. The laminated materials met all tensile and seam strength requirements; however, they failed the tear strength standard. A simple solution might be the addition of a tape or mesh at the ends, thus preventing crack propagation in paper. This research presented and validated PE laminated paper as a new material for medical gown and COVID-19 PPE equipment production.

## Declaration of competing interest

The authors declare that they have no known competing financial interests or personal relationships that could have appeared to influence the work reported in this paper.

## Acknowledgement

This project was supported by ARC Research Hub for Processing Advanced Lignocellulosics (PALS) and the Australian Pulp and Paper Technical Association (APPITA). The authors would also like to thank Norske Skog and Opal (formerly known as Australian Paper and Orora) for preparation of the composites in their mills. Many thanks to Adele Elice-Invaso (Executive Director, Appita), Frank Farchione (Market Development Manager, Amcor Functional Coatings), Russell Allan (Managing Director, Aurelia Group Consulting) and Howard Burvill (Technical Manager, Independent Consultant) for expertise and providing materials. Thanks to Mr. Long Hoh (Laboratory Manager, Department of Civil Engineer), Mr. John Rebollo (Technical Officer, Department of Civil Engineer) and Mr. Ross Ellingham (Workshop Assistant, Department of Chemical Engineering) for helping out to prepare the experimental setup. Thanks to Monash Institute of Medical Engineering (MIME) for use of facilities.

## Appendix A. Supplementary data

Supplementary data to this article can be found online at <https://doi.org/10.1016/j.polymer.2021.123643>.

## References

- [1] N.J. Rowan, J.G. Laffey, Challenges and solutions for addressing critical shortage of supply chain for personal and protective equipment (PPE) arising from Coronavirus disease (COVID-19) pandemic - case study from the Republic of Ireland, *Sci. Total Environ.* 725 (2020) 138532.
- [2] L. Vogel, Canada's PPE crisis isn't over yet, say doctors, *Can. Med. Assoc. J.* 192 (20) (2020) E563, E563.
- [3] N. Shimsski, M. Hara, R. Kikuno, K. Shinohara, A highly sensitive assay using synthetic blood containing test microbes for evaluation of the penetration resistance of protective clothing material under applied pressure, *Biocontrol Sci.* 21 (3) (2016) 141–152.
- [4] F.S. Kilinc, A review of isolation gowns in healthcare: fabric and gown properties, *J. Eng. fibres. Fabr.* 10 (3) (2015), 155892501501000313.
- [5] Y. Guo, Y. Li, P.L. Wong, Environment and body contamination: a comparison of two different removal methods in three types of personal protective clothing, *Am. J. Infect. Contr.* 42 (4) (2014) e39–e45.
- [6] Verbeek, J.H., B. Rajanaki, S. Ijaz, R. Sauni, E. Toomey, B. Blackwood, C. Tikka, J. H. Ruotsalainen, and F.S.K. Balci, Personal protective equipment for preventing highly infectious diseases due to exposure to contaminated body fluids in healthcare staff. *Cochrane Database Syst. Rev.*, (4), 2020.
- [7] U.S. Food and Drug Administration, Enforcement policy for gowns, other apparel, and gloves during the coronavirus disease (COVID-19) public health emergency, in: U.S. Dept. of Health Services, United States of America, 2020.
- [8] Administration, U.S.F.D. Medical gowns [cited 2020 27 May]; Available from: <https://www.fda.gov/medical-devices/personal-protective-equipment-infection-control/medical-gowns>, 2020.

- [19] F.S.K. Balci, Isolation gowns in health care settings: laboratory studies, regulations and standards, and potential barriers of gown selection and use, *Am. J. Infect. Contr.* 44 (1) (2016) 104–111.
- [10] A.A.M.I. PB70, Liquid barrier performance and classification of protective apparel and drapes intended for use in health care facilities, Association for the Advancement of Medical Instrumentation, Arlington (VA), 2012.
- [11] Association for the Advancement of Medical Instrumentation, Selection and use of protective apparel and surgical drapes in health care facilities, Technical Information Report: TIR11: 2005 (2005).
- [12] E. Bowden, C. Campanile, B. Golding, Worker at NYC Hospital where Nurses Wear Trash Bags as Protection Dies from Coronavirus, *New York Post*, 2020.
- [13] Coronavirus BBC, UK Failed to Stockpile Crucial PPE, in BBC, 2020 (United Kingdom).
- [14] Ford Ramps up PPE Production amidst Collaboration with Thermo Fisher on COVID-19 Test Kits, in Legal Monitor Worldwide, 2020, NA.
- [15] HanesBrands, HanesBrands begins production of medical gowns in addition to cloth face coverings to supplement personal protection supply during COVID-19 pandemic, in: Medical Letter on the CDC & FDA, 2020, p. 1342. Atlanta.
- [16] From Sanitizer to Gloves to Gowns, Wisconsin Company Voco Steps up to Combat COVID-19 in America, in Plus Company Updates, 2020, NA.
- [17] Dow, Partners to develop and donate level 2 medical isolation gowns, in: M2 Pharma, NA, 2020.
- [18] PPE company starts production of reusable gowns, coversalls in response to COVID-19, in: Legal Monitor Worldwide, NA, 2020.
- [19] J.W. Granzow, J.W. Smith, R.L. Nichols, R.S. Waterman, A.C. Muzik, Evaluation of the protective value of hospital gowns against blood strike through and methicillin-resistant *Staphylococcus aureus* penetration, *Am. J. Infect. Contr.* 26 (2) (1998) 85–93.
- [20] T. Dargaville, K. Spann, M. Celina, Opinion to address a potential personal protective equipment shortage in the global community during the COVID-19 outbreak, *Polym. Degrad. Stabil.* (2020) 109162.
- [21] M.A. El-Smaali, S.A.A. Mohamed, M.H. Abdel Rehim, M.E. Mohrari, Synthesis of hybrid paper sheets with enhanced air barrier and antimicrobial properties for food packaging, *Carbohydr. Polym.* 168 (Supplement C) (2017) 212–219.
- [22] M. Madhla, M. Herdman, R. Brannan-Smith, M. McDonald, R. Coppel, M. Werrett, P. Andrews, W. Batchelor, Bismuth phosphinate incorporated nanocellulose sheets with antimicrobial and barrier properties for packaging applications, *J. Clean. Prod.* 246 (2019).
- [23] G. Rodionova, M. Lenes, Ø. Eriksen, Ø. Gregersen, Surface chemical modification of microfibrillated cellulose: improvement of barrier properties for packaging applications, *Cellulose* 18 (1) (2011) 127–134.
- [24] L. Mendoza, L. Hossain, E. Downey, C. Seales, W. Batchelor, G. Garnier, Carboxylated nanocellulose foams as superabsorbents, *J. Colloid Interface Sci.* 538 (2019) 433–439.
- [25] M.N. Alam, L.P. Christopher, Natural cellulose-chitosan cross-linked superabsorbent hydrogels with superior swelling properties, *ACS Sustain. Chem. Eng.* 6 (7) (2018) 8736–8742.
- [26] A.M.A. Hasan, M.E.-S. Abdel-Raouf, Cellulose-based superabsorbent hydrogels, in: M.I.H. Mondal (Ed.), *Cellulose-Based Superabsorbent Hydrogels*, Springer International Publishing, Cham, 2019, pp. 245–267.
- [27] R.M. Barajas Ledesma, A.F. Patti, V.N.L. Wong, V.S. Raghuvanshi, G. Garnier, Engineering nanocellulose superabsorbent structure by controlling the drying rate, *Colloid. Surface. Physicochem. Eng. Aspect.* 600 (2020) 124943.
- [28] G. Metreveli, L. Wågberg, E. Emmert, S. Belák, M. Strömme, A. Milarascan, A size-exclusion nanocellulose filter paper for virus removal, *Advanced Healthcare Materials* 3 (10) (2014) 1546–1550.
- [29] A. Onur, A. Ng, G. Garnier, W. Batchelor, Engineering cellulose fibre inorganic composites for depth filtration and adsorption, *Separ. Purif. Technol.* 203 (2018) 209–216.
- [30] A. Basu, G. Celma, M. Strömme, N. Ferraz, In vitro and in vivo evaluation of the wound healing properties of nanofibrillated cellulose hydrogels, *ACS Applied Bio Materials* 1 (6) (2018) 1853–1863.
- [31] E. Caló, V.V. Khutoryanskiy, Biomedical applications of hydrogels: a review of patents and commercial products, *Eur. Polym. J.* 65 (2015) 252–267.
- [32] M. Jorfi, E.J. Foster, Recent Advances in Nanocellulose for Biomedical Applications, 2015 n/a-n/a.
- [33] AATCC TM42-2017e, *Test Method for Water Resistance: Impact Penetration test*, AATCC, North Carolina, USA, 2017.
- [34] AATCC TM127-2018, *Test Method For Water Resistance: Hydrostatic Pressure*, North Carolina, 2018.
- [35] N. Bonilla, M.I. Rojas, G. Netto Flores Cruz, S.H. Hung, F. Rohwer, J.J. Barr, Phage on tap—a quick and efficient protocol for the preparation of bacteriophage laboratory stocks, *PeerJ* 4 (2016), e2261.
- [36] H. Hagemann, R. Snyder, A. Peacock, L. Mandelkern, Quantitative infrared methods for the measurement of crystallinity and its temperature dependence: polyethylene, *Macromolecules* 22 (9) (1989) 3600–3606.
- [37] K. Yazaki, Electron microscopic studies of bacteriophage phi X174 intact and "eclipsing" particles, and the genome by the staining, and shadowing method, *J. Virol Methods* 2 (3) (1981) 159–167.
- [38] M.E. Bayer, R.W. DeBlois, Diffusion constant and dimension of bacteriophage phi X174 as determined by self-beat laser light spectroscopy and electron microscopy, *J. Virol.* 14 (4) (1974) 975–980.
- [39] N. Zhu, D. Zhang, W. Wang, X. Li, B. Yang, J. Song, X. Zhao, B. Huang, W. Shi, R. Lu, P. Niu, F. Zhan, X. Ma, D. Wang, W. Xu, G. Wu, G.F. Gao, W. Tan, A novel coronavirus from patients with pneumonia in China, 2019, *N. Engl. J. Med.* 382 (8) (2020) 727–733.
- [40] Y.M. Bar-On, A. Flamholz, R. Phillips, R. Milo, SARS-CoV-2 (COVID-19) by the numbers, *eLife* 9 (2020), e57309.
- [41] J.M.R. Andrew, B. Mike, At war with no Amox doctors say shortage of protective gear is drive, in: *The New York Times*, *The New York Times*, New York, 2020.
- [42] The Food and Drug Administration, **FAQs on shortages of surgical masks and gowns during the COVID-19 Pandemic** [cited 2020 5/11/2020]; Available from: <https://www.fda.gov/medical-devices/personal-protective-equipment-infection-control/faqs-shortages-surgical-masks-and-gowns-during-covid-19-pandemic>, 2020.
- [43] G. Sollogoub, P. Montmitonnet, Y. Demay, J.-F. Agassant, P. Deparis, Origin of the bubble defect in the extrusion coating process, *Polym. Eng. Sci.* 51 (2) (2011) 347–357.
- [44] Skog Norske, **Newsprint** [cited 2020 1/10/2020]; Available from: <https://www.norskeskog.com/Products/Newsprint>, 2020.
- [45] J. Fernández-Rodríguez, X. Erdocia, F. Hernández-Ramos, M.G. Alriols, J. Labidi, Lignin separation and fractionation by ultrafiltration, in: *Separation of Functional Molecules in Food by Membrane Technology*, Elsevier, 2019, pp. 229–265.
- [46] A. TUTU, U. YILMAZ, M. ÇGÇEKLER, *Effects of physical Properties of some Papers on offset printing quality*, in *IV*, in: International Multidisciplinary Eurasian Congress, 2017. Rome-Italy.
- [47] P.W. Klein, in: Morgan, P. Claypool (Eds.), *Fundamentals of Plastics Thermofforming*, San Rafael, Calif.: San Rafael, Calif, Morgan & Claypool Publishers, 2009.
- [48] F3352-19, A, Standard Specification for Isolation Gowns Intended for Use in Healthcare Facilities, ASTM International, West Conshohocken, PA, 2019.



## ORIGINAL RESEARCH

## High-performance homogenized and spray coated nanofibrillated cellulose-montmorillonite barriers

Kirubanandan Shanmugam · Shaun Ang · Maisha Maliha · Vikram Raghuvanshi · Swambabu Varanasi · Gil Garnier · Warren Batchelor

Received: 2 June 2020 / Accepted: 4 October 2020 / Published online: 19 October 2020  
© Springer Nature B.V. 2020

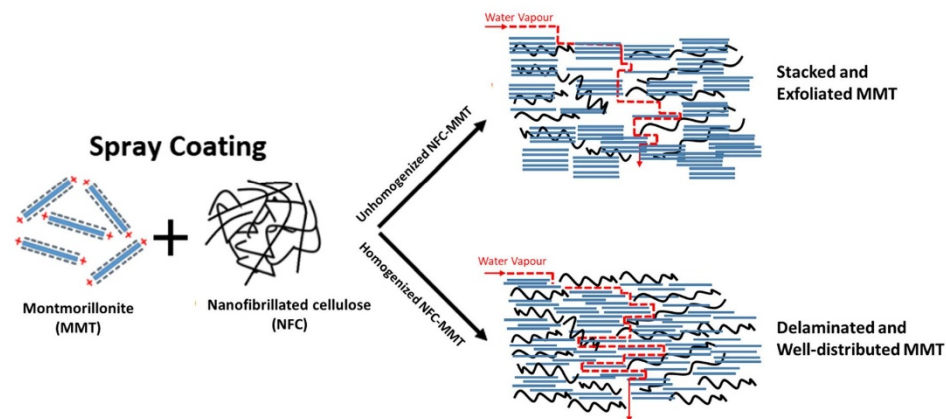
**Abstract** Nanofibrillated cellulose (NFC) is a promising candidate for the development of high-performance renewable packaging. The water vapour permeability (WVP) of NFC sheets can be improved with the addition of inorganic nanoparticles such as montmorillonite nanoclay (MMT). However, these nanoparticles reduce the already poor sheet drainage when layers are formed through vacuum filtration. Spray-coating, on the other hand, is a recently developed rapid method for sheet formation. However, higher WVP of spray-coated NFC sheets compared to its vacuum filtered counterpart still remains a limitation. This work reports a new method for spray-coating a NFC-MMT composite sheet to improve both the ease of preparation and WVP barrier performance. Critically, the WVP of CNF sheets could be significantly reduced by processing the CNF-MMT suspension in a high-pressure homogenizer prior to spray-

coating. X-ray diffraction measurements confirmed that the MMT particles were aligned in the plane of the sheet and were strongly interacting with the NFC matrix. At the optimal MMT loading of 20 wt%, WVP of  $8.3 \times 10^{-12}$  g/m s Pa was achieved. This resulted in comparable barrier performance to vacuum filtered NFC-MMT sheets, with the added benefit of being much easier to produce. Furthermore, spray-coating with 2 wt% suspension reduces the required water removal during drying by almost 90% (291 tonne water/tonne dry NFC product), compared to forming equivalent sheets using vacuum filtration at 0.3 wt%. The spray-coating process is of industrial interest as it is scalable and it is easy to engineer the properties of the NFC composites by varying the MMT content.

**Electronic supplementary material** The online version of this article (<https://doi.org/10.1007/s10570-020-03515-w>) contains supplementary material, which is available to authorized users.

K. Shanmugam · S. Ang · M. Maliha · V. Raghuvanshi · S. Varanasi · G. Garnier · W. Batchelor (✉)  
Department of Chemical Engineering, Bioresource Processing Research Institute of Australia, Monash University, Melbourne, VIC 3800, Australia  
e-mail: warren.batchelor@monash.edu

## Graphic abstract



**Keywords** Spray coating · Nanofibrillated cellulose · Montmorillonite · Nanocomposites · Water vapour permeability

## Introduction

Synthetic plastics are commonly utilised in conventional packaging materials for their good barrier properties against water vapour, oxygen, carbon dioxide, air and water (Silvestre et al. 2011). Despite this, plastics are often linked to a wide range of environmental issues such as poor biodegradability, poor recyclability and plastic microparticulate pollution. Undoubtedly, the need for more sustainable and renewable materials has never been more evident.

Cellulose is an abundant, renewable and eco-friendly biomaterial which has long been utilised in the paper, paperboards, container board, shipping sack and packaging industries (Berk 2013). While paper products have good mechanical properties, they often struggle with issues of poor barrier performance due to the large pores present in paper. These pores allow a significant amount of gas and water vapour to permeate through the fiber network, resulting in oxidation and poor shelf-life of foods and drugs. The barrier performance of paper products is often improved by use of wax coatings and synthetic plastic laminates such as low-density polyethylene and

polypropylene. However, these coated and laminated paper composites are difficult to recycle and reprocess.

Recently, extensive research has been conducted in the field of nanofibrillated cellulose (NFC) as a high-performance barrier material due to its renewable and recyclable nature. NFC materials offer outstanding rigidity, tensile, flexural strength and barrier properties. NFC have high aspect ratio with the fibril diameter varying from 5 to 100 nm and length of a few microns. They form a highly compact network by entanglement via hydrogen bonding. The compact fibril network structure of NFC sheets offers a promising alternative to synthetic packaging materials as a barrier material (Henriksson et al. 2008).

While NFC sheets provide a good barrier against oxygen, they suffer from issues of high water vapour permeability (WVP) under medium and high humidity environments due to the hydrophilic nature of cellulose. The cellulose fiber–fiber bond in the fibril network swells through the absorption of water vapour. The swollen and weakened fibrous network expedites the diffusion pathway for water vapour. As a consequence, the WVP of a NFC sheet increases (Nair et al. 2014) and the stability of cellulose fibril network deteriorates (Spoljaric et al. 2014). To improve the WVP of NFC, inorganic fillers such as nanoclays have been researched and incorporated into the fibrous matrix. The presence of these layered nanoclays in the NFC matrix results in a high-performance nanocomposite which increases the tortuosity of the diffusive

path for a water vapour/gas molecule, resulting in high barrier performance (Azeredo 2009). These nanocomposites are stiff and strong with low gas permeability (Liu and Berglund 2012). The formation of a fiber matrix network with well-dispersed platelet aggregates is critical to obtain good barrier performance of the nanocomposite (Liu et al. 2011).

One of the most promising inorganic fillers is montmorillonite (MMT), an alumina-silicate layered clay hydrated bentonite (Jochen et al. 2006). MMT functions as a nanofiller by producing a structure in the composite that forces the transfer of air/oxygen/water molecules to follow a very tortuous path resulting in lower permeance (Uyama et al. 2003). High-performance NFC-MMT composites were previously prepared via vacuum filtration (Garusinghe et al. 2018). However, the time required to form these nanocomposites via vacuum filtration was long and unattractive as it varied from a minimum of 24 h to 4 days. These MMT nanoparticles were not easily retained during the dewatering stage of vacuum filtration, thereby resulting in sheets with unpredictable properties. Another limitation with filtration is the required separation of the sheet from the filter surface and subsequent manual handling before drying. As a conventional manufacturing method, a limited range of sheet basis weights of the composite can be fabricated using filtration, as the drainage time increases exponentially with sheet thickness and grammage (Shanmugam et al. 2017).

Recently, a rapid spray coating method was developed and successfully implemented to produce pure NFC sheets (Shanmugam et al. 2017, 2018) and NFC nanocomposite sheets with graphite carbon black for electrode applications (Beneventi et al. 2014). Spray coating is a novel process to develop NFC nanocomposites and tailor their properties through the addition of specific nanoparticles or nanofillers. Further, the operation time for spray coating is independent of the NFC concentration and nanoparticle loading. One study reported that a NFC-SiO<sub>2</sub> sheet produced via spray coating could have its properties tailored by varying the SiO<sub>2</sub> loading between 0 and 33 wt% into the suspension (Krol et al. 2015). In that study however, vacuum filtration was applied after spray coating in order to fully dewater the sheet (Krol et al. 2015).

This work investigates the production of high-performance NFC nanocomposite barriers via spray

coating. Here, a scalable, good WVP NFC nanocomposite barrier layer was shown to be achievable with much lower processing times compared to other available NFC sheet formation alternatives.

## Experimental

### Materials

NFC were obtained from DAICEL Chemical Industries Limited Japan as Celish KY-100S grade which has a 75 wt% moisture content and 25 wt% solids content. The NFC in Celish KY-100S were previously reported to have a mean fiber length of 8 μm, mean fiber diameter of approximately 70 nm and fiber aspect ratio of about 140 (Varanasi et al. 2013). MMT nanoclay was obtained from BYK Additives and Instruments, Germany via IMCD Australia Limited as Cloisite-Na + powder. The packed bulk density of Cloisite-Na + is 568 g/L with a dry particle size < 25 μm (d<sub>50</sub>). X-ray results confirmed a d<sub>001</sub> of 1.17 nm for the MMT nanoclay.

### Preparation of NFC-MMT suspension

A 2 wt% NFC suspension was first made with 20 dry g of NFC and 980 g of distilled water. This 1000 g suspension was thoroughly mixed in a 3 L Mavis Engineering (Model No. 8522) standard disintegrator operating at 3000 rpm for 15,000 revolutions. All subsequent MMT addition was based on the NFC dry solids content and varied at a 5 wt%, 10 wt%, 20 wt% and 30 wt% loading. For example, a 10 wt% MMT loading would correspond to the further addition of 2 dry g of MMT powder into the 1000 g NFC suspension. The resulting NFC-MMT suspension was disintegrated again at 3000 rpm and 15,000 revolutions. For each MMT loading, two NFC-MMT batches were produced. One batch was directly sent for spray coating while the other was sent for high-pressure homogenization followed by spray coating.

For comparative purposes, two 2 wt% pure NFC suspensions (without MMT) were also made. The first suspension was directly sent for spray coating while the second suspension was sent for homogenization followed by spray coating. This was done to establish a baseline of pure NFC sheets which would allow for a

fair comparison to the NFC-MMT sheet barrier performance.

#### High-pressure homogenization

Homogenization of the NFC-MMT suspension was performed using a GEA Niro Soavi PANDAPLUS 2000 high-pressure homogenizer operating at 1000 bars for 2 passes. Homogenization was shown to be an effective tool to adequately delaminate the larger stacks of MMT within the NFC suspension while further aiding the fibrillation of the NFC itself. Homogenization of the pure NFC suspension was also performed at the same conditions.

#### Spray coating of NFC-MMT suspension and sheet production

Initially, the pure unhomogenized and homogenized 2 wt% NFC suspensions were spray coated on stainless-steel plates to form pure NFC sheets. This process was then repeated for the NFC-MMT suspensions to form the composite sheets.

In both cases, the suspension was spray coated on square stainless steel plates using a Wagner Pro 117 Professional Spray System at 200 bar with a moving conveyor operating at a fixed velocity of  $1.25 \pm 0.25$  cm/s. A standard 517 spray nozzle was used resulting in an elliptical spray jet with a  $50^\circ$  angle and 22.5 cm suspension coverage. The distance from the nozzle to the surface of the square stainless-steel plate was fixed at 50 cm. During operation, the system was allowed to run to first achieve steady state and prevent any spray jet discontinuities. Multiple sheets could be successfully fabricated in under a minute. All wet spray coated sheets were left to air dry under ambient laboratory conditions. The dried sheets were then peeled from their respective stainless-steel plates resulting in a rough air-exposed surface and a corresponding smooth stainless-steel-exposed surface. The sheets were then conditioned at 50% RH and  $23^\circ\text{C}$  for 24 h prior to property testing. The experimental setup for the spray coating system is shown in Fig. 1.

#### Sheet water vapour permeability

The ASTM E96/E96M-05 standard was used to evaluate the WVP of all sheets. All tests were performed at 50% RH and  $23^\circ\text{C}$ . Prior to testing, all

sheets were oven dried for a minimum of 4 h at  $105^\circ\text{C}$ . Thwing-Albert EZ Vapometer Permeability Cups were filled with 40 g of dried anhydrous  $\text{CaCl}_2$ . The NFC-MMT sheets were then cut into 70 mm diameter circles and were used to cover the cups. The weight of the entire cup,  $\text{CaCl}_2$  and sheet was measured at 4 h intervals. The water vapour transmission rate (WVTR) was then measured based on the slope of the line between weight gain and time. The WVTR of sheets were then normalised with sheet thickness and converted into WVP. Each NFC-MMT sample was repeated for 3 replicates and the average WVP was calculated.

#### Sheet apparent density

The AS/NZS 1301.426 s:2015 standard test method was used to evaluate the apparent density of the spray coated composite sheets. The density of the composite was calculated as the ratio of basis weight ( $\text{g/m}^2$ ) to mean thickness of the composite. A Lorentzen & Wettre AB Thickness Tester Type 21 was used to determine the thickness of the spray coated sheets. The mean thickness was calculated from 25 random points across the sheet surface. The composite sheet was then oven dried for 4 h at  $105^\circ\text{C}$  in order to obtain the oven dried mass. The ratio of the oven dried composite sheet mass to sheet area provides the sheet basis weight ( $\text{g/m}^2$ ).

#### Sheet structure via X-ray diffraction

X-Ray Diffraction (XRD) was conducted on MMT (Cloisite  $\text{Na}^+$ ) powder, pure NFC sheets and spray coated homogenized NFC-MMT composite sheets using a D8 Advance with DAVINCI Design. The device operates at 40 kV and 40 mA with a  $\text{Cu K}\alpha$  X-Ray radiation source. A  $0.02^\circ$  step size and  $2^\circ/\text{min}$  scan speed were used to scatter the radiation from the instrument. The range of diffraction angles for investigation of MMT orientation in the composite varied from  $2^\circ$  to  $34^\circ$ . Bragg's law was used to evaluate the interlayer spacing of MMT. The equation for Bragg's law was given below,

$$d = n\lambda/2\sin\theta \quad (1)$$

where the d-spacing (nm) is the interlayer spacing, n is the order of diffraction,  $\lambda$  is the wavelength of the X-Ray beam (nm) and  $\theta$  is the angle of incidence. The



**Fig. 1** Experimental setup of spray coating system

area under the first peak in the XRD spectrum was evaluated with Origin Software Pro 9.1. The base line was first removed by the software. The corrected spectrum was then fitted with the Gaussian–Lorentzian fit to find the area under the first peak of the MMT region.

#### Sheet mechanical properties

An Instron Model 5965 Universal Testing Machine was used for stress–strain load measurements to determine the mechanical properties of the sheets. The composite sheets were cut into 100 mm long and 15 mm wide strips and tested in accordance with AS/NZS 1301.448 s:2007 standards at a fixed 10 mm/min elongation rate. The sheet tensile index (Nm/g) was calculated as the ratio of tensile strength (N/m) to basis weight ( $\text{g/m}^2$ ). For each NFC-MMT sample, a minimum of 7 strips was tested to obtain a mean value with 95% confidence intervals.

### Results and discussion

#### Sheet appearance

The spray coated NFC-MMT composite sheets produced were noted to be flexible, foldable and of uniform thickness. The physical appearance of the NFC-MMT sheet was increasingly yellow in colour, with increasing MMT content as shown in Fig. 2. The well-distributed deposition of MMT throughout the NFC matrix was also confirmed in the SEM images as

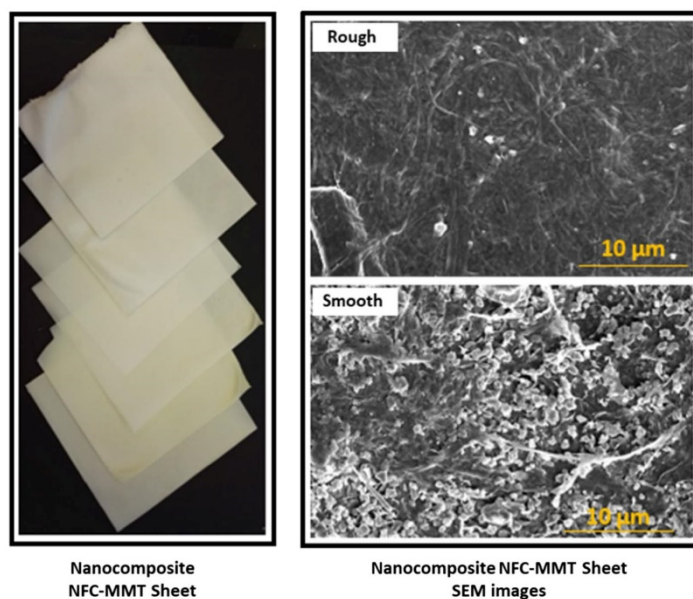
shown in Fig. 2. This is due to absorption spectra of MMT in the nanocomposites.

Fig. S1 in the supplementary information shows an SEM image of the air-exposed rough side and steel-exposed smooth side of the 30 wt% NFC-MMT homogenized composite and pure homogenized NFC sheet. From Fig. S1, the surface of the composite shows scattered MMT throughout the NFC network. After homogenizing both NFC and MMT, the NFC diameter decreased and the MMT was shown to be well dispersed within the NFC network. This results in a compact fibrous network with reduced porosity. Fig S2 in the supplementary information shows SEM images of the cross-sectional view of the NFC-MMT composites. These results are further supported by the XRD analysis of the composites which confirm the adequate dispersion of MMT throughout the NFC network.

#### Sheet water vapour permeability

Figure 3 shows the WVP of the spray coated NFC-MMT composite sheets. Here, the WVP values were also compared with the vacuum filtered NFC-MMT composite sheets previously reported in (Garusinghe et al. 2018). The error bars indicate 95% confidence intervals.

The initial average WVP of a spray coated un-homogenized pure NFC sheet was noted to be  $2.5 \times 10^{-11} \text{ g/m s Pa}$  as shown in Fig. 3. This value is similar to the water vapor permeability of similar pure NFC sheets formed by spraying for packaging applications (Maliha et al. 2019). Here, the addition of 5 wt% MMT loading was shown to decrease this WVP



**Fig. 2** Physical appearance and SEM images of spray coated NFC-MMT sheets

by more than half to  $1.2 \times 10^{-11}$  g/m s Pa. Beyond this loading however, the WVP increased to a maximum of  $3.3 \times 10^{-11}$  g/m s Pa at a 30% MMT loading. This is due to the presence of excessive MMT agglomeration as confirmed by the XRD results in the later sections of this paper.

Interestingly, homogenizing both the MMT and NFC suspension prior to spray coating yielded notable improvements to the WVP results at higher MMT loadings. At an optimum loading of 20% MMT, the average WVP of a spray coated homogenized NFC-MMT composite sheet was  $0.8 \times 10^{-11}$  g/m s Pa, as shown in Fig. 3. It is believed that the process of homogenization breaks down and delaminates the larger MMT particles, thereby increasing their effective surface area (Garusinghe et al. 2018). This in return results in a more even distribution of MMT throughout the NFC matrix which increases the overall tortuosity of the pathway for the permeance of water vapour (Garusinghe et al. 2018). Here, the performance of the spray coated NFC-MMT sheet at  $0.8 \times 10^{-11}$  g/m s Pa was very close to that of the

best vacuum filtered NFC-MMT sheet at about  $0.6 \times 10^{-11}$  g/m s Pa.

#### Sheet apparent density

Figure 4 shows the sheet apparent density values obtained for the spray coated NFC-MMT composite sheets alongside the vacuum filtered sheets (Garusinghe et al. 2018). The error bars indicate 95% confidence intervals.

As shown in Fig. 4, the apparent density of all composite sheets prepared by spray coating were lower than their corresponding vacuum filtered counterparts. The nanofibers in the pure spray coated sheets tend to form small agglomerates and clumps with the spray coating process as previously reported (Shanmugam et al. 2018) which reduces sheet packing density.

This issue is further exacerbated at high MMT loading quantities as shown in Fig. 4. Here, approximately similar sheet apparent density values were obtained despite the increased MMT load for the unhomogenized spray coated NFC-MMT composite

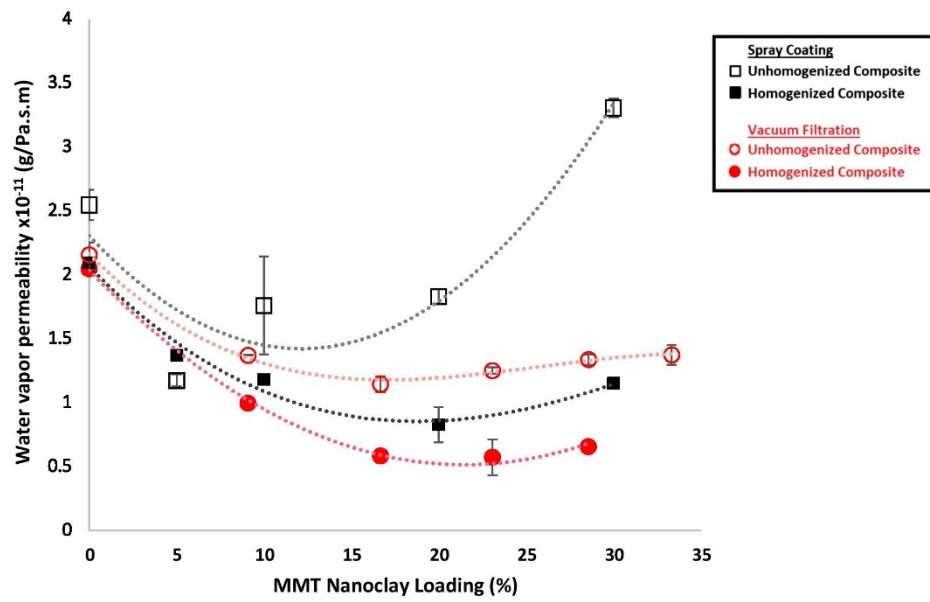


Fig. 3 Water vapour permeability of spray coated and vacuum filtered NFC-MMT sheets containing the same amount of NFC with varying additional MMT loading with respect to the NFC content

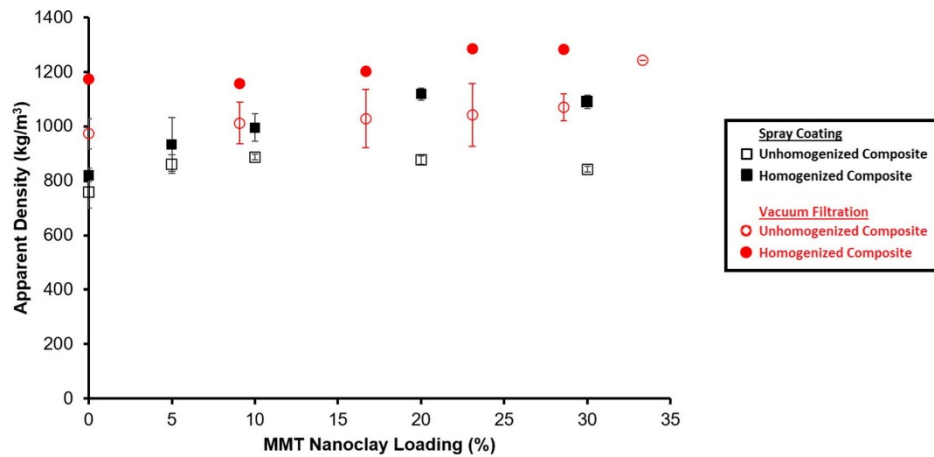


Fig. 4 Apparent density of spray coated and vacuum filtered NFC-MMT sheets

sheet. As previously mentioned, it is believed that the MMT has an increased affinity to form larger stacks at very high loading (Garusinghe et al. 2018). This disrupts the overall packing structure which results in

the increased WVP as shown in Fig. 3. At optimally lower MMT loads however, the nanoclay is able to fill gaps within the fiber network which improves the overall packing structure.

Evidently, the process of homogenization resulted in improved sheet apparent density for all spray coated and vacuum filtered cases. The high mechanical shearing forces in a homogenizer were noted to be effective in breaking down the larger MMT stacks and adequately dispersing them throughout the NFC-MMT suspension. This in return results in a more tightly packed sheet structure which increases the sheet apparent density.

#### Sheet structure

XRD analysis was performed on the spray coated NFC-MMT composites in order to determine the orientation of MMT in the NFC network. Figure 5 shows the XRD patterns of pure MMT, pure NFC and NFC-MMT composites under all MMT loadings. The area under the curve (AUC) provides information on the amount of MMT present in the composite and increases with MMT loading. The AUC of the first peak was chosen because MMT produces a peak from  $2^\circ$  to  $10^\circ$ , which represents the spacing between the MMT layers. As shown in Fig. 5, pure NFC had no characteristic peak in the range of  $2^\circ$  to  $10^\circ$ .

From Fig. 5, the AUC increases sharply from the pure MMT to 10 wt% MMT loading. This is due to the alignment of MMT in the plane of the sheets. In its pure powdered state, MMT is aligned randomly and only flat-oriented platelets will contribute to the diffraction pattern. A more thorough comparison of the AUC of the first peaks in the XRD spectrum versus the MMT loading for the unhomogenized and homogenized composites can be found in Fig. S3 and Fig. S4, respectively in the supplementary information.

Figure 6 shows the effect of MMT loading on the d-spacing of MMT in the composites. The d-spacing of pure MMT was evaluated to be  $11.78 \text{ \AA}$  from the diffraction peak at  $2\theta = 7.5^\circ$  using Eq. 1. The orientation of MMT platelets in the composite shows a peak in this range. The interspacing of MMT platelets barely varies from  $14.7$  to  $14.2 \text{ \AA}$  in the homogenized composites as the MMT content was increased from 10 wt% to 30 wt%. This reveals a strong interaction of MMT platelets and the NFC fiber network. The interspacing is constant and independent of MMT loading, except for the 5 wt% homogenized composite. The effect of charge distribution between the MMT and nanocellulose can be one possible reason for the variation in the MMT interlayer spacing. The diffraction peak of MMT in the 5 wt% and 10 wt% unhomogenized composites were  $6.06^\circ$  and  $6.20^\circ$ , respectively. There is no peak for the 5 wt%

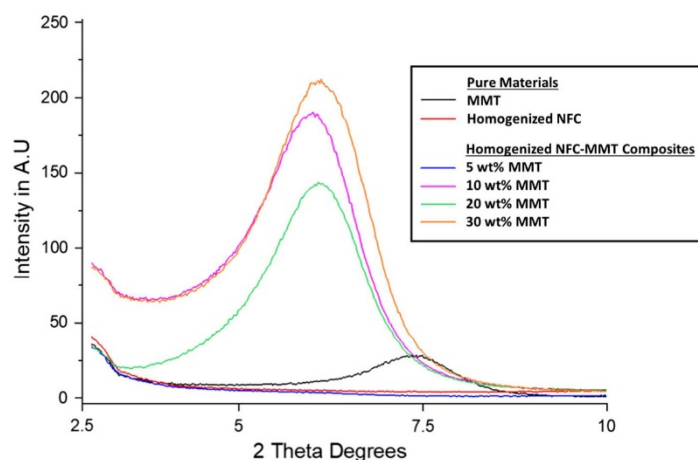


**Fig. 5** First peak in the XRD spectrum of pure MMT, pure NFC and NFC-MMT composites

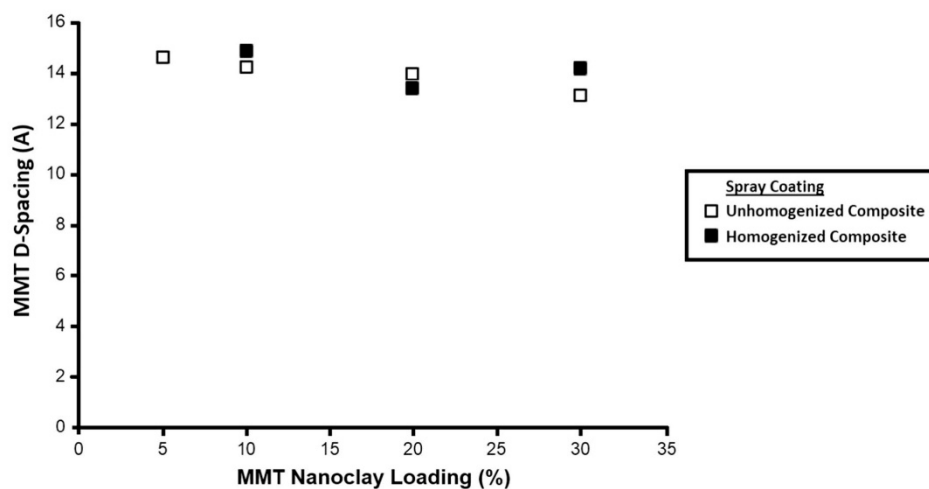


**Fig. 6** Effect of MMT loading on the d-spacing of MMT at the first peak in the XRD spectrum

homogenized sample and a peak at  $6.06^\circ$  for the 10 wt% homogenized composites. The absence of the peak in 5 wt% homogenized composite suggests that MMT platelets completely lose their arrangement on homogenization and are fully dispersed in the CNF fibrous matrix. The composite beyond 5 wt% had peak values due to the stacking of MMT platelets and their subsequent alignment in the plane of the NFC sheet. Thereafter, peak positions increased slightly with MMT content for both types of composites. This means that all the MMT will contribute to the scattering, whereas with pure MMT only the small fraction of platelets that orient in the plane will contribute.

#### Sheet mechanical properties

Figure 7 shows the tensile index of the NFC-MMT composite sheets as a function of MMT nanoclay loading for both unhomogenized and homogenized cases. The error bars indicate 95% confidence intervals. It is worth noting that the aim of this mechanical strength study was to demonstrate that the addition of an optimum amount of MMT nanoclay does not adversely affect sheet strength.

In the case of the unhomogenized composite, the addition of up to 10 wt% MMT resulted in slight

improvements to the sheet tensile index (55 Nm/g) compared to that of the pure NFC sheet (48 Nm/g). However, a decrease in sheet strength performance was observed past a loading of 20 wt% MMT, consistent with the decrease in WVP barrier performance values in the previous section.

In the case of the homogenized composite, the addition of up to 20 wt% MMT resulted in relatively similar sheet tensile index values compared to that of the pure NFC sheet at about 80 Nm/g. The increased tensile index values of homogenized sheets over unhomogenized sheets is due to the increased degree of NFC fibrillation which increases the number of fiber–fiber bonds and the overall capacity of the fiber sheet network to bear load (Ang et al. 2019). A decrease in sheet strength performance was also observed past the optimal 20 wt% MMT loading point and is also consistent with the decrease in WVP barrier performance values in previous section.

Here, we have demonstrated that at the optimal level of MMT loading, the high strength properties of the composite sheet can be retained while still resulting in good sheet barrier performance. The tensile strength and E-modulus of spray coated composites can be found in Fig. S5 and Fig. S6 in the supplementary information.

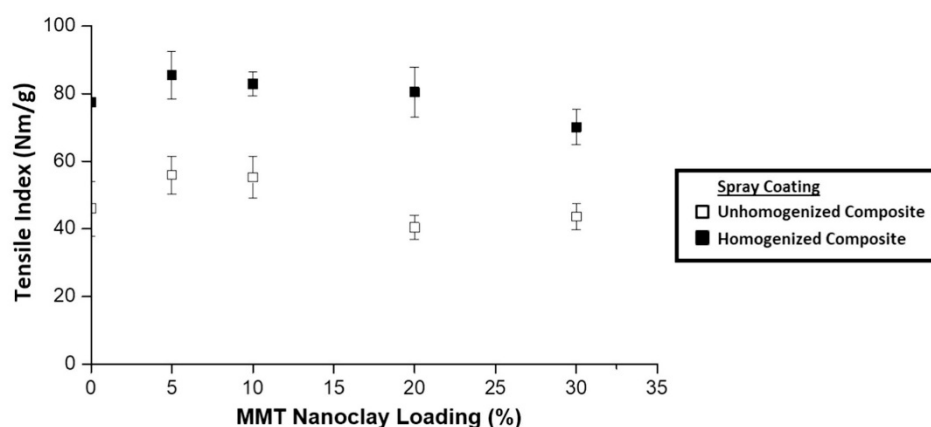


Fig. 7 Tensile index of NFC-MMT composite sheets as a function of MMT nanoclay loading

#### Novelty of process

To the best of our knowledge, there are no readily available industrial methods for the rapid production of NFC composite sheets. The most common method for the fabrication of NFC composites is by use of vacuum filtration. Vacuum filtration is often performed in laboratory-scale settings and has numerous drawbacks. As noted in a previous study, the addition of MMT nanoclays into a 0.3 wt% NFC suspension drastically increased the sheet dewatering time with vacuum filtration from 30 min to 24 h (Garusinghe et al. 2018). Further, the manual-peeling process employed to separate a drained nanocomposite sheet from its filter often leads to surface defects. These issues hinder the rapid production of NFC composite sheets such as NFC-MMT on a commercial scale.

Among the various sheet fabrication technologies, spray coating presents as a viable solution to rapidly form NFC composite sheets. It has the added benefit of being flexible in handling high NFC suspension consistencies compared to vacuum filtration (Shanmugam et al. 2017). As demonstrated in our previous work with pure NFC, the operation time for spray coating was less than 1 min (Shanmugam et al. 2018). This spray coating process could be scalable for the production of self-standing composites or for laminating composites onto a base sheet (Mirmehdi et al. 2018). The spraying of NC onto a continuous steel substrate followed by rapid drying on the same

substrates would be a feasible process. The sheets can be dried in 5 h at 50 °C as reported in our previous work and can be reduced to up to 2 h for modified composites at higher temperatures (Nadeem et al. 2020). In industrial practice, the waste heat recovered to dry the wet film from spraying through the tunnel dryer. Additionally, Yankee dryer and Condebelt technology can be applied for continuous drying process of wet film (Stenström 2019).

Spray coating also drastically reduces the water consumption and water removal required with conventional filtration. For example, vacuum filtering a 0.3 wt% NFC suspension (0.3 g dry fiber in 99.7 g water) requires the removal of 332 tonne water/tonne fiber. In our study, a 2 wt% NFC suspension coupled with an optimum 20 wt% MMT loading (based on dry NFC weight) equates to a total solids content of 2.4 wt% (2.4 g dry fiber in 97.6 g water), which requires the removal of 41 tonne water/tonne fiber. Ultimately, this equates to an almost 90% reduction (291 tonne water/tonne fiber) in water removal requirements using spray coating as opposed to conventional vacuum filtration. However, the water removal mechanism is different in both cases. In the case of vacuum filtration, the water removal can be achieved at the wet end of a paper machine. On the other hand, for spraying evaporative removing of water is required. While this is a promising approach for preparation of high-performance barrier material in terms of material performance and ease of

preparation, future studies to evaluate the energy requirements and the economic feasibility of the process are required.

### Conclusion

In this study, homogenized NFC-MMT composite sheets were spray coated onto impermeable stainless-steel surfaces and their barrier and strength properties were investigated. The resulting NFC-MMT composite sheets had good WVP barrier performance of  $8.3 \times 10^{-12}$  g/m s Pa at an optimal 20 wt% MMT loading. This WVP value was comparable to that obtained from vacuum filtered NFC-MMT composite sheets. Further, spray coating reduced the required water removal during drying by almost 90% (291 tonne water/tonne dry NFC product), compared to forming equivalent sheets using vacuum filtration at 0.3 wt%. XRD analysis confirmed that homogenization was effective in breaking down the larger stacks of MMT nanoclays leading to an even-distribution of MMT throughout the NFC fiber matrix. Even at a high 20 wt% MMT loading, the high mechanical strength of the spray coated NFC-MMT sheets was similar to that of pure NFC sheets at about 80 Nm/g.

Here, we have successfully demonstrated that a high-performance NFC-MMT barrier material can be feasibly and rapidly made by spray coating. Further, the MMT loading quantities have no effect on the operation time for spray coating. This creates a range of opportunities to flexibly tailor the properties of nanocomposite sheets for packaging applications.

### Supplementary material

This manuscript contains the following supplementary materials: The 1  $\mu\text{m}$  micrographs of spray coated composites (Fig. S1), cross-sectional micrograph of spray coated composites (Fig. S2), XRD spectrum of unhomogenized composites (Fig. S3), plot between area under the curve (AUC) of first peak vs MMT loading (Fig. S4) and mechanical properties of spray coated composites (Fig. S5 and Fig. S6).

**Acknowledgments** The authors acknowledge the financial support of the Australian Research Council, Australian Paper, Carter Holt Harvey, Circa, Norske Skog and Visy through the

Industry Transformation Research Hub Grant IH130100016. The use of facilities of the Monash Centre for Electron Microscopy are acknowledged. The authors would like to thank to Dr. Xi-Ya Fang for her help with investigating the cross-sectional view of spray coated nanocomposites under an SEM. The authors also acknowledge the use of facilities within the Monash X-Ray Platform at Monash University, Australia.

### References

- Ang S, Haritos V, Batchelor W (2019) Effect of refining and homogenization on nanocellulose fiber development, sheet strength and energy consumption. *Cellulose* 26:4767–4786. <https://doi.org/10.1007/s10570-019-02400-5>
- Azeredo HMCD (2009) Nanocomposites for food packaging applications. *Food Res Int* 42:1240–1253. <https://doi.org/10.1016/j.foodres.2009.03.019>
- Beneventi D et al (2014) Pilot-scale elaboration of graphite/microfibrillated cellulose anodes for Li-ion batteries by spray deposition on a forming paper sheet. *Chem Eng J* 243:372–379. <https://doi.org/10.1016/j.ccej.2013.12.034>
- Berk Z (2013) Chapter 27—Food packaging. In: Berk Z (ed) *Food process engineering and technology*, 2nd edn. Academic Press, San Diego, pp 621–636. <https://doi.org/10.1016/B978-0-12-415923-5.00027-7>
- Garusinghe UM, Varanasi S, Raghuwanshi VS, Garnier G, Batchelor W (2018) Nanocellulose-montmorillonite composites of low water vapour permeability. *Colloids Surf A Physicochem Eng Asp* 540:233–241. <https://doi.org/10.1016/j.colsurfa.2018.01.010>
- Henriksson M, Berglund LA, Isaksson P, Lindström T, Nishino T (2008) Cellulose nanopaper structures of high toughness. *Biomacromol* 9:1579–1585. <https://doi.org/10.1021/bm800038n>
- Jochen W, Paul T, Julian MD (2006) Functional materials in food nanotechnology. *J Food Sci* 71:R107–R116. <https://doi.org/10.1111/j.1750-3841.2006.00195.x>
- Krol LF, Beneventi D, Alloin F, Chaussy D (2015) Microfibrillated cellulose-SiO<sub>2</sub> composite nanopapers produced by spray deposition. *J Mater Sci* 50:4095–4103. <https://doi.org/10.1007/s10853-015-8965-5>
- Liu A, Berglund LA (2012) Clay nanopaper composites of nacre-like structure based on montmorillonite and cellulose nanofibers—improvements due to chitosan addition. *Carbohydr Polym* 87:53–60. <https://doi.org/10.1016/j.carbpol.2011.07.019>
- Liu A, Walther A, Ikkala O, Belova L, Berglund LA (2011) Clay nanopaper with tough cellulose nanofiber matrix for fire retardancy and gas barrier functions. *Biomacromol* 12:633–641. <https://doi.org/10.1021/bm101296z>
- Malaha M et al (2019) Bismuth phosphinate incorporated nanocellulose sheets with antimicrobial and barrier properties for packaging applications. *J Clean Prod*. <https://doi.org/10.1016/j.jclepro.2019.119016>
- Mirmehdi S, Hein PRG, de Luca Sarantopoulos CIG, Dias MV, Tonoli GHD (2018) Cellulose nanofibrils/nanoclay hybrid composite as a paper coating: effects of spray time, nanoclay content and corona discharge on barrier and

- mechanical properties of the coated papers. *Food Packag Shelf Life* 15:87–94
- Nadeem H et al (2020) An energy efficient production of high moisture barrier nanocellulose/carboxymethyl cellulose films via spray-deposition technique. *Carbohydr Polym* 250:116911. <https://doi.org/10.1016/j.carbpol.2020.116911>
- Nair SS, Zhu J, Deng Y, Ragauskas AJ (2014) High performance green barriers based on nanocellulose. *Sustain Chem Process* 2:23. <https://doi.org/10.1186/s40508-014-0023-0>
- Shanmugam K, Varanasi S, Garnier G, Batchelor W (2017) Rapid preparation of smooth nanocellulose films using spray coating. *Cellulose* 24:2669–2676. <https://doi.org/10.1007/s10570-017-1328-4>
- Shanmugam K, Doosthosseini H, Varanasi S, Garnier G, Batchelor W (2018) Flexible spray coating process for smooth nanocellulose film production. *Cellulose* 25:1725–1741. <https://doi.org/10.1007/s10570-018-1677-7>
- Silvestre C, Duraccio D, Cimmino S (2011) Food packaging based on polymer nanomaterials. *Prog Polym Sci* 36:1766–1782
- Spoljaric S, Salminen A, Dang Luong N, Lahtinen P, Vartiainen J, Tammelin T, Seppälä J (2014) Nanofibrillated cellulose, poly(vinyl alcohol), montmorillonite clay hybrid nanocomposites with superior barrier and thermomechanical properties. *Polym Compos* 35:1117–1131. <https://doi.org/10.1002/pc.22759>
- Stenström S (2019) Drying of paper: a review 2000–2018. *Drying Technol.* <https://doi.org/10.1080/07373937.2019.1596949>
- Uyama H, Kuwabara M, Tsujimoto T, Nakano M, Usuki A, Kobayashi S (2003) Green nanocomposites from renewable resources: plant oil–clay hybrid materials. *Chem Mater* 15:2492–2494. <https://doi.org/10.1021/cm0340227>
- Varanasi S, He R, Batchelor W (2013) Estimation of cellulose nanofibre aspect ratio from measurements of fibre suspension gel point. *Cellulose* 20:1885–1896. <https://doi.org/10.1007/s10570-013-9972-9>

**Publisher's Note** Springer Nature remains neutral with regard to jurisdictional claims in published maps and institutional affiliations.